

# **STAR FORMATION AS A FUNCTION OF ENVIRONMENT USING THE MEERKAT GALAXY CLUSTERS LEGACY SURVEY**



Kabelo Calvin Kesebonye

School of Mathematics, Statistics, and Computer Science

University of KwaZulu-Natal

A thesis submitted in fulfilment of the requirements for the  
degree of

*Doctor of Philosophy*

August, 2023

*For Moratwa.*

## Abstract

Probing the star formation (SF) activity of cluster galaxies paves an important path towards the understanding of cluster evolution. This thesis presents the study of star formation rates (SFR) in clusters using dust-unbiased radio luminosities from the MeerKAT Galaxy Clusters Legacy Survey (MGCLS). Our radio data is complemented by optical data from the Dark Energy Camera Legacy Survey (DECaLS), for photometric redshifts, and also Sunyaev-Zel'dovich (SZ) effect-derived cluster masses from the Atacama Cosmology Telescope (ACT). We present the first statistical study of SFR in clusters using MeerKAT-detected galaxies which takes advantage of MeerKAT's large field of view to investigate the relation between SF activity and cluster environments out to  $2R_{200}$ . Using radio diffuse emission in the form of haloes and relics as a proxy for cluster merger activity, we divide our cluster sample between disturbed/merger clusters and relaxed clusters. We observe a higher fraction of star-forming galaxies ( $f_{\text{SF}}$ ) in disturbed clusters than in relaxed clusters. Disturbed clusters also have higher masses ( $M_{200}$ ) and total SFR ( $\Sigma\text{SFR}$ ) in contrast to relaxed clusters. On analysing the redshift evolution of the mass-normalised  $\Sigma\text{SFR}$ , we observe a  $\approx 4\times$  decline in the SF activity of clusters from the redshift of 0.35 to 0.15, corresponding to  $\approx 2$  Gyr in look-back time. Our result is roughly consistent with the one from cluster studies that used infrared-derived SFR ( $\approx 5\times$  decline) at a similar redshift slice as our sample. We use a subsample of double relic-hosting clusters to investigate the relation between cluster SF activity and the time that has passed since the merger started ( $t_{\text{merger}}$ ) estimated from the relic distances from cluster cores. We observe an anti-correlation between  $\Sigma\text{SFR}$  and  $t_{\text{merger}}$ , suggesting that younger mergers have a higher SF activity. However, we see no clear correlation in the mass-normalised  $\Sigma\text{SFR}$  with  $t_{\text{merger}}$ . We also investigate for differences in the SF activity of galaxies closer to radio relics and those away from the relics and observe no significant differences between the two populations.

## Acknowledgements

Firstly, I would like to thank my supervisors, Professor Matt Hilton and Dr Kenda Knowles, for their guidance and patience over the last three years we have been working together. The lessons I have learned from working with you have proved invaluable to my academic education and my life.

I would also like to convey my thanks to Professor Kavilan Moodley and Dr Edwin Retana-Montenegro for the useful discussions during our weekly group meetings that have contributed to the improvement of my knowledge of the subject and the quality of my research.

A special thank you to the South African Radio Astronomy Observatory (SARAO) Human Capital Development for funding my studies from the first year of my undergraduate degree all the way to my PhD. I would also like to extend my thanks to the MeerKAT and the MGCLS teams. This work would have not been successful without the collective efforts and support of the group.

To Dr Sinenhlanhla Precious Sikhosana, I cannot thank you enough for your support and guidance. I would also like to thank all those from the University of KwaZulu-Natal's Astrophysics Research Centre: the administrative and academic staff, and the students for creating a conducive and safe learning environment.

Finally, to my family and friends, thank you for your love and your endless support. To my soldiers: Kelvin, Galefang, Basto, Ntsoaki, Noki, Dami, Keabaka, Aaron, Diana, Ian, Edward, Vincent, Pamela, Scott, Wesley, Sitwala, Psykes, Gape, Mpho, Tlhompho, Shakes, Kaone, Adila,

Mziyanda, Bismark, Tankiso, Asma, Nada, Elias, thank you all for always having my back and for keeping me sane over the years.

## Preface

The work described in this thesis was carried out in the School of Mathematics, Statistics, and Computer Science, University of KwaZulu-Natal from January 2020 to November 2022. This dissertation was completed under the supervision of Prof. M. Hilton, with co-supervision by Dr. K. Knowles.

This study represents original work by the author and has not been submitted in any form for any degree or diploma to any other tertiary institution. Where use was made of the work of others it has been duly acknowledged in the text.

As the candidate's supervisor I have approved this thesis for submission.

---

Prof. Matthew Hilton

---

Date

---

Dr. Kenda Knowles

---

Date

## **Plagiarism declaration**

I, **Kabelo Calvin Kesebonye**, declare that

1. The research reported in this thesis, except where otherwise indicated, is my original research.
2. This thesis has not been submitted for any degree or examination at any other university.
3. This thesis does not contain other persons' data, pictures, graphs or other information, unless specifically acknowledged as being sourced from other persons.
4. This thesis does not contain other persons' writing, unless specifically acknowledged as being sourced from other researchers. Where other written sources have been quoted, then:
  - (a) Their words have been re-written but the general information attributed to them has been referenced.
  - (b) Where their exact words have been used, then their writing has been placed in italics and inside quotation marks, and referenced.
5. This thesis does not contain text, graphics or tables copied and pasted from the Internet, unless specifically acknowledged, and the source being detailed in the thesis and in the References sections.

Signed: \_\_\_\_\_

## **Declaration of publications**

Details of contribution to publications that form part of and/or include research presented in this thesis:

### **Section 3**

*A Multiwavelength Dynamical State Analysis of ACT-CL J0019.6+0336*  
Pillay D. S., Turner D.J., Hilton M., et al. (2021). Galaxies, 9, 97.

For this paper, I worked on the `zField` analysis code for obtaining photometric data and producing density maps for the cluster in the study.

### **Section 8.2**

*The MeerKAT Galaxy Cluster Legacy Survey I: Survey Overview and Highlights*  
Knowles K., Cotton W. D., Rudnick L., et al. (2022). Astronomy & Astrophysics, 657, A56.

For this paper, I worked on calculations for the astrometric offsets for the MeerKAT catalogues using optical/IR comparisons. I worked on the analysis of star formation rates for cluster Abell 209. I produced optical/IR tables to make data products for optical/IR - radio catalogues for Abell 209 and Abell S295. I produced the data products for star-forming galaxies in Abell 209. Part of the work covered by this thesis is based on the work published in this paper and has been adapted to the formatting requirements of the thesis.

### **Section 3**

*The MeerKAT Galaxy Clusters Legacy Survey: star formation in massive clusters at  $0.15 < z < 0.35$*

Kesebonye K. C., Hilton M., Knowles K., et al. (2023). MNRAS, 518, 3004.

I am the main contributor to this work. I conducted the analysis, coordinated the paper, and wrote the results and discussion of the paper. Part of the work covered by this thesis is based on the work published in this paper and has been adapted to the formatting requirements of the thesis.

Signed in Westville, Durban: \_\_\_\_\_ Date: \_\_\_\_\_

# Contents

<b>Abstract</b>	iii
<b>Acknowledgements</b>	iv
<b>Preface</b>	vi
<b>Declaration of Non-Plagiarism</b>	vii
<b>Declaration of Publications</b>	viii
<b>List of Tables</b>	xiii
<b>List of Figures</b>	xvi
<b>1 Introduction</b>	1
1.1 Cosmic history of the Universe . . . . .	4
1.2 Galaxies . . . . .	7
1.2.1 Star formation in galaxies . . . . .	11
1.2.2 Star formation tracers . . . . .	12
1.2.3 Comparing different SFR tracers . . . . .	19
1.3 Galaxy clusters . . . . .	20
1.3.1 Cluster observational methods . . . . .	22
1.3.2 Cluster morphology and dynamical states . . . . .	26
1.3.3 Non-thermal diffuse emission in galaxy clusters ICM . . . . .	28
1.3.4 Star formation activity of galaxies in clusters . . . . .	34

1.4	Thesis outline	39
<b>2</b>	<b>Parent data samples and method development</b>	<b>40</b>
2.1	MeerKAT Galaxy Clusters Legacy Survey	40
2.1.1	MGCLS astrometry checks with unWISE	43
2.2	Cross-matching MGCLS with DECaLS	49
2.2.1	Photometric redshifts	50
2.3	Star formation in Abell 209	53
2.3.1	Compact source catalogues	53
2.3.2	Cluster membership selection and galaxy star formation rates	54
2.3.3	Star formation activity as a function of clustercentric distance	58
2.4	Summary	61
<b>3</b>	<b>Star formation in massive cluster at <math>0.15 &lt; z &lt; 0.35</math> using the MeerKAT Galaxy Clusters Legacy Survey</b>	<b>62</b>
3.1	Cluster sample	62
3.2	Identifying cluster members	67
3.3	AGN removal	69
3.4	Star formation rates and results	72
3.4.1	Fraction of star-forming galaxies	72
3.4.2	Total star formation rate and cluster mass relation	77
3.4.3	Normalized total star formation rates and redshift relation	82
3.5	Summary	84
<b>4</b>	<b>Star formation activity in MGCLS clusters with haloes and relics</b>	<b>86</b>
4.1	Data sample and analysis	87
4.1.1	Cluster sample	87
4.1.2	Star formation activity relation with time since the merger started	93
4.1.3	The distribution of galaxies and their SFR in relic-hosting clusters	98
4.2	Summary	101
<b>5</b>	<b>Conclusion and future work</b>	<b>102</b>

**A Legacy Survey images of the cluster sample** 105

**Bibliography** 111

# List of Tables

2.1	Median offset values between MeerKAT and unWISE . . . . .	46
3.1	Cluster sample properties . . . . .	65
3.2	Quantities derived from the three clusters in our sample with spec-zs	68
4.1	Properties for relic-hosting clusters . . . . .	88
4.2	Relic properties . . . . .	94
4.3	The $f_{\text{SF}}$ estimates of galaxies in the assumed shock wave path and the cluster . . . . .	99

# List of Figures

1.1	The schematic diagram of the evolution of the Universe . . . . .	5
1.2	The <code>illustrisTNG</code> Simulation of structure in the Universe . . . . .	8
1.3	The Hubble sequence of galaxies . . . . .	10
1.4	A comparison of commonly used IMFs . . . . .	13
1.5	A comparison of SFR estimates between dust-attenuated estimators ( $H_{\alpha}$ and UV) and non-dust-attenuated estimators (radio and IR) . .	19
1.6	The image of the Abell 2744 cluster . . . . .	21
1.7	A schematic diagram of the SZ-effect . . . . .	25
1.8	Properties of a radio halo . . . . .	29
1.9	Image of the Perseus cluster mini-halo . . . . .	31
1.10	Examples of clusters hosting relics . . . . .	33
1.11	Properties of a radio halo . . . . .	34
1.12	Examples of revived fossil plasma . . . . .	35
1.13	The $f_{\text{SF}}$ versus clustercentric radius plot from Haines et al. (2015). .	36
1.14	An example of a galaxy undergoing ram pressure stripping . . . . .	38
1.15	An example of a galaxy undergoing tidal stripping . . . . .	38
2.1	MeerKAT telescope radio image for A209 . . . . .	42
2.2	Offsets in the J0510.2-4519 cluster . . . . .	47
2.3	The distribution of offsets in $\Delta\text{RA}$ for cluster J0510.2-4519 . . . .	48
2.4	A comparison of photo-zs estimated using <code>zCluster</code> on DECaLS photometry with spec-zs from SDSS . . . . .	51

2.5	The flowchart showing the steps followed to produce the star-forming cluster member galaxies for A209 . . . . .	55
2.6	Photometric vs. spectroscopic redshifts for all the A209 galaxies in the MeerKAT field. . . . .	56
2.7	The Legacy Survey DR9 image of the A209 field . . . . .	59
2.8	Star formation activity in the A209 cluster. . . . .	60
3.1	The mass ( $M_{200}$ ) and redshift distribution of the MGCLS cluster subsample . . . . .	66
3.2	Thumbnail images of galaxies with $L_{1.4\text{GHz}} > 10^{23} \text{ WHz}^{-1}$ . . . . .	71
3.3	The fraction of star-forming galaxies in MGCLS comparison with Haines et al. (2015) . . . . .	73
3.4	The comparison of $f_{\text{SF}}$ trends between clusters hosting radio haloes/relics and relaxed clusters . . . . .	76
3.5	Total star formation rates ( $\Sigma\text{SFR}$ ) and cluster mass relation . . . . .	79
3.6	Total SFR of the MGCLS radio-selected and X-ray-selected subsamples	80
3.7	The fraction of star-forming galaxies split by the MGCLS subsamples	81
3.8	Evolution of star formation activity . . . . .	83
4.1	The distribution of galaxies and their SFR in the J2023.4-5535 and Abell 521 clusters . . . . .	90
4.2	The distribution of galaxies and their SFR in the Abell 2744 cluster .	91
4.3	The distribution of galaxies and their SFR in the J0516.6-5430 cluster	92
4.4	$\Sigma$ SFR relation with projected relic distance . . . . .	96
4.5	The relation between relics power and the distance from the centre and also their sizes . . . . .	97
4.6	The comparison of the $f_{\text{SF}}$ in radial bins between galaxies in the assumed shock wave path and those outside the path . . . . .	100
A.1	Legacy Survey images of our cluster sample . . . . .	106
A.2	Legacy Survey images of our cluster sample cont1 . . . . .	107

A.3	Legacy Survey images of our cluster sample cont2	108
A.4	Legacy Survey images of our cluster sample cont3	109
A.5	Legacy Survey images of our cluster sample cont4	110

# Chapter 1

## Introduction

The Universe has always left humankind with more questions than answers on their undying quest to find its origins and evolution. This burning desire to find answers to some of the most challenging questions about the Universe fueled studies of the celestial bodies, giving birth to the disciplines of cosmology and astronomy. For most of human history, the study of celestial bodies was restricted to being done with the naked eye. Major advances in our current knowledge of the Universe have been made largely thanks to the technological development over the last few centuries.

In the 16th century, the first telescope was used to observe celestial bodies at a more detailed level by Galileo Galilei ([Whitehouse, 2009](#)). New information about the solar system and the Milky Way was uncovered. Galileo's discoveries sparked a wave of interest in the study of celestial bodies. As technology advanced in the 19th and 20th centuries, our understanding of astronomy significantly improved. William Herschel discovered infrared radiation ([Rowan-Robinson, 2013](#)), paving a new way to observe the Universe beyond the limits of visible light. The introduction of the first spectroscope by Joseph von Fraunhofer allowed for the probe of the chemical makeup of celestial bodies ([Brand, 1995](#)). Karl Jansky's discovery of radio waves from extraterrestrial objects opened a new window to observe the Universe ([Jansky, 1933](#)).

The technological advancement of the 19th and 20th centuries meant that we could now examine the heavens at a deeper level. As more observations were made,

a debate sparked amongst astronomers in the late 19th and early 20th century about spiral nebulae (galaxies in present terminology), mysterious unresolved gas clouds of uncharacterised nature (see e.g., [Shapley and Curtis, 1921](#)). This debate drove a wedge between astronomers; some argued that the unresolved clouds are part of the Milky Way, which embodies the whole Universe, while others argued that the gas clouds are a group of stars forming their own Universes. Edwin Hubble, a lawyer turned astronomer, settled this debate by studying Cepheid variable stars in the Andromeda nebula (galaxy). Hubble used light fluctuations from the variable stars to determine the distance to the nebula through their periodical fluctuations and luminosity. Hubble's Andromeda distance estimate suggested that it resided outside the Milky Way and could not be a group of stars within it. This new evidence was enough to convince most astronomers of that time that Andromeda is a galaxy and that the Universe, in fact, has a plethora of galaxies.

Hubble continued measuring distances to more galaxies/extragalactic nebulae, this time paying close attention to their motion with respect to Earth. He discovered that galaxies are moving or shifting away from Earth at velocities proportional to their distances ([Hubble, 1929](#)). This observation led to the velocity distance relation, also known as the Hubble Law, defined as  $v = H_0 d$ , where  $v$  is the velocity of the galaxy in  $\text{km s}^{-1}$ ,  $H_0$  is the Hubble constant in  $\text{km s}^{-1} \text{Mpc}^{-1}$  and  $d$  is the distance of the galaxy in Mpc. Hubble's discovery revealed that the farther away a galaxy is from Earth, the faster that galaxy is moving away from us. Galaxy velocities are determined from their redshift ( $z$ ), the shift of the light emitted by the galaxy to the red end of the visible spectrum. The Hubble law implied that nearly all the galaxies are moving away from us, providing the first physical evidence for the expansion of the Universe. Suggestions for an expanding Universe had been theoretically made prior to Hubble's observations by a few scholars (see e.g., [Friedmann, 1922](#); [Lemaître, 1927](#)) using Einstein's field equations ([Einstein, 1915](#)). The sudden marriage between the theoretical and observational implications of an expanding Universe gave birth to the Big Bang cosmological model. It is the current leading model that describes the formation of the Universe all the way from its infancy to the large-scale state that we

inhabit today.

Hubble’s observations pioneered the study of extragalactic bodies, establishing a new branch of extragalactic astrophysics, one of the most prominent fields in modern astronomy. Technological advancement of the last century contributed to tremendous breakthroughs in extragalactic studies being made. This led to numerous discoveries, including the cosmic microwave background (CMB; [Alpher et al., 1948](#); [Penzias and Wilson, 1965](#), suggested to be the vestigial remains of the Big Bang), the discovery of dark energy ([Riess et al., 1998](#); [Perlmutter et al., 1999](#), proposed to be the driving force responsible for the accelerated rate of expansion of the Universe), detection of the first gravitational wave ([Abbott et al., 2016](#)) and the first observation of a black hole in a nearby galaxy ([Event Horizon Telescope Collaboration et al., 2019](#)), to name a few. Even with all these remarkable discoveries made thus far, we have barely scratched the surface and there is still more to be learned about our Universe.

One of the major areas of research in modern astronomy is the study of galaxy clusters. Galaxy clusters are the largest virialized objects in the Universe. They are megaparsecs-wide laboratories populated by hundreds to thousands of galaxies. Since their discovery, they have unlocked multiple avenues to study the Universe and its evolution. Some of these studies include dark matter, dark energy, gravitational lensing, galaxy formation, and environmental effects on galaxy evolution.

The way in which the large-scale properties of galaxy clusters influence the evolution of their member galaxies is yet to be fully understood. The question of whether it is the environmental or internal processes largely at play in the evolution of galaxies is currently under investigation but evidence suggests that both processes influence galaxy evolution and are independent of one another ([Peng et al., 2010](#)). Some studies argue that the environmental influence on galaxy evolution is secondary to the internal influence ([Hahn et al., 2015](#)) while others suggest a redshift dependence where environmental effects are dominant at  $z \leq 1$  and internal processes dominate at  $z \geq 1$  ([Darvish et al., 2016](#)). By investigating galaxy properties, we can attempt to understand the environmental influence of clusters on their member galaxies. One way to study the environmental influence of clusters is through the investigation of the star

formation (SF) activity of their member galaxies. Recent studies of SF activity of member galaxies in clusters of different morphology/dynamical states (relaxed versus disturbed/merger-linked clusters) have yielded contradicting results. Some studies report enhanced SF activity in disturbed clusters compared to relaxed clusters (e.g., [Cohen et al., 2014](#); [Yoon and Im, 2020](#)), others observe no enhanced SF activity in disturbed clusters (e.g., [Shim et al., 2011](#); [Tyler et al., 2014](#)) while other studies observe suppressed SF activity in disturbed clusters than in relaxed clusters (e.g., [Mansheim et al., 2017](#); [Maier et al., 2022](#)).

This study aims to investigate the SFR as a function of the environment in massive clusters of different morphology using radio observations from the MeerKAT telescope. By taking advantage of MeerKAT’s high sensitivity and large field of view, we study the influences of large-scale cluster properties on their member galaxies from the radio perspective, complementing cluster studies that have been done at different wavelengths. Before I talk about the results and implications of this work, I will begin by introducing some of the important astrophysical processes leading to this investigation to provide a wider context of the subject in the sections that follow.

## 1.1 Cosmic history of the Universe

The current leading model of the Universe, the concordance or standard Lambda Cold Dark Matter ( $\Lambda$ CDM) cosmological model, builds on the Big Bang model and provides parameters with which we contextualise the evolution of the Universe. The  $\Lambda$ CDM model proposes that the Universe is a recipe of three main ingredients: the  $\Lambda$  component which represents a cosmological constant for dark energy, the postulated cold dark matter (CDM) component, and the ordinary/baryonic matter component ([Planck Collaboration et al., 2020](#)). The dark energy is attributed to the accelerated expansion of the Universe at late times (see e.g., [Riess et al., 1998](#); [Peebles and Ratra, 2003](#)). Dark matter is the ‘invisible’ component of the Universe whose existence is postulated from its gravitational influence in the evolution of the Universe (see e.g., [Clowe et al., 2006](#)). The latest constraints of the cosmological model estimate that

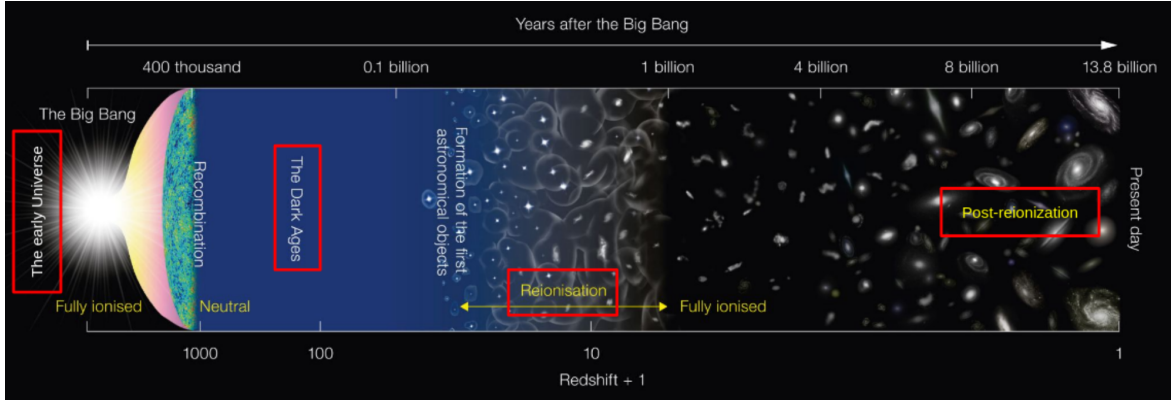


Figure 1.1: The schematic diagram of the evolution of the Universe from the Big Bang till the present day. Image credit: adapted from <https://www.noao.edu/kpno/>

the Universe is  $\approx 70\%$  dark energy,  $\approx 25\%$  cold dark matter, and  $\approx 5\%$  ordinary matter ([Planck Collaboration et al., 2020](#)).

The evolution of the Universe, according to the  $\Lambda$ CDM model, can be summarised into four major epochs as illustrated by Figure 1.1. The first epoch, known as the early Universe, is the period that describes the genesis of the Universe. This epoch ( $\approx 1$  second after the Big Bang) is fairly well understood and characterised thanks to the measurements of signatures that echo events aligned with the Big Bang hypothesis, i.e., the light-element abundance and the CMB. The light elements (helium, deuterium, lithium) are products of the primordial nucleosynthesis estimated to have occurred within a few minutes of the Big Bang. The CMB fluctuations, estimated to have occurred during the age of recombination,  $\approx 380,000$  years post the Big Bang are considered to be the direct evidence of the beginning of the Universe from an explosion. The CMB is the surface of the last scattering from when the Universe cooled to  $\approx 3000\text{ K}$  and neutral atoms could form. Before the CMB was released, photons and ordinary particles were tightly wound together into a single fluid of matter and radiation. As soon as the two species decoupled from one another at the time of recombination, photons carrying a memory of how matter and radiation were distributed at the time of the decoupling started to propagate freely across the Universe.

The second epoch, known as the dark ages, started after the CMB was formed

at  $z \approx 1100$ . This epoch derives its name from the hypothesis that the Universe had no luminous sources at this period. Due to this, we only have a rudimentary understanding of this era from the observation perspective and much of what we know is derived from numerical hydrodynamic simulations (e.g., [Vogelsberger et al., 2014](#); [Schaye et al., 2015](#); [Springel et al., 2018](#)). A number of ground-based and space telescopes have been commissioned (e.g., James Webb Space Telescope (JWST); [Gardner et al., 2006](#)) and proposed (e.g., Radio Experiment for the Analysis of Cosmic Hydrogen (REACH); [de Lera Acedo and L., 2022](#)) to observe this period from just before and during the cosmic dawn. Probing this era proves to be a non-trivial task due to the existence of no luminous objects until the cosmic dawn. Backed by theoretical understanding, highly redshifted 21-cm emission from hydrogen may be the best tool to probe this era ([Loeb and Barkana, 2001](#)). Studies using the JWST early release results have discovered over 100 galaxies at  $z > 9$  ([Naidu et al., 2022](#); [Bradley et al., 2022](#); [Ono et al., 2022](#); [Castellano et al., 2022](#)).

The dark ages ended when the first stars and galaxies emerged at  $z \approx 10 - 30$ , paving a way for the epoch of reionization (EoR), estimated to have taken place at  $z \approx 6 - 13$ . This is the period when the intergalactic medium was reionised by the ultraviolet energy from the first stars. This epoch is marked to be a very important bridge between the physical and cosmological processes of the early Universe and the sophisticated astrophysical processes behind star and galaxy formation. The EoR holds important data about the formation and evolution of matter in the Universe, thus making it one of the most prioritised topics in modern astronomy. Much of what is known about this period is derived from semi-analytical models (e.g., [Cole et al., 1994](#); [De Lucia and Blaizot, 2007](#); [Guo et al., 2011](#)) and numerical hydrodynamic simulations. A number of interferometer instruments have been proposed and established with the aim to probe the EoR using the neutral hydrogen 21-cm emission from this period. Some of these instruments are targeting the 21-cm power spectrum (e.g., Murchison Widefield Array (MWA), Low-Frequency Array (LOFAR), Hydrogen Epoch of Reionisation Array (HERA); [Tingay et al., 2013](#); [van Haarlem et al., 2013](#); [DeBoer et al., 2017](#), respectively) while other instruments are searching

for the global 21-cm signal (see e.g., Shaped Antenna measurement of the background Radio Spectrum (SARAS), Probing Radio Intensity at high-Z (PRIzM); [Singh et al., 2018](#); [Philip et al., 2019](#), respectively). A number of instruments have detected upper limits of the 21-cm fluctuations power spectrum from reionization (e.g., [Parsons et al., 2014](#); [Mertens et al., 2020](#); [Abdurashidova et al., 2022](#)). Although currently under debate, the Experiment to Detect the Global EoR Signature (EDGES) experiment ([Bowman et al., 2018](#)) recently announced a detection of an absorption profile from the EoR centred at frequency 78 MHz ( $z \approx 17$ ). Early release results from the recently launched JWST probing galaxies at this epoch have kick-started thorough investigations of the EoR to provide a more comprehensive view of the Universe at this era ([Curti et al., 2022](#); [Pontoppidan et al., 2022](#)).

The EoR was followed by the post-reionization epoch, occurring at  $z \approx 0 - 6$ . This era presents the Universe at its most interesting and complex state. It is the most accessible of all the epochs and has been studied by the use of multi-wavelength ground-based and space telescopes. Major discoveries have come from this era, shaping our current understanding of the Universe and allowing us to extrapolate our findings through models and simulations to the epochs that are not readily accessible. In the late 1990s, a remarkable revelation from this epoch was observed at  $z \approx 2$ , the accelerated expansion of the Universe, supposedly driven by a ‘dark energy’. This observation was first made by [Riess et al. \(1998\)](#) and [Perlmutter et al. \(1999\)](#) and has since been a fundamental part of the  $\Lambda$ CDM cosmological model. Multiple instruments are underway and built to probe this era to characterise the nature of dark energy using various cosmological targets: type Ia supernovae (SN1a), Baryon Acoustic Oscillations (BAO), CMB, weak gravitational lensing, and galaxy clusters (see e.g., [Huterer and Shafer, 2018](#), for a detailed review of dark energy).

## 1.2 Galaxies

Galaxies are systems that are composed of stars, interstellar medium, and dark matter all bound together by gravity. Galaxies vary in size, shape, and internal activity and

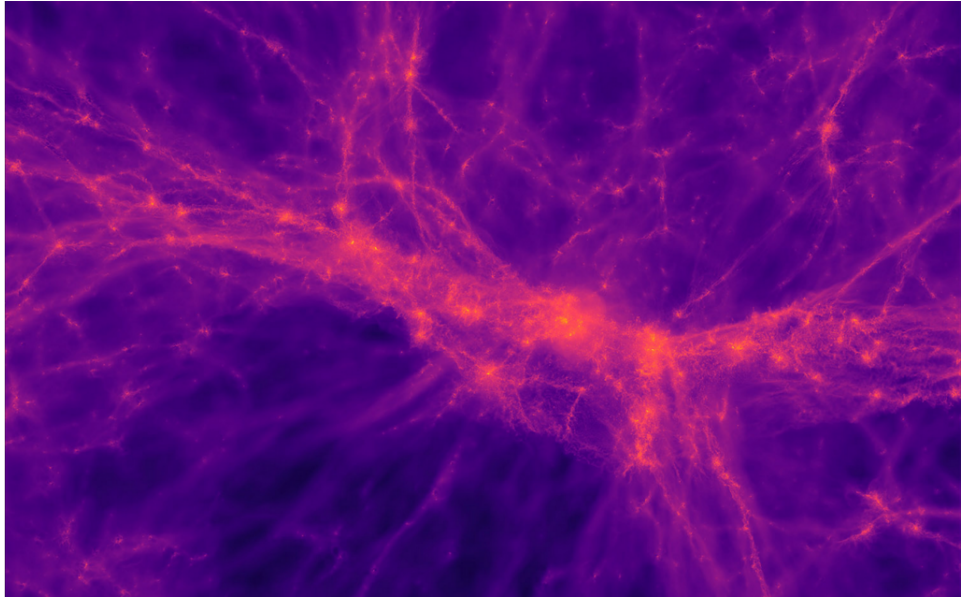


Figure 1.2: The `illustrisTNG` Simulation (Springel et al., 2018) showing the filamentary structure formation in the Universe. The image simulates a region of space 15 Mpc across, showing the filaments connecting together to form galaxies at  $z \approx 3$ . Image credit: <https://www.tng-project.org/media/>

they typically host large numbers of stars ranging from a hundred million to hundreds of billions. They permeate the entire Universe and are estimated in the order of hundreds of billions (Conselice et al., 2016), hence considered to be the building blocks of the Universe and a beacon to map the space-time continuum.

To understand how stars and galaxies were formed, we would need to probe the Universe to the period when the dark ages ended and the first proto-galaxies appeared at  $z \approx 10 - 30$  (a number of galaxies have been reported so far within this redshifts range from the JWST early release results, see e.g., Bradley et al., 2022; Ono et al., 2022; Castellano et al., 2022). The  $\Lambda$ CDM cosmology model proposes that the matter in the Universe forms hierarchically. It starts with small objects being formed, growing through gravitational collapse, and eventually forming large objects. The model further suggests that matter exists in two forms: ordinary/baryonic matter and dark matter. The latter, as the name suggests, has no visual properties and its existence is inferred from the gravitational influence it plays in the formation of stars, galaxies, clusters, and the evolution of the Universe.

The  $\Lambda$ CDM cosmology model postulates that the dark matter haloes that were

formed during the dark ages kept growing as they collapsed gravitationally. In this process, they created potential wells that accreted baryons, leading to the formation of the first stars and galaxies. The process of structure formation is well understood from the theoretical models and simulations perspective but not so much from observations. Various semi-analytical models and numerical hydrodynamic simulations predict structure formation and evolution well enough to match observations of structure seen today (e.g., `illustrisTNG` [Springel et al., 2018](#)). Figure 1.2 shows the simulation of structure in the Universe using hydrodynamic simulations by `illustrisTNG`. Although major processes involving dark matter are yet to be proved observationally, simulations play a major role in bridging our understanding of how structure in the Universe was formed and how it evolved to what we see today.

Galaxies exist in various fashions: they have different shapes, sizes, and colours. The discovery that galaxies differ in morphology raised questions that became the cornerstone of modern astronomical exploration in an attempt to answer them ([Hubble and Humason, 1931](#)). What are the physical processes behind the formation of different forms of galaxies? How does the stellar content of galaxies evolve with time? How do galaxies interact with one another? Upon noticing that galaxies have diverse morphology, Hubble sorted them into groups according to their physical structure, creating what is now known as the Hubble tuning fork or the Hubble sequence, shown in Figure 1.3. Hubble's tuning fork classified galaxies into four broad classes:

- **Elliptical galaxies:** These are galaxy systems with smooth featureless shapes in the form of elliptical isophotes. They are further classified into subtypes ranging between E0–E7. The integer is a rounded value measured from  $10(1 - b/a)$ ,  $a$  and  $b$  being the semi-major and semi-minor axes lengths of the galaxy respectively. The caveat of this classification criteria is that it relies on the projected shape of the galaxy as viewed from Earth so it does not account for the actual three-dimensional structure of the galaxy. This means that systems of similar shapes could be put in different subtypes depending on whether the system is observed face-on or edge-on from our view.

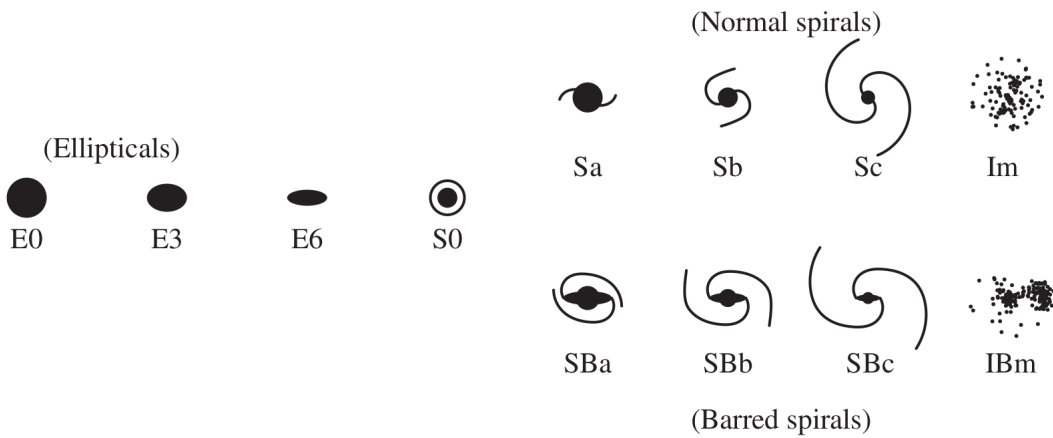


Figure 1.3: The Hubble tuning-fork showing the classification of galaxies based on morphology [Hubble \(1936\)](#). Image credit: [Abraham \(1998\)](#).

- **Spiral galaxies:** These are systems with a bulge of concentrated light in the centre surrounded by a thin flat disk in the form of spiral arms. Spiral galaxies are further broken into two sub-classes: normal spiral (S) systems and barred spiral (SB) systems. The latter types have a bar-like feature across the centre of the galaxy, pivoting the spiral arms on each end of the bar while the former has no central bar features. The sub-classes are further split into three categories, a, b and c, based on three criteria: the light dominance of the central bulge of the system, how tightly wound are the spiral arms, and a measure of HII regions (gas and dust) or what level of the spiral arms is crystallised into stars. For example, Sa/SBa systems will have tightly wound spiral arms and a bright central bulge while Sc/SBc systems will have uneven, loosely wound broken arms, and relatively dimmer/smaller central bulges as seen in Figure 1.3. The tightness of the spiral arms seen in Sa/SBa systems is due to low gas and dust content, which are essential ingredients for the formation of new stars. These systems have low SF, with their central bulges dominated by old stars. The loosely wound spiral arms in Sc/SBc systems are due to their gas and dust richness and are therefore undergoing more SF, resulting in smaller and less dominant central bulges.
- **Lenticular/S0 galaxies:** This is a class of systems with features that lie

between those of elliptical and spiral systems. Like spiral systems, they have a central bulge and like elliptical systems, they have no spiral arms or HII regions. Systems of this nature are classified as S0 galaxies, although some may have a bar-like structure in the centre, and in that case, they are classified as SB0 galaxies.

- **Irregular galaxies:** These are systems with no distinctive features. They have disturbed morphology and are dominated by HII regions. They were not included in the initial Hubble sequence of galaxies but have been added as an extension of spiral systems in recent years ([Abraham, 1998](#)).

The terms early-type and late-type galaxies are often used to label systems based on morphology. The former is used to refer to elliptical and lenticular galaxies while the latter label refers to spiral and irregular galaxies. It is worth noting that galaxies have more classification criteria beyond their morphological properties noted in the Hubble sequence. Further classifications can be done based on their surface brightness, luminosity, gas content, SF activity, and galactic nucleus activity (normal or active). Multiple efforts have been made in the last few decades to study various properties of galaxies to understand the evolution of the Universe.

### 1.2.1 Star formation in galaxies

Stars are the fundamental building blocks of galaxies, much in the same way galaxies are building blocks of the Universe. The cosmic history and evolution of a galaxy are encoded in the age and composition of the stars belonging to it. Stars form from the gravitational collapse of gas clouds (giant molecular clouds) in the interstellar medium (ISM, see e.g., [Williams et al., 2000](#); [McKee and Ostriker, 2007](#), for reviews). Tracing the physical processes behind SF, especially in distant galaxies is a non-trivial task. The direct representation of recent SF activity is emission from young, massive stellar populations ( $\geq 8 M_{\odot}$ ). However, young massive populations burn up their hydrogen reserves rapidly and are short-lived ( $10^{7-8}$  years). The massive stars produce colossal explosions known as supernovae at the end of their life, injecting heavier elements

into the ISM and ultimately enriching the giant molecular clouds ([Sandstrom et al., 2009](#)). Galaxies can also accrete more gas from the inter-galactic medium (IGM) and galaxy mergers, which give them more fuel to form new stars.

SF activity is often estimated using the star formation rate (SFR)

$$\psi = \frac{M_*}{t}, \quad (1.1)$$

where  $M_*$  denotes the total stellar mass of newly formed stars in time  $t$ . The mass distribution of newly formed stellar populations is called the initial mass function (IMF). The IMF is an empirical function that extrapolates the mass distribution of stars from their initial masses when they were formed ([Bastian et al., 2010](#)). It is often quantified by a simple power law

$$\xi(M) = cM^{-\alpha}, \quad (1.2)$$

where  $\alpha$  is a dimensionless constant and  $c$  is a constant relating to the local stellar density.  $\xi(M)$  is generally assumed to fall within the lower and upper limit of  $0.1 - 100 M_\odot$  to allow comparison of results from different IMFs. There are a number of various formulae for IMFs in the literature and the commonly used ones are [Salpeter \(1955\)](#), [Kroupa \(2001\)](#), [Chabrier \(2003\)](#) and are shown in Figure 1.4. The Salpeter IMF has  $\alpha = 2.35$  and was first estimated for more massive stars than the Sun. The Kroupa and Chabrier IMFs both predict fewer low-mass stars but coincide with the Salpeter IMF for masses  $> 1 M_\odot$ .

### 1.2.2 Star formation tracers

Integrated emission from unresolved young stars in galaxies can be observed at various wavelengths in the spectrum. The most common SF tracers are ultraviolet (e.g., [Salim et al., 2007](#)), emission line tracers ( $H\alpha$ ,  $Lya$ ,  $[OII]$ , e.g., [Twite et al., 2012](#); [Dijkstra and Westra, 2010](#); [Kewley et al., 2004](#), respectively), infrared (e.g., [Elbaz](#)

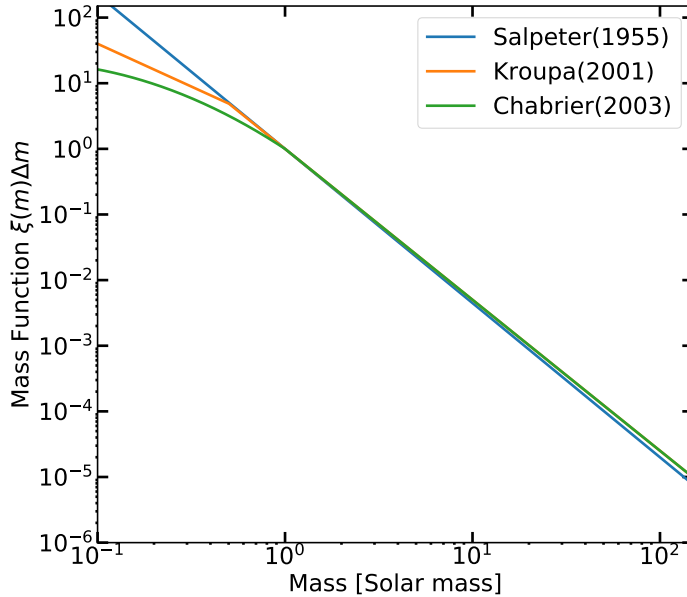


Figure 1.4: A comparison of commonly used IMFs. The Salpeter (1995) IMF is shown by the blue line, the Kroupa (2001) IMF is shown by the orange line and the Chabrier (2003) IMF is shown by the green line.

et al., 2007), X-ray (e.g., Ranalli et al., 2003) and radio emission (e.g., Karim et al., 2011). The SF tracers probe the stellar populations at varying stellar mass ranges and different sensitivities. However, no specific SF tracer is perfect and there are some discrepancies observed when comparing different SF tracers (e.g., Hopkins et al., 2001; Lee et al., 2009; Figueira et al., 2022). We cover each SF tracer in the following sections, discussing the way in which they are used to estimate SF as well as their strong and weak points.

### Ultraviolet emission

Ultraviolet (UV) emission is a direct tracer of radiation from young stars living in galaxies. The bulk of the observed UV radiation in galaxies arises from massive, short-lived young stars emitting at short wavelengths (150–280 nm). The wavelength range is longward of the Ly $\alpha$  emission but also optimised to block contamination from old star populations. As a result, UV emission is often regarded as the “instantaneous”

SF tracer. Synthesis population models (e.g., [Conroy et al., 2009](#)) are used to convert UV flux density integrated over a wavelength range to SFR. With the assumption that SFR remains constant over longer timescales than those of the dominant UV emitting population, [Kennicutt \(1998, K98 henceforth\)](#), derived an approximation for integrated SFR from UV emission using a [Salpeter \(1955\)](#) IMF within mass limits  $0.1 - 100 M_{\odot}$  as

$$\text{SFR}_{\text{UV}} (M_{\odot} \text{yr}^{-1}) = 1.4 \times 10^{-28} L_v (\text{ergs s}^{-1} \text{Hz}^{-1}), \quad (1.3)$$

where  $L_v$  is the intrinsic UV luminosity. The composite UV spectrum is approximately flat in  $L_v$  at the  $150 - 280$  nm wavelength range in the Salpeter IMF. The advantage of estimating SFR with UV emission is that it directly traces radiation from young stars and it can be probed over a wide range of redshifts. The major disadvantage arising from UV radiation as an SF tracer is that it is highly sensitive to dust attenuation. Integrated UV magnitudes are typically corrected for dust attenuation using  $\approx 0 - 3$  magnitudes but corrections can be higher depending on how dusty the galaxy is.

### Emission line emitters

UV radiation can also be traced through nebular line emission from excited and ionised gas by young stars in HII regions. Hydrogen recombination lines such as  $H\alpha$  and  $Ly\alpha$  are commonly used to directly estimate SFR because they scale with photo-ionization rates resulting from high UV radiation. Emission lines from heavier elements like [OII], [OII 3727 Å] are also used to estimate SFR but require a careful calibration due to their convoluted relation with ISM conditions such as metallicity and excitation ([Madau and Dickinson, 2014](#)). The heavier elements lines such as [OII] are useful in estimating SFR of distant galaxies where the  $H\alpha$  and  $Ly\alpha$  are not sensitive. Emission line tracers also face the challenge of dust attenuation and thus require corrections to obtain reliable SFR estimates.  $H\alpha$  is deemed the most accurate estimator of SFR among the easily observable nebular line tracers. K98 derived a relation to converting the ionising flux to SFR for  $H\alpha$  emitters as

$$\text{SFR}_{H\alpha} (M_{\odot} \text{yr}^{-1}) = 7.9 \times 10^{-42} L_{H\alpha} (\text{ergs s}^{-1}), \quad (1.4)$$

where  $L_{H\alpha}$  is the H $\alpha$  luminosity. The main advantage of H $\alpha$  line emission is due to its high sensitivity and its ability to directly trace high SF activity in nearby galaxies using high-resolution maps.

### Infrared emission

Infrared (IR) emission is a byproduct of the bolometric emission from young stars in galaxies. When the UV emission from newly formed stars interacts with the dust in galaxies, it heats the dust which then re-emits at infrared wavelengths ( $8 - 1000 \mu\text{m}$ ), paving a way to trace SFR from obscured UV emission. The total IR (TIR) emission from the dust is a direct measure of the UV radiation that gets attenuated by the dust, providing a fractional estimate of the SFR ([Kennicutt and Evans, 2012](#)). A combination of UV and IR SFR measurements are often used to represent the total SFR estimate from young stellar populations (see e.g., [Rodríguez-Muñoz et al., 2019](#)).

The TIR luminosity is converted to SFR using synthesis models. K98 derived an IR luminosity to SFR relation for starbursts of age limit  $10 - 100$  Myr using the Salpeter IMF

$$\text{SFR}_{\text{IR}} (M_{\odot} \text{yr}^{-1}) = 4.5 \times 10^{-44} L_{\text{TIR}} (\text{ergs s}^{-1}), \quad (1.5)$$

where  $L_{\text{TIR}}$  is the IR luminosity integrated over the full IR spectrum ( $8 - 1000 \mu\text{m}$ ).

There are a number of caveats that come with IR-based SFR estimates. Firstly, dust heating can be a result of more than one contribution alongside the UV radiation from young stars. Emissions from old stars can also heat up the dust. Dust-gas AGN toruses also emit at IR wavelengths and can also add to the radiation. Secondly, IR observations are challenging and often rely on the use of space telescopes to achieve this since most of the IR gets blocked by Earth's atmosphere. Lastly, to get accurate estimates of IR luminosities, the process relies on spectral energy distribution (SED) fitting (K98; [Madau and Dickinson, 2014](#)). IR emission at a single rest-frame

detection is not a true SFR indicator since the total IR SED of a galaxy traces a combination of dust components at varying temperatures (heated dust surrounding young stars, cooler dust in the interstellar medium (ISM), and perhaps also the heated AGN torus dust). Despite the aforementioned challenges associated with IR emission, it provides a good estimator of SFR in dusty circum-nuclear starbursts.

### X-ray emission

The integrated rest-frame X-ray emission can be used to trace SFR in galaxies thanks to its tight correlation with far-infrared and radio fluxes even though there is no first principle calibration between X-ray luminosities and SFR. Non-AGN powered X-ray fluxes arise from X-ray binaries, massive stars, supernovae and supernova remnants, all of which are associated with young stellar populations with ongoing/recent SF. Using the IR calibration, [Ranalli et al. \(2003\)](#) formulated a relation to converting X-ray luminosities to SFR from the K98 relation and the Salpeter IMF as

$$\text{SFR}_{\text{X-ray}} (\text{M}_\odot \text{ yr}^{-1}) = \begin{cases} 2.2 \times 10^{-40} L_{0.5-2 \text{ keV}} (\text{ergs s}^{-1}) \\ 2.0 \times 10^{-40} L_{2-10 \text{ keV}} (\text{ergs s}^{-1}) \end{cases}, \quad (1.6)$$

where  $L$  is the X-ray luminosity at the rest-frame band. The main limitation of X-ray-derived SFR is that X-ray emission is dominated by AGN activity, which limits X-ray as an extensive tracer of SFR due to contamination. Furthermore, the correlation between X-ray luminosity and SFR could depend on stellar population age and additional parameters in the galaxy, leading to significant disparities between X-ray-derived SFR calibrations ([Kennicutt and Evans, 2012](#)).

### Radio continuum emission

Radio continuum emission from star-forming galaxies with no AGN activity is made up of thermal free-free (bremsstrahlung) radiation and non-thermal synchrotron radiation. The thermal free-free emission is a direct tracer of SFR from ionised hydrogen in HII regions caused by massive stars in young stellar populations. The non-thermal

component originates from cosmic ray electrons spiralling in the magnetic field of the galaxy (Condon, 1992). At frequencies,  $\leq 5$  GHz, thermal free-free radiation contributes weakly to the radio continuum flux and non-thermal radiation accounts for 90% of the signal (Condon, 1992). The physics that describes SF from radio emission is complicated and still poorly understood. Radio emission as an SF tracer is bootstrapped from the IR calibrations due to the tight correlation between radio emission and far-infrared (FIR) emission at 1.4 GHz (e.g., Helou et al., 1985; Condon et al., 1991; Yun et al., 2001).

Unlike the other SFR tracers, non-thermal radio emission is not an ‘instantaneous’ tracer as it mostly arises from supernovae activity. It is often regarded as the ‘delayed’ SF indicator. Being free from dust interactions, radio emission is regarded to be an advantageous SFR tracer for galaxies compared to other SFR tracers. The main challenge of using radio observations to study SFR is AGN contamination. Previous studies (e.g., Sadler et al., 2002; Condon et al., 2002; Mauch and Sadler, 2007) have shown that radio-AGN may contribute up to 50% of the radio luminosities in the local Universe at luminosities just below  $L_{1.4\text{GHz}} \approx 10^{23}$  W Hz $^{-1}$ , and that at luminosities over  $10^{23}$  W Hz $^{-1}$  AGN dominate the population over star-forming galaxies. Separating star-forming galaxies from AGN-hosting galaxies remains a significant challenge and relies on the use of various non-extensive methods to identify them.

Bell (2003) deduced the calibration for estimating SFR from radio continuum emission using the radio–FIR correlation and the Salpeter IMF as

$$\text{SFR} (\text{M}_\odot \text{ yr}^{-1}) = \begin{cases} 5.52 \times 10^{-22} L, & L > L_c \\ \frac{5.52 \times 10^{-22} L}{0.1 + 0.9(L/L_c)^{0.3}}, & L \leq L_c, \end{cases} \quad (1.7)$$

where  $L = L_{1.4\text{GHz}}$  is the radio luminosity in W Hz $^{-1}$  derived from the total flux density.  $L_c = 6.4 \times 10^{21}$  W Hz $^{-1}$  is taken to be the typical radio luminosity of a  $L_*$ -like galaxy (where  $L_*$  is the characteristic luminosity from the galaxy luminosity function). Bell (2003) argues that galaxies with low luminosities could have their non-thermal emission significantly suppressed and therefore need to be separated from the

population with higher luminosities.

## Spectral energy distribution

In contrast to using monochromatic SFR tracers mentioned in the previous sections, SFR can also be estimated from spectral energy distribution (SED) fitting. Galaxies radiate energy over the full electromagnetic spectrum mostly dominated by contributions from their stellar population, dust and AGN (Walcher et al., 2011; Conroy, 2013). Each galaxy component dominates and radiates at different wavelengths and can be identified in the galaxy spectrum. The distribution of energy emitted from a galaxy as a function of wavelength is called the SED. SEDs over a large range of wavelengths reveal vital properties of galaxies such as the SFR, stellar mass, IMF, stellar and gas metallicities.

Significant efforts have been made in the past decade to acquire information from galaxy SEDs by modelling the stellar, dust and AGN components of galaxies (see reviews by Walcher et al., 2011; Conroy, 2013). A number of SED-fitting codes designed to extract galaxy properties from broadband galaxy SEDs have been developed, including Code Investigating GALaxy Emission (CIGALE; Boquien et al., 2019), BayEsian Analysis of GaLaxy sEds (BEAGLE; Chevallard and Charlot, 2016), Python code for Stellar Population Inference from Spectra and SEDs (Prospector; Leja et al., 2017), Multi-wavelength Analysis of Galaxy Physical Properties (MAGPHYS; da Cunha et al., 2008).

Estimating SFR from SED fitting can be very challenging due to a number of reasons: (1) the evolution of the IMF, (2) the age-dust-metallicity degeneracy makes it difficult to reliably measure ages and hence SFR, unless high quality data are available (Conroy, 2013), (3) the choice of model priors on the dust model library imposes often severe biases on the resulting ages and SFR (Trayford et al., 2020).

Several studies have been done to directly compare SED-derived SFR to other SFR tracers and they show overall agreement (e.g., Salim et al., 2007).

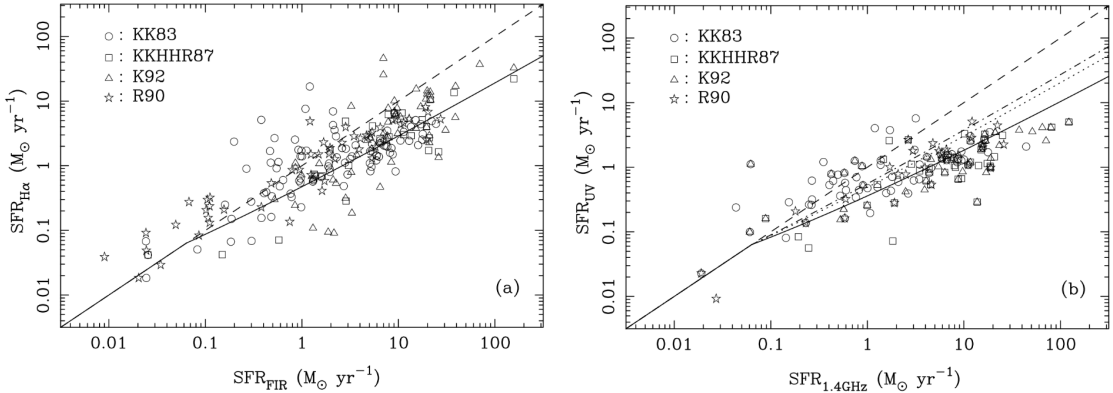


Figure 1.5:  $\text{SFR}_{\text{H}\alpha}$  vs  $\text{SFR}_{\text{FIR}}$  on the left and  $\text{SFR}_{\text{UV}}$  vs  $\text{SFR}_{1.4\text{GHz}}$  on the right from Hopkins et al. (2001). The  $\text{SFR}_{\text{UV}}$  and  $\text{SFR}_{\text{H}\alpha}$  values are both uncorrected for dust extinction. The solid black line shows the SFR-dependent attenuation. The dashed line shows the one-to-one relationship while the dotted lines and the dot-dashed lines on the right plot show the attenuation levels at  $\lambda = 0.365 \mu\text{m}$  and  $0.28 \mu\text{m}$  respectively. The marker labels indicate the data used to make the plots, and their corresponding references can be found in Hopkins et al. (2001).

### 1.2.3 Comparing different SFR tracers

As already outlined by the discussions of different SFR tracers above, no individual tracer is perfect and is able to probe SF activity at all epochs. Nonetheless, using various tracers to probe SF activity at different stages of evolution should put us closer to understanding more about the SF history of the Universe.

When estimates from the aforementioned SFR tracers are compared, a large scatter is observed between the measurements (see e.g., Hopkins et al., 2001; Hopkins et al., 2003; Figueira et al., 2022). Systematic effects and inconsistencies in observational methods are some of the challenges that amplify the observed scatter. Furthermore, the challenge of calibrating for dust-extinction for optical observations (UV and  $\text{H}\alpha$ ) adds to the discrepancy between them and the non-dust-attenuated tracers (Radio and IR). Figure 1.5 shows the scatter that arises from comparing radio and IR SFR estimates to those measured from  $\text{H}\alpha$  and UV emission. A visible discrepancy can be seen between radio and IR estimates compared to dust-extinction uncorrected  $\text{H}\alpha$  and UV SFR estimates.

Various efforts have been made to get robust dust-extinction corrections for UV observations (e.g., Meurer et al., 1999; Bouwens et al., 2009) and for  $\text{H}\alpha$  observations

(e.g., Domínguez et al., 2013; Momcheva et al., 2013). Recent studies have shown that using combined measurements of optical (UV/H $\alpha$ ) and IR to estimate SFR provides more reliable estimates than individual tracers. Combined measurements have been used to estimate SFR using H $\alpha$  and IR fluxes (e.g., Kennicutt et al., 2009) and using UV and IR fluxes (e.g., Kennicutt and Evans, 2012; Rodríguez-Muñoz et al., 2019).

### 1.3 Galaxy clusters

Most galaxies are often found in high-density environments in the form of galaxy groups and clusters. It is estimated that well over 50% of galaxies live in group and cluster environments (Eke et al., 2004). Galaxy clusters are the largest gravitationally bound objects in the Universe and about 10–20% of galaxies are estimated to reside in cluster environments. The  $\Lambda$ CDM model proposes that structure forms hierarchically (see Section 1.2), and this implies that the most massive objects in the Universe, galaxy clusters, are formed last and therefore the most dynamically immature (e.g., Boylan-Kolchin et al., 2009; Gao et al., 2012).

Since their discovery eight decades ago (Zwicky, 1938), they have been a major topic of interest due to their unique nature. Clusters span a few megaparsecs (Mpc) in size, contain hundreds to thousands of galaxies and have total masses ranging  $10^{14\text{--}15} M_\odot$ . They originate from merging galaxy groups as well as galaxies accreting through gravity, clumping together to form clusters (Mann and Ebeling, 2012). Cluster mass distribution is  $\approx 80\%$  dark matter,  $\approx 15\%$  intra-cluster medium (ICM, a hot dense plasma), and  $\approx 5\%$  is the ordinary matter found in galaxies. The galaxy clusters ICM is made up of hot ( $10^{7\text{--}8}$  K) gas emitting bremsstrahlung X-ray radiation at luminosities  $L_X \approx 10^{43\text{--}45}$  ergs/s. The hot gas X-ray emission reveals the deep gravitational potential wells of clusters (Rosati et al., 2002). Figure 1.6 shows the composite image (optical and X-ray) of the Abell 2744 cluster, suggested to have formed from a merger of 4 sub-clusters (Owers et al., 2011).

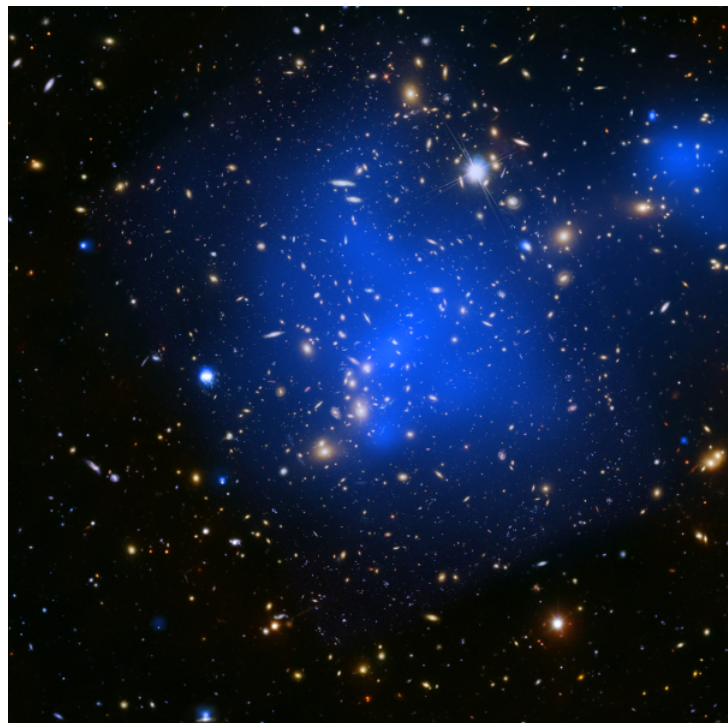


Figure 1.6: The composite image of the Abell 2744 cluster showing the *Hubble* space telescope optical image of the galaxies and the ICM observed from the hot diffuse X-ray emission (blue hue) by the *Chandra* X-ray telescope. Image credit: NASA/STScI: [https://www.nasa.gov/mission\\_pages/chandra/images/abell-2744.html](https://www.nasa.gov/mission_pages/chandra/images/abell-2744.html)

### 1.3.1 Cluster observational methods

Galaxy clusters are massive unique objects through which astrophysical processes involving dark matter, the ICM and galaxies can be probed to get critical insight into the history (and the future) of the Universe. They enable us to test hierarchical cosmological models (e.g., [Planck Collaboration et al., 2020](#); [Abbott et al., 2022](#)), study the physics behind cosmic rays ([Bell, 1978](#); [Brunetti and Jones, 2014](#)), and investigate the evolution of galaxies and their star formation properties in dense environments (e.g., [Stroe et al., 2014](#); [Haines et al., 2015](#)).

The first few decades of cluster exploration were done at optical wavelengths. As technology and analytical tools improved, new methods to observe and identify galaxy clusters were developed. In the sections below, we discuss ways of identifying clusters through various techniques at different wavelengths.

#### Optical Surveys

Observations and studies of galaxy clusters were pioneered by George Abell with the study of over 2000 rich galaxy clusters in the northern hemisphere using data from the Palomar Observatory Sky Survey ([Abell, 1958](#)). Abell extended his study of galaxy clusters to the southern hemisphere using data from the ESO-SERC Southern Sky Survey, releasing a catalogue of 4073 clusters which combined into an all-sky catalogue ([Abell et al., 1989](#)). Clusters from the Abell catalogue were identified by visually inspecting photographic plates from the telescopes and they adhered to set criteria that were established to classify objects as clusters:

- **Richness:** The clusters should have a minimum number of 50 member galaxies with apparent magnitudes in the range  $m_3 < m < m_3 + 2$  ( $m_3$  being the apparent magnitude of the third brightest cluster member).
- **Compactness:** The 50 or more member galaxies must lie within  $1.5 h^{-1}\text{Mpc}$  (Abell radius), where  $h$  is the dimensionless Hubble constant.
- **Distance:** Abell's cluster classification criteria were limited to clusters within

$0.02 < z < 0.2$ . The lower limit was due to clusters with  $z < 0.02$  spanning more than one photographic plate used by the telescope and the upper limit was dictated by the magnitude detection limit.

Although Abell and his team maintained consistency and strict criteria to identify clusters, this method was prone to errors and bias as it relied on visual inspection. As optical telescopes became more sensitive and sophisticated with computing power enabling high survey speeds over wider fields of view, faster and more objective methods to identify clusters using algorithms were developed. Building on the evidence that clusters are dominated by early-type galaxies, [Gladders and Yee \(2000\)](#) developed an algorithm that identifies clusters using the red-sequence (from a colour-magnitude relation that includes most red galaxies, which are generally elliptical galaxies) as a tracer of over-dense regions. [Koester et al. \(2007b\)](#) developed a technique that also uses the red-sequence to identify clusters and also tracks the brightest cluster galaxies (BCGs) which are often located at the centre of massive clusters. They applied their algorithm to the Sloan Digital Sky Survey (SDSS) data, identifying over 13,000 clusters ([Koester et al., 2007a](#)). The red-sequence approach has since become a standard cluster identifier employed by large optical surveys, with improved algorithms being developed and used to identify clusters in recent years (e.g., [Gladders and Yee, 2005](#); [Hao et al., 2010](#); [Murphy et al., 2012](#); [Rykoff et al., 2014](#); [Rykoff et al., 2016](#)).

The limitation of detecting clusters with optical surveys is that they are only sensitive to galaxies, which are  $\approx 5\%$  of the total cluster mass. Optical surveys also face the challenge of projection effects, making them vulnerable to contamination by sources along the line of sight. This challenge can be particularly hard to mitigate at higher redshifts. Although optical surveys are powerful instruments at identifying clusters and characterising their dynamical state (e.g., [Einasto et al., 2012](#); [Wen and Han, 2013](#)), the data they provide is still not enough to paint a full picture that shows the extensive properties of a cluster. This motivated the need for multi-wavelength observations to get a broad understanding of the physical properties of galaxy clusters.

## X-ray Surveys

Galaxy clusters can also be detected at X-ray wavelengths by probing the thermal bremsstrahlung radiation and the line emission from the ICM. The first catalogue of X-ray clusters was released five decades ago from observations by the *Uhuru* space telescope (Giacconi et al., 1972). Shortly after that, it was shown that the X-ray emission from the hot gas provides a powerful tool to trace the gravitational potential wells of galaxy clusters (Cavaliere and Fusco-Femiano, 1976) and their total gravitating masses (Fabricant et al., 1980).

A number of instruments have been commissioned to observe clusters at X-ray wavelengths and these include the *ROSAT* telescope (Vikhlinin et al., 1998), *Chandra* X-ray Observatory (Weisskopf et al., 2000) and *XMM-Newton* (Jansen et al., 2001). The on-going all-sky survey, *eROSITA*, is expected to detect  $\approx 100,000$  galaxy clusters out to  $z > 1$  (Brunner et al., 2022; Liu et al., 2022).

The advantage of detecting clusters with thermal bremsstrahlung X-ray radiation is that clusters are the only extended extragalactic X-ray sources. This makes cluster-finding with X-ray emission less prone to projection effects from the objects in the line of sight. Also, the X-ray observables (luminosity, ICM temperature) scale with the mass of the cluster, making X-ray observations a useful tool to estimate cluster masses and also probe the morphology/dynamical state of the cluster (e.g., Lovisari et al., 2017; Yuan and Han, 2020). X-ray luminosity is also a good probe of the depth of the cluster gravitational potential (Rosati et al., 2002). The challenge facing X-ray cluster studies is that flux-limited observations lead to a bias in the selection function due to differences in the detection efficiency of X-ray instruments for centrally-peaked and flat objects (Eckert et al., 2011). Also, low-resolution X-ray surveys like *ROSAT* ( $30''$ ), can have a challenge of cluster-cluster projection effects as demonstrated by Ramos-Ceja et al. (2019). However, this bias can be mitigated by conducting follow-up studies with high-resolution instruments like *Chandra* ( $0.5''$ ) and *XMM-Newton* ( $5'' - 14''$ ).

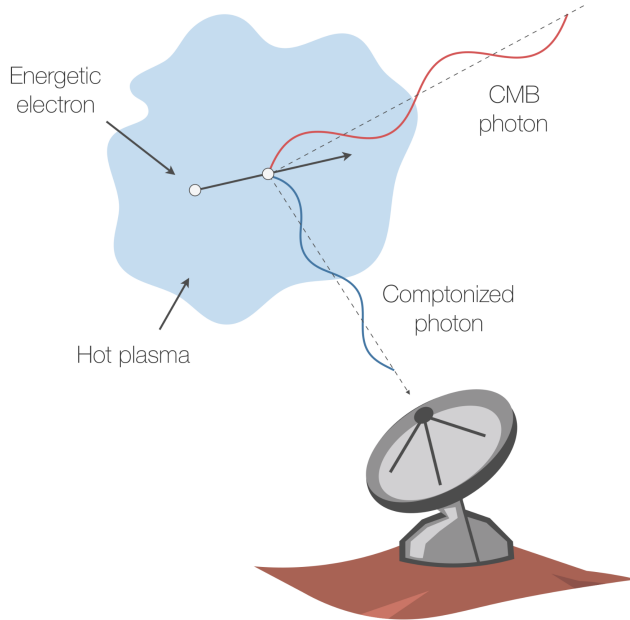


Figure 1.7: A schematic diagram of the SZ-effect. Image credit: [Mroczkowski et al. \(2019\)](#).

### Sunyaev-Zel'dovich Surveys

When the electrons in the ICM interact with the background photons from the CMB passing through the cluster, an inverse Compton scattering of the CMB photons occurs which is detectable at millimetre wavelengths ([Mroczkowski et al., 2019](#), demonstrated in Figure 1.7). This phenomenon is known as the thermal Sunyaev-Zel'dovich (SZ) effect ([Sunyaev and Zeldovich, 1980](#)) and was first observed in clusters four decades ago ([Birkinshaw, 1990](#)). The signal from SZ-effect is redshift-independent, and this makes it a powerful tool for detecting mass-limited clusters out to high redshifts. The lowest SZ-detectable cluster mass depends on the survey noise level limit ([Birkinshaw, 1999; Mroczkowski et al., 2019](#)).

Just like X-ray, the SZ cluster physical properties scale with mass and hence provide estimates for cluster masses and dynamical states. On the other hand, SZ surveys do not face the challenge of flux limitations and therefore provide accurate estimates for the selection function ([Melin et al., 2005](#)). Observations from *Planck* ([Tauber, 2001](#)), the Atacama Cosmology Telescope (ACT; [Fowler, 2004](#)), and the South Pole Telescope (SPT; [Ruhl et al., 2004](#)) have collectively contributed nearly

7000 SZ-detected clusters out to  $z \approx 2$  over the past decade and a half. Most of the SZ-detected clusters so far were observed by ACT, contributing  $> 4000$  clusters in the latest data release (ACT DR5; [Hilton et al., 2021](#)).

Although both the X-ray and SZ-effect arise from the ICM, these observables probe its distribution around the cluster differently. The X-ray emission scales with the square of the ICM density while the SZ scales linearly with the ICM density ([Lovisari and Maughan, 2022](#)). This implies that X-ray surveys are biased towards detecting relaxed and centrally peaked clusters as compared to SZ detections, and this has been shown to be the case by various studies (e.g., [Rossetti et al., 2016](#); [Andrade-Santos et al., 2017](#); [Lovisari et al., 2017](#)). However, even with the noted differences between these observables, they both depend on the total ICM amount in a cluster and therefore share a bias in detecting clusters with high gas content (e.g., [Andreon et al., 2016](#)), leading to a mass-dependence in their selection. Combining efforts from all the cluster observables (optical, X-ray and SZ-effect) could help mitigate some of the biases faced by each observable. Using optical surveys to identify clusters, then doing a follow-up with X-ray/SZ surveys to create an optically-selected sample. A comparison between this sample and the X-ray and SZ-selected samples could possibly shed some light on the information missed by biased samples. However, as mentioned in Section 1.3.1, optical surveys face a challenge of projection effects and have also been shown to falsely identify cluster centres  $> 25\%$  of the time (e.g., [Zhang et al., 2019](#)).

### 1.3.2 Cluster morphology and dynamical states

Galaxy clusters can be grouped into various classes based on their physical properties (masses/galaxy population, cluster core dynamical state). Clusters with high galaxy number densities are regarded as rich clusters (hosting thousands of galaxies, e.g., Coma cluster) while clusters with low number densities are regarded as poor clusters or groups (hosting less than a thousand galaxies, e.g., the Local Group).

Clusters can also be classified by the dynamical state of their cores which is re-

vealed by the state of the ICM as seen at X-ray wavelengths. Depending on the symmetry of the cluster ICM, a cluster can be identified as either relaxed or disturbed from the evidence of substructure in the ICM (e.g., [Cassano et al., 2010](#); [Lovicari et al., 2017](#)). The morphology of the hot dense plasma in the ICM changes during a merger and can be seen in the X-ray surface brightness distribution of the cluster.

Clusters are also classified as either cool-core or non-cool-core based on the specific entropy floor of the cluster centre ([Hudson et al., 2010](#); [Giacintucci et al., 2017](#)). Cool-core clusters are characterised as having low central entropy and a systematic central temperature drop while non-cool-core clusters have high central entropies.

The size of a galaxy cluster is often estimated within the radius ( $R_{200}$ ) which the average density is 200 times the critical density ( $\rho_{\text{crit}} \approx 10^{-29} \text{ g cm}^{-3}$ ) of the universe at the cluster redshift. This follows the spherical collapse of an over-dense region using an analytical model that parametrises the motion of spherical shells and then matches it to the results of linear structure formations ([Peebles, 1980](#)). This leads to a solution where an overdensity  $\Delta = 18\pi^2 \approx 177$  times the critical density will collapse. The value  $\Delta = 200$  is commonly used, which is rounded up from 177 as the virial radius estimation relies on approximate assumptions.

Massive clusters grow hierarchically through merging with other clusters and sub-clusters or groups of galaxies (e.g., [Sarazin, 2002](#)). When clusters merge, they release an enormous amount of kinetic energy ( $\approx 10^{63-64} \text{ ergs}$ ) into the ICM over a period of a few Gyrs (see e.g., [Brunetti and Jones, 2014](#)). This makes cluster mergers the most energetic events in the Universe since the Big Bang. The bulk of the merger-induced energy is transferred to thermal energy by heating up the ICM ([Hoang et al., 2018](#)). Through large-scale shocks and turbulence, a small fraction of the released energy is converted into non-thermal energy of relativistic particles that permeate the ICM, emitting synchrotron diffuse emission observable at radio wavelengths (see e.g., [Feretti et al., 2012](#); [Brunetti and Jones, 2014](#)). Cluster observations at X-ray and radio wavelengths show that the ICM has both thermal and non-thermal properties ([Cassano et al., 2010](#)). The X-ray observations probe the thermal properties of the

cluster while radio observations reveal the Mpc-scale non-thermal relativistic diffuse emission in the form of radio haloes and radio relics.

### 1.3.3 Non-thermal diffuse emission in galaxy clusters ICM

The first discovery of non-thermal diffuse radio emission in clusters was observed in the Coma cluster six decades ago by Large et al. (1959) and was later confirmed by various observations (e.g., Willson, 1970; Venturi et al., 1990; Giovannini et al., 1993). This discovery confirmed that the ICM produced ultra-relativistic electrons and magnetic fields which result in Mpc-scale synchrotron emission in clusters (Ferrari et al., 2008; Brunetti and Jones, 2014; van Weeren et al., 2019). The diffuse radio emission can be classified into groups depending on size and morphology with the main groups being radio haloes, radio mini-haloes, radio relics and revived fossil plasma. The processes involved in the formation of the different types of diffuse radio emission in clusters are still poorly constrained and a number of theories have been formulated in an attempt to explain the origins of the diffuse emission. The descriptions and distinctions of the different types of diffuse emission in clusters are summarised in the following sections.

#### Radio haloes

Radio haloes (RHs) are diffuse radio emission of spherical morphology found in cluster centres. They have typical sizes of  $\approx 1 - 2$  Mpc with physical structures resembling the cluster X-ray morphology (see examples in Figures 1.8 and 1.10). RHs are often found in dynamically disturbed clusters and have been strongly linked with the re-acceleration of relativistic particles by cluster mergers (e.g., Brunetti et al., 2009; Cassano et al., 2013; Lindner et al., 2014; Kale et al., 2015). RHs are generally unpolarised ( $< 10\%$ ) (Feretti, 2003) except in some rare instances observed in a few clusters thus far: Abell 2255, Govoni et al. (2005); MACS J0717.5+3745, Bonafede et al. (2009); Abell 523, Girardi et al. (2016). They have a low surface brightness of  $\approx 1 \mu\text{J arcsec}^{-2}$  at 1.4 GHz (Feretti et al., 2012). Halos are mostly observed in

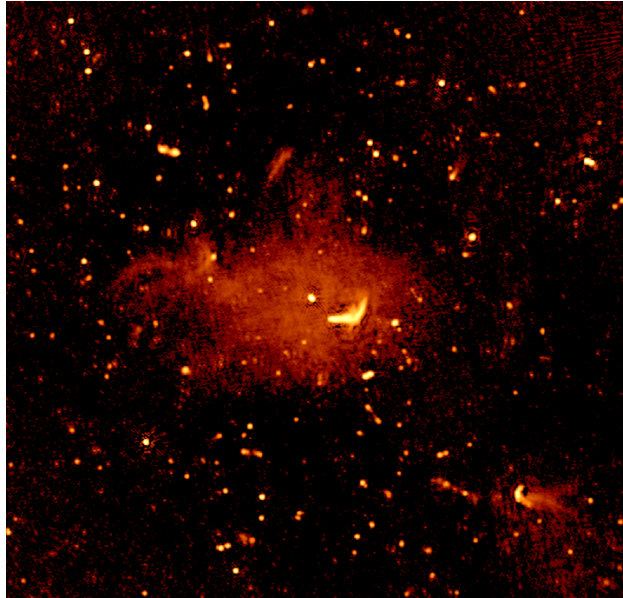


Figure 1.8: *Left:* The image of a radio halo in the Coma cluster observed by LOFAR at 20'' resolution. Image credit: [van Weeren et al. \(2019\)](#).

luminous X-ray clusters ( $L_X > 5 \times 10^{45} \text{ erg s}^{-1}$ ) and form a radio power – X-ray luminosity correlation ( $P - L_X$ ) ([Giovannini et al., 1999](#); [Feretti and Giovannini, 2008](#); [Cassano et al., 2011](#)) shown in Figure 1.11. Halos have steep radio spectral indices ( $\alpha \leq -1$ ) estimated from multi-frequency radio observations using the scaling of radio flux density with frequency ( $S_\nu \propto \nu^\alpha$ ).

The leading model for the formation of RHs is the re-acceleration model which proposes that pre-existing electrons are re-accelerated by magnetohydrodynamical turbulent energy from cluster mergers ([Jaffe, 1977](#); [Petrosian, 2001](#); [Donnert and Brunetti, 2014](#)). The merger-induced turbulent energy is insufficient to accelerate the thermal electrons in the ICM, suggesting that pre-existing relativistic electrons get re-accelerated out to Mpc scales, forming RHs. Although widely accepted, the re-acceleration model has outstanding questions that are yet to be addressed such as, what is the source of the pre-existing electrons? What are the re-acceleration mechanisms involved and what role does the magnetic field play? Another outstanding challenge is providing constraints for cases where RHs are observed in clusters with no evidence of merger activity (e.g., [Kale et al., 2019](#)).

Another model that has been proposed to describe the processes behind the for-

mation of RHs is the hadronic model which suggests that relativistic electrons are secondary products from the interactions between cosmic ray protons and thermal protons in the ICM (Dennison, 1980; Blasi and Colafrancesco, 1999; Enßlin et al., 2011). This formation process leads to the cosmic ray electrons permeating the ICM, which is backed by the observed scaling relation between radio power and X-ray luminosity. The proton-proton collisions also lead to  $\gamma$ -rays being emitted and one of the difficulties faced by this model is the reported non-detection of the  $\gamma$ -rays by the *Fermi*  $\gamma$ -ray Space Telescope (e.g., Ackermann et al., 2010; Zandanel and Ando, 2014; Brunetti et al., 2017), leading only to upper-limits on the  $\gamma$ -ray fluxes of clusters. Another challenge facing the hadronic model is the missing constraints for the observed large amounts of energy in some RHs with ultra-steep spectra (e.g., Brunetti, 2004; Brunetti et al., 2008).

## Radio mini-haloes

Radio mini-haloes (RMHs) are a faint diffuse radio emission that resides in the central region of dynamically relaxed, cool-core clusters around the brightest cluster galaxies (BCGs; see e.g., Gitti et al., 2015; Giacintucci et al., 2017). RMHs have typical sizes of  $\approx 100 - 500$  kpc. They have similar properties with RHs in terms of morphology and polarisation but differ in sizes and the dynamical state of their host clusters. Only about thirty mini-haloes have been detected thus far through X-ray and radio observations (Giacintucci et al., 2019), which both need to have coinciding centres for a source to be classified as RMH. The seed electrons forming the RMH are thought to originate from activity around a supermassive black hole in the centre of the BCG (Richard-Laferrière et al., 2020). This leads to the injection of relativistic particles into the ICM around the BCG, leading to the formation of a RMH. Figure 1.9 shows the RMH around the NGC 1275 galaxy in the Perseus cluster, which was one of the first prototypes used for observing RMHs.

The formation mechanism of RMHs can be derived using the hadronic model where relativistic electrons are assumed to be a by-product of the collision of the cosmic ray protons and the thermal protons from the supermassive black hole jets

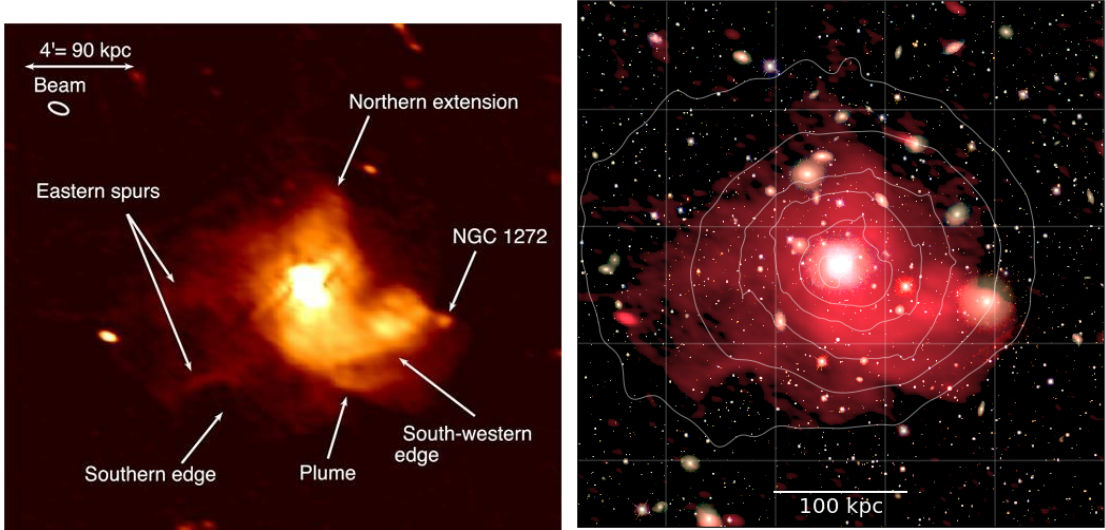


Figure 1.9: The VLA observation of the RMH around the NGC 1275 galaxy in the Perseus cluster. Image credit: [Gendron-Marsolais et al. \(2017\)](#). Right: The radio-optical composite overlay of the mini-halo in the Perseus cluster. The background image is from SDSS and the pink hue is radio data from VLA. White contours are from the X-ray surface brightness from the *XMM-Newton* observations. Image credit: [van Weeren et al. \(2019\)](#).

([Zandanel and Ando, 2014](#); [Ignesti et al., 2020](#)). The injection of the cosmic ray protons leads to turbulence that heats the ICM, thus reducing gas cooling. This mechanism is also used to explain the *cooling flow problem* (e.g., [McDonald et al., 2019](#)). According to the re-acceleration model, the seed electrons are deposited in the ICM by AGN activity or type Ia supernovae and then re-accelerated by turbulent activity to form RMHs ([Fujita et al., 2007](#); [Richard-Laferrière et al., 2020](#)). The re-acceleration formation model is still unclear since RMHs are known to reside in relaxed cool-core clusters with little or no merger activity. However, recent results from a study of turbulent motion in the Perseus cluster suggest that the cool-core cluster had turbulence that could be efficient for electrons re-acceleration ([Hitomi Collaboration et al., 2016](#)).

## Radio relics

Radio relics (RRs) are arc-shaped/elongated Mpc-scale diffuse radio emission sources residing in the periphery of galaxy clusters. They are thought to result from shock

fronts induced in the ICM during cluster mergers (e.g., [Ogreal et al., 2013](#); [Weeren et al., 2016](#); [van Weeren et al., 2019](#)). Results from cosmological simulations reveal that when massive clusters merge, they produce shock waves that propagate through the ICM from the cluster centre out to the cluster periphery (e.g., [Brüggen et al., 2011](#); [Vazza et al., 2012](#); [Skillman et al., 2013](#)). In several cases, shock waves have been observed in merger clusters with Mach numbers of  $M_{\text{shock}} < 4$  (e.g., [Brunetti and Jones, 2014](#)). According to the re-acceleration formation model, these shock waves produce radio relics via diffusive shock acceleration (DSA, see e.g., [Kang et al., 2012](#); [Vazza and Brüggen, 2014](#)). In the DSA mechanism, CR protons and electrons are accelerated from the thermal pool up to relativistic energies at the cluster merger shocks (see e.g., [Drury, 1983](#); [Yokoyama and Ohira, 2020](#)). The energy of the thermal electrons is boosted when they cross the cluster shock region while flowing up or downstream. The spatial co-location of shocks in the ICM and radio relics has been determined in some clusters, supporting the DSA theory (e.g., Abell 3667; [Finoguenov et al. \(2010\)](#), RX J0603.3+4212; [Ogreal et al. \(2013\)](#), 1E 0657-56; [Shimwell et al. \(2014\)](#), Abell 115 [Botteon et al. \(2016\)](#)).

Radio relics have typical sizes  $\geq 1 \text{ Mpc}$  and steep spectral indices ( $\alpha \leq -1$ ). Like haloes, they have a low surface brightness. Unlike haloes, relics are highly polarised sources, generally,  $\approx 30\%$  ([Brunetti and Jones, 2014](#)) and in some cases as high as  $\approx 50 - 60\%$  of polarisation has been observed ([Vazza et al., 2016](#)). The polarisation levels, spectrum steepness, and the degree of the surface brightness can vary considerably over the morphology of one relic.

Some clusters host double relics in the form of two arcs opposite each other in the cluster peripheries (e.g., [van Weeren et al., 2011a](#); [Kale et al., 2012](#); [de Gasperin et al., 2014](#); [Lindner et al., 2014](#)). In some cases, cluster systems hosting both a halo and relics have also been observed (e.g., [van Weeren et al., 2011c](#); [Bonafede et al., 2012](#); [de Gasperin et al., 2015](#)). Figure 1.10 shows examples of various clusters with different types of relics configurations.

Numerical simulations reveal that a merger between clusters with approximately equal masses can lead to the formation of two symmetrical relics when the merger

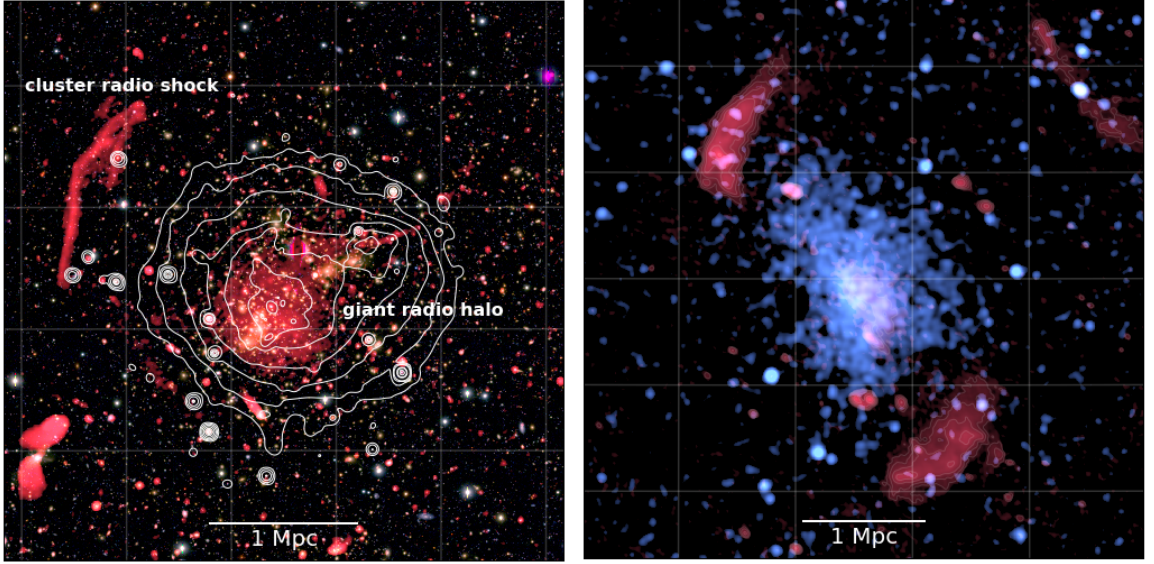


Figure 1.10: *Left:* The VLA image of the merging Abell 2744 cluster showing the radio halo at the centre and the radio relic (radio shock). The white contours are from the *Chandra* X-ray observations. Image credit: [van Weeren et al. \(2019\)](#). *Right:* A composite image of the PSZ1 G108.18–11.53 cluster showing the double radio relics (red) observed by GMRT and the cluster observation in X-ray by *Chandra*. Image credit: [van Weeren et al. \(2019\)](#).

axis is approximately perpendicular to the line of sight (e.g., [van Weeren et al., 2011a](#); [Brüggen et al., 2011](#)). Symmetric double relic systems are suggested to form from cluster mergers with a low mass ratio while single relic system arises from mergers with higher mass ratios ([van Weeren et al., 2011a](#)). Results from recent studies suggest that double-relic systems are the most disturbed clusters (e.g., [Bonafede et al., 2017](#)).

Studies of double relic clusters show a correlation between the linear size of the relics against their radio power and their distance from the cluster centre (e.g., [Bonafede et al., 2012](#)). Other studies also found that radio relics with high largest linear size (LLS) have high radio powers and are usually found at larger distances from the cluster centre, while smaller relics are closer to the cluster cores (see e.g., [de Gasperin et al., 2014](#), and the right panel of Figure 1.11). According to simulation studies, this is due to shocks getting larger in less dense and lower temperature regions ([Vazza et al., 2012](#); [Skillman et al., 2013](#)). [de Gasperin et al. \(2014\)](#) also found that the radio power of double relics steeply scales with the cluster mass and that this relation is still maintained when single radio relics are included.

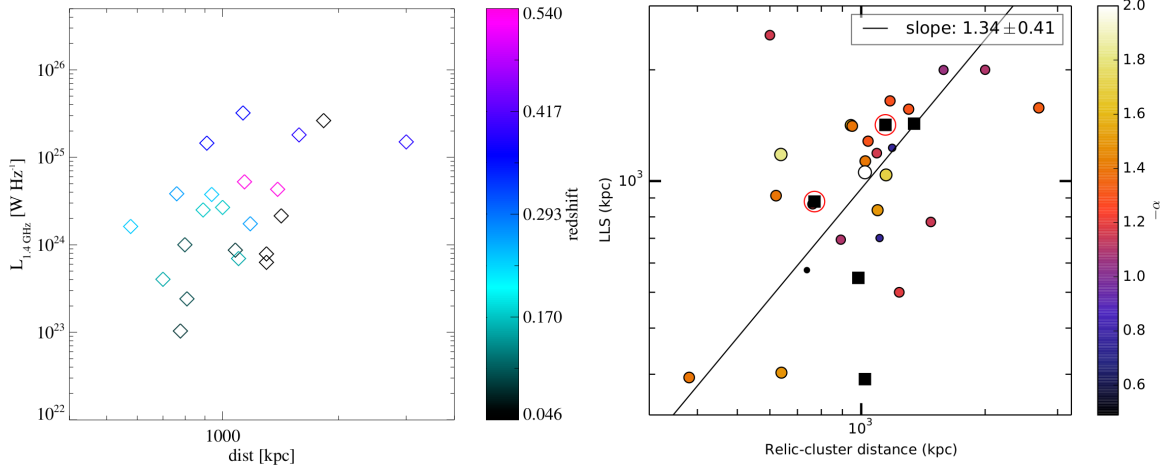


Figure 1.11: The monochromatic radio power of a halo at 1.4 GHz versus the bolometric X-ray luminosity of the cluster from [Feretti and Giovannini \(2008\)](#).

### Revived fossil plasma

Radio observations of clusters at low frequencies have uncovered the presence of faint diffuse radio sources with steep spectra ( $\alpha < -1.5$ ) and ambiguous morphology. These sources can be classified into two groups: radio phoenixes (considered to be a subclass of radio relics), which are thought to be re-energised fossil plasma from AGN lobes ([van Weeren et al., 2019](#); [Giacintucci et al., 2020](#)), and the gently re-energised tails (GReETs [de Gasperin et al., 2017](#); [Bîrzan et al., 2020](#)). GReETs have been suggested to form from the compression of radio tails by weak shocks or from the tail re-energisation due to turbulence from the Rayleigh-Taylor and the Kelvin-Helmholtz instabilities ([de Gasperin et al., 2017](#); [van Weeren et al., 2019](#)). Only a few sources from revived fossil plasma have been detected to date and more observations are required to further understand their origin and physical properties. Figure 1.12 shows examples of some of the observed revived fossil plasma.

### 1.3.4 Star formation activity of galaxies in clusters

Most galaxies can be classified into two distinct groups: a population of red and quiescent galaxies with little to no SF activity and spherical/elliptical morphology; and a population of blue star-forming galaxies with spiral/disky morphology ([Baldry et al., 2004](#); [Skibba et al., 2009](#); [Taylor et al., 2015](#)). Discerning the physical processes

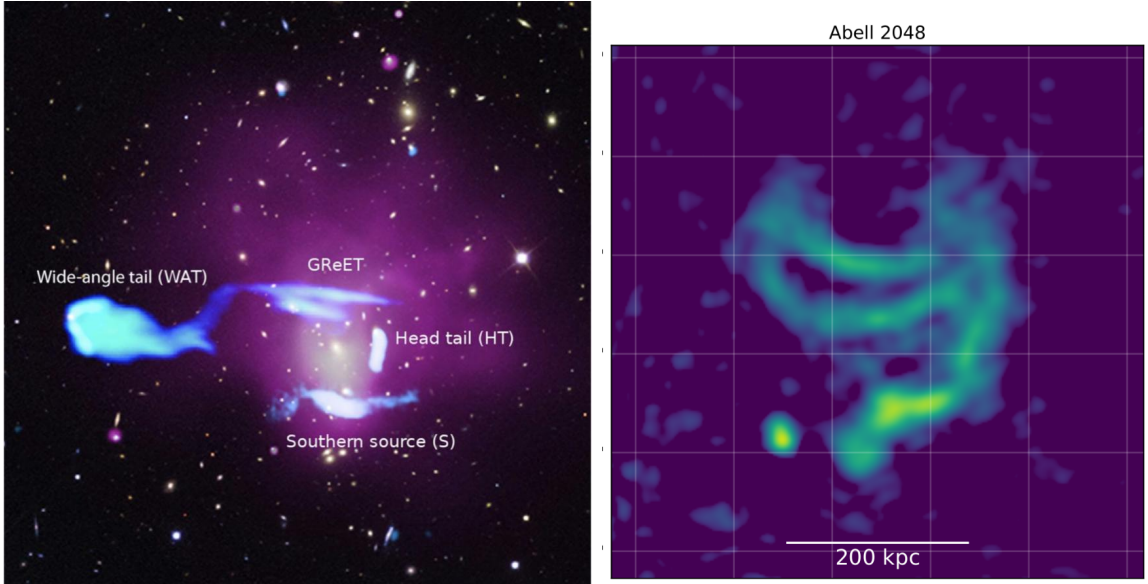


Figure 1.12: *Left:* The composite image of the Abell 1033 galaxy cluster showing a GReET. The composite image was made from optical (SDSS, background image), X-ray emission (*Chandra* X-ray Observatory, purple hue) and radio (Low-Frequency Array, LOFAR, in blue). Image credit: [de Gasperin et al. \(2017\)](#). *Right:* The image of a radio phoenix in the Abell 2048 cluster observed by the Giant Millimetre Radio Telescope (GMRT). Image credit: [van Weeren et al. \(2011b\)](#).

involved in making a galaxy a member of either population group at any cosmological epoch remains an unsolved problem of modern astrophysics. Multiple studies have investigated the SF activity of galaxies in clusters at various redshifts to measure the environmental influence of high-density environments on galaxy evolution (e.g., Dressler et al., 1997; De Lucia et al., 2007; Vulcani et al., 2011; Rodríguez-Muñoz et al., 2019). Results from this extensive investigation provide evidence for a significant change in galaxy populations in clusters since  $z \approx 1$ . Galaxies in dense environments like clusters are expected to evolve quicker than those in less dense environments (Oemler et al., 1997), thus making clusters an area of interest in studying galaxy evolution. Nearly five decades ago, Butcher and Oemler (1978) discovered the increase in the fraction of blue galaxies with redshift, rising from zero in the Local Universe to  $\approx 20\%$  by  $z \approx 0.5$ . This observation has been linked to an in-falling population of SF galaxies into cluster environments which later evolve into quiescent systems.

In the Local Universe, SF activity in galaxies has been shown to be strongly

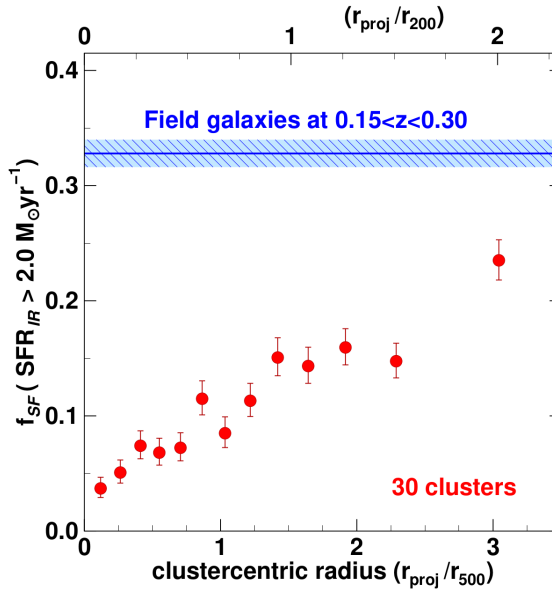


Figure 1.13: The radial population gradient of the star-forming galaxies from Haines et al. (2015). The red points show the  $f_{\text{SF}}$  as a function of the projected clustercentric radius ( $r_{500}$  in the bottom axis and  $r_{200}$  in the top axis). The horizontal blue line at the top shows the corresponding  $f_{\text{SF}}$  for field galaxies and their  $1\sigma$  uncertainties in the shaded area.

dependent on the galaxy environment through comparative studies of galaxies in high-density (groups/clusters) environments and galaxies in the field (e.g., Balogh et al., 1998; Lewis et al., 2002; Gómez et al., 2003; Haines et al., 2015). These studies conclude that the fraction of star-forming galaxies in cluster environments is lower compared to low-density/field environments. These studies also reveal a population distribution in cluster galaxies with most of the red ellipticals mainly found in cluster cores and blue spirals dominant in the cluster outskirts. This population distribution means that the fraction of star-forming galaxies ( $f_{\text{SF}}$ ) decreases as you get closer to the core of the cluster, leading to a relation between  $f_{\text{SF}}$  and the radius of the cluster. Figure 1.13 shows the  $f_{\text{SF}}$  - radius relation from the Haines et al. (2015) study of 30 clusters at  $0.15 < z < 0.30$  out to  $2R_{200}$  in comparison with the  $f_{\text{SF}}$  of field galaxies.

A number of physical processes have been suggested over the years to be responsible for the removal of gas and the suppression of SF activity of galaxies in cluster environments. These processes include ram pressure stripping, galaxy-to-galaxy interactions and galaxy starvation. Evidence suggests that these quenching processes are

effective in different regions of the cluster (e.g., Treu et al., 2003; Boselli and Gavazzi, 2006). The description and distinction of these processes are briefly summarised in the bullet points below:

- **Ram pressure stripping:** When an in-falling field galaxy enters the cluster environment, it experiences a drag force known as *ram pressure* due to its motion relative to the ICM. This drag force is responsible for stripping the interstellar gas out of the galaxy and the strength of this interaction crucially depends on the orbit of the galaxy as it enters the ICM (see Gunn and Gott, 1972; Fujita and Nagashima, 1999). Ram pressure-stripped galaxies are often seen with a large trailing tail of interstellar medium, gaining them the name “jellyfish galaxies” (Poggianti et al., 2016). As galaxies get closer to the cluster core, more and more of their gas is stripped out, including the cold gas reservoir which fuels the formation of new stars (Cortese et al., 2021). Simulations reveal that the stripping process has timescales ranging between 100 million years (Quilis et al., 2000) and a few billion years (Balogh et al., 2000) for 100% of the gas to be stripped out.
- **Galaxy-galaxy interactions:** Galaxy-to-galaxy interactions (harassment or tidal stripping) play a significant role in galaxy and cluster evolution (Moore et al., 1996). Results from several studies suggest that the transformation of star-forming spiral galaxies to quiescent ellipticals is mainly driven by both minor and major galaxy mergers (see e.g., Toomre and Toomre, 1972; Barnes, 1992; Bournaud et al., 2005). The interaction of matter between the merging galaxies leads to intense flashes of SF, which in turn depletes the gas supply in short timescales.
- **Galaxy starvation:** Spiral galaxies form stars by using up the gas reservoir in the ISM, which they continuously replenish from their extended haloes (Larson et al., 1980). When the accretion of gas from the extended halo is halted due to the removal of the extended halo by the ICM, the galaxy undergoes a period of *starvation* as it depletes the last of its remaining gas through SF, eventually

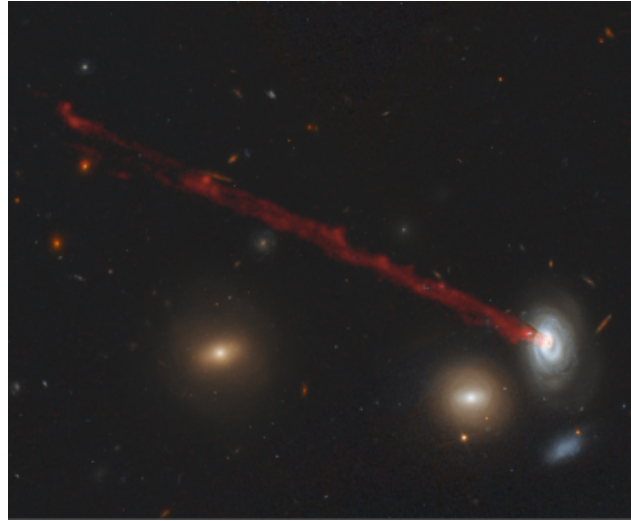


Figure 1.14: The image of a galaxy undergoing ram pressure stripping from Cramer et al. (2019). This observation is from the *Hubble* Space Telescope false colour image overlayed with H $\alpha$  data in red from Subaru Suprime-Cam.



Figure 1.15: The image of a galaxy to galaxy interaction showing tidal stripping.  
Image credit: <http://www.hubblesite.org/gallery/>

turning into a gas-poor passively evolving galaxy (Larson et al., 1980; Balogh et al., 2000; van den Bosch et al., 2008).

This thesis aims to investigate the relation between SF activity and cluster environments. This study uses MeerKAT-detected radio luminosities from clusters to compare and complement cluster studies from other SFR tracers. This will put us closer to answering questions such as: does the SF activity in galaxy clusters depend on their dynamical state? How do radio-derived SFR results compare with IR-derived

SFR on the evolution of SF activity? And how does the presence of relics/shock waves affect the SF activity of the cluster and the member galaxies around them?

## 1.4 Thesis outline

The layout of this thesis is as follows:

- Chapter 2 introduces the parent data samples required for this study. We discuss the tools and method development process by initially focusing our study on the Abell 209 cluster.
- Chapter 3 looks at the statistical analysis of multiple clusters to investigate the environmental dependence of SF activity with the dynamical states of clusters. We compare our radio-derived results to IR-derived results from the literature.
- Chapter 4 covers the investigation of the relation of SF activity with the time that passed since the merger started in double-relics clusters. This chapter also include the investigation of the differences in SF activity between galaxies close to relics and those away from the relics.
- Chapter 5 covers the summary of our main results and future work.

In this thesis, we assume a flat  $\Lambda$ CDM cosmology with  $H_0 = 70 \text{ km s}^{-1} \text{ Mpc}^{-1}$ ,  $\Omega_{\text{m},0} = 0.3$  and  $\Omega_{\Lambda,0} = 0.7$ .  $M_{200}$  denotes the mass enclosed within a sphere of radius  $R_{200}$  in which the mean enclosed overdensity is equal to 200 times the critical density of the Universe at the cluster redshift.

# Chapter 2

## Parent data samples and method development

The aim of this chapter is to provide a comprehensive introduction to the parent data samples utilised in this study and to develop a methodology for studying SF rates in clusters. This entails radio and optical/IR data acquisition, estimation of photometric redshifts (photo-zs), and the cross-matching of radio and optical catalogues. We test our method by initially focusing on the study of the Abell 209 (A209) cluster, which would then pave the way to the study of the larger MeerKAT Galaxy Clusters Legacy Survey (MGCLS) sample. Our initial focus on A209 was due to the availability of extensive spectroscopic redshifts (spec-zs) for the cluster in the literature. The spec-zs not only allows us to accurately classify cluster members but also gives us a yardstick to utilise in our photo-zs member selection criteria. I end the chapter by discussing the results of the investigation of the SF activity in A209. The material covered in this chapter appears in [Knowles et al. \(2022\)](#), and in here I describe the contributions I have made to that work.

### 2.1 MeerKAT Galaxy Clusters Legacy Survey

The MeerKAT Galaxy Clusters Legacy Survey (MGCLS DR1, [Knowles et al., 2022](#)) is a heterogeneous sample of 115 clusters in the southern sky observed between a declina-

tion range of  $-85^\circ < \delta < 0^\circ$ . The MGCLS clusters were observed using the MeerKAT radio telescope ([Jonas and MeerKAT Team, 2016](#); [Camilo et al., 2018](#)). MeerKAT is an interferometer of 64, 13.5 m diameter antennas located in the Karoo desert of South Africa. MeerKAT antennas operate in the *UHF*-band (580 – 1015 MHz), the *L*-band (900 – 1670 MHz) and the *S*-band (1.75 – 3.5 GHz). MGCLS clusters were observed with a primary beam full-width at half-maximum (FWHM) of  $1.2^\circ$  at 1.28 GHz in 4096 channels and 8 seconds integration time. This produced radio images at  $\approx 8''$  resolution and  $< 5 \mu\text{Jy beam}^{-1}$  rms sensitivities. Figure [2.1](#) shows MeerKAT’s observation of A209, which is one of the clusters in MGCLS DR1.

MGCLS provides long-track *L*-band observations of clusters with a total of  $\approx 1000$  hours of observation. Each MGCLS cluster was observed at full polarisation for  $\approx 6 - 10$  hours. The first data release (DR1) of the MGCLS sample provides basic image cubes at  $\approx 8''$  resolution and enhanced spectral and polarisation cubes observed at  $\approx 8''$  and  $15''$  resolution. The MGCLS image products have rms sensitivities ranging between  $2 - 7 \mu\text{Jy beam}^{-1}$  at  $8''$  resolution and  $7 - 15 \mu\text{Jy beam}^{-1}$  at  $15''$  resolution. The MGCLS basic cubes span a  $2 \text{ deg}^2$  field of view (FoV) and the enhanced data products have been primary beam corrected within a  $1.2 \text{ deg}^2$  FoV. The MGCLS data processing was handled by the MGCLS team and the imaging procedure is described in [Mauch et al. \(2020\)](#). The MGCLS clusters have a median redshift of 0.14 with only four clusters with redshifts  $z > 0.4$ .

The MGCLS cluster targets had no standard selection criteria based on redshift or X-ray/radio luminosity. It is a combination of two subsamples: the radio-selected subsample and the X-ray-selected subsample. The MGCLS radio-selected subsample consists of 41 clusters (36%) that were targeted based on previously done searches by other studies that were looking for diffuse radio emission in clusters. This subsample includes clusters with and without previously detected diffuse emission. The clusters that were targeted by previous studies were of high mass,  $M_{200} \gtrsim 9 \times 10^{14} M_\odot$ , derived from X-ray or SZ-effect data. The radio-selected subsample is therefore strongly biased towards massive clusters with diffuse radio emission, covering a redshift range of  $0.018 < z < 0.870$  and a median at  $z = 0.22$ . The X-ray-selected subsample

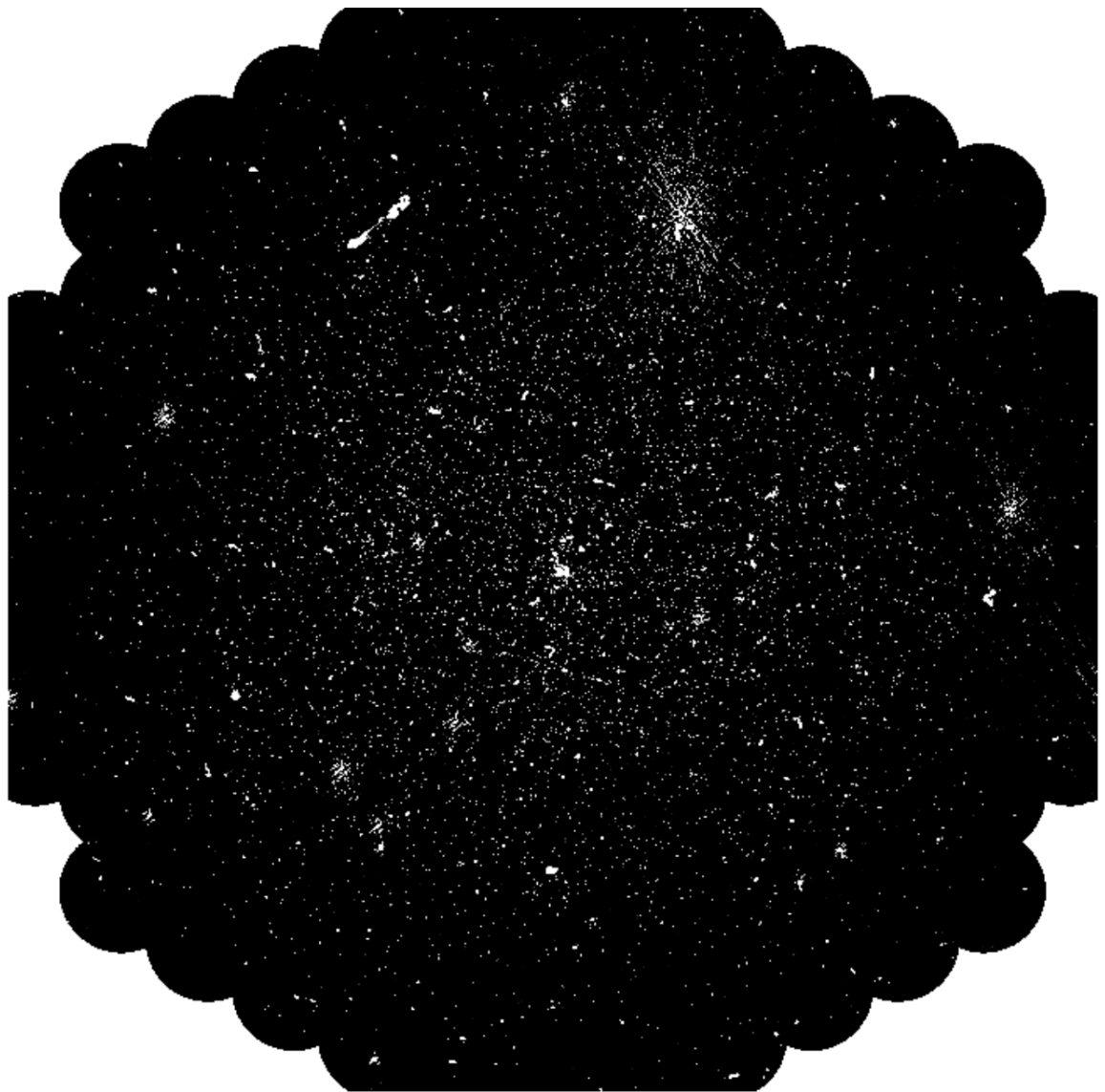


Figure 2.1: MeerKAT telescope radio image with coordinates centred at the A209 cluster and a diameter of  $\approx 2$  deg.<sup>1</sup> The North is in the direction towards the top of the image and the left of the image is East. Given MeerKAT’s large FoV, the radio image contains a myriad of sources, many of which are not part of the A209 cluster.

consists of 74 clusters (64%), contributing the bulk of the clusters in the MGCLS sample. It was targeting clusters from the Meta-Catalogue of X-ray-detected Clusters (MCXC Catalogue, Piffaretti et al., 2011), with the aim to produce a sample with no direct prior biases towards or against clusters with diffuse radio emission. This sample includes MCXC clusters below  $-39^\circ$  which were selected to fill gaps during the MeerKAT observing schedule. The X-ray-selected subsample covers a redshift range of  $0.011 < z < 0.640$  with a median of  $z = 0.13$ .

The MGCLS team created a compact source catalogue of galaxies from all the 115 clusters using the Python Blob Detection and Source Finder (PYBDSF; Mohan and Rafferty, 2015). The released catalogue contains compact sources from detections that have a single Gaussian component. Compact sources were searched in full resolution, primary beam corrected MeerKAT images at a threshold of  $5\sigma$  source detection on the local image rms (see Knowles et al., 2022, for more details). The MGCLS DR1<sup>1</sup> data archive includes a compact source catalogue of over 720,000 sources from all the 115 clusters in the catalogue.

### 2.1.1 MGCLS astrometry checks with unWISE

During the commissioning of an instrument, it is essential to ensure that it is calibrated to take measurements accurately and within nominal uncertainties. One way of checking if a telescope is calibrated correctly is by the test of its astrometric accuracy. An accurate understanding of the astrometric errors of a telescope is crucial in optimising the quality of the data measured by the instrument.

Through the process of producing radio-optical/IR catalogues between the MGCLS compact sources and the Dark Energy Camera Legacy Survey catalogue (DECaLS; Dey et al., 2019), systematic offsets of up to  $2''$  were discovered on a handful of clusters that were initially cross-matched. We extended the investigation of offsets for all MGCLS fields to gauge the number of observations with large offsets by cross-matching with the Wide-field Infrared Survey Explorer (WISE; Wright et al., 2010) as

<sup>1</sup><https://doi.org/10.48479/7epd-w356>

the unWISE catalogue (Schlafly et al., 2019) for its all-sky coverage with deeper imaging and accurate photometry and astrometry. We use the `Astropy` package (Astropy Collaboration, 2013; Astropy Collaboration, 2018) for our cross-matching routine and use `Astroquery`<sup>2</sup>, to access the unWISE catalogue through the Vizier<sup>3</sup> database. A cross-matching radius of  $10''$  was used to obtain corresponding sources between the MeerKAT fields and unWISE. The compact sources between the two catalogues were matched according to the nearest neighbour. We then estimated the median offsets ( $\Delta\text{RA} = \text{RA}_{\text{unWISE}} - \text{RA}_{\text{MeerKAT}}$  and  $\Delta\text{DEC} = \text{DEC}_{\text{unWISE}} - \text{DEC}_{\text{MeerKAT}}$ ) between the MeerKAT and unWISE source positions.

Table 2.1 shows the median offset values for compact sources in the 47/115 MeerKAT fields with systematic offset values between  $1'' - 6.2''$  in  $\Delta\text{RA}$ . The biggest median offset in  $\Delta\text{DEC}$  is  $1.9''$ . It should be noted that although offsets are identified with cluster names in Table 2.1, all the compact sources in the MeerKAT field of view were used to deduce them and were not based on clusters. Much of the offset values were attributed to the instrument calibrator position errors from the list of calibrators that were initially used for MeerKAT. This was mitigated by re-imaging the affected fields and adding or subtracting offset values. Table 2.1 also includes the offset values calculated from the re-imaged fields. After re-imaging, only 4/47 fields have  $\Delta\text{RA} > 1''$  from fields with corrected calibrator offsets. These offsets could result from the time offset and half-channel frequency errors noted in the initial observations made by MeerKAT (see Section 4.4.4 in Knowles et al., 2022, for more details). For re-imaged MeerKAT fields with corrected offsets, there are 39/47 fields with  $\Delta\text{RA} < 0.5''$  and 43/47 with  $\Delta\text{RA} < 1''$ . All but one field has  $\Delta\text{DEC} > 1''$  after re-imaging.

In Figure 2.2, we show plots of the offsets of galaxies in the field of J0510.2-4519 as an example. The left panel of Figure 2.2 shows the difference in RA and DEC between galaxy positions in MeerKAT and unWISE and the right panel shows the number count of sources with respect to the difference in source positions. We re-calculated the difference in RA after the fields were re-imaged and corrected for calibrator offsets

<sup>2</sup><https://doi.org/10.6084/m9.figshare.805208.v2>

<sup>3</sup><https://vizier.cds.unistra.fr/>

and we show the difference in  $\Delta\text{RA}$  between uncorrected and corrected fields in Figure 2.3.

MeerKAT Field	$\Delta\text{RA}$	$\Delta\text{DEC}$	$\Delta\text{RA}_{\text{re-imaged}}$	$\Delta\text{DEC}_{\text{re-imaged}}$
	["]	["]	["]	["]
J0014.3-6604	2.203	1.793	0.094	0.079
J0027.3-5015	1.051	1.902	0.049	0.078
J0145.0-5300	1.081	0.142	0.052	-0.003
J0145.2-6033	-2.427	0.198	-0.062	-0.005
J0217.2-5244	1.244	0.257	0.008	0.014
J0303.7-7752	-3.329	0.718	-0.164	0.047
J0328.6-5542	-1.926	-0.174	-0.162	-0.018
J0336.3-4037	1.315	0.349	0.062	-0.001
J0351.1-8212	-6.192	0.455	-1.077	0.106
J0352.4-7401	-3.076	0.568	-0.374	0.018
J0406.7-7116	-1.020	0.222	0.013	0.024
J0416.7-5525	-1.238	-0.915	-0.047	-0.033
J0431.4-6126	-1.294	-0.957	-0.072	-0.034
J0449.9-4440	1.517	0.512	0.053	0.011
J0510.2-4519	2.295	1.067	0.088	0.035
J0525.8-4715	2.289	1.131	0.128	0.054
J0528.9-3927	2.068	1.228	2.049	1.222
J0540.1-4050	1.949	1.238	0.273	0.260
J0540.1-4322	1.983	1.273	0.306	0.121
J0542.8-4100	2.072	1.233	0.085	0.055
J0543.4-4430	2.025	1.262	0.071	0.055
J0545.5-4756	2.282	1.324	0.097	0.068
J0607.0-4928	2.469	1.289	0.206	0.116
J0610.5-4848	2.095	1.330	0.112	0.072
J0616.8-4748	1.899	1.441	0.081	0.076
J0626.3-5341	2.380	1.394	0.125	0.083
J0627.2-5428	2.239	1.535	0.209	0.100
J0631.3-5610	2.432	1.528	0.148	0.075
J0637.3-4828	2.000	1.558	0.092	0.147
J0638.7-5358	2.329	1.629	0.176	0.043
J0645.4-5413	1.835	1.583	0.125	0.074
J0712.0-6030	1.854	-0.831	0.100	-0.039
J0738.1-7506	4.364	-0.796	0.236	-0.044
J0943.4-7619	5.418	-0.147	0.495	-0.033
J0948.6-8327	1.804	0.615	0.171	-0.014
J1040.7-7047	3.920	0.065	0.648	0.049
J1423.7-5412	1.574	0.649	0.466	0.281
J1518.3-4632	-2.639	-0.342	-0.910	-0.141
J1535.1-4658	-2.038	-0.441	-0.934	-0.154
J1539.5-8335	-5.109	0.322	-1.255	-0.009
J1601.7-7544	-2.290	0.127	-0.936	0.047
J1653.0-5943	-1.067	-1.699	0.277	-0.474
J1705.1-8210	-4.483	0.021	-0.183	-0.017
J1840.6-7709	-2.533	-0.348	-1.056	0.128
J2104.9-8243	-2.662	-0.469	-0.269	-0.050
J2319.2-6750	3.411	1.281	-0.055	0.076
J2340.1-8510	1.354	-0.648	-0.205	-0.012

Table 2.1: Median offset values from differences between MeerKAT source positions and unWISE positions. Columns 2 and 3 show the initial offset values of the MeerKAT fields and column 4 and 5 show the offsets calculated after re-imaging to fix the initial offsets.

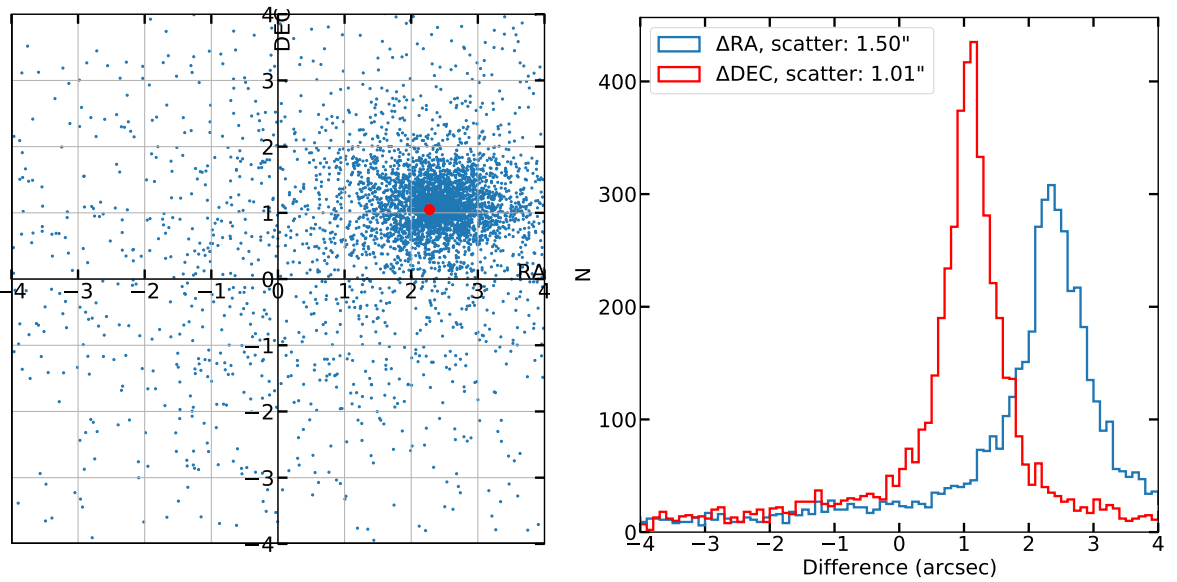


Figure 2.2: *Top left panel:* Offset values in both RA and DEC between MeerKAT and unWISE positions for sources in cluster J0510.2-4519. The red dot is the median offset that is applied during the correction. *Top right panel:* The number distribution of the offsets in both RA (blue) and DEC (red). We estimated the scatter using the bi-weight scale estimator (e.g., [Beers et al., 1990](#)).

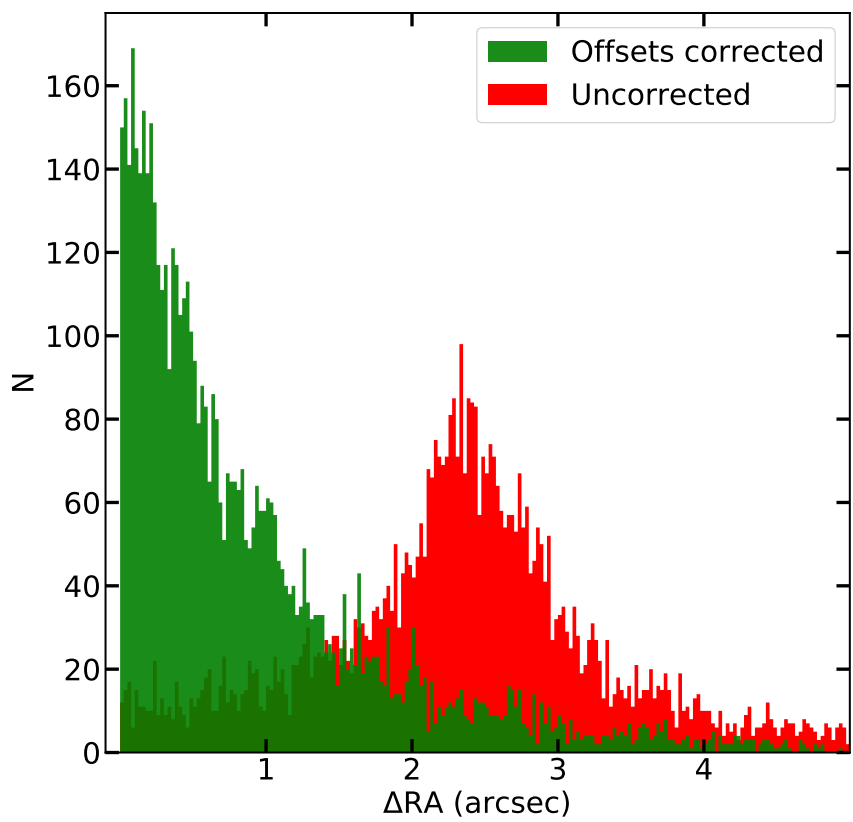


Figure 2.3: The distribution of offsets in  $\Delta\text{RA}$  for cluster J0510.2-4519. We show the distribution of offsets before (red) and after (green) the correction was made.

## 2.2 Cross-matching MGCLS with DECaLS

For the MGCLS clusters in the Dark Energy Survey (DES; [Dark Energy Survey Collaboration et al., 2016](#)) footprint, we produced cross-matched radio-optical catalogues which include estimated photo-zs using photometry from the eighth DECaLS data release (DR8; [Dey et al., 2019](#)). The crossmatching between MeerKAT and DECaLS was conducted by Ilani Loubser, a member of the MGCLS team, through a procedure that uses the likelihood ratio method (similar to that in; [Sutherland and Saunders, 1992](#); [Laird et al., 2009](#); [Smith et al., 2011](#)), described in detail in ([Knowles et al., 2022](#)). Of the 115 MGCLS clusters, 66 have complete coverage in DECaLS DR8 (DECaLS henceforth). We rely on photo-zs to assign cluster membership for the study of a larger MGCLS sample. Although spec-zs are more accurate and a preferred way to classify cluster members, extensive coverage of spectroscopic surveys is not available for most of the clusters in MGCLS. While less accurate compared to spec-zs, photo-zs provide a vital means to study galaxies in fields where spec-zs are not available. Their extensive and deep coverage of the sky allows for statistical analysis of larger samples which would not be easy to attain with the resource-costly and sensitivity-limited spectroscopic surveys. A growing number of studies have been conducted using accurate photo-zs to study the universe in recent years. Some of these studies looked at galaxy properties over cosmic evolution (e.g., [Fontana et al., 2000](#)), properties of multiple clusters (e.g., [Finoguenov et al., 2007](#)), and the evolution of AGN-hosting galaxies (e.g., [Miyaji et al., 2015](#)), to mention a few.

The concept of using galaxy photometry to estimate redshifts was initially proposed by [Baum \(1957\)](#) in an attempt to work out redshifts of elliptical galaxies beyond what spectroscopic observations could measure at the time. Further studies on photo-zs have been conducted since (see e.g., [Baldwin, 1977](#); [Puschell et al., 1982](#); [Benítez, 2000](#); [Ilbert et al., 2006](#); [Brammer et al., 2008](#)). Various techniques have been developed to estimate photo-zs and can be mainly classified into two groups: SED template-fitting methods and machine learning algorithms.

The SED template-fitting methods employ spectral template libraries of galaxies

(spirals, ellipticals and starbursts) and AGN (quasars, seyferts) from observations and models (e.g., [Coleman et al., 1980](#); [Blanton and Roweis, 2007](#)) to estimate photo- $zs$ . The machine learning techniques rely on the use of algorithms to estimate photo- $zs$  (e.g., [Carliles et al., 2010](#); [Beck et al., 2017](#)). Some approaches use a hybrid of the SED template-fitting and machine learning techniques to estimate photo- $zs$  (e.g., [Beck et al., 2016](#)). For our study, we rely on a SED template fitting method which is discussed in detail in the following section. For extensive details on the other photo- $z$  estimation techniques, the reader is referred to the [Salvato et al. \(2019\)](#) review on the various photo- $z$  methods.

We relied on photometry from the DECaLS DR8 ([Dey et al., 2019](#)) to estimate photo- $zs$  for galaxies in our cluster sample. The DECaLS photometry was captured by the Dark Energy Camera (DECam  $\approx 3.2 \text{ deg}^2$  FoV, 570 Mpixel; [Flaugher et al., 2015](#)) at the 4-m Blanco telescope at the Cerro Tololo Inter-American Observatory in Chile. DECam is a highly sensitive camera optimized for a wide-field survey across a broad wavelength range ( $\approx 400 - 1000 \text{ nm}$ ) with a plate scale of  $0.262''$  per pixel. DECam has a median point spread function FWHM of  $1.29''$  at the  $g$ -band,  $1.18''$  at the  $r$ -band and  $1.11''$  at the  $z$ -band. DECaLS is part of the three surveys that integrate to make the DESI Legacy Survey, alongside the Beijing-Arizona Sky Survey (BASS; [Zou et al., 2017](#)) and the Mayall z-band Legacy Survey (MzLS; [Silva et al., 2016](#)), all combining to cover  $\approx 14000 \text{ deg}^2$  of the extragalactic sky. DECaLS provides optical  $grz$  photometry combined with  $3.4, 4.6 \mu\text{m}$  photometry from the Wide-field Infrared Survey Explorer mission (WISE; [Wright et al., 2010](#)). The DECaLS  $grz$  photometry data has  $5\sigma$  depth levels of  $g = 24.0$ ,  $r = 23.4$  and  $z = 22.5$  in AB magnitudes.

### 2.2.1 Photometric redshifts

To estimate the photo- $zs$  for galaxies in our cluster sample, I developed `zField`, a template-fitting algorithm. `zField` exists as part of the `zCluster` code ([Hilton et al., 2018](#); [Hilton et al., 2021](#)) which is designed to estimate cluster redshifts. `zCluster`'s main operation is to take advantage of the full photometric data available while

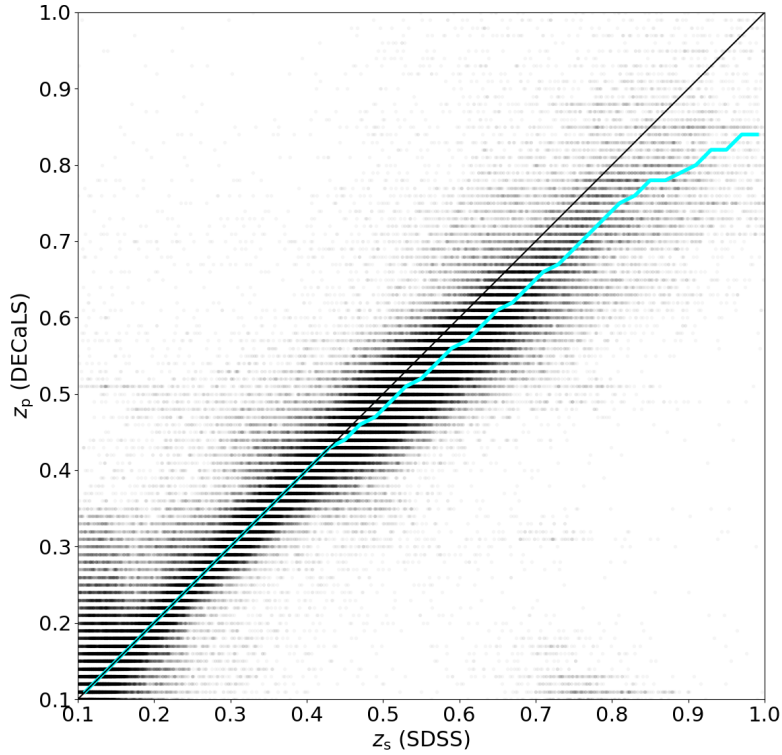


Figure 2.4: A comparison of photo-zs estimated using `zCluster` on DECaLS photometry with spec-zs from SDSS (219,380 galaxies,  $0.1 < z < 1$ ). The photo-zs are evaluated on a grid with step size  $\Delta z = 0.01$ , hence the linear order of data points along the vertical axis. The black solid line shows the one-to-one relation for  $z_s$  and  $z_p$ . The cyan line shows the median redshift residual in bins of width  $\Delta z_s = 0.2$ . It becomes slightly biased at higher redshift, but this is well above our cluster samples. The photo-zs do not perform well at  $z_s < 0.15$  due to the lack of  $u$ -band magnitudes in DECaLS.

minimising assumptions based on the optical properties of the cluster. This is due to the fact that `zCluster` was designed to measure redshifts of clusters observed through other methods besides the optical approach. `zField` builds on the `zCluster` framework and is developed to estimate photo-zs for any galaxy at any point in the sky.

The `zField` algorithm measures the maximum likelihood photo- $z$  and the probability distribution  $p(z)$  of each galaxy in the line of sight of specified coordinates within a radius via a template-fitting technique. `zField` follows a similar method used by photo- $z$  algorithms like the Bayesian Photometric Redshift Estimation (BPZ;

Benítez, 2000) and the Easy and Accurate Z(photo-zs) from Yale (EAZY; Brammer et al., 2008). `zField` uses the default set of galaxy spectral energy distribution (SED) templates used by both BPZ and EAZY. For DECaLS photometry, `zField` also uses a combination of the Coleman et al. (1980) templates and a subset of the spectral templates used in the COSMOS survey (Ilbert et al., 2009; Salvato et al., 2011), representing a range of normal galaxies and AGNs. For each template SED and filter transmission function ( $g, r, z, W1, W2$ , in the case of DECaLS), we calculate magnitudes that would be observed at each redshift  $z_i$  over the range of  $0 < z < 1$  in steps of 0.01 in redshift. The observed broadband SED of each galaxy is then compared with each template SED at each  $z_i$ . The  $p(z)$  distribution is then constructed from the minimum  $\chi^2$  value (over the template set) for each galaxy at each  $z_i$ . The peak of the  $p(z)$  distribution gives the maximum likelihood galaxy redshift, which we use to assign cluster membership in Section 2.3.2. `zCluster` makes use of the full  $p(z)$  distribution to estimate the cluster photometric redshift from the weighted sum of the individual galaxy  $p(z)$ .

We tested the accuracy of the `zField` photo-zs was against spec-zs in the SDSS DR16 (Ahumada et al., 2020) using 219,380 galaxies between the redshift range of  $0.1 < z < 1$ . The mean of the photo-zs offsets  $\Delta z/(1+z_s) = 0.008$  (where  $\Delta z = z_s - z_p$  is the photo-zs residuals,  $z_s$  are the spec-zs, and  $z_p$  are the photo-zs), with a scatter of  $\sigma_{\text{bw}} = 0.03$ , as estimated using the biweight scale (e.g., Beers et al., 1990). This means 93% of the galaxies have  $\Delta z/(1 + z_s) < 0.09$ , i.e., 7% of the photo-zs are expected to be “catastrophic outliers”. This sample was also used to calibrate zero-point offsets to the DECaLS photometry to minimise the bias of the photo- $z$  residuals. Figure 2.4 shows a comparison of the photo-zs and spec-zs for this test sample. We observe a redshift-dependent bias for redshifts  $> 0.5$  as seen in Figure 2.4. However, this does not affect us as clusters in our sample are in a lower redshift range ( $0.15 < z < 0.35$ ).

In addition to photo-zs estimates, `zField` also provides density maps made from integrating the probability distribution for each galaxy in the line of sight of specified coordinates. The integral is on a redshift range centred at a specified  $z$  and within  $\pm \Delta z$ , where  $\Delta z$  is also user specified. The density maps are produced in a  $4 \text{ Mpc} \times$

4 Mpc grid with a pixel size of  $0.2 \text{ Mpc} \times 0.2 \text{ Mpc}$ . The `zField` density maps have been used in the [Pillay et al. \(2021\)](#) study of the dynamical state of the ACT-CL J0019.6+0336 cluster. The density map revealed substructure in the cluster and also allowed for estimates of the centre shift and asymmetry cluster parameters.

## 2.3 Star formation in Abell 209

As an example of how MeerKAT observations may be used to estimate star formation activity in clusters, we used the MGCLS compact source catalogue to estimate the SFRs of galaxies in A209, a rich cluster at redshift  $z = 0.206$ . This analysis forms part of the study presented in Section 8.2 of [Knowles et al. \(2022\)](#). The MGCLS compact source catalogue provides us with dust-unbiased  $L$ -band radio continuum luminosities over a  $\approx 1 \text{ deg}^2$  field centred on the cluster, allowing us to study the SF activity of A209 out well beyond twice the  $R_{200}$  (2.15 Mpc) of the cluster. We estimate the value of the cluster's  $R_{200}$  from its cluster mass ( $M_{200} = 11.1 \times 10^{14} \text{ M}_\odot$ , [Hilton et al. \(2021\)](#)), assuming the virial theorem. We use SZ-derived cluster masses from the Atacama Cosmology Telescope catalogue (ACT DR5; [Hilton et al., 2021](#)).

We chose to focus on this particular cluster in this analysis due to the availability of extensive spectroscopic catalogues from the Cluster Lensing And Supernova survey with Hubble (CLASH-VLT; [Annunziatella et al., 2016](#)) and the Arizona Cluster Redshift Survey (ACReS; described in [Haines et al., 2015](#)).

### 2.3.1 Compact source catalogues

To estimate the SF activity in the A209 cluster, we use multiple catalogues to compile a dataset that has radio luminosities for estimating SFR as well as photo-zs and spec-zs to assign cluster membership. Firstly, we cross-match our MeerKAT compact sources catalogue with the `zField` DECaLS catalogue in the A209 field to form a radio-optical catalogue. We then crossmatch our radio-optical catalogue with the spec-zs catalogue to calibrate variables that will be used in the photo- $z$  cluster membership selection criteria described in the following section. As mentioned in Section

[2.1](#), the MeerKAT source catalogues were produced using the PYBDSF code. In the primary beam corrected field of A209, there are 4456 radios sources, 3288 of which have been identified to have optical counterparts in DECaLS.

Using the `zField` algorithm, we get 39,783 galaxies with estimated photo-zs from DECaLS in the A209 field. We obtain a combined total of 1425 galaxies with spec-zs in the A209 field from the literature ([Haines et al., 2015](#); [Annunziatella et al., 2016](#)).

### 2.3.2 Cluster membership selection and galaxy star formation rates

We assigned cluster membership using a combination of spec-zs and photo-zs. Photo-zs were estimated using photometry from DECaLS through the `zField` code described in Section [2.2.1](#). The spec-zs were obtained from the Cluster Lensing And Supernova survey with Hubble (CLASH-VLT [Annunziatella et al., 2016](#)) and the Arizona Cluster Redshift Survey (ACReS; [Haines et al., 2015](#)) spectroscopic datasets. CLASH-VLT and ACReS contain secure redshifts for 1256 and 345 galaxies in the A209 field respectively, with a combined total of 1425 non-overlapping galaxies. We consider galaxies with peculiar velocities within  $\pm 3\sigma_v$  of the cluster redshift to be spec- $z$ -selected cluster members of A209, where  $\sigma_v = 1320 \text{ km s}^{-1}$ , is the line of sight velocity dispersion as measured by [Annunziatella et al. \(2016\)](#). To select cluster members using photo-zs, we consider galaxies with maximum likelihood photo-zs within  $|z_p - z_c| < 3\sigma_{bw}(1 + z_c)$  to be cluster members. The photo-zs selection criteria identified galaxies within  $0.1 < z < 0.32$  as cluster members while the spec-zs selection criteria identified galaxies within  $0.19 < z < 0.22$  as cluster members. The scatter,  $\sigma_{bw} = 0.03$ , estimated using the biweight scale ([Beers et al., 1990](#)) on the photo- $z$  residuals ( $\Delta z/(1 + z_s)$ ). Figure [2.5](#) shows the schematic of the procedure followed in assembling star-forming sample for member galaxies using both the photo-zs and spec-zs selection criteria.

We used the galaxies that have both spec-zs and photo-zs to determine the amount of contamination from field galaxy populations and the number of confirmed spec-

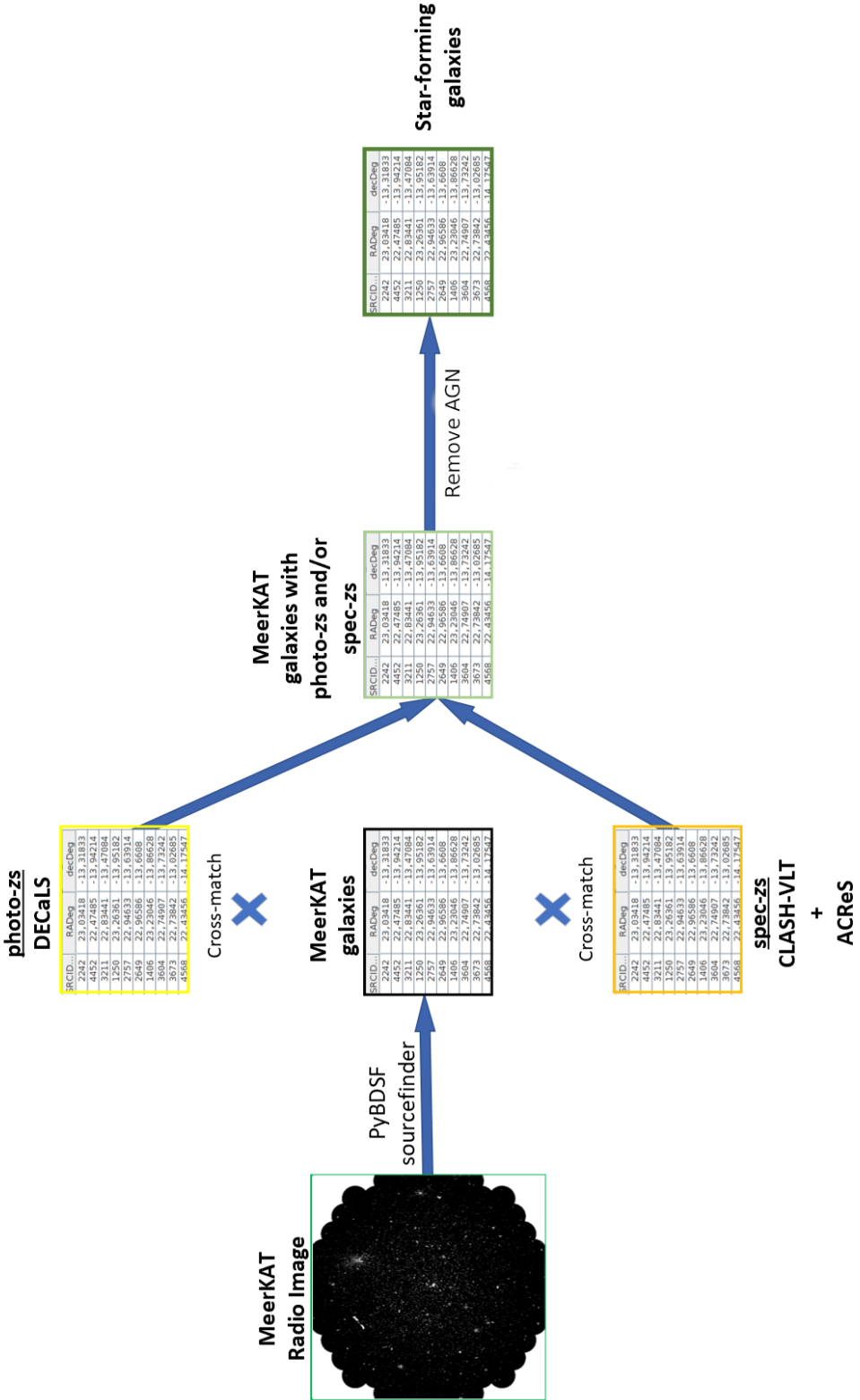


Figure 2.5: The flowchart showing the steps followed to produce the star-forming cluster member galaxies for A209.

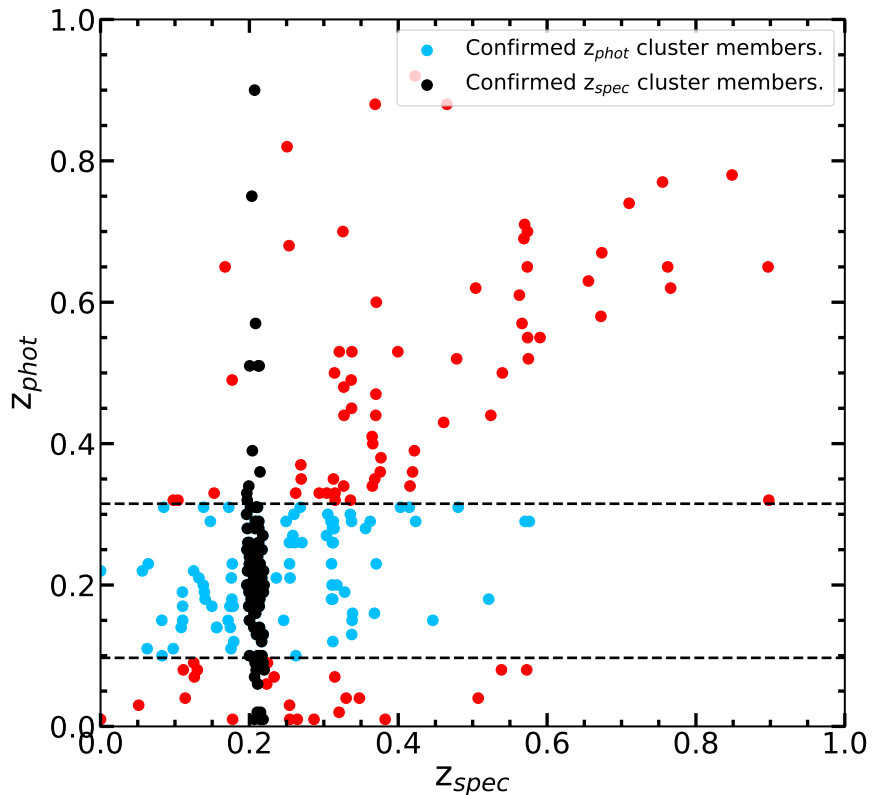


Figure 2.6: Photometric vs. spectroscopic redshifts for all the A209 galaxies in the MeerKAT field. The blue dots represent the galaxies assigned cluster membership based on the photo- $z$  cut. The black dashed lines show the lower and upper bound cut applied on photo- $zs$  to classify cluster members. Galaxies within this range without  $z_{spec}$  counterparts are counted as members. The black dots indicate selected cluster members using spectroscopic redshifts criteria. We estimate  $\approx 16\%$  field contamination in our sample and  $\approx 23\%$  of the spec- $z$  members are missed by the photo- $z$  cut.

$z$  members left out by the photo- $z$  selection criteria. Figure 2.6 shows the relation between spec- $zs$  and photo- $zs$  in radio-detected galaxies. We obtain 16% field contamination, while 23% of the galaxies that are identified as members using their spec- $zs$  are missed by the photo- $z$  selection. The level of field contamination is  $< 20\%$ , which is often used as a limiting value by studies that rely on photo- $zs$  to select cluster members (e.g., Pelló et al., 2009; Rodríguez-Muñoz et al., 2019). After combining cluster members from both the spec- $zs$  and photo- $zs$  selection criteria, we obtain a final catalogue of 523 cluster members with radio emission out to  $3.5R_{200}$ .

As discussed in Section 1.2.2, radio observations face the challenge of AGN contamination. To achieve a star-forming sample unbiased by AGN, we used a method developed by Assef et al. (2018), that relies on WISE W1 and W2 colours to separate star-forming galaxies from AGN-dominated galaxies. We use equation 4 of Assef et al. (2018) to flag out sources that may be AGN

$$W1 - W2 > \begin{cases} \alpha_R \exp\{\beta_R(W2 - \gamma_R)^2\}, & W2 > \gamma_R \\ \alpha_R, & W2 \leq \gamma_R \end{cases} \quad (2.1)$$

where  $\alpha_R$ ,  $\beta_R$  and  $\gamma_R$  are constants whose values depend on the targeted reliability fraction. To achieve 90% reliability on our sample, we adopt the values  $(\alpha_{R90}, \beta_{R90}, \gamma_{R90}) = (0.650, 0.092, 13.70)$  from Assef et al. (2018). We classified 64 galaxies as AGN with this selection method, bringing down the full sample to 459 radio-detected cluster members, which we assume to be powered by SF in the sections that follow.

We used the Bell (2003) calibration (from Equation 1.7 in Section 1.2.2) of the radio–FIR correlation (see also Karim et al., 2011) to convert radio luminosities to SFR scaled down by 1.74 from the Salpeter IMF to the Chabrier IMF

$$\text{SFR (M}_\odot \text{yr}^{-1}\text{)} = \begin{cases} 3.18 \times 10^{-22}L, & L > L_c \\ \frac{3.18 \times 10^{-22}L}{0.1 + 0.9(L/L_c)^{0.3}}, & L \leq L_c \end{cases} \quad (2.2)$$

where  $L = L_{1.4\text{GHz}}$  is the radio luminosity in  $\text{W Hz}^{-1}$  derived from the MGCLS 1.28 GHz total flux density, using a power-law scaling and assuming a non-thermal spectral

index of -0.8 (Condon, 1992).

### 2.3.3 Star formation activity as a function of clustercentric distance

There are a number of ways to investigate the internal SF activity of a cluster and one of the commonly used approaches is the measurement of the fraction of star-forming galaxies ( $f_{\text{SF}}$ ). It is well known that clusters are hostile environments for star-forming galaxies with their cores dominated by quiescent elliptical galaxies and their outskirts dominated by spiral star-forming galaxies. This cluster population distribution leads to a  $f_{\text{SF}}-\text{radius}$  relation which has been observed in various cluster SF studies at different wavelengths (Lewis et al., 2002; Gómez et al., 2003; Haines et al., 2015).

We measure the population trend for our MeerKAT-detected star-forming sample and compare our results with a population trend of Spitzer/MIPS 24  $\mu\text{m}$  IR-derived results from a study of 30 clusters at  $0.15 < z < 0.3$  by Haines et al. (2015) in the left panel of Figure 2.8. We only plot MGCLS sources with SFR greater than the  $5\sigma$  detection limit of  $\text{SFR } 5\sigma = 2 \text{ M}_\odot \text{yr}^{-1}$ , which matches the same detection limit reached by the Haines et al. study. We define the fraction of star-forming galaxies as  $f_{\text{SF}} = N_{\text{MGCLS}}/N_{\text{optIR}}$ , where  $N_{\text{MGCLS}}$  is the number of cluster members detected by MeerKAT within  $3.5R_{200}$  (429) and  $N_{\text{optIR}}$  is the total number of star-forming cluster members from DECaLS (2476) within the same field of view.

We observe a similar trend out to  $2R_{200}$  for both the radio and IR-derived  $f_{\text{SF}}$  estimates. The  $f_{\text{SF}}$  rises steadily from less than 0.1 to just over 0.2 by  $2R_{200}$ , consistent within  $1\sigma$  with the radial trend observed by Haines et al. (2015) out to  $2R_{200}$ . We observe a significant decline in the  $f_{\text{SF}}$  of the last three radial bins which could be a result of decreased sensitivity in the MGCLS observations due to the MeerKAT primary beam. The Haines et al. (2015) study investigated the difference between the  $f_{\text{SF}}$  of cluster galaxies and coeval field galaxies. They observed that field galaxies have a higher  $f_{\text{SF}}$  than cluster galaxies, noting an  $f_{\text{SF}}$  of  $\approx 0.23$  at  $2R_{200}$  in cluster galaxies and  $\approx 0.33$  in field galaxies. They extrapolate that the cluster  $f_{\text{SF}}$  and field

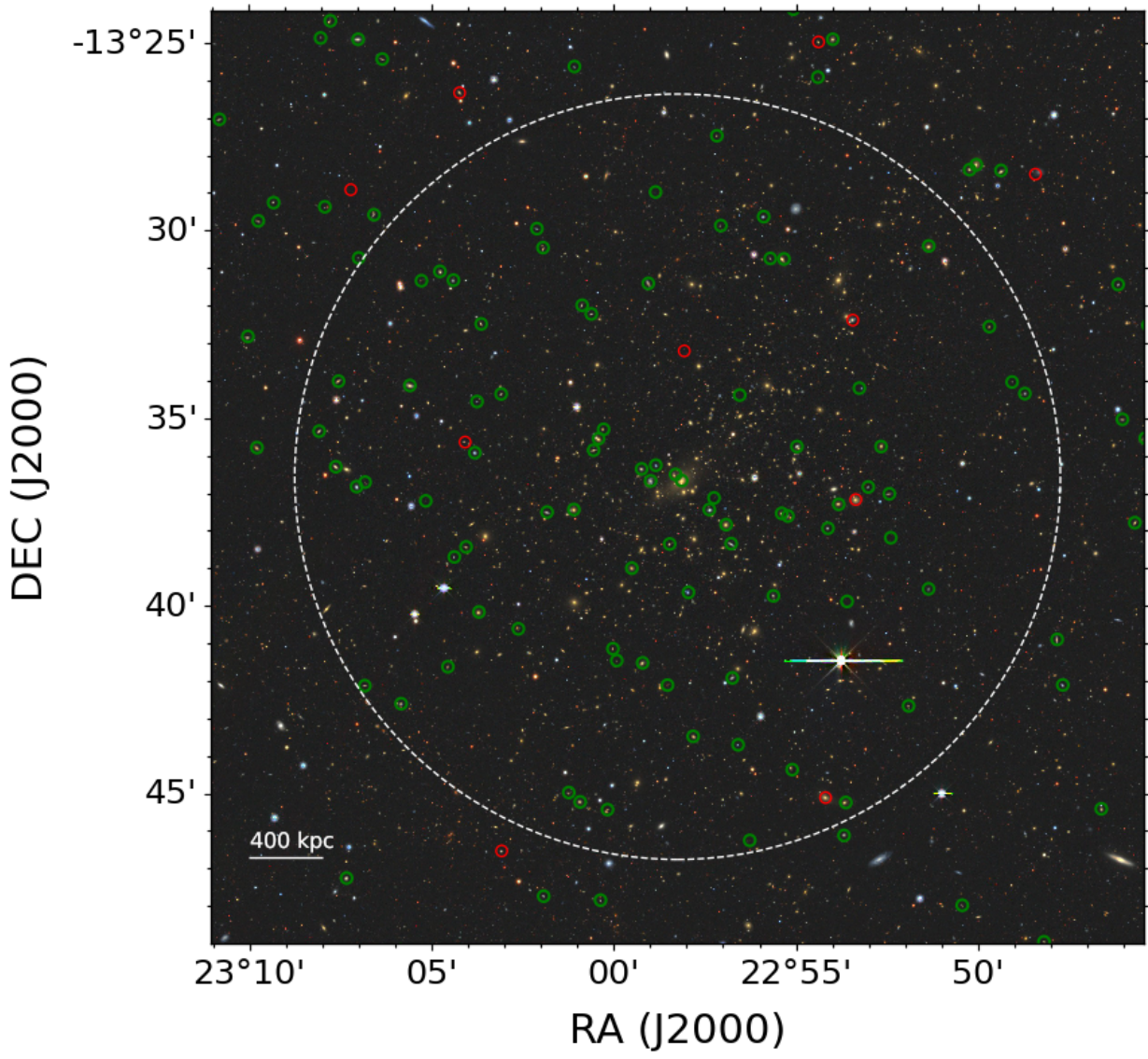


Figure 2.7: The Legacy Survey DR9 image of the A209 field. The green circles show the MeerKAT-detected star-forming galaxies and the red circles show the MeerKAT-detected galaxies identified as AGN. The dashed circle encloses galaxies within the cluster's  $R_{200}$  (2.0 Mpc).

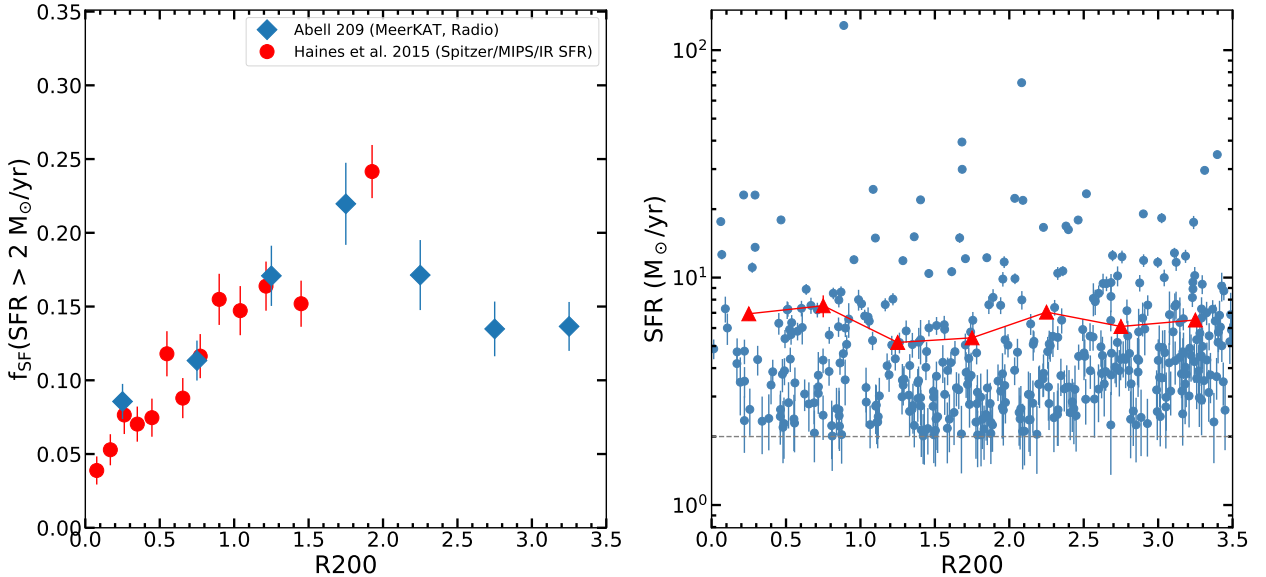


Figure 2.8: *Left panel:* The fraction ( $f_{SF}$ ) of star-forming cluster members in A209 detected by MeerKAT (blue diamonds) as a function of projected radial distance from the cluster centre in units of  $R_{200}$  (2.15 Mpc). The red circles show the fraction of star-forming galaxies from Haines et al. (2015) for 30 clusters observed in IR. Error bars show  $1\sigma$  uncertainties. *Right panel:* SFR versus projected radial distance for A209 cluster members detected by MeerKAT. The red triangles indicate the median SFR plotted in radial bins. The grey dashed line is the SFR at the MGCLS  $5\sigma$  sensitivity limit. All error bars show the  $1\sigma$  uncertainty.

$f_{SF}$  values intersect at  $\approx 4.5R_{200}$ , suggesting that the quenching of cluster galaxies must begin long before a galaxy enters the cluster environment. This means that galaxies are pre-processed in lower-density environments such as galaxy groups prior to entering cluster environments.

We also investigate the relation of SFR as a function of clustercentric radius for the A209 star-forming galaxies shown in the right panel of Figure 2.8. The red triangles show the median SFR plotted in radial bins and show no obvious dependence of SFR with radial distance from the cluster centre. This is consistent with the SF quenching process taking place over longer periods than the infall time, i.e., galaxies that are forming stars are not immediately quenched upon encountering the cluster environment.

## 2.4 Summary

We have introduced the parent data samples required to conduct the study of SF activity in clusters. These comprise of MeerKAT observations, providing us with radio luminosities, DECaLS DR8 observations which are used to generate photo-zs for galaxies, and the ACT DR5, providing us with cluster masses that we use to estimate the  $R_{200}$  of a cluster.

We also create and describe `zField`, a template-fitting algorithm that exists within `zCluster`, made to estimate photo-zs for galaxies at any point in the sky. We note an increased scatter in photo-zs at  $z < 0.15$  caused by the lack of  $u$ -band magnitudes in DECaLS, leading to poor estimates of the photo-zs at lower redshifts. We also note a bias towards spec-zs at redshifts  $z > 0.5$ . Due to the aforementioned observations, we limit the redshift of our cluster studies with `zField` photo-zs to  $z > 0.15$  and  $z < 0.5$ .

We then present a case study for A209, which allowed us to craft a methodology to study the SF activity in MGCLS clusters. With a defined cluster membership criteria, we identify members for Abell 209 and obtain a result consistent with the [Haines et al. \(2015\)](#)  $f_{\text{SF}}$  gradient out to  $2R_{200}$ . Due to MeerKAT’s loss of sensitivity outside the primary beam, the binned  $f_{\text{SF}}$  falls off beyond  $2R_{200}$ , which we set as a limit to map the  $f_{\text{SF}}$  gradient for the larger sample studies. We now turn our attention to studying the larger MGCLS sample in the following chapter.

# Chapter 3

## Star formation in massive cluster at $0.15 < z < 0.35$ using the MeerKAT Galaxy Clusters Legacy Survey

This chapter presents a statistical study of SF activity in 20 clusters using radio observations from the first data release of the MeerKAT Galaxy Cluster Legacy Survey (MGCLS DR1; [Knowles et al., 2022](#)). We investigate the SF activity of clusters with respect to their the dynamical state. We compare our results to previous studies of multiple clusters carried out using FIR as a tracer for SFR.

This study has been published in the journal Monthly Notices of the Royal Astronomical Society ([Kesebonye et al., 2023](#)) and has been adapted to the formatting requirements of this thesis.

### 3.1 Cluster sample

As discussed in Section [2.1](#), the MGCLS catalogue is made up of a heterogeneous sample of 115 clusters with no general selection criteria guided by cluster mass or redshift. MGCLS comprises two subsamples grouped as “radio-selected” and “X-

ray-selected” with each subsample contributing 41 and 74 clusters respectively. The MGCLS radio-selected subsample was picked to be biased towards high-mass clusters with extended radio emission. The X-ray-selected subsample was guided by the Meta-Catalogue of X-ray-detected Clusters (MCXC; [Piffaretti et al., 2011](#)), which is a heterogeneous compilation of X-ray-selected clusters with no direct prior biases towards or against clusters with extended radio emission.

Of the total 115 MGCLS clusters, 66 had optical counterparts with complete coverage in DECaLS DR8 and 38 of the 66 clusters have cluster masses from the ACT DR5 catalogue. The MGCLS fields are given an image data quality rank ranging from 0 to 3. The data quality from 0 to 1 is classified as a good to moderate dynamic range whereas 2 to 3 is classified as a poor dynamic range with ripples and/or source artefacts on the image. For this study, we only work with fields that are ranked 0 and 1 to ensure that our data has the least amount of contamination.

The selection of the clusters from the parent MGCLS sample was guided by the availability of cluster photometric data in the eighth data release of the Dark Energy Camera Legacy Survey (DECaLS DR8; [Dey et al., 2019](#)) as well as the availability of cluster masses ( $M_{200}$ ) from the latest cluster release from the Atacama Cosmology Telescope (ACT DR5; [Hilton et al., 2021](#)). The ACT DR5 catalogue has a homogeneous selection of clusters with consistently derived mass estimates and contains 4195 optically confirmed Sunyaev-Zel’dovich (SZ) galaxy clusters with redshift measurements. The ACT DR5 catalogue provides a set of mass estimates that have been re-scaled according to a richness-based weak-lensing mass calibration through a technique described in [Hilton et al. \(2018\)](#).

The DECaLS DR8 photometric data is complete for WISE ( $3.4\,\mu\text{m}$ ) W1 band apparent magnitude (mag)  $m_{3.4} \leq 19.7$ . This corresponds to an absolute mag limit  $M_{3.4} = -20.8$ , K-corrected to our sample median redshift ( $z = 0.25$ ). We are sensitive down to a limit of  $\approx M_{3.4}^* + 1.5$ , using  $m^*$  (18.2) of the IR-selected cluster sample luminosity function best-fit from the Spitzer Infrared Array Camera (IRAC)  $3.6\,\mu\text{m}$ -band ([Mancone et al., 2010](#)).  $M^*$  is scaled down by 0.08 mag to correct for the colour difference between W1 ( $3.4\,\mu\text{m}$ ) and Spitzer IRAC channel one ( $3.6\,\mu\text{m}$ ). The

IR luminosity function is a good tracer of the stellar mass function since the  $3.6\,\mu\text{m}$  photometry probes the peak of the stellar light.

The cluster sample selection was also limited to clusters with  $z > 0.15$  due to the large scatter observed in photo- $z$  estimates at  $z < 0.15$ , making them unreliable (see Section 2.2.1 and Figure 2.4). We also excluded clusters with  $z > 0.5$  due to the observed bias on the photo-zs. After identifying all the clusters that satisfy our set conditions, we were left with 20 clusters in the redshift of  $0.15 < z < 0.35$ . Our final sample has ten clusters from the radio-selected subsample, nine of which are hosts of extended diffuse emission in the form of a radio halo and/or relic and one cluster with no extended diffuse emission. The other ten clusters in our final sample are from the X-ray-selected subsample with five hosting extended diffuse emission in the form of a radio halo and/or relic, one hosting extended diffuse emission in the form of a mini-halo and 4 with no extended diffuse emission. The cluster sample properties are listed in Table 3.1. Figure 3.1 shows the mass and redshift distribution of our final cluster sample.

In total, 14/20 clusters in our sample host large-scale extended diffuse emission (haloes and relics) linked to ongoing merger activity. The presence or lack of large-scale extended diffuse emission has been linked to the dynamical state of the cluster by Cassano et al. (e.g., 2010, where the large scale sources are linked to merger activity). The six clusters with no large-scale extended diffuse emission are assumed to be relatively dynamically relaxed or undergoing minor mergers and likely to be less disturbed in contrast to the 14 clusters hosting haloes and relics. We conducted a visual inspection on the dynamical state of 4 of the 6 non-halo/relic-hosting clusters in our sample using archival X-ray imaging from *Chandra* and *XMM Newton* surveys. The X-ray images indicate that the clusters are likely to be dynamically relaxed. Lovisari et al. (2017) classified the dynamical state of some of the clusters that overlap with our sample as either ‘disturbed’, ‘relaxed’, or ‘mixed’, using criteria based on seven parameters. Clusters J0449.9-4440 and J0525.8-4715 are classified as relaxed systems while J0510.2-4519 (hosting a mini-halo) is noted as a mixed system by the Lovisari et al. (2017) classification criteria. They point out that the classification of

Cluster	(1)	(2)	(3)	(4)	(5)	(6)	(7)	(8)	(9)	(10)
	RA	DEC	z	RMS ( $\mu\text{J b}^{-1}$ )	$M_{200}$ ( $10^{14} \text{M}_\odot$ )	$R_{200}$ (Mpc)	$f_{\text{SF}}$	$\Sigma \text{SFR}$ $\text{M}_\odot \text{yr}^{-1}$	State	
Abell 209	22.970833	-13.609444	0.206	3.6	$11.1_{-2.3}^{+2.7}$	2.0	0.228	$322.39 \pm 39.18$	halo (disturbed)	
Abell 2744	3.578333	-30.383333	0.307	2.9	$19.2_{-3.7}^{+4.2}$	2.3	0.059	$163.38 \pm 34.65$	halo, relic (disturbed)	
Abell 2813	10.851667	-20.621389	0.292	3.4	$15.0_{-2.9}^{+3.3}$	2.1	0.060	$210.66 \pm 35.99$	halo <sup>‡</sup> (disturbed)	
Abell 2895	19.546250	-26.973056	0.228	3.0	$11.0_{-2.2}^{+2.6}$	2.0	0.188	$208.57 \pm 26.35$	phoenix <sup>‡</sup> (disturbed)	
Abell 521	73.537917	-10.238611	0.248	3.4	$9.6_{-2.0}^{+2.3}$	1.9	0.110	$346.76 \pm 43.02$	halo, relic (disturbed)	
Abell S1063	342.181250	-44.528889	0.348	2.6	$28.1_{-5.4}^{+6.1}$	2.6	0.163	$497.71 \pm 84.99$	halo (disturbed)	
Abell S295	41.399167	-53.038056	0.300	2.3	$15.6_{-3.0}^{+3.4}$	2.2	0.092	$302.60 \pm 45.66$	halo (disturbed)	
J0051.1-4833	12.796667	-48.559722	0.187	2.6	$4.9_{-1.1}^{+1.3}$	1.5	0.107	$70.10 \pm 4.61$	relaxed	
J0217.2-5244	34.302500	-52.746944	0.343	2.8	$4.9_{-1.1}^{+1.2}$	1.4	0.105	$162.51 \pm 33.37$	relic <sup>‡</sup> (disturbed)	
J0225.9-4154	36.477500	-41.909722	0.220	2.7	$4.8_{-1.0}^{+1.2}$	1.5	0.135	$78.62 \pm 11.75$	halo (disturbed)	
J0232.2-4420	38.070000	-44.347500	0.284	2.6	$18.1_{-3.5}^{+4.0}$	2.3	0.171	$310.24 \pm 48.73$	halo (disturbed)	
J0336.3-4037	54.077917	-40.622222	0.172	3.5	$10.9_{-2.3}^{+2.7}$	2.0	0.087	$124.05 \pm 8.43$	relaxed	
J0449.9-4440	72.480000	-44.678056	0.150	2.6	$6.1_{-1.4}^{+1.7}$	1.7	0.060	$71.93 \pm 2.82$	relaxed	
J0510.2-4519	77.557500	-45.321111	0.200	3.0	$8.1_{-1.7}^{+2.0}$	1.8	0.086	$121.30 \pm 7.72$	relaxed, mini-halo <sup>‡</sup>	
J0516.6-5430	79.158333	-54.514167	0.295	3.1	$9.0_{-1.8}^{+2.0}$	1.8	0.089	$182.61 \pm 27.51$	halo,relic (disturbed)	
J0525.8-4715	81.465000	-47.250556	0.191	3.0	$9.9_{-2.1}^{+2.4}$	1.9	0.107	$161.26 \pm 19.17$	relaxed	
J2023.4-5535	305.850000	-55.591700	0.232	2.7	$13.9_{-2.8}^{+3.2}$	2.1	0.171	$248.19 \pm 35.75$	halo, relic (disturbed)	
MACS J0257.6-2209	44.422083	-22.153889	0.322	3.2	$11.8_{-2.3}^{+2.6}$	2.0	0.071	$237.35 \pm 37.89$	relic <sup>‡</sup> (disturbed)	
RXC J0528.9-3927	82.234583	-39.462778	0.284	2.6	$13.1_{-2.6}^{+2.9}$	2.1	0.137	$267.02 \pm 39.92$	halo (disturbed)	
RXC J0543.4-4430	85.851667	-44.505278	0.164	3.6	$4.2_{-1.1}^{+1.3}$	1.5	0.109	$96.79 \pm 9.41$	relaxed	

Table 3.1: The cluster sample. Columns: (1) Name of the cluster; (2,3) MeerKAT pointing coordinates: J2000 Right Ascension and Declination in degrees; (4) Cluster redshift; (5) MeerKAT image sigma-clipped standard deviation in micro-Jy per beam; (6) Cluster mass in  $10^{14} \text{M}_\odot$ ; (7) Cluster  $R_{200}$  in Mpc; (8) The fraction of all star forming galaxies within  $R_{200}$  (see Section 3.4.1); (9) Total SFR for galaxies within  $R_{200}$  (see Section 3.4.2); (10) The dynamical state of a cluster. The clusters with newly detected extended radio emission in the MGCLS are marked as candidates based on their morphology are indicated by <sup>‡</sup>.

the mixed systems may be subjective and that a cluster falling under this category depends on the parameters chosen to optimize completeness and purity.

Given the high masses of clusters in our sample, the clusters without large-scale extended emission are likely to be relaxed systems or have only minor mergers and can be considered to be less disturbed environments for star-forming galaxies.

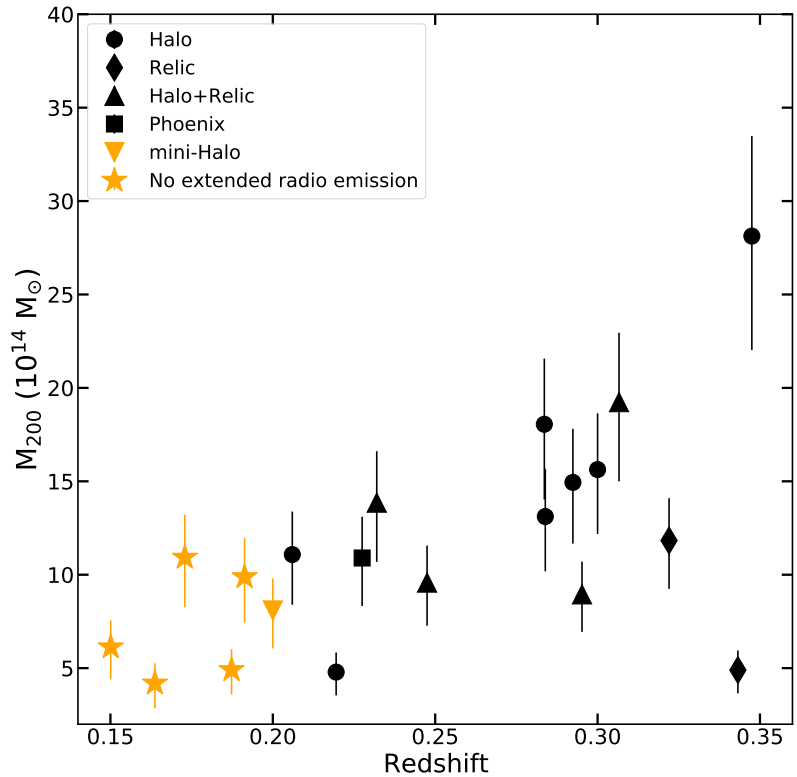


Figure 3.1: The mass ( $M_{200}$ ) and redshift distribution of the cluster sample used in this work. We use only the SZ-selected ACT DR5 clusters ([Hilton et al., 2021](#)) to ensure a homogeneous set of cluster mass estimates. The black markers show clusters with merger-linked extended radio emission and the orange markers show relaxed clusters with no extended diffuse emission and non-merger-linked extended diffuse emission. Each symbol represents the type of extended radio emission a cluster hosts as per the MGCLS DR1 survey paper ([Knowles et al., 2022](#)).

## 3.2 Identifying cluster members

The most unequivocal way to select cluster members is by use of reliable spec-zs. However, extensive spec-z catalogues covering all our cluster sample are not available. For this study, we rely solely on photo-zs to achieve a homogeneous dataset. In Section 2.2.1, we discuss the process for deducing the photo- $z$  using `zCluster` and their accuracy.

Instead of relying on individual photo-zs from galaxies, our membership selection process uses the redshift probability distribution  $P(z)$  provided by `zCluster`. We follow a method developed by [Pelló et al. \(2009\)](#) to identify cluster members. This method builds-on a technique by [Brunner and Lubin \(2000\)](#), which calculates the probability ( $P_{\text{member}}$ ) of being a member galaxy at a redshift range centred at the cluster redshift ( $z_{\text{cl}}$ ), with a width ( $\delta z$ ) that depends on the accuracy of the photo-zs (see Section 2.2.1),

$$P_{\text{member}} = \int_{z_{\text{cl}} - \delta z}^{z_{\text{cl}} + \delta z} P(z) dz . \quad (3.1)$$

For our case,  $\delta z = n\sigma_{\text{bw}}(1 + z_{\text{cl}})$ , where  $n$  is the number of  $\sigma_{\text{bw}}$  to be used in the integration of  $P(z)$  and the  $\sigma_{\text{bw}}$  is the scatter in the redshift residual derived from the biweight scale ([Beers et al., 1990](#)). This approach works well for this study as we mainly focus on the integrated properties of the cluster galaxy population (i.e., total cluster SFR or fraction of star-forming galaxies), rather than the properties of individual galaxies. We use the three clusters in our sample with available extensive spec-zs in the literature (A209, A2744, AS1063) to calibrate cluster membership selection for the rest of the sample. We classify galaxies with spec-zs as members that satisfy the condition  $|z_{\text{cl}} - z_{\text{spec}}| < 3\sigma_{\text{cl}}(1 + z_{\text{cl}})$ , where  $\sigma_{\text{cl}}$  is the cluster velocity dispersion. The Abell 209 spec-zs were obtained from the Cluster Lensing And Supernova survey with Hubble (CLASH-VLT; [Annunziatella et al., 2016](#)) and the Arizona Cluster Redshift Survey (ACReS; described in [Haines et al., 2015](#)), see also Section 2.3.2. The spec-zs for Abell 2744 are from the Multi Unit Spectroscopic Explorer (MUSE; [Mahler et al., 2018](#)) and Anglo-Australian Telescope (AAT; [Owers et al., 2011](#)) catalogues. The

(1)	(2)	(3)	(4)	(5)	(6)
Cluster	$z_{\text{cl}}$	No. of spec-zs	$\sigma_{\text{bw}}$	$C$ (%)	$F$ (%)
Abell 209	0.206	2377 (753)	0.10	81	15
Abell 2744	0.307	971 (463)	0.06	81	13
Abell S1063	0.348	1626 (751)	0.08	84	25

Table 3.2: Quantities derived from the three clusters in our sample with spec-zs: (1) Cluster name; (2) cluster redshift; (3) the total number of matched spectroscopic galaxies within  $R_{200}$ . The number of spec- $z$  galaxies within  $|z_{\text{cl}} - z_{\text{spec}}| < 3\sigma_{\text{cl}}(1 + z_{\text{cl}})$  is shown in brackets; (4) the scatter in the redshift residual derived from the biweight estimator; (5) spec-zs completeness level; (6) fraction of spec- $z$  field galaxies.

Abell S1063 spec-zs were obtained from the CLASH-VLT catalogue ([Mercurio et al., 2021](#)).

From the stacked catalogue from the three clusters with spec-zs, we get  $\sigma_{\text{bw}} = 0.08$  from the redshift residuals,  $\Delta z/(1 + z_s)$ . The spectroscopic completeness level  $C = 82\%$  and the field contamination  $F = 17\%$  using  $n = 2$  and  $P_{\text{member}} \geq 0.5$ . The  $n$  and  $P_{\text{member}}$  values were chosen to maximise  $C$  and minimise  $F$  while selecting galaxies that are likely to be members using redshift probability distribution functions. The spectroscopic completeness level describes the number of confirmed spec- $z$  members correctly identified as members by the photo-zs selection criteria. The field contamination shows the percentage level of spec-zs that are non-members/field galaxies but selected by the photo-zs membership criteria.

The  $\sigma_{\text{bw}}$  from the stacked catalogue is higher than the one estimated with the SDSS spec-zs mentioned in section [2.2.1](#). We adopt the larger value as a more conservative estimate of the cluster member photometric redshift accuracy. Table [3.2](#) shows the  $C$  and  $F$  percentage levels reached for each cluster. We use the same selection parameters to identify members using only photo-zs for all 20 clusters, assuming a  $C > 80\%$  and  $F < 20\%$  for our full sample. We further attempt to mitigate the field contamination in two ways: (1) we check the effect of using a higher  $P_{\text{member}}$  on our results, and (2) we use  $P_{\text{member}}$  as a weight for each galaxy when investigating integrated cluster properties. We find that increasing the  $P_{\text{member}}$  threshold has

minimal effect on our overall conclusions while reducing the completeness level in the spectroscopic sample and with little change in the field contamination level.

We obtain a total of 14,419 galaxies out to  $2R_{200}$  for the W1 complete DECaLS DR8 membership sample for the 20 clusters. This gave us a sample of 3054 cluster member galaxies observed by MeerKAT. The MeerKAT-detected member galaxies sample is complete above a  $5\sigma_{\text{RMS}}$  detection limit of  $\text{SFR} = 1.9 \text{ M}_\odot \text{ yr}^{-1}$  in our most distant cluster ( $z = 0.35$ ).

### 3.3 AGN removal

Galaxies hosting active galactic nuclei (AGN) pose a significant challenge when using radio observations to estimate SFR in galaxies. Previous studies (e.g., [Sadler et al., 2002](#); [Condon et al., 2002](#); [Mauch and Sadler, 2007](#)) have shown that radio-AGN may contribute up to 50% of the radio luminosities in the local Universe at luminosities just below  $L_{1.4\text{GHz}} \approx 10^{23} \text{ W Hz}^{-1}$ , and that at luminosities over  $10^{23} \text{ W Hz}^{-1}$  AGN dominate the population over star-forming galaxies. It is therefore essential for us to remove AGN-hosting galaxies from our dataset to achieve an unbiased star-forming sample. To identify X-ray AGN, we cross-matched our member galaxies sample with the *Chandra* serendipitous source catalogue (CSC 2.0; [Evans et al., 2019](#)) and the fourth *XMM-Newton* serendipitous source catalogue (4XMM-DR11; [Webb et al., 2020](#)). X-ray sources above the rest-frame (2-10 keV) X-ray luminosity,  $L_X > 10^{42} \text{ erg s}^{-1}$  are expected to be AGN, whereas those below this limit are expected to be powered by star formation. We used the cross-matching radius of  $4''$  for both X-ray catalogues, yielding 65 and 54 sources respectively. There are four clusters in our sample with no coverage or matches within the X-ray catalogues. Of the 119 galaxies with X-ray cross-matches, we remove 94 galaxies that are above the X-ray AGN luminosity cut.

To determine additional AGN, we adopt the ‘R90’ WISE IR-selection criteria by [Assef et al. \(2018\)](#) (see also [Stern et al., 2012](#); [Assef et al., 2013](#)) for AGN classification. This uses only the WISE W1 and W2 bands to identify AGN based on their W1-W2

colour, compared to a threshold that depends on the W2 band mag (see equation 4 of [Assef et al., 2018](#), which identifies AGNs with 90% reliability). With this AGN separation method, we removed 28 sources classified as AGN-hosting galaxies from our sample.

Finally, to reduce contamination from radio-loud AGN, we apply a radio luminosity cut on our sample for galaxies with  $L_{1.4\text{GHz}} > 10^{23} \text{ W Hz}^{-1}$  ([Condon et al., 2002](#)). This cut removes 80 galaxies, some of which may be star-forming, but a relatively small number (< 3%) of the total sample. Only 30 galaxies with the luminosity above the radio-loud AGN cut are within our total sample  $R_{200}$ . Figure 3.2 shows Legacy Surveys DR9 ([Schlegel et al., 2021](#)) images of the 30 radio-loud galaxies within  $R_{200}$  of our cluster sample to visually confirm AGN status. Most of the galaxies show evidence of early-type morphology and are likely to be AGN hosts and not star-forming. A handful of galaxies show disk morphology with observed dust lanes visible across their images. We observe three galaxies within the radio-loud sample with ambiguous morphology. These are MKTCS J024536.66-525542.0 and MKTCS J224833.25-443538.0, which shows the structure that is consistent with quasar morphology and the MKTCS J051033.09-451647.8, which appears to be two galaxies colliding with two noticeable bulges and disturbed spiral arms. It is also worth noting that low luminosity radio-loud AGN may be left out by the radio luminosity cut and we assume that their number does not significantly affect our results.

After removing 203 galaxies identified as AGN hosts through the methods described above, we obtain a total sample of 2851 MeerKAT-detected galaxies out to  $2R_{200}$ , which we assume to be powered by star formation in the sections that follow. After removing 436 X-ray and WISE AGN from the photometric DECaLS DR8 selected members sample, we obtain 13,983 star-forming galaxies. Appendix A shows the Legacy Surveys DR9 ([Schlegel et al., 2021](#)) optical images of all the 20 clusters overlayed with green markers at the positions of the galaxies classified as members and radio-loud AGN.

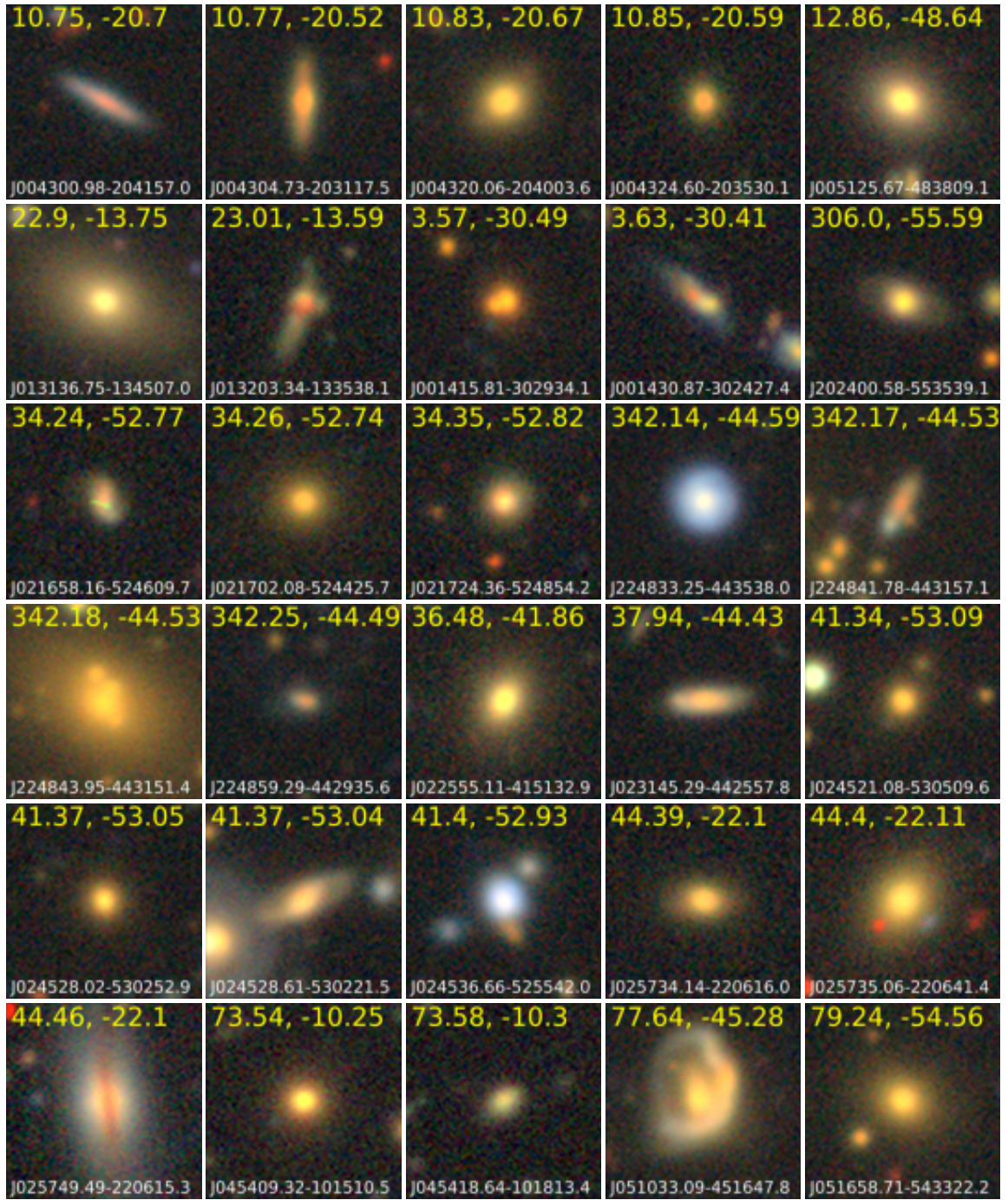


Figure 3.2: Thumbnail images of galaxies with  $L_{1.4\text{GHz}} > 10^{23} \text{ WHz}^{-1}$ . The images were produced from the Legacy Surveys DR9 (Schlegel et al., 2021) archive.

## 3.4 Star formation rates and results

To estimate the star formation rates for our cluster member galaxies identified as star-forming, we use the Bell relation showed in Equation 2.2. With a sample of galaxies with SFR estimates, we now focus our attention on investigating the SF activity of clusters with respect to the environment in the sections that follow.

### 3.4.1 Fraction of star-forming galaxies

Previous studies have shown that SF activity is suppressed with decreasing distance from the cluster centre (Balogh et al., 1998; Lewis et al., 2002; Haines et al., 2015). We study the population distribution of our radio-derived SFR for the 20 clusters with respect to their clustercentric radius in units of  $R_{200}$ . We define the fraction of star-forming galaxies as  $f_{\text{SF}} = N_{\text{SF}}/N_{\text{tot}}$ , where  $N_{\text{SF}}$  is the number of galaxies classified as star-forming cluster members and  $N_{\text{tot}}$  is the total number of cluster members. Figure 3.3 shows the  $f_{\text{SF}}$  for MeerKAT-detected sources in radial bins compared with  $f_{\text{SF}}$  results from Haines et al. (2015), obtained from infrared-derived SFR using *Spitzer*/MIPS 24 $\mu\text{m}$  observations for 30 clusters at  $0.15 < z < 0.30$  and a  $5\sigma$  detection limit of  $2 \text{ M}_\odot \text{yr}^{-1}$ . The Haines et al. (2015) study calculates SFR using the Kroupa (2002) IMF, which yields results that are nearly identical to the Chabrier (2003) IMF. The fraction of star-forming galaxies from radio observations falls within  $1\sigma$  of the  $f_{\text{SF}}$  of Haines et al. (2015) well out to  $\approx 1.7R_{200}$  and falls within  $3\sigma$  difference at  $\approx 1.9R_{200}$ . The Haines et al. (2015) cluster sample is comprised of uniformly selected clusters with no significant bias towards either merger or relaxed clusters. They notice that even at large radii,  $2R_{200}$ , the  $f_{\text{SF}}$  of clusters ( $\approx 0.23$ ) remained well below that of field galaxies ( $f_{\text{SF}} = 0.33 \pm 0.01$ ). They conclude that this is not due to cluster galaxies having higher stellar masses than field galaxies, as it is known for  $f_{\text{SF}}$  to decrease with increasing stellar mass (e.g., Haines et al., 2007). They suggest that  $f_{\text{SF}}$  being low out to large clustercentric radii may be due to the star-forming galaxies being pre-processed in lower-density environments such as galaxy groups before they enter cluster environments.

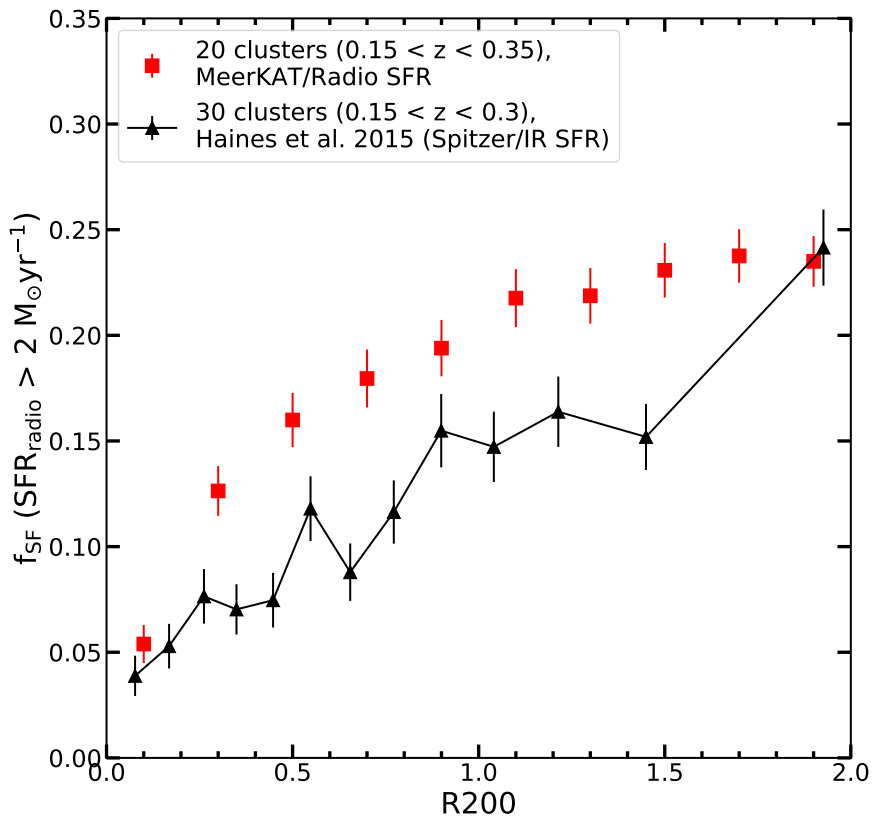


Figure 3.3: The fraction of star-forming galaxies,  $f_{\text{SF}}$  as a function of projected radial distance, in units of  $R_{200}$  from the cluster centre. We only plot MGCLS cluster members with SFR greater than the  $5\sigma$  detection limit of  $\text{SFR} = 2 \text{ M}_\odot \text{yr}^{-1}$  for comparison with IR-derived results from Haines et al. (2015) using *Spitzer*/MIPS  $24 \mu\text{m}$  fluxes down to the same SFR limit. The red squares indicate  $f_{\text{SF}}$  values for MeerKAT-detected cluster members in 20 clusters at  $0.15 < z < 0.35$  and their  $1\sigma$  uncertainties. The black triangles show the  $f_{\text{SF}}$  values by Haines et al. (2015) in 30 clusters at  $0.15 < z < 0.30$  with binomial statistics derived uncertainties.

We estimate a 23% higher SF activity in clusters with radio haloes and/or relics within  $R_{200}$  and 34% out to  $2R_{200}$ . We note that our dynamical state subsamples are unevenly distributed across the full sample redshift range as shown in Figure 3.1. The relaxed clusters fall within the lower redshift bin while unrelaxed/merging clusters are all above  $z = 0.2$ . The  $f_{\text{SF}}$  in clusters has been shown to increase with redshift, forming a relation known as the [Butcher and Oemler \(1978\)](#), hereafter BO) effect. The BO effect is the increase in the fraction of blue galaxies in clusters with redshift. Since our study uses  $f_{\text{SF}}$  to compare SF activity between subsamples, we expect some fraction of the differences in the overall cluster  $f_{\text{SF}}$  to be due to the BO effect. However, as suggested by this investigation as well as previous studies that have investigated SF activity in clusters, the dynamical state of a cluster plays an influential role in its SF activity ([Cohen et al., 2014](#); [Cohen et al., 2015](#); [Yoon and Im, 2020](#); [Stroe and Sobral, 2021](#)). Observing a homogeneous sample (not subject to MGCLS heterogeneous nature) will allow us to confirm this result and rule out whether or not the BO effect affected our results and by how much.

Figure 3.4 shows the  $f_{\text{SF}}$  of the MeerKAT cluster sample split by whether they have radio haloes/relics. Our sample has 14 clusters with extended diffuse emission in the form of radio haloes and relics (found in merging clusters) and their  $f_{\text{SF}}$  trend is shown in blue stars. The  $f_{\text{SF}}$  trend for the 6 relaxed clusters without radio haloes/relics is shown in green circles. The relaxed clusters have a shallower decline from  $1.9R_{200}$  to the centre in contrast to the steeper decline noticed in the merging clusters. Recent studies ([Cohen et al., 2014](#); [Cohen et al., 2015](#); [Yoon and Im, 2020](#)) estimate that the fraction of star-forming galaxies is 20 – 30% higher in merging clusters than in relaxed clusters. The median  $f_{\text{SF}}$  for clusters with merger activity ( $0.148 \pm 0.016$ ) in our sample is  $\approx 23\%$  higher than the relaxed clusters ( $0.120 \pm 0.011$ ) for all star-forming galaxies within  $R_{200}$ . The difference rises to  $\approx 34\%$  for all star-forming galaxies within  $2R_{200}$  between merging clusters ( $0.225 \pm 0.019$ ) and relaxed clusters ( $0.168 \pm 0.012$ ). The  $1\sigma$  errorbars are calculated using bootstrap resampling of the SF galaxies in the clusters.

Results from our study are consistent with observations made by previous studies

that looked at the effect of cluster dynamical state on SF activity. [Cohen et al. \(2014\)](#) studied 107 clusters at  $0.04 < z < 0.1$  using the Sloan Digital Sky Survey (SDSS) and uses substructure within clusters to identify clusters with multiple substructure components (mergers) from single component clusters (relaxed). They found merging clusters to have  $\approx 30\%$  more SF activity than relaxed clusters. [Yoon and Im \(2020\)](#) estimates up to  $\approx 24\%$  more SF activity within  $R_{200}$  in multiple component clusters compared to single component clusters from their study of 105 clusters at  $0.015 < z < 0.060$  using SDSS. The enhanced SF activity in merging clusters has also been observed by [Stroe and Sobral \(2021\)](#) from their study of H $\alpha$  emitters in 14 clusters at  $0.15 < z < 0.31$ . Various processes have been suggested to occur from cluster mergers that lead to the enhanced SF activity that is observed in merging clusters. [Bekki et al. \(2010\)](#) used numerical simulations to show that compressed cold gas from the rising external pressure of ICM during mergers could explain the SF activity enhancement in merging clusters. [Stroe et al. \(2017\)](#) suggests that the observed enhanced SF activity in merging clusters may be caused by shock waves in the ICM resulting from merging clusters or galaxy groups as well as the accretion of filaments. They studied the difference between merging and relaxed clusters using H $\alpha$  luminosity functions of 19 clusters at  $0.15 < z < 0.31$ , and found that merging systems have a higher characteristic density compared to relaxed systems.

In contrast to the results of these low-redshift studies, [Mansheim et al. \(2017\)](#) observed that SF activity may be suppressed in merging clusters from the study of an individual cluster system at high redshift ( $z \approx 1.105$ ). More recently, [Maier et al. \(2022\)](#) observed higher SF activity in clusters with an actively star-forming BCG (indicative of a relaxed cool-core cluster) than in clusters with passive BCGs (indicative of a non-relaxed cool-core cluster) using a study of 18 clusters at  $0.15 < z < 0.26$  from the Local Cluster Substructure Survey (LoCuSS). The [Chung et al. \(2010\)](#) study of the merging Bullet cluster argues that, depending on the cluster, mergers may not be the driver for the enhanced SF activity but could be a result of the infalling galaxy population. [Wittman \(2019\)](#) suggests that claims made by various studies that cluster mergers suppress, enhance or have no effect on SF activity may not

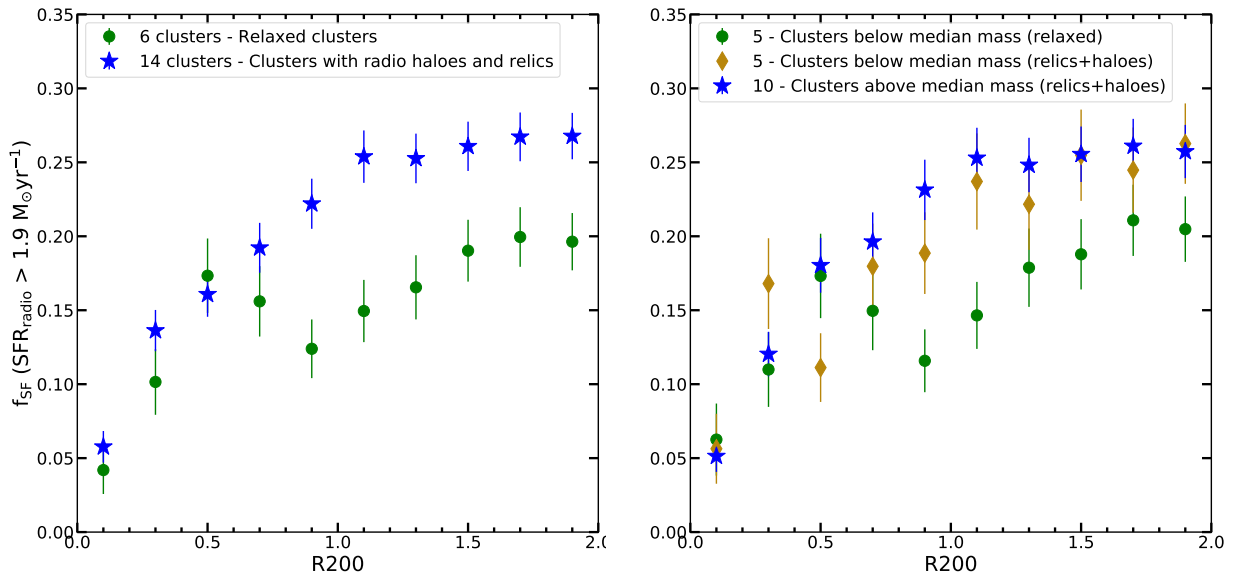


Figure 3.4: *Left panel:* The comparison of  $f_{\text{SF}}$  trends between clusters hosting radio haloes/relics (blue star markers) and relaxed clusters (green circles). *Right panel:* The  $f_{\text{SF}}$  trends of clusters split by median cluster mass ( $1.09 \times 10^{15} M_{\odot}$ ) and by cluster dynamical state. The clusters above the median mass are shown by blue star markers and the clusters below the median mass are shown in green circles (those hosting relics and haloes) and brown diamond markers (relaxed systems).

be conflicting but can be explained by how much time has passed since the pericenter passage (the age of the merger), the relative velocity at the first pericenter, and the viewing angle.

### 3.4.2 Total star formation rate and cluster mass relation

To investigate how our cluster sample SFR relates with cluster mass, we summed the SFR for member galaxies within  $R_{200}$  and plotted them against cluster masses as shown in Figure 3.5. The clusters that have been identified to have merger-related extended radio emission are plotted in black markers and relaxed clusters are plotted in orange markers. Figure 3.5 shows that the total SFR ( $\Sigma\text{SFR}$ ) correlates not only with cluster mass but is also dependent upon the dynamical state of the cluster. This result is consistent with recent claims that mergers enhance SF activity in clusters at low redshifts (e.g., Cassano et al., 2013; Cohen et al., 2014; Stroe and Sobral, 2021). We observe a marginal difference (within  $3\sigma$ ) between median values for mass normalised total SFR in relaxed clusters ( $21.5 \pm 1.9 \text{ M}_\odot \text{yr}^{-1}/10^{14}\text{M}_\odot$ ) and clusters with merger activity ( $26.1 \pm 1.6 \text{ M}_\odot \text{yr}^{-1}/10^{14}\text{M}_\odot$ ). The errors on the median values were estimated from bootstrap resampling.

We observe a linear correlation between  $\Sigma\text{SFR}$  and cluster mass ( $M_{200}$ ), consistent with results from previous studies (e.g., Goto, 2004; Popesso et al., 2006). This correlation has been described as a richness effect,  $\Sigma\text{SFR} \propto N_{\text{gal}}$ , where  $N_{\text{gal}}$  is the number of galaxies in a cluster. The number of galaxies in a cluster scales with cluster mass in that the higher the mass, the higher the number of star-forming galaxies. Figure 3.5 shows the linear correlation of  $\Sigma\text{SFR}$  and  $M_{200}$ . We also observe the contribution of cluster dynamical state to the  $\Sigma\text{SFR}$ , something that was not considered by previous studies. The contribution of cluster dynamical state is particularly evident along clusters with mass estimates within  $1\sigma$  of each other but with different relaxation states. This difference is noticeable in clusters within the mass range  $0.8 - 1.2 \times 10^{15} \text{ M}_\odot$ . There are eight clusters that fall within this range and we observe that the median  $\Sigma\text{SFR}$  for relaxed clusters ( $172.3 \pm 12.1 \text{ M}_\odot \text{yr}^{-1}$ ) is  $\approx 0.5 \times$  lower than the one for clusters with radio haloes and/or relics ( $309.2 \pm 42.9 \text{ M}_\odot \text{yr}^{-1}$ ). The errors on the median

values were estimated from bootstrap resampling.

As described in Section 2.1, the MGCLS catalogue is a heterogeneous sample composed of two non-uniformly selected subsamples. One from the radio-selected subsample (biased towards massive clusters with extended diffuse emission) and the other from the X-ray-selected subsample with no prior biases towards or against clusters with extended diffuse emission but selected with no redshift or X-ray luminosity criteria followed. Our cluster sample is biased towards clusters with extended radio emission, albeit equally split between clusters from each MGCLS subsample. To check our results, we look at clusters from the X-ray-selected subsample by splitting clusters in our sample by their MGCLS subsamples and re-plotting Figure 3.5.

Figure 3.6 shows the plot of  $\Sigma\text{SFR}$  versus  $M_{200}$  for clusters in our sample separated into each respective subsample. The left panel shows the plot of the clusters from the radio-selected subsample and the right panel shows the plot of the clusters from the X-ray-selected subsample. Although clusters from the X-ray-selected sample are limited in quantity, a correlation between  $\Sigma\text{SFR}$  and  $M_{200}$  is observed in the right panel of Figure 3.6. Results from the X-ray-selected clusters are consistent with merging clusters having higher SF activity than relaxed clusters. Due to the limitation of a small cluster sample, future observations of a larger sample will be required to confirm these results.

We observe one halo-hosting cluster, J0225.9-4154 (J0225 hereafter), that has a  $\Sigma\text{SFR}$  profile of relaxed clusters at its mass on the X-ray subsample. Dynamical state studies of J0225 reveal that it is an interesting binary cluster system of two merging clusters (A3017 and A3016) connected by an X-ray filament (see Foëx et al., 2017b; Parekh et al., 2017; Chon et al., 2019, for detailed reviews of the on-going merger). Dynamical studies show that J0225 is a face-on merger at its early stage with multiple substructures within its virial radius. The dynamical mass estimate ( $M_{200}$ ) for J0225 according to Foëx et al. (2017b) is  $18.6^{+2.6}_{-2.0} \times 10^{14} M_\odot$  but after accounting for the substructure in the line of sight they obtain an estimate of  $8.4^{+1.3}_{-1.5} \times 10^{14} M_\odot$ . Their estimate is in good agreement with the mass estimate from the Planck Sunyaev-Zeldovich sources catalogue (PSZ2, Planck Collaboration et al., 2016) re-scaled to

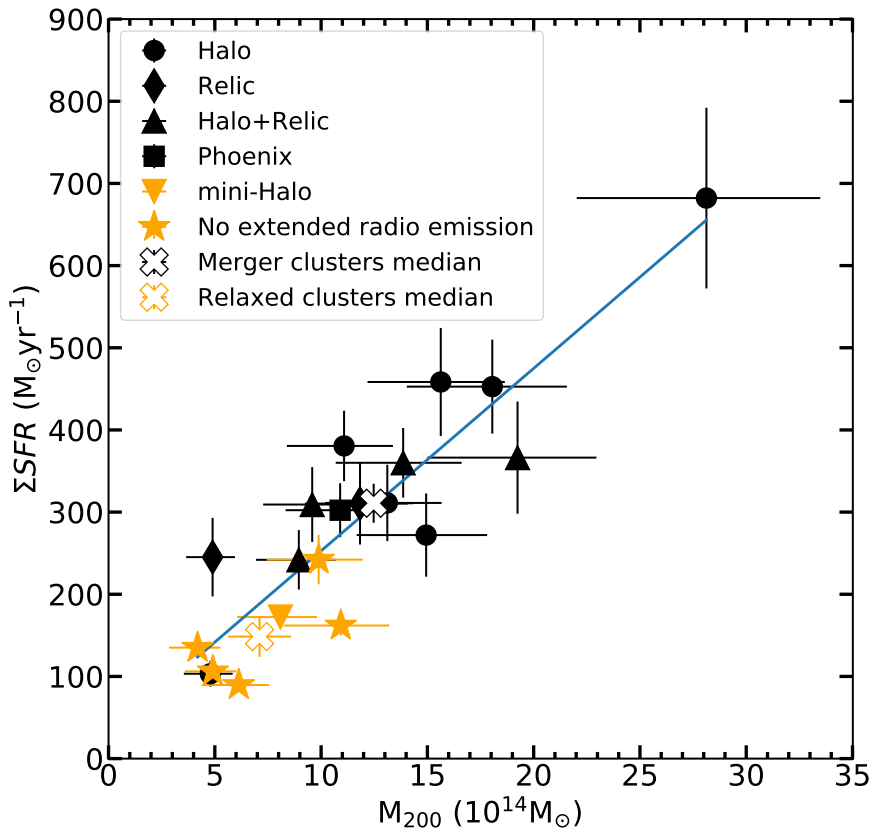


Figure 3.5: Total SFR in MGCLS clusters plotted against their cluster masses. Clusters with extended radio emission linked to merger activity are plotted in black markers (Clusters hosting only haloes are plotted in dots, those hosting haloes and relics are in upward-facing triangles and the ones with only relics and a phoenix are in diamonds and squares respectively). Relaxed clusters are plotted in orange markers (relaxed clusters with no diffuse emission are shown in star markers and the mini-halo is indicated by a downward-facing triangle). The error bars indicate  $1\sigma$  uncertainties. The median values for relaxed and merging clusters are shown by the X-shaped markers with bootstrapped resampled errorbars. The blue line shows the least-squares line of best fit derived from the full cluster sample between the mass limits  $4.19 < M_{200}(10^{14}M_\odot) < 28.13$

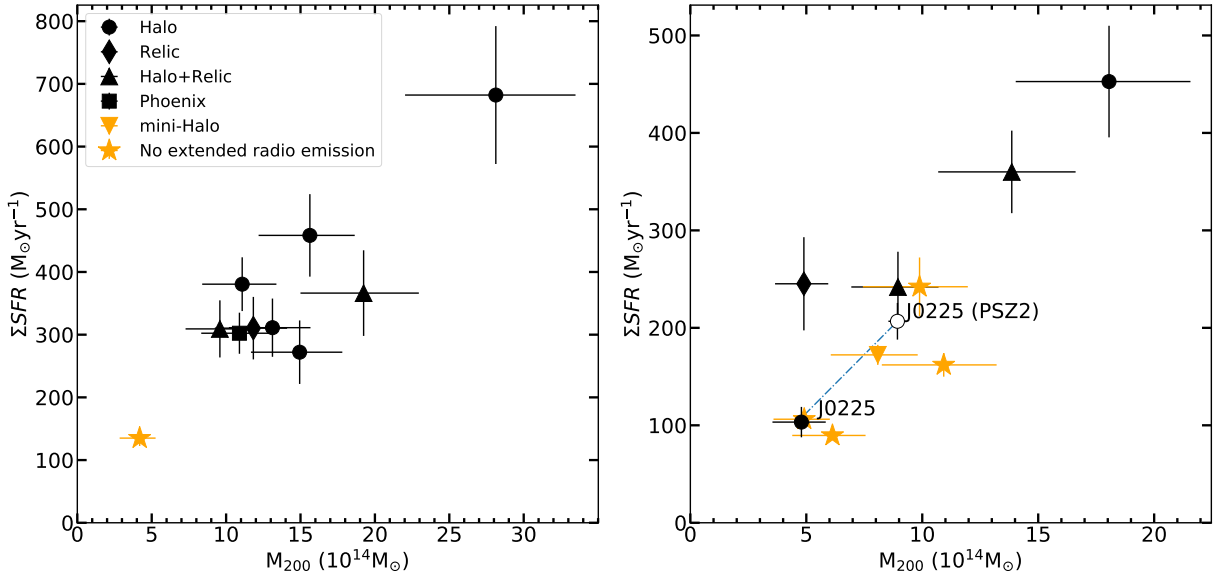


Figure 3.6:  $\Sigma\text{SFR} - M_{200}$  relation for clusters from the MGCLS radio-selected (*left*) and the X-ray-selected (*right*) subsamples. The open symbol shows the  $\Sigma\text{SFR} - M_{200}$  for cluster J0225.9-4154 (J0225) at the Planck SZ mass estimate from the Planck Sunyaev-Zeldovich sources catalogue (PSZ2, [Planck Collaboration et al., 2016](#)). The dashed blue line shows the difference between the  $\Sigma\text{SFR} - M_{200}$  from the ACT DR5 mass estimate and the PSZ2 mass estimate.

$M_{200}, 8.9 \pm 0.4 \times 10^{14} M_\odot$ . The [Foëx et al. \(2017b\)](#) and the PSZ2 mass estimate for J0225 are approximately double the ACT DR5 mass estimate ( $4.8_{-1.0}^{+1.2} \times 10^{14} M_\odot$ ) but fall within  $3\sigma$  of each other. The right panel of Figure 3.6 includes the data point for  $\Sigma\text{SFR}$  at the PSZ2 mass estimate for J0225 and shows the difference in  $\Sigma\text{SFR}$  between the two mass estimates of the cluster. The  $\Sigma\text{SFR}$  from the PSZ2 mass estimate is higher by a factor of 1.6 and has  $R_{200}$  at 1.9 Mpc, 1.3 $\times$  higher than  $R_{200}$  from the ACT DR5 mass estimate. The extraordinary nature of J0225 raises the need for a multi-wavelength analysis to get a clear picture of its properties.

Figure 3.7 shows the  $f_{\text{SF}}$  profiles of our clusters broken down by their subsample. The radio-selected subsample comprises 9 merger-linked extended diffuse emission clusters and one relaxed cluster in the redshift range  $0.15 < z < 0.35$ . The X-ray-selected clusters subsample is evenly distributed between 5 merger-linked extended diffuse emission clusters and 5 relaxed clusters also in the redshift range of  $0.15 <$

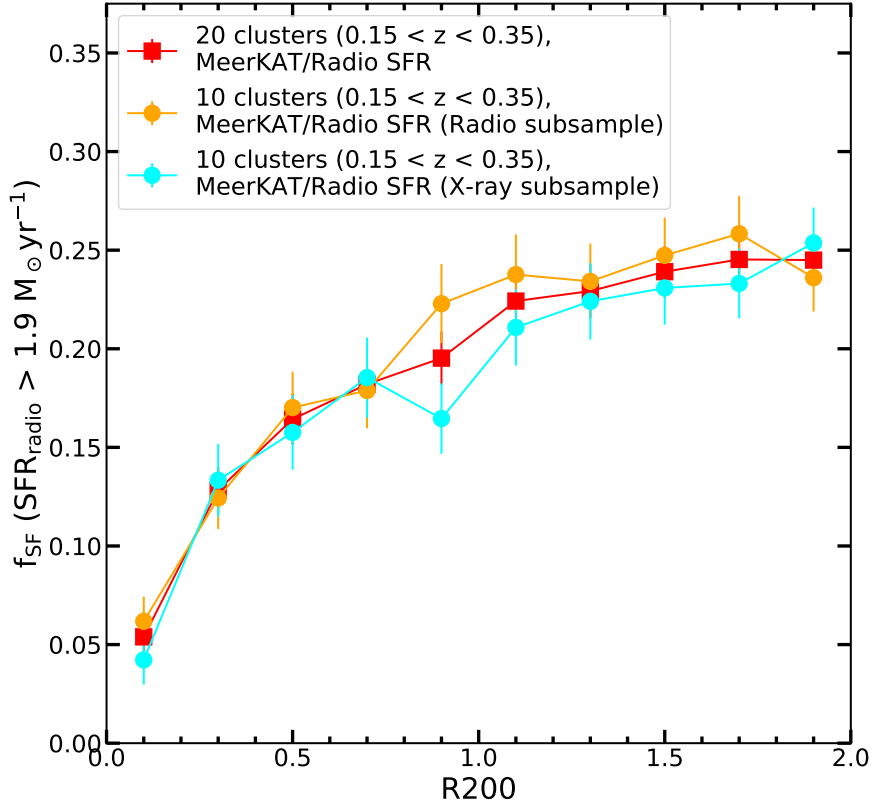


Figure 3.7: The fraction of star-forming galaxies including trends for clusters split by their MGCLS subsamples. The  $f_{\text{SF}}$  trend for clusters from the radio-selected subsample is plotted in orange dots and the trend for clusters from the X-ray-selected subsample is plotted in cyan dots.

$z < 0.35$ . The radio-selected subsample has an  $f_{\text{SF}}$  of  $0.253 \pm 0.019$  within  $2R_{200}$  while the X-ray-selected subsample is  $0.241 \pm 0.012$  out to the same radius. The  $1\sigma$  errorbars are calculated using bootstrap resampling of the SF galaxies in the clusters. The radio-selected  $f_{\text{SF}}$  trend is slightly higher than that of the X-ray-selected sample and the  $f_{\text{SF}}$  values lie within  $1 - 1.5\sigma$  between the subsamples. The observed higher  $f_{\text{SF}}$  trend of the radio-selected subsample is likely due to the selection bias towards massive merger-linked clusters with haloes and/or relics.

### 3.4.3 Normalized total star formation rates and redshift relation

A number of recent studies have examined the evolution of SF activity with redshift in clusters by using the total SFR per cluster mass for clusters hosting luminous infrared galaxies (LIRGs) (e.g., Popesso et al., 2012; Haines et al., 2013; Webb et al., 2013). This is done by summing the SFR of individual galaxies that are confirmed to be members within  $R_{200}$  for each cluster and normalising it by  $M_{200}$ ,  $\Sigma(\text{SFR})/M_{200}$ . This approach enables the comparison of SF activity for clusters with different masses. Although methods employed by the various studies to define cluster properties differ from one another, including this one, they all consistently come to the conclusion of a rapid decline in SF activity within clusters with decreasing redshift.

To understand the evolution of SF activity within our sample, we follow the analysis of Popesso et al. (2012), hereafter Po12, which studies the  $\Sigma(\text{SFR})/M_{200}$  – redshift relation for LIRGs in rich/massive clusters and groups/poor clusters at  $0.1 < z < 1.6$  using infrared luminosities from *Herschel*/PACS  $100\mu\text{m}$  and  $160\mu\text{m}$ . Following Po12, we summed up the SFR of all the MeerKAT galaxies with SFR values above the LIRG luminosity limit corresponding to  $L_{1.4\text{GHz}} \approx 3.14 \times 10^{22} \text{ W Hz}^{-1}$  or  $10 \text{ M}_\odot \text{yr}^{-1}$  in SFR for each of the 20 clusters in our sample. All clusters in our sample contain at least one LIRG within  $R_{200}$ . Figure 3.8 shows a plot of  $\Sigma(\text{SFR})/M_{200}$  – redshift relation for our sample including results from Po12 scaled down by 1.74 from the Salpeter IMF to Chabrier IMF. Figure 3.8 includes results from Haines et al. (2013), hereafter Ha13, which also followed the Po12 study of LIRGs at  $0.15 < z < 0.3$  using infrared luminosities from *Spitzer*/MIPS  $24\mu\text{m}$ . It is worth noting that there are differences in cluster mass estimation methods between our study and both the Po12 and the Ha13 studies. The Po12 study uses dynamical mass estimates derived from optical spectroscopy and the Ha13 study relies on X-ray-derived masses. This means that for clusters that are common among the studies, the total SFR within  $R_{200}$  would be estimated out to different radii, due to differences in the mass measurements between the studies.

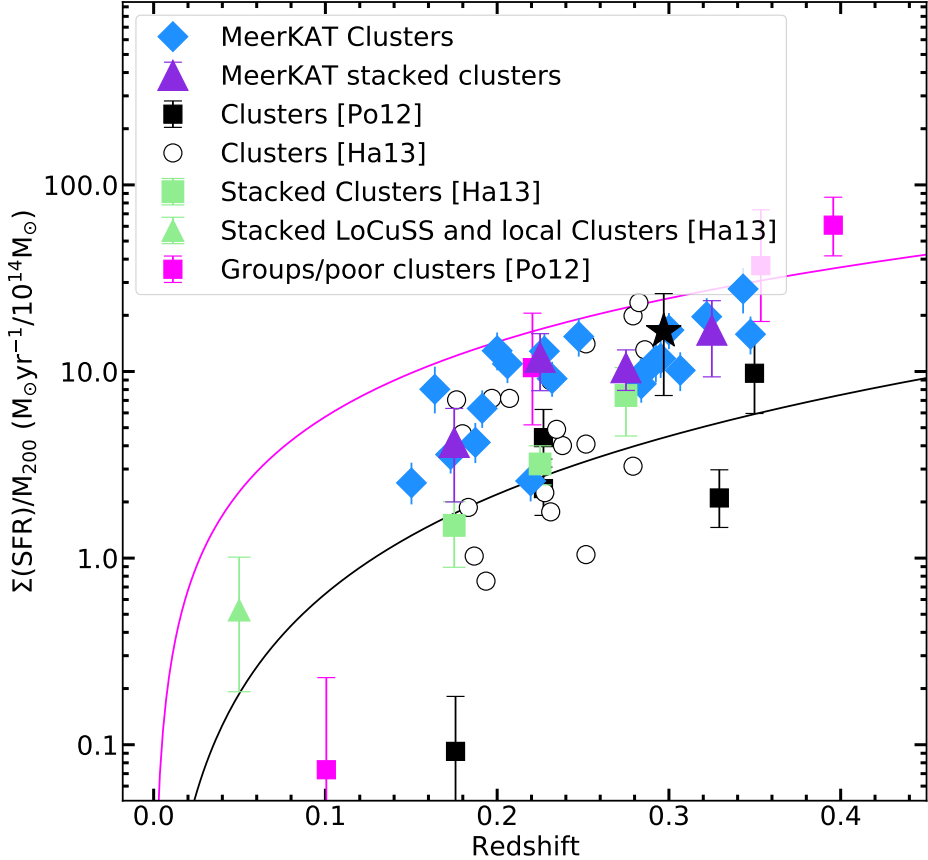


Figure 3.8: The Evolution of  $\Sigma(\text{SFR})/M_{200}$  - redshift relation among cluster LIRGs. The blue diamonds indicate the total SFR normalised by the cluster mass for all the cluster LIRGs within  $R_{200}$  for each MGCLS cluster as a function of redshift. The purple triangles indicate the averaged values for the MGCLS clusters in four redshift bins in steps of 0.5. There are six clusters at  $0.15 < z < 0.20$ , six clusters at  $0.20 < z < 0.25$ , six clusters at  $0.25 < z < 0.30$  and five clusters at  $0.30 < z < 0.35$ . We use bootstrap resampling in the  $\Sigma(\text{SFR})/M_{200}$  scatter of clusters in each bin to estimate  $1\sigma$  uncertainties. The Ha13 clusters are indicated by black rings and their redshift binned average values are shown in green squares. Ha13 also included the analysis of local clusters at  $0.02 < z < 0.05$  shown by the green triangle. The black and magenta squares are from the Po12 clusters and groups respectively which are made up of composite systems from GOODS, COSMOS and individual systems. The black star indicates the merging Bullet cluster also from Po12. The black curve shows the best fit  $\Sigma(\text{SFR})/M_{200}$  relation for the Po12 cluster sample excluding the Bullet cluster and the magenta curve shows the relation for the group/poor clusters sample. The Po12 clusters and groups best-fit lines were deduced from their study of clusters and groups at  $0.1 < z < 1.6$ . For our study, we plot the Po12 best-fit lines at the part that highlights our redshift slice.

None of the clusters in our sample overlap with the Po12 cluster sample and only one cluster from our sample (Abell 209) appears in the Ha13 study. The  $\Sigma(\text{SFR})/M_{200}$  value for Abell 209 from Ha13 is  $\approx 7.1 \text{ M}_\odot \text{yr}^{-1}/10^{14} \text{M}_\odot$ . This is within  $1.5\sigma$  of our estimated value for the same cluster,  $(10.99 \pm 2.69) \text{ M}_\odot \text{yr}^{-1}/10^{14} \text{M}_\odot$ .

We estimate the overall evolutionary trend by dividing our cluster sample into four redshift bins as indicated by the purple triangles in Figure 3.8. We observe a  $\approx 4\times$  decline in the level of SF activity per cluster mass in MeerKAT clusters in contrast to the  $\approx 5\times$  decline seen by Ha13 in green squares over the  $0.15 < z < 0.3$  redshift slice. Just as observed in Ha13, we also see a decline in the number of cluster LIRGs with redshift bins, reducing from 87 LIRGs in 5 cluster systems at  $0.3 < z < 0.35$  to 10 LIRGs in 5 systems at  $0.15 < z < 0.20$ .

Figure 3.8 includes the  $\Sigma(\text{SFR})/M_{200}$  of the Bullet cluster from Po12 (indicated by the black star), which is known to have an ongoing violent merger. The Bullet cluster has a higher  $\Sigma(\text{SFR})/M_{200}$ , consistent within errorbars with the clusters in our sample, most of which host extended radio emission linked to merger activity. Even with noted differences in our study and those from other authors, the evolutionary trend for MGCLS clusters also indicate that there is a rapid decline in star formation activity among cluster galaxies at lower redshifts, roughly consistent with observations made by Po12 and Ha13.

### 3.5 Summary

We have studied SF activity in cluster environments at low redshifts ( $0.15 < z < 0.35$ ) using dust-unbiased radio continuum data from the MGCLS. This provides the first-look at SFR in clusters using radio data from the MeerKAT telescope. The investigation of SF activity in and around clusters is crucial in understanding how galaxies evolve with time in high-density environments and how the dynamical state of a cluster affects SF activity in galaxies. Below is the summary of our main results:

We measure a  $f_{\text{SF}}$  population trend out to a similar limit at  $2R_{200}$  with the Haines et al. (2015) study, noting a  $1-3\sigma$  difference between the radio SFR and IR SFR

data points which is likely due to the MGCLS selection bias towards merger-linked clusters. Both the radio-derived and IR-derived  $f_{\text{SF}}$  are lower than the [Haines et al. \(2015\)](#) field galaxies  $f_{\text{SF}}$  even at  $2R_{200}$ . This is consistent with the suggestion that in-falling galaxies may be pre-processed in their prior environments such as galaxy groups, before they enter cluster environments, which could explain the lower  $f_{\text{SF}}$  even at radii over  $2R_{200}$ .

There is a difference in SF activity between clusters that host extended radio emission (relics and haloes) linked to cluster mergers and clusters that are non-halo/relic hosting, likely to be dynamically relaxed or only minor mergers. We see the differences in the  $f_{\text{SF}}$  as well as the  $\Sigma\text{SFR}$  between merging clusters and relaxed clusters. merging clusters have a higher fraction of star-forming galaxies and consequently a higher  $\Sigma\text{SFR}$  compared to relaxed clusters.

We find a rapid decline in the SF evolutionary trend among radio-selected galaxies with SFR corresponding to those of cluster LIRGs in our sample. We observe a  $\approx 4\times$  decline in  $\Sigma\text{SFR}/M_{200}$  from redshift of 0.35 till 0.15, corresponding to 2 Gyr in lookback time. This observation is roughly consistent with IR-derived SFR studies by [Popesso et al. \(2012\)](#) and [Haines et al. \(2013\)](#).

# Chapter 4

## Star formation activity in MGCLS clusters with haloes and relics

As discussed in the previous Chapters, galaxy clusters grow hierarchically through merging with other clusters and sub-clusters/groups (see e.g., Sarazin, 2002, and Section 1.3.2 of this thesis). Some merging clusters have been observed to host both radio haloes and relics. Suggestions have been made about both the present radio haloes and relics in merging clusters originating from the same formation mechanisms (Feretti et al., 2012). Systems hosting radio haloes and relics are uncommon and only about a dozen have been discovered so far (Feretti et al., 2012). Half a decade ago, Bonafede et al. (2017) conducted a study to assess the period when haloes appear during a merger using clusters with radio relics as a proxy for the time passed since the merger started. They found that clusters without haloes fall either in the early or later stages of the merger while halo and relic-hosting systems lie at a similar evolutionary stage.

The aim of this chapter is to study a sample of clusters hosting radio haloes and double relics to investigate how their SF activity relates to their environment. We investigate the relation of the SF activity to the time that has passed since the merger started using the distance of the relics from the cluster cores. We also investigate the differences in the SF activity between galaxies close to or along the path of the relic/shock wave and those away from the relic.

## 4.1 Data sample and analysis

We select a subsample of radio haloes and relics-hosting clusters from the sample that was constructed and described in Chapter 3 under Section 3.1. We identify four clusters that host at least one previously detected relic by other instruments. The relic-hosting clusters each have a radio halo, two double relics each (Abell 2744 and J0516.6-5430) while the other two clusters also host one double relic, and contain one candidate relic (J2023.4-5535 and Abell 521) each.

Below, we briefly discuss the properties of each cluster and list their MeerKAT observed properties in Table 4.1. The properties of the radio relics are shown in Table 4.2. These include the integrated flux densities (provided by Kolokythas et al., *in preparation*) and derived mean spectral indices for the radio relics obtained from the spectral index maps that are in the MGCLS DR1 image cubes. The spectral index maps were derived over the 908–1656 MHz frequency range (see Knowles et al., 2022). We compare the MeerKAT-derived spectral indices to those from the literature for previously detected radio relics under each cluster discussion.

### 4.1.1 Cluster sample

The Abell 521 cluster has had extensive coverage at X-ray (e.g., Ferrari et al., 2006; Bourdin et al., 2013; Yoon et al., 2020) and at radio wavelengths which reveal a radio halo ( $\approx 1$  Mpc) and a prominent relic ( $\approx 1.35$  Mpc) South East of the cluster (see e.g., Ferrari et al., 2006; Giacintucci et al., 2008; Macario et al., 2013). Multiwavelength observations show that Abell 521 is a highly disturbed system of at least three sub-clusters undergoing a complex merger (Yoon et al., 2020). Knowles et al. (2022) reported the detection of a new candidate relic (see Figure 4.1) in the North West direction of the cluster which is smaller and fainter than the previously observed South East relic. The Abell 521 relic pair has a configuration in the North-West South-East direction and has been noted as a double relic system (Stuardi et al., 2022). The Abell 521 South East relic spectral index has been estimated to be  $-1.45 \pm 0.02$  between the 153 MHz and 5 GHz frequency range (Macario et al., 2013). The MeerKAT-derived

(1)	(2)	(3)	(4)	(5)	(6)	(7)	(8)	(9)
Cluster	RA	DEC	z	$M_{200}$	$R_{200}$	$f_{SF}$	$\Sigma SFR$	$T_X$
				( $10^{14} M_\odot$ )	(Mpc)		( $M_\odot \text{yr}^{-1}$ )	(keV)
Abell 2744	3.578333	-30.383333	0.307	$19.2^{+4.2}_{-3.7}$	2.3	0.113	$366.31 \pm 68.29$	$8.5 \pm 0.3$ [a]
Abell 521	73.537917	-10.238611	0.248	$9.6^{+2.3}_{-2.0}$	1.9	0.132	$309.21 \pm 45.54$	$5.9 \pm 0.2$ [b]
J0516.6-5430	79.158333	-54.514167	0.295	$9.0^{+2.0}_{-1.8}$	1.8	0.108	$241.93 \pm 36.16$	$7.5 \pm 0.3$ [c]
J2023.4-5535	305.850000	-55.591700	0.232	$13.9^{+3.2}_{-2.8}$	2.1	0.201	$360.01 \pm 42.34$	$8.0 \pm 0.8$ [d]

Table 4.1: Properties for relic-hosting clusters. Columns: (1) Name of the cluster; (2,3) MeerKAT pointing coordinates: J2000 Right Ascension and Declination in degrees; (4) cluster redshift; (5) cluster mass in  $10^{14} M_\odot$ ; (6) cluster  $R_{200}$  in Mpc; (7) the fraction of all star-forming galaxies within  $R_{200}$  (see Section 3.4.1); (8) total SFR for galaxies within  $R_{200}$  (see Section 3.4.2); (9) the global X-ray temperature of the cluster. References: [a] [Mantz et al. \(2010\)](#); [b] [Ferrari et al. \(2006\)](#); [c] [Zhang et al. \(2006\)](#); [d] [HyeongHan et al. \(2020\)](#).

value ( $\alpha = -1.48 \pm 0.15$ ) is consistent with the estimate from [Macario et al. \(2013\)](#).

The J2023.4-5535 cluster's radio halo and relic have been recently reported by [HyeongHan et al. \(2020\)](#) through a multiwavelength study at optical, X-ray and radio wavelengths. [HyeongHan et al. \(2020\)](#) reports a  $\approx 2$  Mpc giant radio halo and a  $\approx 0.5$  Mpc radio relic West of the cluster from deep observations using the Australian Square Kilometre Array Pathfinder - Evolutionary Map of the Universe (ASKAP-EMU; [Norris et al., 2011](#)). MeerKAT observations also reveal the radio halo and the prominent West relic. Although this was not reported on the MGCLS first data release, MeerKAT also reveals what could be a very faint twin relic along a chain of galaxies in the South East direction of the cluster (see Knowles et al., *in preparation* and Figure 4.1 for a visual). [HyeongHan et al. \(2020\)](#) estimates the spectral index of  $-0.76 \pm 0.06$  for the West relic from a narrow bandwidth between 800 MHz and 1088 MHz. The MeerKAT-derived spectral index is  $-1.48 \pm 0.15$ , and has a  $5\sigma$  difference with the one estimated by [HyeongHan et al. \(2020\)](#) from the narrowband.

Abell 2744 is one of the most studied clusters and has been extensively observed at optical, X-ray, and radio wavelengths (e.g., [Owers et al., 2011](#); [Merten et al., 2011](#); [Pearce et al., 2017](#)). Its dynamical state has been revealed to be highly disturbed

by optical and X-ray observations (Owers et al., 2011; Merten et al., 2011), with evidence of four sub-clusters undergoing a merger. Abell 2744 is known to host a giant  $\approx 2.1$  Mpc radio halo and an  $\approx 1.5$  Mpc radio relic in the North East direction (see e.g., Pearce et al., 2017; Paul et al., 2019; Rajpurohit et al., 2021). Using the deep observations from the Very Large Array radio telescope, Pearce et al. (2017) discovered three new faint radio relics (see also, Rajpurohit et al., 2021, using the VLA and upgraded Giant Metre Radio Telescope (uGMRT) multiwavelength observations). MeerKAT detected two of the four relics: the prominent North East relic, and the faint South East relic (see Figure 4.2). MeerKAT-derived spectral indices for the North East relic and South East relic are  $-1.28 \pm 0.13$  and  $-1.21 \pm 0.08$  respectively. These values are consistent within  $1\sigma$  of those reported by Rajpurohit et al. (2021) from wide bandwidth observations between 150 MHz and 3 GHz. They estimated  $-1.17 \pm 0.03$  for the North East relic, and  $-1.19 \pm 0.05$  for the South East relic.

J0516.6-5430 has been detected and studied in detail at X-ray wavelengths (Böhringer et al., 2004; Zhang et al., 2006; Weißmann et al., 2013). J0516.6-5430 also featured in the optical Abell et al. (1989) supplementary southern catalogue. Foëx et al. (2017a) studied the cluster at X-ray and optical wavelengths and reports a large amount of substructure seen in the galaxy surface density map and a bimodal core in the North-South axis. There have not been many observations at radio wavelengths. The halo and double relics in the cluster are from observations done by MeerKAT and will be covered in more detail in Kolokythas et al., *in preparation*. The J0516.6-5430 relic pair has a North-South configuration and comprise a prominent relic in the North and a smaller fainter relic in the South (see Figure 4.3). This relic pair has the largest radius from the cluster centre. The MeerKAT-derived spectral indices for this pair are  $-1.28 \pm 0.11$  for the North relic and  $-1.11 \pm 0.11$  for the South relic.

With an identified and briefly discussed sample of haloes and double relic systems, we now move on to analysing the sample to look for any signatures of environmental dependence of the SF activity in the clusters. The cluster membership selection criteria, estimation of SFR and  $f_{\text{SF}}$  are described in Sections 3.2 and 3.4.

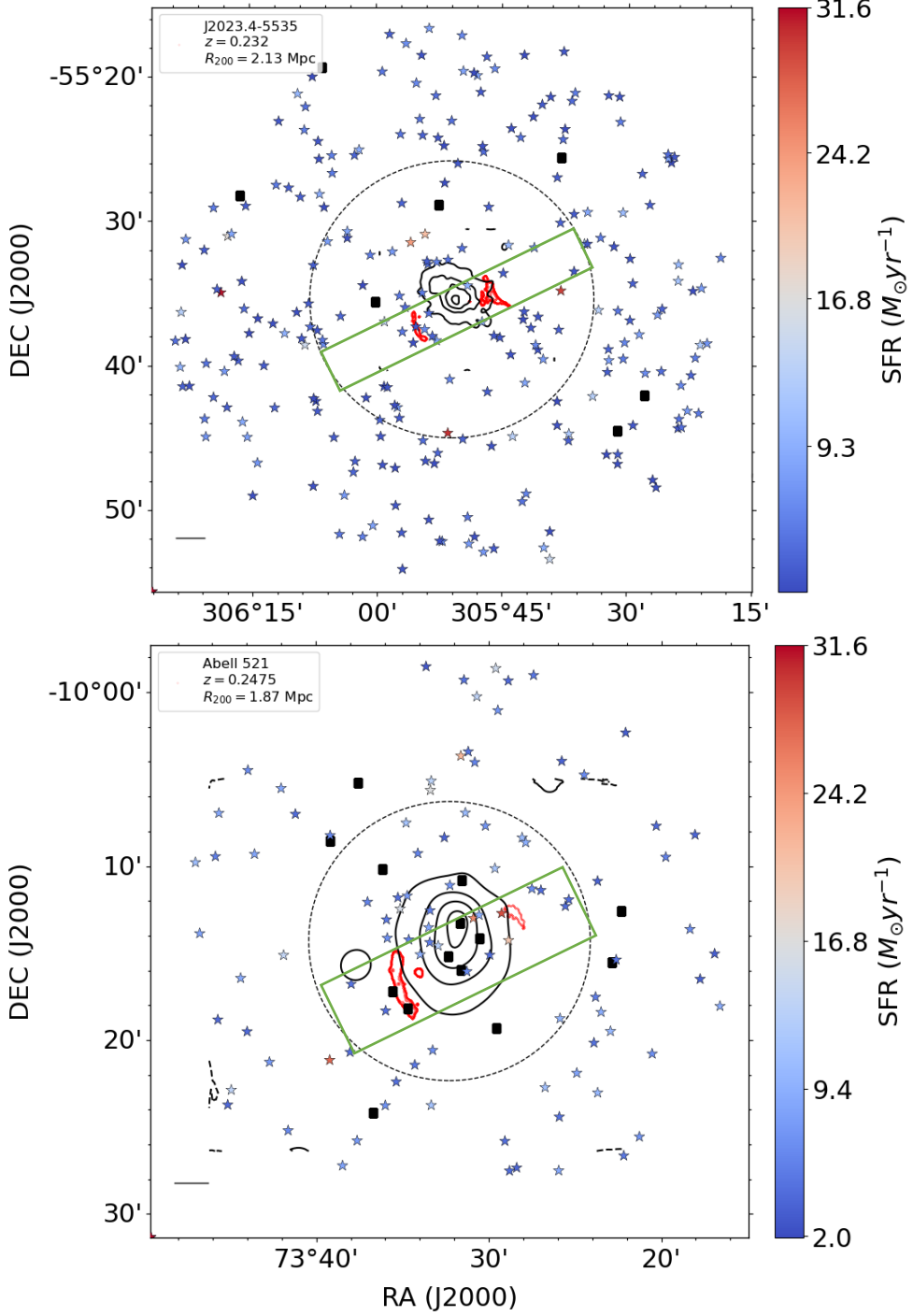


Figure 4.1: *Top*: The view of the J2023.4-5535 cluster with MeerKAT-detected galaxies identified as members shown in star symbols. A divergent colour scheme shows the SFR of each galaxy based on the colour scale on the right. The black squares show the galaxy members flagged as AGN. The red contour lines show the position and relative sizes of the radio relics detected by MeerKAT. Only the relic contours are included from the radio images. The radio contours around the relics are at the levels of  $[1, 2, 3, 4] \times 3\sigma_{\text{rms}}$ ,  $\sigma_{\text{rms}} = 3.8 \mu\text{Jy beam}^{-1}$ . The black contours show the smoothed archival *XMM-Newton* X-ray contours. The straight black line at the bottom left shows the 2' scalebar. *Bottom*: The view of the Abell 521 cluster and its identified member galaxies. The radio contours around the relics are at the levels of  $[1, 2, 3, 4] \times 3\sigma_{\text{rms}}$ ,  $\sigma_{\text{rms}} = 4.8 \mu\text{Jy beam}^{-1}$ .

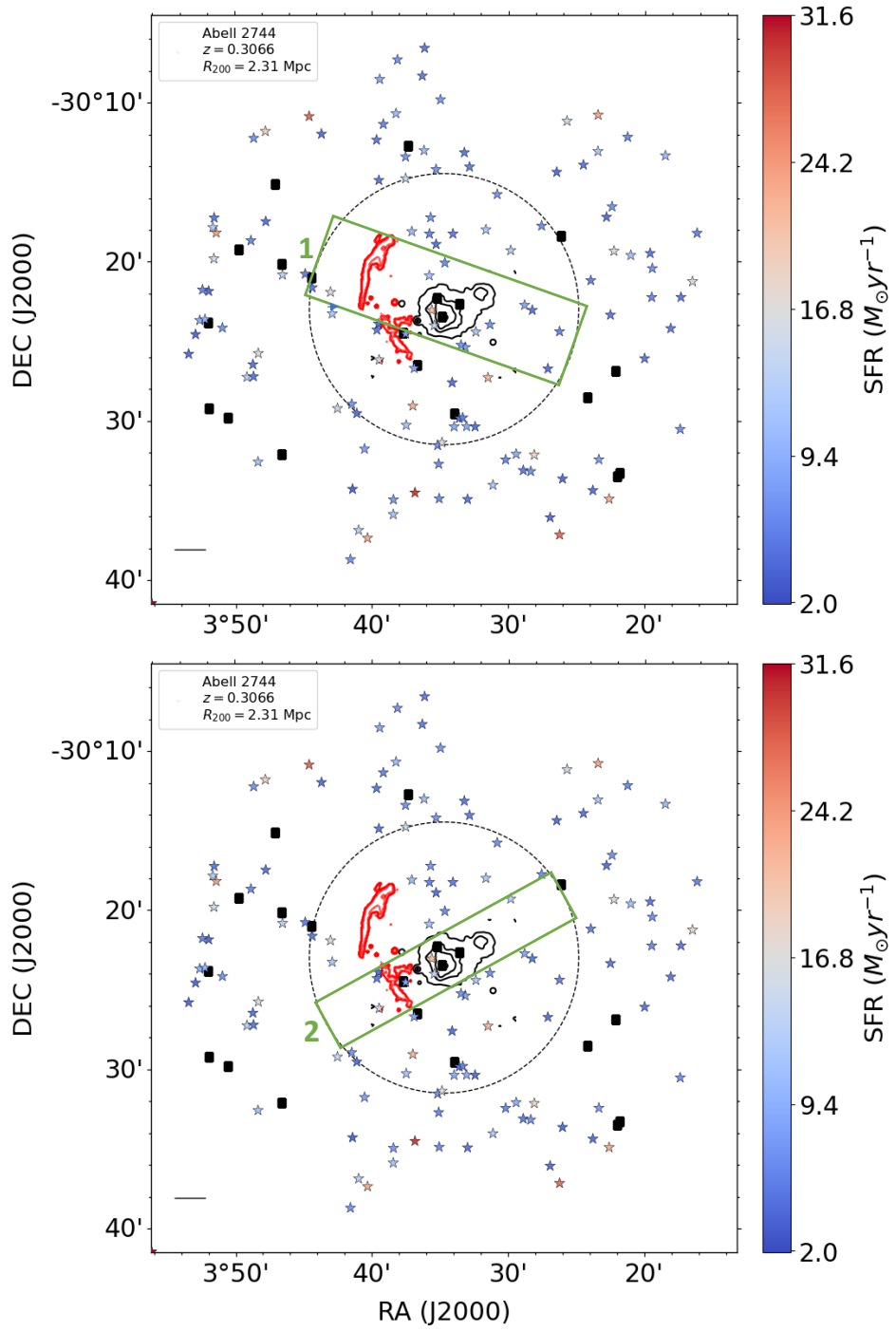


Figure 4.2: *Top:* The view of the Abell 2744 cluster and the assumed shock wave path for relic 1. *Bottom row:* The view of the Abell 2744 cluster and the assumed shock wave path for relic 2. The symbols, shapes and contours are described in Figure 4.1. The radio contour levels for Abell 2744 are  $[1, 2, 3, 4] \times 3\sigma_{\text{rms}}$ ,  $\sigma_{\text{rms}} = 4.1 \mu\text{Jy beam}^{-1}$ .

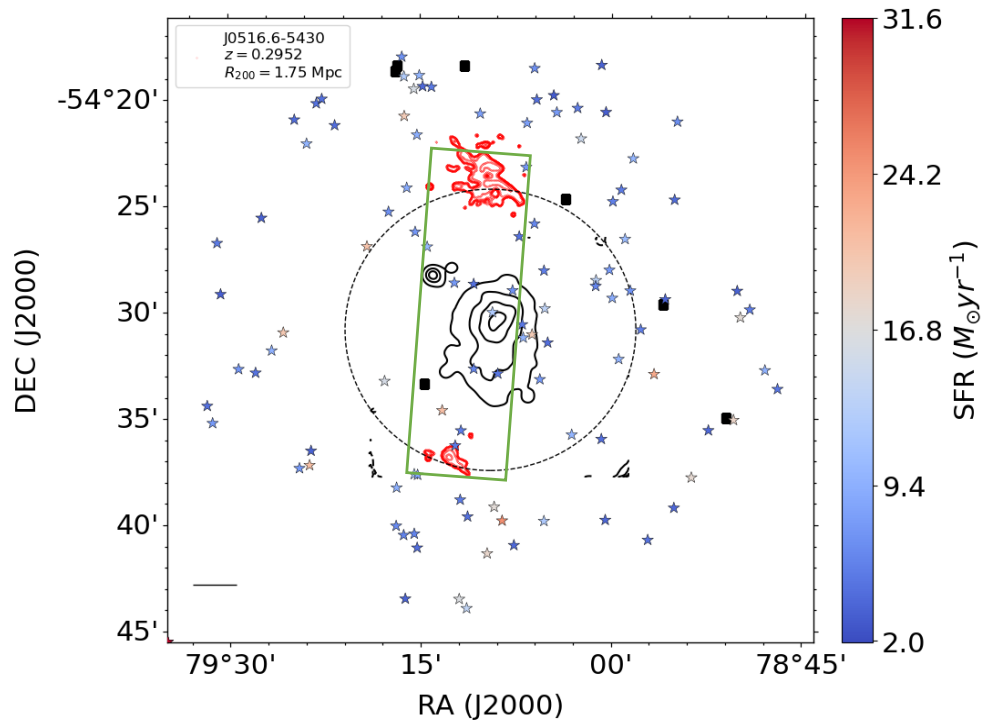


Figure 4.3: The view of the J0516.6-5430 cluster. The symbols, shapes and contours are described in Figure 4.1. The radio contour levels are  $[1, 2, 3, 4] \times 3\sigma_{\text{rms}}$ ,  $\sigma_{\text{rms}} = 4.2 \mu\text{Jy beam}^{-1}$ .

### 4.1.2 Star formation activity relation with time since the merger started

In this section, we attempt to estimate the SF activity of the clusters with respect to the time that passed since the merger started. Estimating the time that passed since the merger started from observations is a challenging task with limited data available in the literature. Assuming that radio relics are powered by diffusive shock acceleration (DSA, propagating through shock waves from the cluster cores to the outskirts, see Section 1.3.3) and that the cluster merger is in the plane of the sky, we can use the distance of the relic from the cluster centre as a rough estimate of the time passed since the merger started.

Using the distance of the radio relic from the cluster centre as a proxy for time since the merger started has been previously implemented by [Bonafede et al. \(2017\)](#) as a way to investigate the period at which radio haloes form during a merger. They used a sample of clusters hosting symmetric relics (some also hosting haloes and others without haloes). They use the Mach number of the shock wave and the speed of sound ( $c_s$ ) in the ICM to derive the shock velocity ( $v_{\text{shock}}$ ) and estimate the time the shock wave took to reach the relic position  $t_{\text{merger}}$ . [Bonafede et al. \(2017\)](#) relied on a number of assumptions to estimate  $t_{\text{merger}}$ . They assume that:

- The ICM is isothermal.
- The radio relics are tracing two symmetric shock waves induced in the ICM at the same time.
- The radio relics are fueled by DSA.
- The shock wave Mach number has a shallow radial dependence ( $M \propto r^{1/2}$ ).
- The merger occurs in the plane of the sky and has minimal projection effects.

Following the same approach and assumptions as [Bonafede et al. \(2017\)](#), we estimate  $t_{\text{merger}}$  for clusters in our sample. This also assumes that the shock waves travelled an equal distance from the cluster centre which is equal to half the distance

(1) Name	(2) z	(3) $S_{1.28\text{ GHz}}$ (mJy)	(4) $L_{1.4\text{ GHz}}$ ( $10^{24}\text{ WHz}^{-1}$ )	(5) Size (kpc $\times$ kpc)	(6) $R_{\text{Mpc}}$	(7) $\alpha$	(8) $M_{\text{shock}}$
Abell 2744 NE	0.307	17.7	4.6	$450 \times 1570$	1.5	$-1.28 \pm 0.13$	$2.85 \pm 0.48$
Abell 2744 SE	0.307	3.0	0.7	$210 \times 1210$	1.0	$-1.21 \pm 0.08$	$3.24 \pm 0.37$
Abell 521 SE	0.248	16.6	2.7	$240 \times 1260$	0.9	$-1.48 \pm 0.15$	$2.27 \pm 0.35$
Abell 521 NW (c)	0.248	0.5	0.08	$125 \times 330$	1.0	-	-
J0516.6-5430 N	0.295	33.6	7.8	$650 \times 1500$	1.9	$-1.28 \pm 0.11$	$2.85 \pm 0.40$
J0516.6-5430 S	0.295	3.3	0.8	$270 \times 770$	1.8	$-1.32 \pm 0.10$	$2.7 \pm 0.33$
J2023.4-5535 W	0.232	8.5	1.1	$150 \times 640$	0.6	$-1.52 \pm 0.09$	$2.20 \pm 0.19$
J2023.4-5535 SE (c)	0.232	0.9	0.1	$100 \times 590$	0.7	-	-

Table 4.2: The properties of MeerKAT-detected relics. Columns: (1) name of the cluster with the location of the relic in the cluster. The relics with ‘(c)’ are those identified as candidate relics; (2) cluster redshift; (3) the integrated flux densities of the relics as observed by MeerKAT at the frequency of 1.28 GHz (Kolokythas et al., *in preparation*); (4) the relic radio luminosities k-corrected and scaled to the 1.4 GHz frequency. For candidate relics with no integrated spectral index, we assume  $\alpha = -1.3$  (Feretti et al., 2012); (5) the size of the relic; (6) the distance of the relic from the cluster centre; (7) the integrated spectral index. MeerKAT-derived mean spectral indices over the 908 – 1656 MHz frequency range; (8) the Mach number of the shock.

between the two radio relics. Using the cluster ICM temperature obtained from X-ray studies in the literature (see Table 4.1 for references), we use the relation from Sarazin (1988) to estimate the speed of sound in the ICM

$$c_s = 1480 \left( \frac{T_X}{10^8 \text{ K}} \right)^{\frac{1}{2}} \text{ km s}^{-1} \quad (4.1)$$

where  $T_X$  is the global X-ray temperature of the cluster. We then estimate the Mach number of the shock wave using

$$M_{\text{shock}} = \left( \frac{2\alpha_{\text{inj}} - 3}{2\alpha_{\text{inj}} + 1} \right)^{\frac{1}{2}} \quad (4.2)$$

where  $M_{\text{shock}}$  is the Mach number of the shock wave estimated from the integrated spectral index of the radio relic ( $\alpha$ , see Table 4.2), and  $\alpha_{\text{inj}}$  is the injected spectral index. To properly find the injection spectral index, resolved spectral modelling is

required (see Harwood et al., 2013; Harwood et al., 2015; Harwood, 2017). For this study, we use the relation,  $\alpha = \alpha_{\text{inj}} - 0.5$  to estimate the injection spectral index.

We then estimate  $t_{\text{merger}}$  from the shock velocity ( $v_{\text{shock}} = M_{\text{shock}} \times c_s$ ) and the distance travelled by the shock to reach the position of the relic, using the most dominant radio (brightest and largest) relic in the cluster.

Figure 4.4 shows the relation between the total SFR ( $\Sigma\text{SFR}$ ) within the cluster's  $R_{200}$  and  $t_{\text{merger}}$ . Figure 4.4 also includes the relation between mass normalised total SFR ( $\Sigma\text{SFR}/M_{200}$ ) and  $t_{\text{merger}}$ . We note an anti-correlation between  $\Sigma\text{SFR}$  and  $t_{\text{merger}}$ . This could suggest that more recent mergers, which also have a higher count of star-forming galaxies and larger cluster masses (see  $\Sigma\text{SFR}-M_{200}$  correlation in Section 3.4.2), have higher SF activity  $R_{200}$  compared to older mergers which have a higher  $t_{\text{merger}}$ . The more recent mergers also exhibit more ICM disturbances seen through the *XMM-Newton* X-ray contours in Figures 4.1 and 4.3 (described in the following section). There is no clear correlation between the mass normalised  $\Sigma\text{SFR}$  and  $t_{\text{merger}}$ . The small cluster sample provides very little data to draw any preliminary conclusions. This motivates the need for more cluster samples to further investigate the relation between SF activity and  $t_{\text{merger}}$ .

We also note that the sizes and the integrated radio luminosities of the relics in our sample increase with the distance away from the centre as shown in Figure 4.5. This is consistent with the relations found by van Weeren et al. (2011a) and Bonafede et al. (2012), that distant relics have high radio luminosities and a higher largest linear size (LLS). This is in agreement with predictions made by cosmological simulation models that shocks are more powerful in low-density regions, hence the observation of larger and brighter relics in the peripheral regions of the clusters (Feretti et al., 2012).

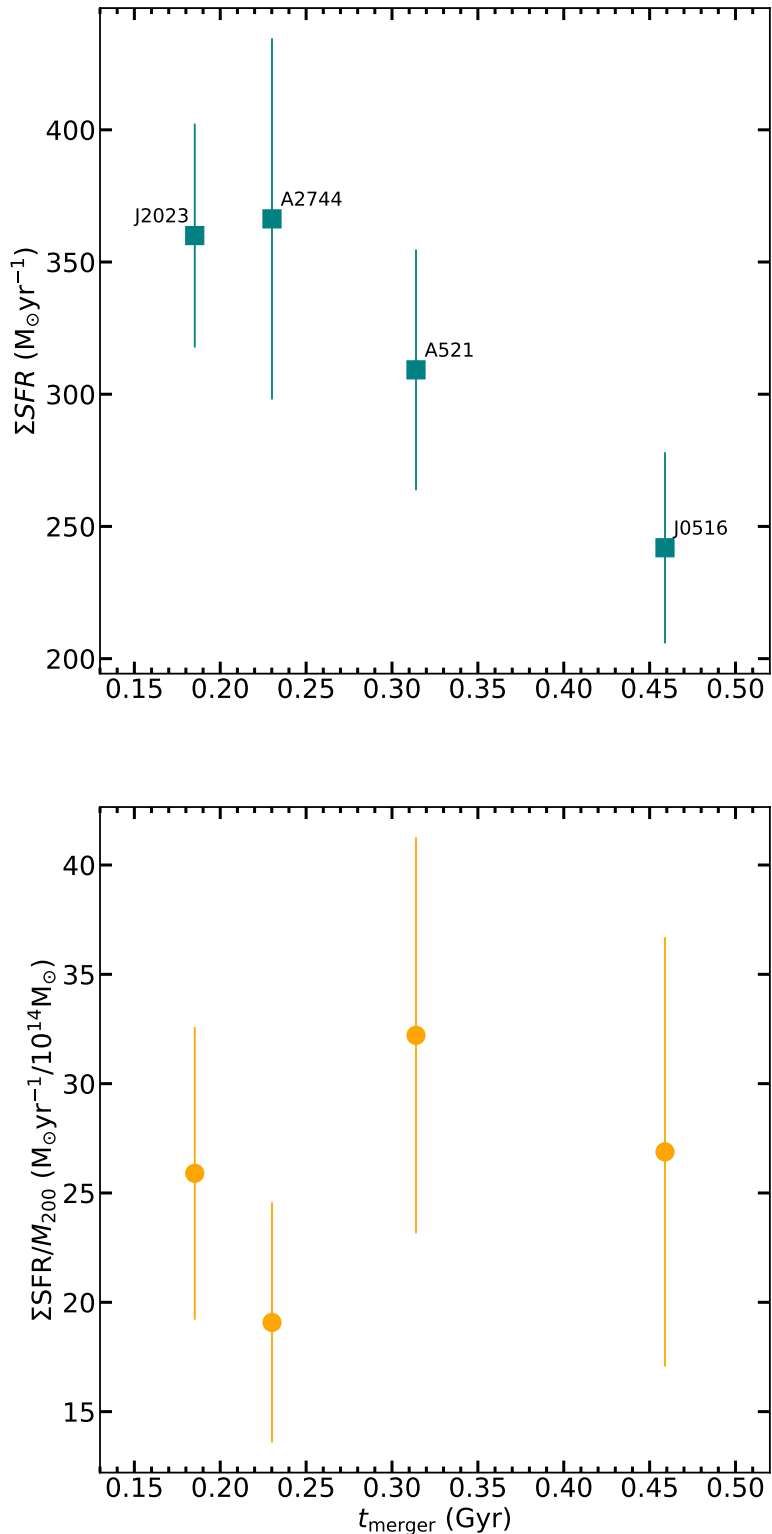


Figure 4.4: *Top:* The relation between total star formation rates ( $\Sigma \text{SFR}$ ) and the estimated time that has passed since merger ( $t_{\text{merger}}$ ). *Bottom:* The relation between the mass normalised total star formation rates ( $\Sigma \text{SFR}/M_{200}$ ) and the time passed since merger  $t_{\text{merger}}$ .

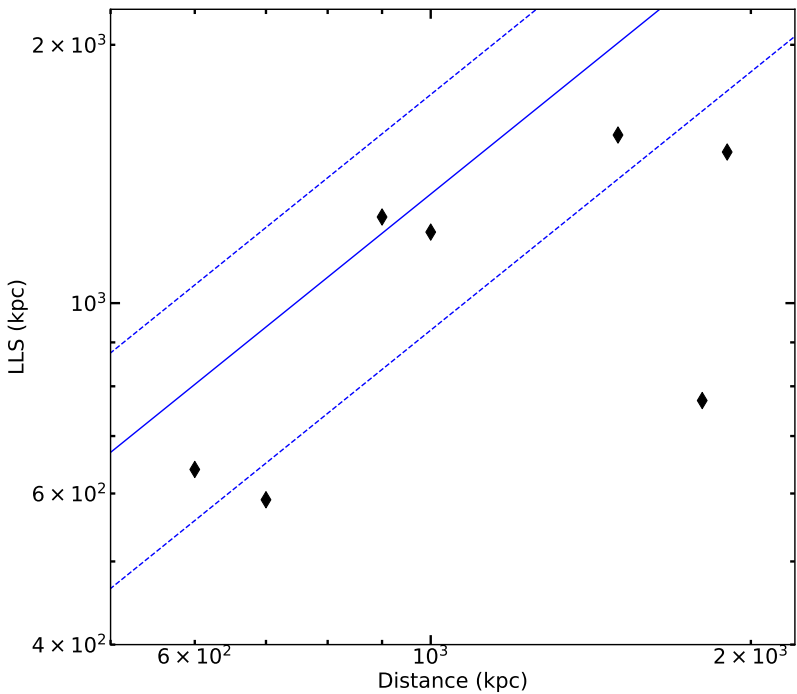
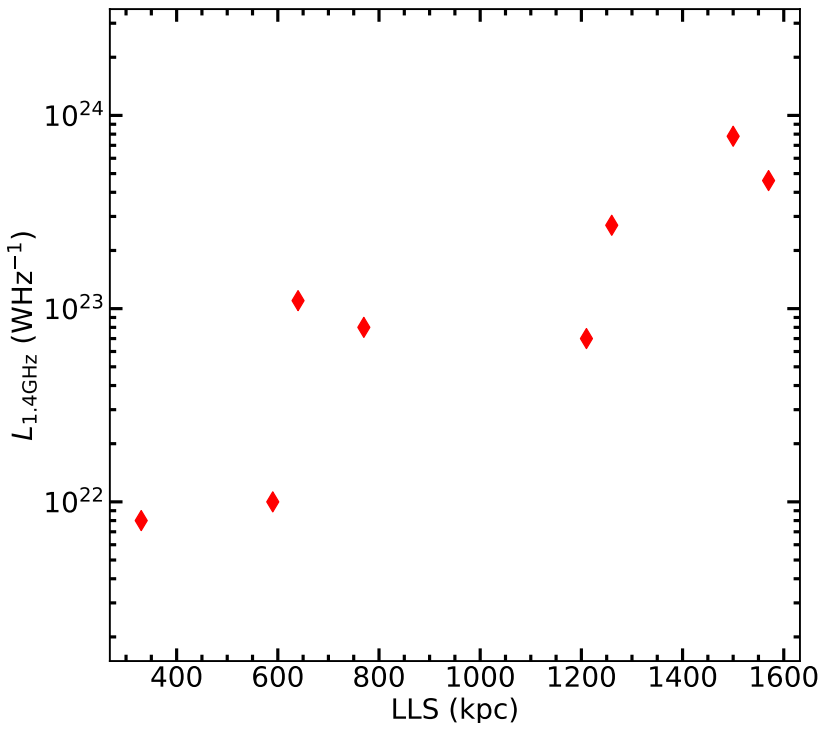


Figure 4.5: *Top*: The relation between the radio relics power and their size (LLS). *Bottom*: The relation between the radio relics LLS and their distance from the cluster centre. The blue solid line shows the LLS - relic distance relation from [de Gasperin et al. \(2014\)](#) and its uncertainty in the blue dashed lines.

### 4.1.3 The distribution of galaxies and their SFR in relic-hosting clusters

In this section, we investigate the impact of radio relics/shock waves on the SF activity of the galaxies in the clusters, looking for any signs of increased or suppressed SF activity around and along the relic environment. We divide the galaxies in the cluster into two groups: the population along the path between the relics going out to  $R_{200}$ , and another population of galaxies outside this path. The relic/shock wave paths used to separate the galaxy groups are shown in Figures 4.1 - 4.3. This assumes that the shock wave propagated the ICM within that path and will continue moving along it. We then attempt to study the SF activity of galaxies within the assumed shock wave path to compare it with the SF activity of galaxies outside the shock wave path.

[Stroe et al. \(2014\)](#) employed a similar approach on their study of shocks/relics in influencing the H $\alpha$  luminosity function (LF). They used two clusters at  $z \approx 0.2$  hosting relics, CIZA J2242.8+5301 ('sausage' cluster) and 1RXS J0603.3+4213 ('toothbrush' clusters), to study the H $\alpha$  LFs using galaxies in the clusters and also within a selected area around the relics in the clusters. For the 'sausage' cluster, they reported the normalisation of the H $\alpha$  LF that is an order of magnitude above LFs for relaxed and disturbed clusters. They also noted a high number count of luminous H $\alpha$  emitters around the relic and suggest this could be due to the passage of the shock wave inducing SF in the galaxies. However, they do not find a boosted H $\alpha$  LF normalisation or a high number count of luminous H $\alpha$  emitters for the 'toothbrush' cluster, and they suggest that the observed differences in the two clusters could have to do with their merger histories, especially the time since core-passage.

For this study, we focus on finding differences in SF activity within the clusters using the fraction of star-forming ( $f_{\text{SF}}$ ) as a proxy for SF. We also investigate the distribution of the galaxies within the cluster and their SFR. Figures 4.1 - 4.3 show the distribution of galaxies within each relic hosting cluster. They include radio contours around the radio relics as observed by MeerKAT, and the *XMM-Newton* X-ray contours. Table 4.3 shows a comparison of the fraction of star-forming galaxies

(1)	(2)	(3)	(4)	(5)	(6)
Cluster	$f_{\text{SF},\text{shock}}$	$f_{\text{SF},\text{non-shock}}$	$f_{\text{SF},\text{cluster}}$	$N_{\text{gal},\text{shock}}$	$N_{\text{gal},\text{cluster}}$
Abell 2744	$0.09 \pm 0.02$	$0.13 \pm 0.01$	$0.11 \pm 0.02$	18	40
Abell 521	$0.16 \pm 0.02$	$0.11 \pm 0.02$	$0.13 \pm 0.02$	15	36
J0516.6-5430	$0.11 \pm 0.02$	$0.11 \pm 0.01$	$0.11 \pm 0.02$	13	28
J2023.4-5535	$0.21 \pm 0.03$	$0.20 \pm 0.03$	$0.20 \pm 0.03$	10	62

Table 4.3: The fraction of star-forming galaxies ( $f_{\text{SF}}$ ) estimates in the shock wave path and the cluster. Columns: (1) Name of the cluster; (2) the  $f_{\text{SF}}$  estimate for galaxies within the assumed shock wave path; (3) the  $f_{\text{SF}}$  estimate for galaxies outside the shock wave path; (4) the  $f_{\text{SF}}$  estimate for all member galaxies within the cluster's  $R_{200}$ ; (5) the number of member galaxies within the assumed shock wave path; (6) the number of member galaxies within the cluster's  $R_{200}$ .

in the shock wave path with those outside the path and the overall  $f_{\text{SF}}$  of the cluster. It also includes the number of galaxies in the assumed shock wave path ( $N_{\text{gal},\text{shock}}$ ) and the total number of galaxies in the cluster  $N_{\text{gal},\text{cluster}}$ .

Looking at the distribution of galaxies in clusters and their SFR indicated by the divergent colour scale, we observe no clear evidence of enhanced SF activity of the individual galaxies in the shock wave paths. The comparison of  $f_{\text{SF}}$  of galaxies (within  $R_{200}$ ) inside the shock path and those outside shows no significant differences (mostly  $< 1\sigma$ ). The Abell 2744 MeerKAT image has two asymmetric radio relics, and for each relic, we mark a shock wave path to compare it with the rest of the cluster environment as shown in Figure 4.2, although we combine their statistics to estimate the  $f_{\text{SF}}$  in Table 4.3.

As a further test, we stacked all the galaxies within the assumed shock wave paths and outside the paths from all the clusters and then plotted their  $f_{\text{SF}}$  relation with clustercentric radius in Figure 4.6. We observe no significant difference between the two samples although at  $R_{200}$ ,  $f_{\text{SF}}$  reaches  $\approx 0.22 \pm 0.06$  for galaxies in the assumed shock wave path compared to  $\approx 0.14 \pm 0.03$  for galaxies outside it. The overall  $f_{\text{SF}}$  within  $R_{200}$  is  $\approx 0.14 \pm 0.02$  for the shock wave path population and  $\approx 0.15 \pm 0.02$  for the galaxy population outside the assumed shock wave path. The individual and stacked  $f_{\text{SF}}$  comparison for our two samples are within  $1\sigma$  of each other, suggesting

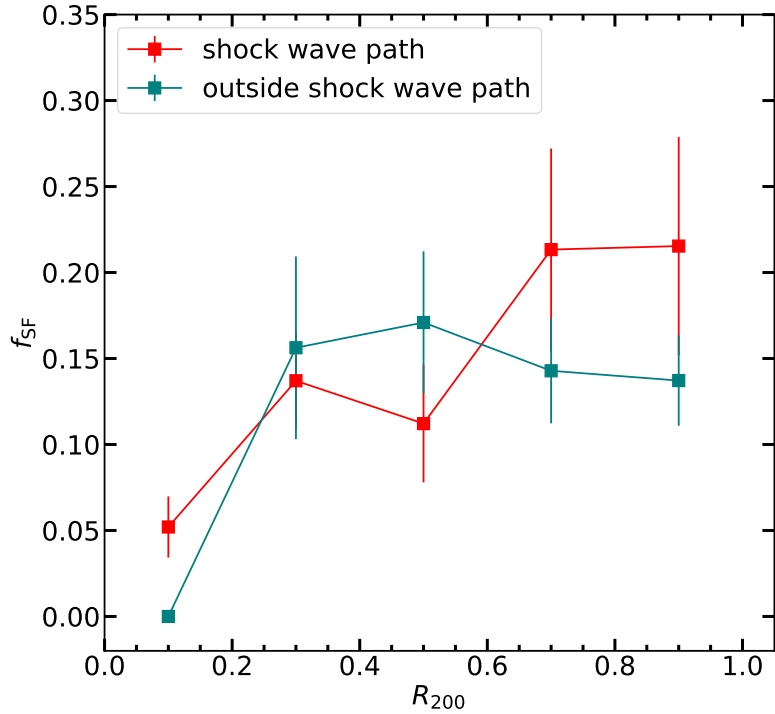


Figure 4.6: The comparison of the  $f_{SF}$  in radial bins between galaxies in the assumed shock wave paths (red markers) and those outside the path (teal markers). We note no significant  $f_{SF}$  differences between the two populations. However, the  $f_{SF}$  gradient for galaxies outside the assumed shock wave paths appears to be flatter compared to the  $f_{SF}$  gradient of galaxies in the shock wave paths, but still remains within  $1\sigma$  uncertainties at all radial bins.

that the overall  $f_{SF}$  of the cluster stays consistent throughout the cluster with no suppressed or enhanced SF activity around shocks/relics for clusters in our sample. However, we note that the uncertainties are large, as a result of the small cluster sample considered here.

## 4.2 Summary

We used a sample of haloes and relic-hosting clusters to investigate the dependence of the SF activity on the cluster environment. Following the approach from Bonafede et al. (2017), we rely on a number of assumptions to estimate the time that has passed since the merger started ( $t_{\text{merger}}$ ). We note an anti-correlation between  $\Sigma\text{SFR}$  with increasing distances of the relics from the cluster centres but see no correlation with relation to the mass normalised  $\Sigma\text{SFR}$ . We observe a correlation between  $L_{1.4\text{GHz}}$  and LLS as well as between the LLS and relic distances from the centre. This is consistent with correlations seen previous studies of double-relic clusters.

Taking a closer look into the clusters and separating galaxies between those in the assumed environment of the relic and those outside, we see no significant differences in the SFR and the  $f_{\text{SF}}$  of the galaxies in the assumed relic/shock wave paths and the rest of the galaxies in the clusters. We note the small size and large uncertainties in this study. Although there could be an effect, it may too subtle to see due to this limitation.

# Chapter 5

## Conclusion and future work

The aim of this thesis was to investigate galaxy star formation rates as a function of their environment in the MeerKAT Galaxy Clusters Legacy Survey (MGCLS). We do so by identifying a sample of MGCLS clusters with optical coverage in the Dark Energy Camera Legacy Survey (DECaLS) and SZ-effect coverage in the Atacama Cosmology Telescope. This allowed us to classify cluster members with photometric redshifts estimated from DECaLS photometry within a radius derived from the ACT cluster masses. In this chapter, we summarise the results and the conclusions reached. We end the chapter by laying out the planned follow-up work for this study.

In Chapter 1, we provided a brief history of astronomy and discussed the current leading cosmological model, the  $\Lambda$ CDM model, alongside the major stages of the Universe’s evolution. We provided a literature review on star formation, galaxies and galaxy clusters. We discussed large-scale cluster properties, highlighting the non-thermal diffuse emission (radio haloes, mini-haloes, relics, phoenices), which we use as the basis for defining the dynamical state of our cluster sample. We covered the large-scale properties of clusters and their influence in suppressing the star formation of their member galaxies, highlighting a result from Haines et al. (2015) that shows that galaxies in clusters have their SF suppressed at levels below the SF of field galaxies even at  $2R_{200}$  of the clusters.

Chapter 2 introduces the parent data samples used in this study. This chapter also develops the methodology and tools to study the larger MGCLS sample. We developed `zField`, which forms part of `zCluster`, and uses a template-fitting method to estimate photo-zs using DECaLS photometry. The accuracy test for `zField` photo-zs against SDSS spec-zs showed that the photo-zs do well between  $0.15 < z < 0.5$  but are unreliable for redshifts outside that redshift range. To minimise contamination, we restricted our study of the MGCLS clusters to those with redshifts within this redshift range. To test our methodology and analytical tools, we studied SFR in Abell 209. Our results show a steady increase in the fraction of star-forming galaxies ( $f_{\text{SF}}$ ) with radial bins, rising from  $\approx 0.08$  at the cluster core to  $\approx 0.22$  outside the cluster outskirts near  $2R_{200}$ . This result is consistent with the Haines et al. (2015)  $f_{\text{SF}}$  gradient out to the same radius, although it uses a different SF tracer. Based on the Haines et al. (2015) estimation of  $f_{\text{SF}}$  for field galaxies, we note that even for Abell 209, the  $f_{\text{SF}}$  is still below that of field galaxies  $\approx 0.33$  at  $2R_{200}$ . This is consistent with the Haines et al. (2015) suggestion of the *pre-processing* of galaxies in galaxy groups before they enter cluster environments.

Chapter 3 presents a study of 20 MGCLS clusters at  $0.15 < z < 0.35$  guided by a methodology developed in Chapter 2. The results in Chapter 3 show that using  $f_{\text{SF}}$  comparisons, clusters with merger-linked diffuse emission have a higher SF activity than relaxed clusters. However, our sample has a bias towards clusters with radio haloes and relics due to the heterogeneous nature of the underlying MGCLS sample in our cluster sample and will require a homogeneously selected sample to confirm our results. With that noted, the results from this chapter are consistent with suggestions made by previous studies that merger-induced turbulence and shocks affect the star formation activity within clusters (Ferrari et al., 2003; Pranger et al., 2013; Ebeling et al., 2014). Consistent with infrared studies using LIRGs, we observe a redshift-dependent  $4\times$  decline in SF activity from  $z = 0.35$  to  $z = 0.15$ . The decline in SF activity with redshift since  $z \approx 2.5$  has been reported by various studies (e.g., Lilly et al., 1996; Karim et al., 2011; Sobral et al., 2014) and has been shown to be the case in all environments (Koyama et al., 2013).

Chapter 4 investigated the SF activity in a subsample of radio haloes and relics-hosting MGCLS clusters. The results presented in this chapter reveal an anti-correlation in the  $\Sigma\text{SFR}$  -  $t_{\text{merger}}$  relation, suggesting that more recent mergers have a higher SF than older mergers. From the  $f_{\text{SF}}$  comparisons of member galaxies in the assumed relic/shock wave path and the galaxies away from the path, we see no significant difference in the SF activity between the two populations. We suggest sample size limitations as a possible hindrance to seeing shock-induced differences in galaxy clusters of this nature.

## Future work

We aim to conduct a follow-up study of the results presented in Chapter 3 using an unbiased mass-selected cluster sample from the MeerKAT Exploration of Relics, Giant Halos, and Extragalactic Radio Sources (MERGHERS; [Knowles et al., 2022](#)). This will also allow us to investigate if the [Butcher and Oemler \(1978\)](#) effect affected our results.

Using a combination of clusters from MGCLS, MERGHERS and the recently observed high redshift clusters by MeerKAT (at  $1 < z < 1.2$ ), we will conduct a study of the evolution of the radio luminosity function from  $z = 0.15$  out to  $z \approx 1.2$ . We will also produce the radio luminosity functions for clusters based on their environments.

## Appendix A

### Legacy Survey images of the cluster sample

Here we present Legacy Surveys DR9 images for our cluster sample. See discussion in Section 3.1.

Figures A.1 - A.5 show the Legacy Surveys DR9 images of our cluster sample with the identified MeerKAT-detected cluster members and the radio-loud AGN.

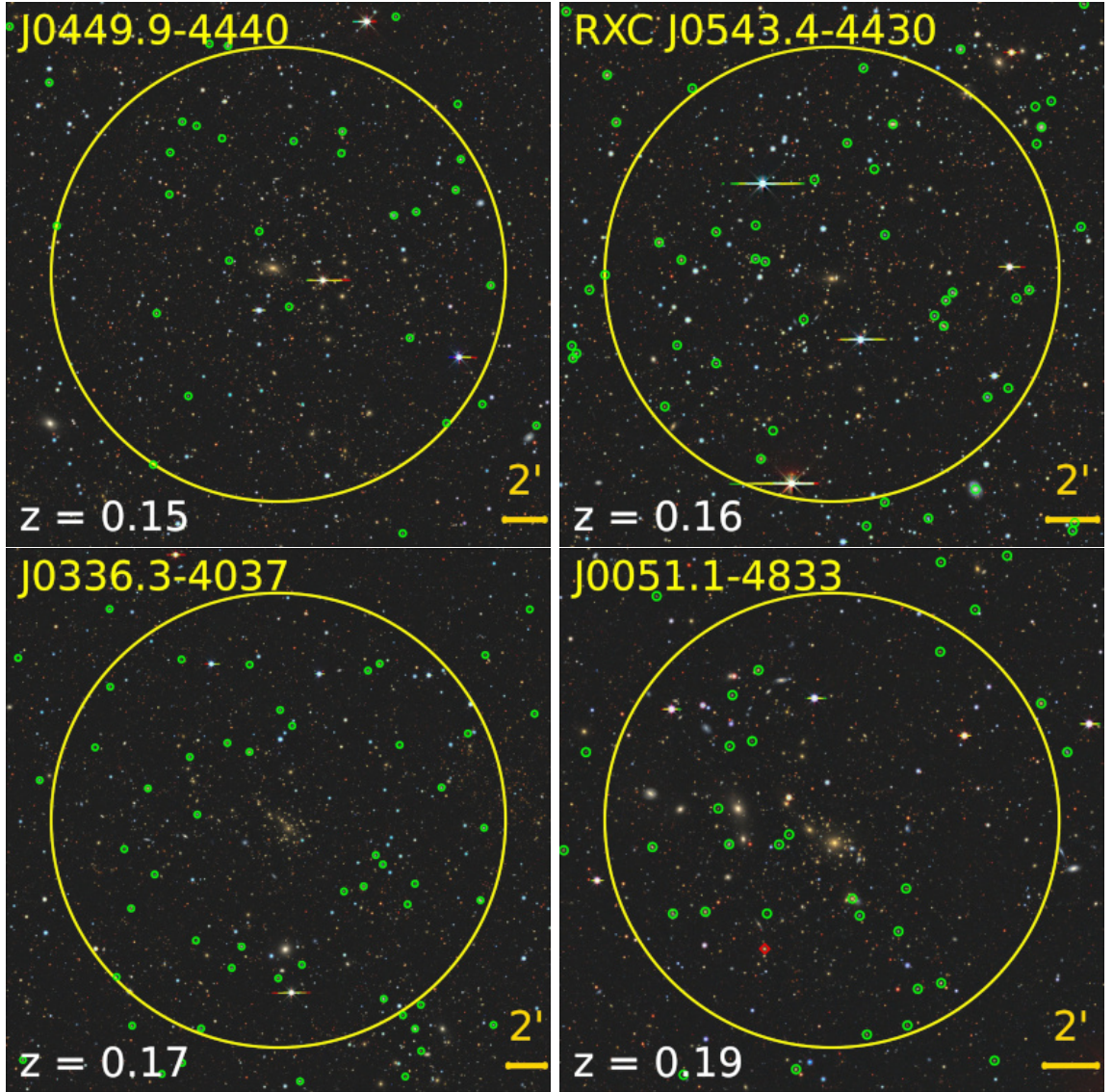


Figure A.1: The Legacy Survey image of clusters: J0449.9-4440, RXC J0543.4-4430, J0336.3-4037, J0051.1-4833. MeerKAT-detected galaxies are highlighted in small green and red circles representing star-forming galaxies and radio-loud AGN respectively. The large yellow circles show the  $R_{200}$  of the cluster.

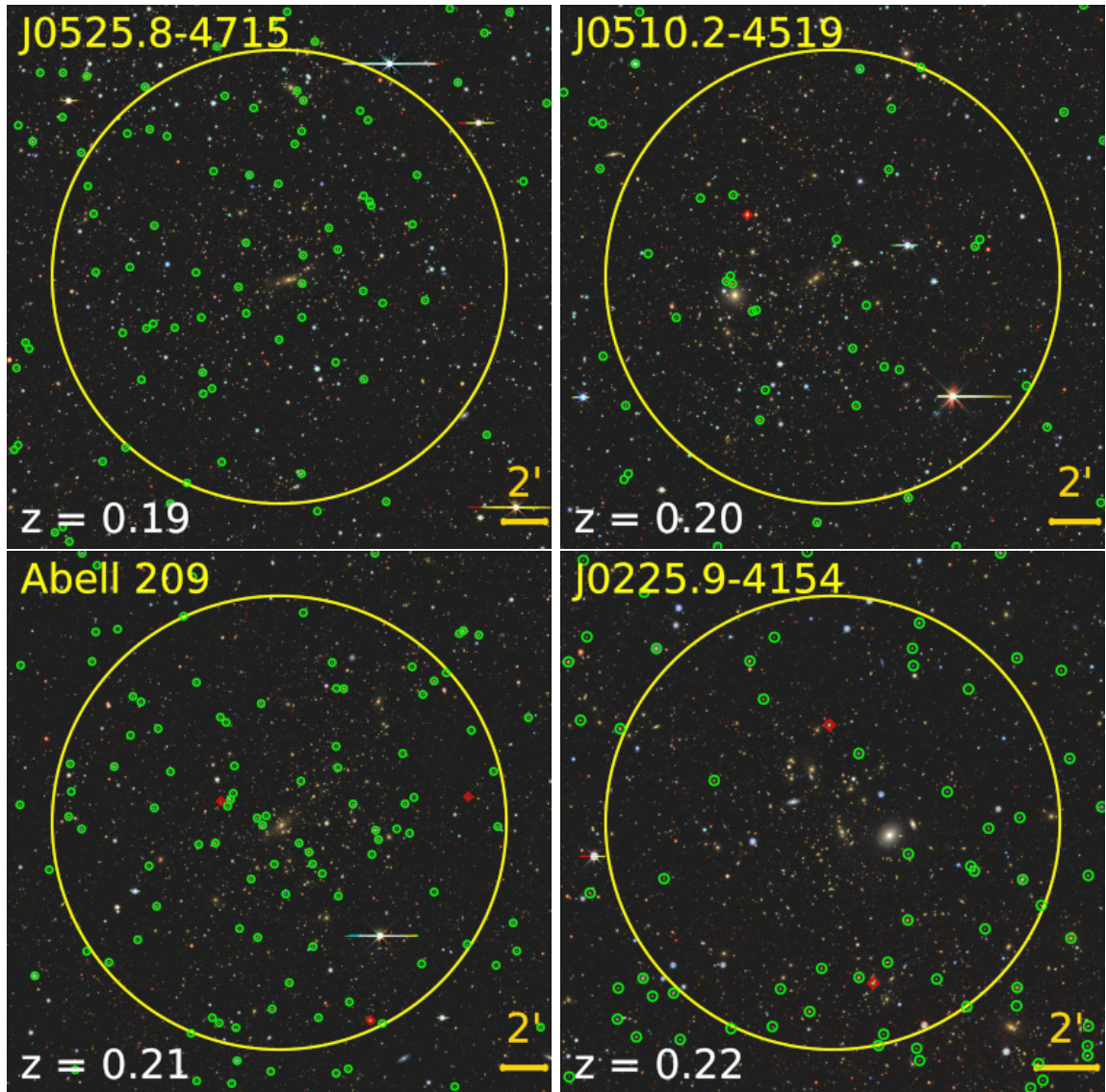


Figure A.2: The Legacy Survey images of clusters: J0525.8-4715, J0510.2-4519, Abell 209, J0225.9-4154.

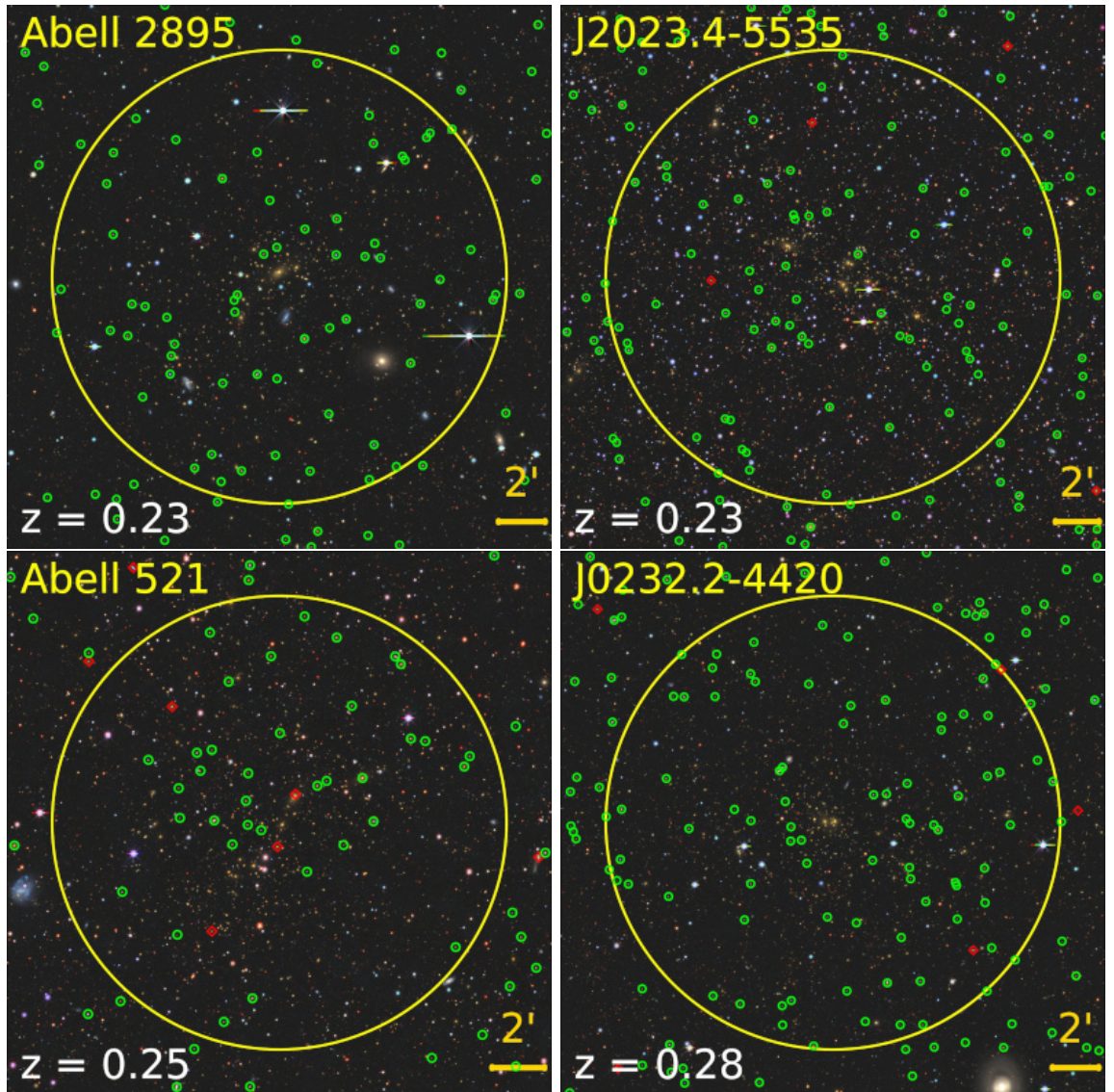


Figure A.3: The Legacy Survey images of clusters: Abell 2895, J2023.4-5535, Abell 521, J0232.2-4420.

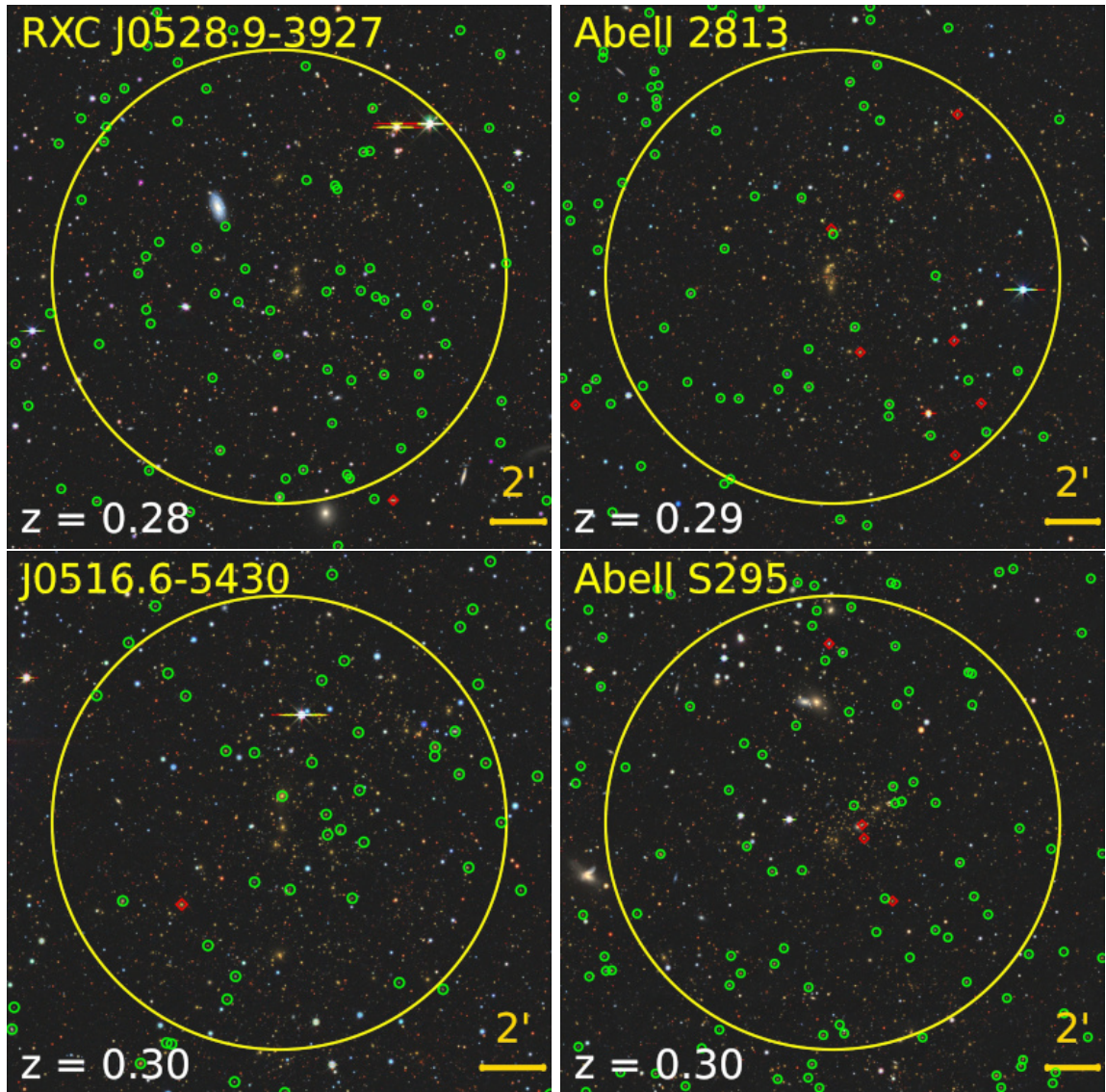


Figure A.4: The Legacy Survey images of clusters: RXC J0528.9-3927, Abell 2813, J0516.6-5430, Abell S295.

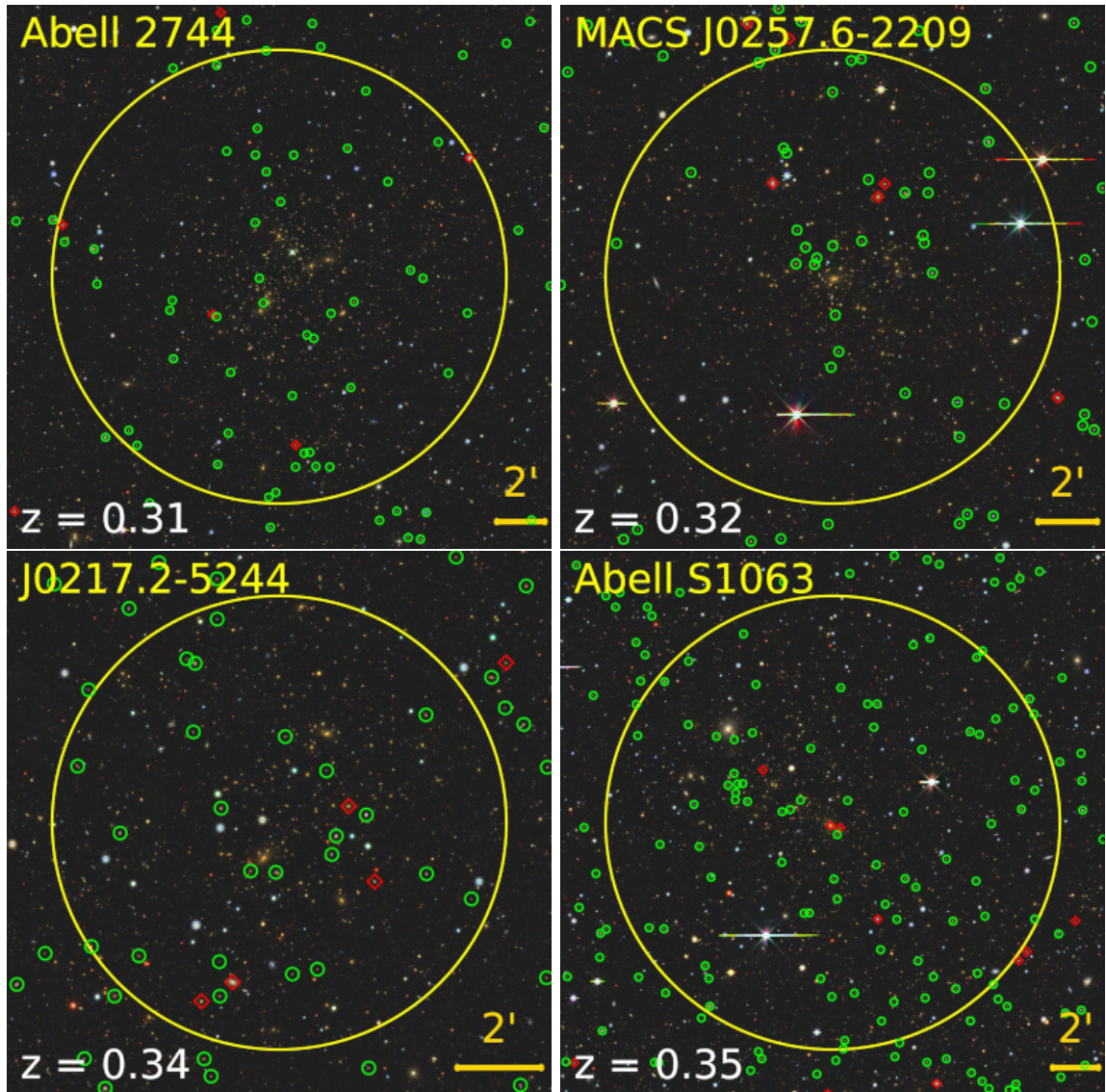


Figure A.5: The Legacy Survey images of clusters: Abell 2744, MACS J0257.6-2209, J0217.2-5244, Abell S1063.

# Bibliography

- Abbott, B. P. et al. (Feb. 2016). “Observation of Gravitational Waves from a Binary Black Hole Merger”. In: *Physical Review Letters* 116.6, 061102, p. 061102. DOI: [10.1103/PhysRevLett.116.061102](https://doi.org/10.1103/PhysRevLett.116.061102). arXiv: [1602.03837 \[gr-qc\]](https://arxiv.org/abs/1602.03837).
- Abbott, T. M. C. et al. (Jan. 2022). “Dark Energy Survey Year 3 results: Cosmological constraints from galaxy clustering and weak lensing”. In: *Physical Review D*. 105.2, 023520, p. 023520. DOI: [10.1103/PhysRevD.105.023520](https://doi.org/10.1103/PhysRevD.105.023520). arXiv: [2105.13549 \[astro-ph.CO\]](https://arxiv.org/abs/2105.13549).
- Abdurashidova, Zara et al. (Feb. 2022). “First Results from HERA Phase I: Upper Limits on the Epoch of Reionization 21 cm Power Spectrum”. In: *Astrophys. J.* 925.2, 221, p. 221. DOI: [10.3847/1538-4357/ac1c78](https://doi.org/10.3847/1538-4357/ac1c78). arXiv: [2108.02263 \[astro-ph.CO\]](https://arxiv.org/abs/2108.02263).
- Abell, George O. (May 1958). “The Distribution of Rich Clusters of Galaxies.” In: *Astrophys. J. Supp.* 3, p. 211. DOI: [10.1086/190036](https://doi.org/10.1086/190036).
- Abell, George O. et al. (May 1989). “A Catalog of Rich Clusters of Galaxies”. In: *Astrophys. J. Supp.* 70, p. 1. DOI: [10.1086/191333](https://doi.org/10.1086/191333).
- Abraham, R. G. (Sept. 1998). “Perspectives in Physical Morphology”. In: *arXiv e-prints*, astro-ph/9809131, astro-ph/9809131. arXiv: [astro-ph/9809131 \[astro-ph\]](https://arxiv.org/abs/astro-ph/9809131).
- Ackermann, M. et al. (July 2010). “GeV Gamma-ray Flux Upper Limits from Clusters of Galaxies”. In: *Astrophys. J. Lett.* 717.1, pp. L71–L78. DOI: [10.1088/2041-8205/717/1/L71](https://doi.org/10.1088/2041-8205/717/1/L71). arXiv: [1006.0748 \[astro-ph.HE\]](https://arxiv.org/abs/1006.0748).
- Ahumada, Romina et al. (July 2020). “The 16th Data Release of the Sloan Digital Sky Surveys: First Release from the APOGEE-2 Southern Survey and Full Release of eBOSS Spectra”. In: *Astrophys. J. Supp.* 249.1, 3, p. 3. DOI: [10.3847/1538-4365/ab929e](https://doi.org/10.3847/1538-4365/ab929e). arXiv: [1912.02905 \[astro-ph.GA\]](https://arxiv.org/abs/1912.02905).
- Alpher, R. A. et al. (Apr. 1948). “The Origin of Chemical Elements”. In: *Physical Review* 73.7, pp. 803–804. DOI: [10.1103/PhysRev.73.803](https://doi.org/10.1103/PhysRev.73.803).
- Andrade-Santos, Felipe et al. (July 2017). “The Fraction of Cool-core Clusters in X-Ray versus SZ Samples Using Chandra Observations”. In: *Astrophys. J.* 843.1, 76, p. 76. DOI: [10.3847/1538-4357/aa7461](https://doi.org/10.3847/1538-4357/aa7461). arXiv: [1703.08690 \[astro-ph.CO\]](https://arxiv.org/abs/1703.08690).
- Andreon, S. et al. (Jan. 2016). “The amazing diversity in the hot gas content of an X-ray unbiased massive galaxy clusters sample”. In: *Astron. Astrophys.* 585, A147, A147. DOI: [10.1051/0004-6361/201527408](https://doi.org/10.1051/0004-6361/201527408). arXiv: [1511.04195 \[astro-ph.CO\]](https://arxiv.org/abs/1511.04195).
- Annunziatella, M. et al. (Jan. 2016). “CLASH-VLT: Environment-driven evolution of galaxies in the  $z = 0.209$  cluster Abell 209”. In: *Astron. Astrophys.* 585, A160, A160. DOI: [10.1051/0004-6361/201527399](https://doi.org/10.1051/0004-6361/201527399). arXiv: [1510.05659 \[astro-ph.GA\]](https://arxiv.org/abs/1510.05659).

- Assef, R. J. et al. (July 2013). “Mid-Infrared Selection of Active Galactic Nuclei with the Wide-Field Infrared Survey Explorer. II. Properties of WISE Selected Active Galactic Nuclei in the NDWFS Bootes Field”. In: *The Astrophysical Journal* 772.1, p. 26. DOI: [10.1088/0004-637x/772/1/26](https://doi.org/10.1088/0004-637x/772/1/26). URL: <https://doi.org/10.1088/0004-637x/772/1/26>.
- Assef, R. J. et al. (Jan. 2018). “The WISE AGN Catalog”. In: *The Astrophysical Journal Supplement Series* 234.2, p. 23. ISSN: 1538-4365. DOI: [10.3847/1538-4365/aaa00a](https://doi.org/10.3847/1538-4365/aaa00a). URL: <http://dx.doi.org/10.3847/1538-4365/aaa00a>.
- Astropy Collaboration (Oct. 2013). “Astropy: A community Python package for astronomy”. In: *Astron. Astrophys.* 558, A33, A33. DOI: [10.1051/0004-6361/201322068](https://doi.org/10.1051/0004-6361/201322068). arXiv: [1307.6212 \[astro-ph.IM\]](https://arxiv.org/abs/1307.6212).
- (Sept. 2018). “The Astropy Project: Building an Open-science Project and Status of the v2.0 Core Package”. In: *Astron. J.* 156.3, 123, p. 123. DOI: [10.3847/1538-3881/aabc4f](https://doi.org/10.3847/1538-3881/aabc4f). arXiv: [1801.02634 \[astro-ph.IM\]](https://arxiv.org/abs/1801.02634).
- Baldry, Ivan K. et al. (Jan. 2004). “Quantifying the Bimodal Color-Magnitude Distribution of Galaxies”. In: *Astrophys. J.* 600.2, pp. 681–694. DOI: [10.1086/380092](https://doi.org/10.1086/380092). arXiv: [astro-ph/0309710 \[astro-ph\]](https://arxiv.org/abs/astro-ph/0309710).
- Baldwin, Jack A. (June 1977). “Luminosity Indicators in the Spectra of Quasi-Stellar Objects”. In: *Astrophys. J.* 214, pp. 679–684. DOI: [10.1086/155294](https://doi.org/10.1086/155294).
- Balogh, Michael L. et al. (Sept. 2000). “The Origin of Star Formation Gradients in Rich Galaxy Clusters”. In: *Astrophys. J.* 540.1, pp. 113–121. DOI: [10.1086/309323](https://doi.org/10.1086/309323). arXiv: [astro-ph/0004078 \[astro-ph\]](https://arxiv.org/abs/astro-ph/0004078).
- Balogh, Mike L. et al. (Sept. 1998). “The Dependence of Cluster Galaxy Star Formation Rates on the Global Environment”. In: *The Astrophysical Journal* 504.2, L75–L78. ISSN: 0004-637X. DOI: [10.1086/311576](https://doi.org/10.1086/311576). URL: <http://dx.doi.org/10.1086/311576>.
- Barnes, Joshua E. (July 1992). “Transformations of Galaxies. I. Mergers of Equal-Mass Stellar Disks”. In: *Astrophys. J.* 393, p. 484. DOI: [10.1086/171522](https://doi.org/10.1086/171522).
- Bastian, Nate et al. (Sept. 2010). “A Universal Stellar Initial Mass Function? A Critical Look at Variations”. In: *Annu. Rev. Astron. Astrophys.* 48, pp. 339–389. DOI: [10.1146/annurev-astro-082708-101642](https://doi.org/10.1146/annurev-astro-082708-101642). arXiv: [1001.2965 \[astro-ph.GA\]](https://arxiv.org/abs/1001.2965).
- Baum, W. A. (Feb. 1957). “Photoelectric determinations of redshifts beyond 0.2 c.” In: *Astron. J.* 62, pp. 6–7. DOI: [10.1086/107433](https://doi.org/10.1086/107433).
- Beck, R. et al. (July 2017). “On the realistic validation of photometric redshifts”. In: *Mon. Not. R. Astron. Soc.* 468.4, pp. 4323–4339. DOI: [10.1093/mnras/stx687](https://doi.org/10.1093/mnras/stx687). arXiv: [1701.08748 \[astro-ph.GA\]](https://arxiv.org/abs/1701.08748).
- Beck, Róbert et al. (Aug. 2016). “Photometric redshifts for the SDSS Data Release 12”. In: *Mon. Not. R. Astron. Soc.* 460.2, pp. 1371–1381. DOI: [10.1093/mnras/stw1009](https://doi.org/10.1093/mnras/stw1009). arXiv: [1603.09708 \[astro-ph.GA\]](https://arxiv.org/abs/1603.09708).
- Beers, T. C. et al. (July 1990). “Measures of location and scale for velocities in clusters of galaxies - A robust approach”. In: *AJ* 100, pp. 32–46.
- Bekki, Kenji et al. (July 2010). “Synchronized Formation of Starburst and Post-starburst Galaxies in Merging Clusters of Galaxies”. In: *Astrophys. J. Lett.* 718.1, pp. L27–L31. DOI: [10.1088/2041-8205/718/1/L27](https://doi.org/10.1088/2041-8205/718/1/L27). arXiv: [1006.3399 \[astro-ph.CO\]](https://arxiv.org/abs/1006.3399).

- Bell, A. R. (Feb. 1978). “The acceleration of cosmic rays in shock fronts - II.” In: *Mon. Not. R. Astron. Soc.* 182, pp. 443–455. DOI: [10.1093/mnras/182.3.443](https://doi.org/10.1093/mnras/182.3.443).
- Bell, Eric F. (Apr. 2003). “Estimating Star Formation Rates from Infrared and Radio Luminosities: The Origin of the Radio-Infrared Correlation”. In: *The Astrophysical Journal* 586.2, pp. 794–813. DOI: [10.1086/367829](https://doi.org/10.1086/367829). URL: <https://doi.org/10.1086/367829>.
- Benítez, Narciso (June 2000). “Bayesian Photometric Redshift Estimation”. In: *Astrophys. J.* 536.2, pp. 571–583. DOI: [10.1086/308947](https://doi.org/10.1086/308947). arXiv: [astro-ph/9811189 \[astro-ph\]](https://arxiv.org/abs/astro-ph/9811189).
- Birkinshaw, M. (Jan. 1990). “Observations of the Sunyaev-Zel Effect”. In: *The Cosmic Microwave Background: 25 Years Later*. Ed. by N. Mandolesi and N. Vittorio. Vol. 164. Astrophysics and Space Science Library, p. 77. DOI: [10.1007/978-94-009-0655-6\\_6](https://doi.org/10.1007/978-94-009-0655-6_6).
- Birkinshaw, Mark (May 1999). “The Sunyaev-Zel'dovich effect: an update”. In: *3K cosmology*. Ed. by Luciano Maiani et al. Vol. 476. American Institute of Physics Conference Series, pp. 298–309. DOI: [10.1063/1.59334](https://doi.org/10.1063/1.59334).
- Blanton, Michael R. and Sam Roweis (Feb. 2007). “K-Corrections and Filter Transformations in the Ultraviolet, Optical, and Near-Infrared”. In: *Astron. J.* 133.2, pp. 734–754. DOI: [10.1086/510127](https://doi.org/10.1086/510127). arXiv: [astro-ph/0606170 \[astro-ph\]](https://arxiv.org/abs/astro-ph/0606170).
- Blasi, Pasquale and Sergio Colafrancesco (Nov. 1999). “Cosmic rays, radio halos and nonthermal X-ray emission in clusters of galaxies”. In: *Astroparticle Physics* 12.3, pp. 169–183. DOI: [10.1016/S0927-6505\(99\)00079-1](https://doi.org/10.1016/S0927-6505(99)00079-1). arXiv: [astro-ph/9905122 \[astro-ph\]](https://arxiv.org/abs/astro-ph/9905122).
- Böhringer, H. et al. (Oct. 2004). “The ROSAT-ESO Flux Limited X-ray (REFLEX) Galaxy cluster survey. V. The cluster catalogue”. In: *Astron. Astrophys.* 425, pp. 367–383. DOI: [10.1051/0004-6361:20034484](https://doi.org/10.1051/0004-6361:20034484). arXiv: [astro-ph/0405546 \[astro-ph\]](https://arxiv.org/abs/astro-ph/0405546).
- Bonafede, A. et al. (Sept. 2009). “Revealing the magnetic field in a distant galaxy cluster: discovery of the complex radio emission from MACS J0717.5 +3745”. In: *Astron. Astrophys.* 503.3, pp. 707–720. DOI: [10.1051/0004-6361/200912520](https://doi.org/10.1051/0004-6361/200912520). arXiv: [0905.3552 \[astro-ph.CO\]](https://arxiv.org/abs/0905.3552).
- Bonafede, A. et al. (Oct. 2012). “Discovery of radio haloes and double relics in distant MACS galaxy clusters: clues to the efficiency of particle acceleration”. In: *Mon. Not. R. Astron. Soc.* 426.1, pp. 40–56. DOI: [10.1111/j.1365-2966.2012.21570.x](https://doi.org/10.1111/j.1365-2966.2012.21570.x). arXiv: [1206.6102 \[astro-ph.CO\]](https://arxiv.org/abs/1206.6102).
- Bonafede, A. et al. (Sept. 2017). “On the absence of radio haloes in clusters with double relics”. In: *Mon. Not. R. Astron. Soc.* 470.3, pp. 3465–3475. DOI: [10.1093/mnras/stx1475](https://doi.org/10.1093/mnras/stx1475). arXiv: [1706.04203 \[astro-ph.CO\]](https://arxiv.org/abs/1706.04203).
- Boquien, M. et al. (Feb. 2019). “CIGALE: a python Code Investigating GALaxy Emission”. In: *Astron. Astrophys.* 622, A103, A103. DOI: [10.1051/0004-6361/201834156](https://doi.org/10.1051/0004-6361/201834156). arXiv: [1811.03094 \[astro-ph.GA\]](https://arxiv.org/abs/1811.03094).
- Boselli, Alessandro and Giuseppe Gavazzi (Apr. 2006). “Environmental Effects on Late-Type Galaxies in Nearby Clusters”. In: *Publications of the Astronomical Society of the Pacific* 118.842, 517–559. ISSN: 1538-3873. DOI: [10.1086/500691](https://doi.org/10.1086/500691). URL: <http://dx.doi.org/10.1086/500691>.

- Botteon, A. et al. (July 2016). “A shock at the radio relic position in Abell 115”. In: *Mon. Not. R. Astron. Soc.* 460.1, pp. L84–L88. DOI: [10.1093/mnrasl/slw082](https://doi.org/10.1093/mnrasl/slw082). arXiv: [1604.07823 \[astro-ph.HE\]](https://arxiv.org/abs/1604.07823).
- Bourdin, H. et al. (Feb. 2013). “Shock Heating of the Merging Galaxy Cluster A521”. In: *Astrophys. J.* 764.1, 82, p. 82. DOI: [10.1088/0004-637X/764/1/82](https://doi.org/10.1088/0004-637X/764/1/82). arXiv: [1302.0696 \[astro-ph.CO\]](https://arxiv.org/abs/1302.0696).
- Bournaud, F. et al. (July 2005). “Galaxy mergers with various mass ratios: Properties of remnants”. In: *Astron. Astrophys.* 437.1, pp. 69–85. DOI: [10.1051/0004-6361:20042036](https://doi.org/10.1051/0004-6361:20042036). arXiv: [astro-ph/0503189 \[astro-ph\]](https://arxiv.org/abs/astro-ph/0503189).
- Bouwens, R. J. et al. (Nov. 2009). “UV Continuum Slope and Dust Obscuration from  $z \sim 6$  to  $z \sim 2$ : The Star Formation Rate Density at High Redshift”. In: *Astrophys. J.* 705.1, pp. 936–961. DOI: [10.1088/0004-637X/705/1/936](https://doi.org/10.1088/0004-637X/705/1/936). arXiv: [0909.4074 \[astro-ph.CO\]](https://arxiv.org/abs/0909.4074).
- Bowman, Judd D. et al. (Mar. 2018). “An absorption profile centred at 78 megahertz in the sky-averaged spectrum”. In: *Nature*. 555.7694, pp. 67–70. DOI: [10.1038/nature25792](https://doi.org/10.1038/nature25792). arXiv: [1810.05912 \[astro-ph.CO\]](https://arxiv.org/abs/1810.05912).
- Boylan-Kolchin, Michael et al. (Sept. 2009). “Resolving cosmic structure formation with the Millennium-II Simulation”. In: *Mon. Not. R. Astron. Soc.* 398.3, pp. 1150–1164. DOI: [10.1111/j.1365-2966.2009.15191.x](https://doi.org/10.1111/j.1365-2966.2009.15191.x). arXiv: [0903.3041 \[astro-ph.CO\]](https://arxiv.org/abs/0903.3041).
- Bradley, Larry D. et al. (Oct. 2022). “High-Redshift Galaxy Candidates at  $z = 9 - 13$  as Revealed by JWST Observations of WHL0137-08”. In: *arXiv e-prints*, arXiv:2210.01777, arXiv:2210.01777. arXiv: [2210.01777 \[astro-ph.GA\]](https://arxiv.org/abs/2210.01777).
- Brammer, Gabriel B. et al. (Oct. 2008). “EAZY: A Fast, Public Photometric Redshift Code”. In: *Astrophys. J.* 686.2, pp. 1503–1513. DOI: [10.1086/591786](https://doi.org/10.1086/591786). arXiv: [0807.1533 \[astro-ph\]](https://arxiv.org/abs/0807.1533).
- Brand, J.C.D. (1995). *Lines Of Light: The Sources Of*. Taylor & Francis. ISBN: 9782884491624. URL: <https://books.google.co.za/books?id=spYSK-g8DrkC>.
- Brüggen, M. et al. (Jan. 2011). “Magnetic fields and shock waves in cluster outskirts”. In: *Mem. Societa Astronomica Italiana* 82, p. 627. arXiv: [1102.1926 \[astro-ph.CO\]](https://arxiv.org/abs/1102.1926).
- Brunetti, G. et al. (Oct. 2008). “A low-frequency radio halo associated with a cluster of galaxies”. In: *Nature*. 455.7215, pp. 944–947. DOI: [10.1038/nature07379](https://doi.org/10.1038/nature07379). arXiv: [0810.4288 \[astro-ph\]](https://arxiv.org/abs/0810.4288).
- Brunetti, G. et al. (Nov. 2009). “On the evolution of giant radio halos and their connection with cluster mergers”. In: *Astron. Astrophys.* 507.2, pp. 661–669. DOI: [10.1051/0004-6361/200912751](https://doi.org/10.1051/0004-6361/200912751). arXiv: [0909.2343 \[astro-ph.CO\]](https://arxiv.org/abs/0909.2343).
- Brunetti, G. et al. (Dec. 2017). “Relativistic protons in the Coma galaxy cluster: first gamma-ray constraints ever on turbulent reacceleration”. In: *Mon. Not. R. Astron. Soc.* 472.2, pp. 1506–1525. DOI: [10.1093/mnras/stx2092](https://doi.org/10.1093/mnras/stx2092). arXiv: [1707.02085 \[astro-ph.HE\]](https://arxiv.org/abs/1707.02085).
- Brunetti, Gianfranco (Dec. 2004). “Particle Acceleration and Non-Thermal Emission from Galaxy Clusters”. In: *Journal of Korean Astronomical Society* 37.5, pp. 493–500. DOI: [10.5303/JKAS.2004.37.5.493](https://doi.org/10.5303/JKAS.2004.37.5.493). arXiv: [astro-ph/0412529 \[astro-ph\]](https://arxiv.org/abs/astro-ph/0412529).

- Brunetti, Gianfranco and Thomas W. Jones (Mar. 2014). “Cosmic Rays in Galaxy Clusters and Their Nonthermal Emission”. In: *International Journal of Modern Physics D* 23.4, 1430007-98, pp. 1430007–98. DOI: [10.1142/S0218271814300079](https://doi.org/10.1142/S0218271814300079). arXiv: [1401.7519 \[astro-ph.CO\]](https://arxiv.org/abs/1401.7519).
- Brunner, H. et al. (May 2022). “The eROSITA Final Equatorial Depth Survey (eFEDS). X-ray catalogue”. In: *Astron. Astrophys.* 661, A1, A1. DOI: [10.1051/0004-6361/202141266](https://doi.org/10.1051/0004-6361/202141266). arXiv: [2106.14517 \[astro-ph.HE\]](https://arxiv.org/abs/2106.14517).
- Brunner, R. J. and L. M. Lubin (Dec. 2000). “A Probabilistic Quantification of Galaxy Cluster Membership”. In: *The Astronomical Journal* 120.6, pp. 2851–2858. DOI: [10.1086/316849](https://doi.org/10.1086/316849). URL: <https://doi.org/10.1086/316849>.
- Butcher, H. and Jr. Oemler A. (Jan. 1978). “The evolution of galaxies in clusters. I. ISIT photometry of Cl 0024+1654 and 3C 295.” In: *Astrophys. J.* 219, pp. 18–30. DOI: [10.1086/155751](https://doi.org/10.1086/155751).
- Bîrzan, L et al. (June 2020). “LOFAR observations of X-ray cavity systems”. In: *Monthly Notices of the Royal Astronomical Society* 496.3, pp. 2613–2635. ISSN: 0035-8711. DOI: [10.1093/mnras/staa1594](https://doi.org/10.1093/mnras/staa1594). eprint: <https://academic.oup.com/mnras/article-pdf/496/3/2613/33484638/staa1594.pdf>. URL: <https://doi.org/10.1093/mnras/staa1594>.
- Camilo, F. et al. (Apr. 2018). “Revival of the Magnetar PSR J1622-4950: Observations with MeerKAT, Parkes, XMM-Newton, Swift, Chandra, and NuSTAR”. In: *Astrophys. J.* 856.2, 180, p. 180. DOI: [10.3847/1538-4357/aab35a](https://doi.org/10.3847/1538-4357/aab35a). arXiv: [1804.01933 \[astro-ph.HE\]](https://arxiv.org/abs/1804.01933).
- Carliles, Samuel et al. (Mar. 2010). “Random Forests for Photometric Redshifts”. In: *Astrophys. J.* 712.1, pp. 511–515. DOI: [10.1088/0004-637X/712/1/511](https://doi.org/10.1088/0004-637X/712/1/511).
- Cassano, R. et al. (Oct. 2010). “On the Connection Between Giant Radio Halos and Cluster Mergers”. In: *Astrophys. J. Lett.* 721.2, pp. L82–L85. DOI: [10.1088/2041-8205/721/2/L82](https://doi.org/10.1088/2041-8205/721/2/L82). arXiv: [1008.3624 \[astro-ph.CO\]](https://arxiv.org/abs/1008.3624).
- Cassano, R. et al. (Dec. 2011). “The Connection between Radio Halos and Cluster Mergers and the Statistical Properties of the Radio Halo Population”. In: *Journal of Astrophysics and Astronomy* 32, pp. 519–527. DOI: [10.1007/s12036-011-9117-1](https://doi.org/10.1007/s12036-011-9117-1). arXiv: [1108.0291 \[astro-ph.CO\]](https://arxiv.org/abs/1108.0291).
- Cassano, R. et al. (Nov. 2013). “Revisiting Scaling Relations for Giant Radio Halos in Galaxy Clusters”. In: *Astrophys. J.* 777.2, 141, p. 141. DOI: [10.1088/0004-637X/777/2/141](https://doi.org/10.1088/0004-637X/777/2/141). arXiv: [1306.4379 \[astro-ph.CO\]](https://arxiv.org/abs/1306.4379).
- Castellano, Marco et al. (Oct. 2022). “Early Results from GLASS-JWST. III. Galaxy Candidates at z 9-15”. In: *Astrophys. J. Lett.* 938.2, L15, p. L15. DOI: [10.3847/2041-8213/ac94d0](https://doi.org/10.3847/2041-8213/ac94d0). arXiv: [2207.09436 \[astro-ph.GA\]](https://arxiv.org/abs/2207.09436).
- Cavaliere, A. and R. Fusco-Femiano (May 1976). “X-rays from hot plasma in clusters of galaxies.” In: *Astron. Astrophys.* 49, pp. 137–144.
- Chabrier, Gilles (July 2003). “Galactic Stellar and Substellar Initial Mass Function”. In: *Pub. Astron. Soc. Pacific* 115.809, pp. 763–795. DOI: [10.1086/376392](https://doi.org/10.1086/376392). arXiv: [astro-ph/0304382 \[astro-ph\]](https://arxiv.org/abs/astro-ph/0304382).
- Chevallard, Jacopo and Stéphane Charlot (Oct. 2016). “Modelling and interpreting spectral energy distributions of galaxies with BEAGLE”. In: *Mon. Not. R. As-*

- tron. Soc.* 462.2, pp. 1415–1443. DOI: [10.1093/mnras/stw1756](https://doi.org/10.1093/mnras/stw1756). arXiv: [1603.03037 \[astro-ph.GA\]](https://arxiv.org/abs/1603.03037).
- Chon, Gayoung et al. (Jan. 2019). “Interaction of the massive cluster system Abell 3016/3017 embedded in a cosmic filament”. In: *Astron. Astrophys.* 621, A77, A77. DOI: [10.1051/0004-6361/201833068](https://doi.org/10.1051/0004-6361/201833068). arXiv: [2105.14000 \[astro-ph.CO\]](https://arxiv.org/abs/2105.14000).
- Chung, Sun Mi et al. (Dec. 2010). “Star Formation in the Bullet Cluster. I. The Infrared Luminosity Function and Star Formation Rate”. In: *Astrophys. J.* 725.2, pp. 1536–1549. DOI: [10.1088/0004-637X/725/2/1536](https://doi.org/10.1088/0004-637X/725/2/1536). arXiv: [1005.3847 \[astro-ph.CO\]](https://arxiv.org/abs/1005.3847).
- Clowe, Douglas et al. (Sept. 2006). “A Direct Empirical Proof of the Existence of Dark Matter”. In: *Astrophys. J. Lett.* 648.2, pp. L109–L113. DOI: [10.1086/508162](https://doi.org/10.1086/508162). arXiv: [astro-ph/0608407 \[astro-ph\]](https://arxiv.org/abs/astro-ph/0608407).
- Cohen, Seth A. et al. (Mar. 2014). “Star Formation and Substructure in Galaxy Clusters”. In: *Astrophys. J.* 783.2, 136, p. 136. DOI: [10.1088/0004-637X/783/2/136](https://doi.org/10.1088/0004-637X/783/2/136). arXiv: [1401.6171 \[astro-ph.CO\]](https://arxiv.org/abs/1401.6171).
- Cohen, Seth A. et al. (June 2015). “Star Formation and Relaxation in 379 Nearby Galaxy Clusters”. In: *Astrophys. J.* 806.1, 85, p. 85. DOI: [10.1088/0004-637X/806/1/85](https://doi.org/10.1088/0004-637X/806/1/85). arXiv: [1504.05191 \[astro-ph.GA\]](https://arxiv.org/abs/1504.05191).
- Cole, S. et al. (Dec. 1994). “A recipe for galaxy formation.” In: *Mon. Not. R. Astron. Soc.* 271, pp. 781–806. DOI: [10.1093/mnras/271.4.781](https://doi.org/10.1093/mnras/271.4.781). arXiv: [astro-ph/9402001 \[astro-ph\]](https://arxiv.org/abs/astro-ph/9402001).
- Coleman, G. D. et al. (July 1980). “Colors and magnitudes predicted for high redshift galaxies”. In: *Astrophys. J. Supp.* 43, pp. 393–416. DOI: [10.1086/190674](https://doi.org/10.1086/190674).
- Condon, J. J. (Jan. 1992). “Radio emission from normal galaxies.” In: *Annu. Rev. Astron. Astrophys.* 30, pp. 575–611. DOI: [10.1146/annurev.aa.30.090192.003043](https://doi.org/10.1146/annurev.aa.30.090192.003043).
- Condon, J. J. et al. (July 1991). “Correlations between Far-Infrared, Radio, and Blue Luminosities of Spiral Galaxies”. In: *Astrophys. J.* 376, p. 95. DOI: [10.1086/170258](https://doi.org/10.1086/170258).
- Condon, J. J. et al. (Aug. 2002). “Radio Sources and Star Formation in the Local Universe”. In: *Astron. J.* 124.2, pp. 675–689. DOI: [10.1086/341650](https://doi.org/10.1086/341650).
- Conroy, Charlie (Aug. 2013). “Modeling the Panchromatic Spectral Energy Distributions of Galaxies”. In: *Annu. Rev. Astron. Astrophys.* 51.1, pp. 393–455. DOI: [10.1146/annurev-astro-082812-141017](https://doi.org/10.1146/annurev-astro-082812-141017). arXiv: [1301.7095 \[astro-ph.CO\]](https://arxiv.org/abs/1301.7095).
- Conroy, Charlie et al. (July 2009). “The Propagation of Uncertainties in Stellar Population Synthesis Modeling. I. The Relevance of Uncertain Aspects of Stellar Evolution and the Initial Mass Function to the Derived Physical Properties of Galaxies”. In: *Astrophys. J.* 699.1, pp. 486–506. DOI: [10.1088/0004-637X/699/1/486](https://doi.org/10.1088/0004-637X/699/1/486). arXiv: [0809.4261 \[astro-ph\]](https://arxiv.org/abs/0809.4261).
- Conselice, Christopher J. et al. (Oct. 2016). “The Evolution of Galaxy Number Density at  $z \geq 8$  and Its Implications”. In: *Astrophys. J.* 830.2, 83, p. 83. DOI: [10.3847/0004-637X/830/2/83](https://doi.org/10.3847/0004-637X/830/2/83). arXiv: [1607.03909 \[astro-ph.GA\]](https://arxiv.org/abs/1607.03909).
- Cortese, L. et al. (Aug. 2021). “The Dawes Review 9: The role of cold gas stripping on the star formation quenching of satellite galaxies”. In: *Pub. Astron. Soc. Australia* 38, e035, e035. DOI: [10.1017/pasa.2021.18](https://doi.org/10.1017/pasa.2021.18). arXiv: [2104.02193 \[astro-ph.GA\]](https://arxiv.org/abs/2104.02193).

- Cramer, W. J. et al. (Jan. 2019). “Spectacular Hubble Space Telescope Observations of the Coma Galaxy D100 and Star Formation in Its Ram Pressure-stripped Tail”. In: *Astrophys. J.* 870.2, 63, p. 63. DOI: [10.3847/1538-4357/aaefff](https://doi.org/10.3847/1538-4357/aaefff). arXiv: [1811.04916 \[astro-ph.GA\]](https://arxiv.org/abs/1811.04916).
- Curti, Mirko et al. (Sept. 2022). “The chemical enrichment in the early Universe as probed by JWST via direct metallicity measurements at  $z \approx 8$ ”. In: *Mon. Not. R. Astron. Soc.* DOI: [10.1093/mnras/stac2737](https://doi.org/10.1093/mnras/stac2737). arXiv: [2207.12375 \[astro-ph.GA\]](https://arxiv.org/abs/2207.12375).
- da Cunha, Elisabete et al. (Aug. 2008). “A simple model to interpret the ultraviolet, optical and infrared emission from galaxies”. In: *Mon. Not. R. Astron. Soc.* 388.4, pp. 1595–1617. DOI: [10.1111/j.1365-2966.2008.13535.x](https://doi.org/10.1111/j.1365-2966.2008.13535.x). arXiv: [0806.1020 \[astro-ph\]](https://arxiv.org/abs/0806.1020).
- Dark Energy Survey Collaboration et al. (Aug. 2016). “The Dark Energy Survey: more than dark energy - an overview”. In: *Mon. Not. R. Astron. Soc.* 460.2, pp. 1270–1299. DOI: [10.1093/mnras/stw641](https://doi.org/10.1093/mnras/stw641). arXiv: [1601.00329 \[astro-ph.CO\]](https://arxiv.org/abs/1601.00329).
- Darvish, Behnam et al. (July 2016). “The Effects of the Local Environment and Stellar Mass on Galaxy Quenching to  $z \sim 3$ ”. In: *Astrophys. J.* 825.2, 113, p. 113. DOI: [10.3847/0004-637X/825/2/113](https://doi.org/10.3847/0004-637X/825/2/113). arXiv: [1605.03182 \[astro-ph.GA\]](https://arxiv.org/abs/1605.03182).
- de Gasperin, F. et al. (Nov. 2014). “A new double radio relic in PSZ1 G096.89+24.17 and a radio relic mass-luminosity relation”. In: *Mon. Not. R. Astron. Soc.* 444.4, pp. 3130–3138. DOI: [10.1093/mnras/stu1658](https://doi.org/10.1093/mnras/stu1658). arXiv: [1408.2677 \[astro-ph.CO\]](https://arxiv.org/abs/1408.2677).
- de Gasperin, F. et al. (Nov. 2015). “A powerful double radio relic system discovered in PSZ1 G108.18-11.53: evidence for a shock with non-uniform Mach number?” In: *Mon. Not. R. Astron. Soc.* 453.4, pp. 3483–3498. DOI: [10.1093/mnras/stv1873](https://doi.org/10.1093/mnras/stv1873). arXiv: [1508.02901 \[astro-ph.HE\]](https://arxiv.org/abs/1508.02901).
- de Gasperin, Francesco et al. (Oct. 2017). “Gentle reenergization of electrons in merging galaxy clusters”. In: *Science Advances* 3.10, e1701634. DOI: [10.1126/sciadv.1701634](https://doi.org/10.1126/sciadv.1701634). arXiv: [1710.06796 \[astro-ph.HE\]](https://arxiv.org/abs/1710.06796).
- de Lera Acedo, E. and de Villiers D. I. L. (July 2022). “The REACH radiometer for detecting the 21-cm hydrogen signal from redshift  $z \approx 7.5-28$ ”. In: *Nature*. 2397.3366, pp. 67–70. DOI: <https://doi.org/10.1038/s41550-022-01709-9>.
- De Lucia, Gabriella and Jérémie Blaizot (Feb. 2007). “The hierarchical formation of the brightest cluster galaxies”. In: *Mon. Not. R. Astron. Soc.* 375.1, pp. 2–14. DOI: [10.1111/j.1365-2966.2006.11287.x](https://doi.org/10.1111/j.1365-2966.2006.11287.x). arXiv: [astro-ph/0606519 \[astro-ph\]](https://arxiv.org/abs/astro-ph/0606519).
- De Lucia, Gabriella et al. (Jan. 2007). “The build-up of the colour-magnitude relation in galaxy clusters since  $z \approx 0.8$ ”. In: *Mon. Not. R. Astron. Soc.* 374.3, pp. 809–822. DOI: [10.1111/j.1365-2966.2006.11199.x](https://doi.org/10.1111/j.1365-2966.2006.11199.x). arXiv: [astro-ph/0610373 \[astro-ph\]](https://arxiv.org/abs/astro-ph/0610373).
- DeBoer, David R. et al. (Apr. 2017). “Hydrogen Epoch of Reionization Array (HERA)”. In: *Pub. Astron. Soc. Pacific* 129.974, p. 045001. DOI: [10.1088/1538-3873/129/974/045001](https://doi.org/10.1088/1538-3873/129/974/045001). arXiv: [1606.07473 \[astro-ph.IM\]](https://arxiv.org/abs/1606.07473).
- Dennison, B. (Aug. 1980). “Formation of radio halos in clusters of galaxies from cosmic-ray protons.” In: *Astrophys. J. Lett.* 239, pp. L93–L96. DOI: [10.1086/183300](https://doi.org/10.1086/183300).

- Dey, Arjun et al. (May 2019). “Overview of the DESI Legacy Imaging Surveys”. In: *Astron. J.* 157.5, 168, p. 168. DOI: [10.3847/1538-3881/ab089d](https://doi.org/10.3847/1538-3881/ab089d). arXiv: [1804.08657 \[astro-ph.IM\]](https://arxiv.org/abs/1804.08657).
- Dijkstra, Mark and Eduard Westra (Feb. 2010). “Star formation indicators and line equivalent width in Ly-alpha galaxies”. In: *Mon. Not. R. Astron. Soc.* 401.4, pp. 2343–2348. DOI: [10.1111/j.1365-2966.2009.15859.x](https://doi.org/10.1111/j.1365-2966.2009.15859.x). arXiv: [0911.1357 \[astro-ph.CO\]](https://arxiv.org/abs/0911.1357).
- Domínguez, A. et al. (Feb. 2013). “Dust Extinction from Balmer Decrement of Star-forming Galaxies at  $0.75 \leq z \leq 1.5$  with Hubble Space Telescope/Wide-Field-Camera 3 Spectroscopy from the WFC3 Infrared Spectroscopic Parallel Survey”. In: *Astrophys. J.* 763.2, 145, p. 145. DOI: [10.1088/0004-637X/763/2/145](https://doi.org/10.1088/0004-637X/763/2/145). arXiv: [1206.1867 \[astro-ph.CO\]](https://arxiv.org/abs/1206.1867).
- Donnert, J. and G. Brunetti (Oct. 2014). “An efficient Fokker-Planck solver and its application to stochastic particle acceleration in galaxy clusters”. In: *Mon. Not. R. Astron. Soc.* 443.4, pp. 3564–3577. DOI: [10.1093/mnras/stu1417](https://doi.org/10.1093/mnras/stu1417). arXiv: [1407.2735 \[astro-ph.CO\]](https://arxiv.org/abs/1407.2735).
- Dressler, Alan et al. (Dec. 1997). “Evolution since  $z = 0.5$  of the Morphology-Density Relation for Clusters of Galaxies”. In: *Astrophys. J.* 490.2, pp. 577–591. DOI: [10.1086/304890](https://doi.org/10.1086/304890). arXiv: [astro-ph/9707232 \[astro-ph\]](https://arxiv.org/abs/astro-ph/9707232).
- Drury, L. Oc. (Aug. 1983). “REVIEW ARTICLE: An introduction to the theory of diffusive shock acceleration of energetic particles in tenuous plasmas”. In: *Reports on Progress in Physics* 46.8, pp. 973–1027. DOI: [10.1088/0034-4885/46/8/002](https://doi.org/10.1088/0034-4885/46/8/002).
- Ebeling, H. et al. (Feb. 2014). “Jellyfish: Evidence of Extreme Ram-pressure Stripping in Massive Galaxy Clusters”. In: *Astrophys. J. Lett.* 781.2, L40, p. L40. DOI: [10.1088/2041-8205/781/2/L40](https://doi.org/10.1088/2041-8205/781/2/L40). arXiv: [1312.6135 \[astro-ph.GA\]](https://arxiv.org/abs/1312.6135).
- Eckert, D. et al. (Feb. 2011). “The cool-core bias in X-ray galaxy cluster samples. I. Method and application to HIFLUGCS”. In: *Astron. Astrophys.* 526, A79, A79. DOI: [10.1051/0004-6361/201015856](https://doi.org/10.1051/0004-6361/201015856). arXiv: [1011.3302 \[astro-ph.CO\]](https://arxiv.org/abs/1011.3302).
- Einasto, M. et al. (Apr. 2012). “Multimodality in galaxy clusters from SDSS DR8: substructure and velocity distribution”. In: *Astron. Astrophys.* 540, A123, A123. DOI: [10.1051/0004-6361/201118697](https://doi.org/10.1051/0004-6361/201118697). arXiv: [1202.4927 \[astro-ph.CO\]](https://arxiv.org/abs/1202.4927).
- Einstein, Albert (Jan. 1915). “Die Feldgleichungen der Gravitation”. In: *Sitzungsberichte der Königlich Preußischen Akademie der Wissenschaften (Berlin)*, pp. 844–847.
- Eke, V. R. et al. (Mar. 2004). “Galaxy groups in the 2dFGRS: the group-finding algorithm and the 2PIGG catalogue”. In: *Mon. Not. R. Astron. Soc.* 348.3, pp. 866–878. DOI: [10.1111/j.1365-2966.2004.07408.x](https://doi.org/10.1111/j.1365-2966.2004.07408.x). arXiv: [astro-ph/0402567 \[astro-ph\]](https://arxiv.org/abs/astro-ph/0402567).
- Elbaz, D. et al. (June 2007). “The reversal of the star formation-density relation in the distant universe”. In: *Astron. Astrophys.* 468.1, pp. 33–48. DOI: [10.1051/0004-6361:20077525](https://doi.org/10.1051/0004-6361:20077525). arXiv: [astro-ph/0703653 \[astro-ph\]](https://arxiv.org/abs/astro-ph/0703653).
- Enßlin, T. et al. (Mar. 2011). “Cosmic ray transport in galaxy clusters: implications for radio halos, gamma-ray signatures, and cool core heating”. In: *Astron. Astrophys.* 527, A99, A99. DOI: [10.1051/0004-6361/201015652](https://doi.org/10.1051/0004-6361/201015652). arXiv: [1008.4717 \[astro-ph.CO\]](https://arxiv.org/abs/1008.4717).

- Evans, Ian N. et al. (Mar. 2019). “Chandra Source Catalog Release 2.0 - The State of the Art Serendipitous X-ray Source Catalog”. In: *AAS/High Energy Astrophysics Division*. Vol. 17. AAS/High Energy Astrophysics Division, 114.01, p. 114.01.
- Event Horizon Telescope Collaboration et al. (Apr. 2019). “First M87 Event Horizon Telescope Results. I. The Shadow of the Supermassive Black Hole”. In: *Astrophys. J. Lett.* 875.1, L1, p. L1. DOI: [10.3847/2041-8213/ab0ec7](https://doi.org/10.3847/2041-8213/ab0ec7). arXiv: [1906.11238 \[astro-ph.GA\]](https://arxiv.org/abs/1906.11238).
- Fabricant, D. et al. (Oct. 1980). “X-ray measurements of the mass of M 87.” In: *Astrophys. J.* 241, pp. 552–560. DOI: [10.1086/158369](https://doi.org/10.1086/158369).
- Feretti, L. and G. Giovannini (2008). “Clusters of Galaxies in the Radio: Relativistic Plasma and ICM/Radio Galaxy Interaction Processes”. In: *A Pan-Chromatic View of Clusters of Galaxies and the Large-Scale Structure*. Ed. by M. Plionis et al. Vol. 740, p. 24. DOI: [10.1007/978-1-4020-6941-3\\_5](https://doi.org/10.1007/978-1-4020-6941-3_5).
- Feretti, Luigina (Sept. 2003). “Non-Thermal Phenomena in Galaxy Clusters”. In: *Texas in Tuscany. XXI Symposium on Relativistic Astrophysics*. Ed. by R. Bandiera et al., pp. 209–220. DOI: [10.1142/9789812704009\\_0019](https://doi.org/10.1142/9789812704009_0019). arXiv: [astro-ph/0309221 \[astro-ph\]](https://arxiv.org/abs/astro-ph/0309221).
- Feretti, Luigina et al. (May 2012). “Clusters of galaxies: observational properties of the diffuse radio emission”. In: *Astron. Astrophys. Rev.* 20, 54, p. 54. DOI: [10.1007/s00159-012-0054-z](https://doi.org/10.1007/s00159-012-0054-z). arXiv: [1205.1919 \[astro-ph.CO\]](https://arxiv.org/abs/1205.1919).
- Ferrari, C. et al. (Mar. 2003). “Multiple merging events in Abell 521”. In: *Astron. Astrophys.* 399, pp. 813–828. DOI: [10.1051/0004-6361:20021741](https://doi.org/10.1051/0004-6361:20021741). arXiv: [astro-ph/0211592 \[astro-ph\]](https://arxiv.org/abs/astro-ph/0211592).
- Ferrari, C. et al. (Feb. 2006). “Chandra observation of the multiple merger cluster Abell 521”. In: *Astron. Astrophys.* 446.2, pp. 417–428. DOI: [10.1051/0004-6361:20053946](https://doi.org/10.1051/0004-6361:20053946). arXiv: [astro-ph/0508585 \[astro-ph\]](https://arxiv.org/abs/astro-ph/0508585).
- Ferrari, C. et al. (Feb. 2008). “Observations of Extended Radio Emission in Clusters”. In: *Space Sci. Rev.* 134.1-4, pp. 93–118. DOI: [10.1007/s11214-008-9311-x](https://doi.org/10.1007/s11214-008-9311-x). arXiv: [0801.0985 \[astro-ph\]](https://arxiv.org/abs/0801.0985).
- Figueira, M. et al. (Nov. 2022). “SFR estimations from  $z = 0$  to  $z = 0.9$ . A comparison of SFR calibrators for star-forming galaxies”. In: *Astron. Astrophys.* 667, A29, A29. DOI: [10.1051/0004-6361/202141701](https://doi.org/10.1051/0004-6361/202141701). arXiv: [2209.04390 \[astro-ph.GA\]](https://arxiv.org/abs/2209.04390).
- Finoguenov, A. et al. (Sept. 2007). “The XMM-Newton Wide-Field Survey in the COSMOS Field: Statistical Properties of Clusters of Galaxies”. In: *Astrophys. J. Suppl.* 172.1, pp. 182–195. DOI: [10.1086/516577](https://doi.org/10.1086/516577). arXiv: [astro-ph/0612360 \[astro-ph\]](https://arxiv.org/abs/astro-ph/0612360).
- Finoguenov, Alexis et al. (June 2010). “XMM-Newton Observation of the Northwest Radio Relic Region in A3667”. In: *Astrophys. J.* 715.2, pp. 1143–1151. DOI: [10.1088/0004-637X/715/2/1143](https://doi.org/10.1088/0004-637X/715/2/1143). arXiv: [1004.2331 \[astro-ph.CO\]](https://arxiv.org/abs/1004.2331).
- Flaugher, B. et al. (Oct. 2015). “THE DARK ENERGY CAMERA”. In: *The Astronomical Journal* 150.5, p. 150. ISSN: 1538-3881. DOI: [10.1088/0004-6256/150/5/150](https://doi.org/10.1088/0004-6256/150/5/150). URL: <http://dx.doi.org/10.1088/0004-6256/150/5/150>.
- Foëx, G. et al. (Oct. 2017a). “Comparison of hydrostatic and dynamical masses of distant X-ray luminous galaxy clusters”. In: *Astron. Astrophys.* 606, A122, A122. DOI: [10.1051/0004-6361/201731104](https://doi.org/10.1051/0004-6361/201731104). arXiv: [1707.05985 \[astro-ph.CO\]](https://arxiv.org/abs/1707.05985).

- Foëx, G. et al. (May 2017b). “From the core to the outskirts: structure analysis of three massive galaxy clusters”. In: *Astron. Astrophys.* 601, A145, A145. DOI: [10.1051/0004-6361/201630086](https://doi.org/10.1051/0004-6361/201630086). arXiv: [1703.02763 \[astro-ph.CO\]](https://arxiv.org/abs/1703.02763).
- Fontana, Adriano et al. (Nov. 2000). “Photometric Redshifts and Selection of High-Redshift Galaxies in the NTT and Hubble Deep Fields”. In: *Astron. J.* 120.5, pp. 2206–2219. DOI: [10.1086/316803](https://doi.org/10.1086/316803). arXiv: [astro-ph/0009158 \[astro-ph\]](https://arxiv.org/abs/astro-ph/0009158).
- Fowler, Joseph W. (Oct. 2004). “The Atacama Cosmology Telescope Project”. In: *Z-Spec: a broadband millimeter-wave grating spectrometer: design, construction, and first cryogenic measurements*. Ed. by C. Matt Bradford et al. Vol. 5498. Society of Photo-Optical Instrumentation Engineers (SPIE) Conference Series, pp. 1–10. DOI: [10.1117/12.553054](https://doi.org/10.1117/12.553054).
- Friedmann, A. (Jan. 1922). “Über die Krümmung des Raumes”. In: *Zeitschrift für Physik* 10, pp. 377–386. DOI: [10.1007/BF01332580](https://doi.org/10.1007/BF01332580).
- Fujita, Yutaka and Masahiro Nagashima (May 1999). “Effects of Ram Pressure from the Intracluster Medium on the Star Formation Rate of Disk Galaxies in Clusters of Galaxies”. In: *Astrophys. J.* 516.2, pp. 619–625. DOI: [10.1086/307139](https://doi.org/10.1086/307139). arXiv: [astro-ph/9812378 \[astro-ph\]](https://arxiv.org/abs/astro-ph/9812378).
- Fujita, Yutaka et al. (July 2007). “Nonthermal Emission Associated with Strong AGN Outbursts at the Centers of Galaxy Clusters”. In: *Astrophys. J. Lett.* 663.2, pp. L61–L64. DOI: [10.1086/520337](https://doi.org/10.1086/520337). arXiv: [0705.4284 \[astro-ph\]](https://arxiv.org/abs/0705.4284).
- Gao, L. et al. (Sept. 2012). “The Phoenix Project: the dark side of rich Galaxy clusters”. In: *Mon. Not. R. Astron. Soc.* 425.3, pp. 2169–2186. DOI: [10.1111/j.1365-2966.2012.21564.x](https://doi.org/10.1111/j.1365-2966.2012.21564.x). arXiv: [1201.1940 \[astro-ph.CO\]](https://arxiv.org/abs/1201.1940).
- Gardner, Jonathan P. et al. (Apr. 2006). “The James Webb Space Telescope”. In: *Space Sci. Rev.* 123.4, pp. 485–606. DOI: [10.1007/s11214-006-8315-7](https://doi.org/10.1007/s11214-006-8315-7). arXiv: [astro-ph/0606175 \[astro-ph\]](https://arxiv.org/abs/astro-ph/0606175).
- Gendron-Marsolais, M. et al. (Aug. 2017). “Deep 230-470 MHz VLA observations of the mini-halo in the Perseus cluster”. In: *Mon. Not. R. Astron. Soc.* 469.4, pp. 3872–3880. DOI: [10.1093/mnras/stx1042](https://doi.org/10.1093/mnras/stx1042). arXiv: [1701.03791 \[astro-ph.CO\]](https://arxiv.org/abs/1701.03791).
- Giacconi, R. et al. (Dec. 1972). “The Uhuru catalog of X-ray sources.” In: *Astrophys. J.* 178, pp. 281–308. DOI: [10.1086/151790](https://doi.org/10.1086/151790).
- Giacintucci, S. et al. (Aug. 2008). “Shock acceleration as origin of the radio relic in A 521?” In: *Astron. Astrophys.* 486.2, pp. 347–358. DOI: [10.1051/0004-6361:200809459](https://doi.org/10.1051/0004-6361:200809459). arXiv: [0803.4127 \[astro-ph\]](https://arxiv.org/abs/0803.4127).
- Giacintucci, S. et al. (Mar. 2020). “Discovery of a Giant Radio Fossil in the Ophiuchus Galaxy Cluster”. In: *Astrophys. J.* 891.1, 1, p. 1. DOI: [10.3847/1538-4357/ab6a9d](https://doi.org/10.3847/1538-4357/ab6a9d). arXiv: [2002.01291 \[astro-ph.GA\]](https://arxiv.org/abs/2002.01291).
- Giacintucci, Simona et al. (June 2017). “Occurrence of Radio Minihalos in a Mass-limited Sample of Galaxy Clusters”. In: *Astrophys. J.* 841.2, 71, p. 71. DOI: [10.3847/1538-4357/aa7069](https://doi.org/10.3847/1538-4357/aa7069). arXiv: [1701.01364 \[astro-ph.HE\]](https://arxiv.org/abs/1701.01364).
- Giacintucci, Simona et al. (Aug. 2019). “Expanding the Sample of Radio Minihalos in Galaxy Clusters”. In: *Astrophys. J.* 880.2, 70, p. 70. DOI: [10.3847/1538-4357/ab29f1](https://doi.org/10.3847/1538-4357/ab29f1). arXiv: [1906.07087 \[astro-ph.HE\]](https://arxiv.org/abs/1906.07087).
- Giovannini, G. et al. (Apr. 1993). “The Halo Radio Source Coma C and the Origin of Halo Sources”. In: *Astrophys. J.* 406, p. 399. DOI: [10.1086/172451](https://doi.org/10.1086/172451).

- Giovannini, G. et al. (Mar. 1999). “Radio halo and relic candidates from the NRAO VLA Sky Survey”. In: *New Astron.* 4.2, pp. 141–155. DOI: [10.1016/S1384-1076\(99\)00018-4](https://doi.org/10.1016/S1384-1076(99)00018-4). arXiv: [astro-ph/9904210 \[astro-ph\]](https://arxiv.org/abs/astro-ph/9904210).
- Girardi, M. et al. (Mar. 2016). “A multiwavelength view of the galaxy cluster Abell 523 and its peculiar diffuse radio source”. In: *Mon. Not. R. Astron. Soc.* 456.3, pp. 2829–2847. DOI: [10.1093/mnras/stv2827](https://doi.org/10.1093/mnras/stv2827). arXiv: [1510.05951 \[astro-ph.GA\]](https://arxiv.org/abs/1510.05951).
- Gitti, M. et al. (Apr. 2015). “The SKA view of cool-core clusters: evolution of radio mini-halos and AGN feedback”. In: *Advancing Astrophysics with the Square Kilometre Array (AASKA14)*, 76, p. 76. DOI: [10.22323/1.215.0076](https://doi.org/10.22323/1.215.0076). arXiv: [1412.5664 \[astro-ph.CO\]](https://arxiv.org/abs/1412.5664).
- Gladders, Michael D. and H. K. C. Yee (Oct. 2000). “A New Method For Galaxy Cluster Detection. I. The Algorithm”. In: *Astron. J.* 120.4, pp. 2148–2162. DOI: [10.1086/301557](https://doi.org/10.1086/301557). arXiv: [astro-ph/0004092 \[astro-ph\]](https://arxiv.org/abs/astro-ph/0004092).
- (Mar. 2005). “The Red-Sequence Cluster Survey. I. The Survey and Cluster Catalogs for Patches RCS 0926+37 and RCS 1327+29”. In: *Astrophys. J. Supp.* 157.1, pp. 1–29. DOI: [10.1086/427327](https://doi.org/10.1086/427327). arXiv: [astro-ph/0411075 \[astro-ph\]](https://arxiv.org/abs/astro-ph/0411075).
- Gómez, Percy L. et al. (Feb. 2003). “Galaxy Star Formation as a Function of Environment in the Early Data Release of the Sloan Digital Sky Survey”. In: *Astrophys. J.* 584.1, pp. 210–227. DOI: [10.1086/345593](https://doi.org/10.1086/345593). arXiv: [astro-ph/0210193 \[astro-ph\]](https://arxiv.org/abs/astro-ph/0210193).
- Goto, Tomotsugu (Dec. 2004). “Do star formation rates of galaxy clusters depend on mass? Blue/late-type fractions and total star formation rates of 115 galaxy clusters as a function of cluster virial mass”. In: *Monthly Notices of the Royal Astronomical Society: Letters* 356.1, pp. L6–L10. DOI: [10.1111/j.1745-3933.2005.08566.x](https://doi.org/10.1111/j.1745-3933.2005.08566.x). URL: <https://doi.org/10.1111%2Fj.1745-3933.2005.08566.x>.
- Govoni, F. et al. (Jan. 2005). “A2255: The first detection of filamentary polarized emission in a radio halo”. In: *Astron. Astrophys.* 430, pp. L5–L8. DOI: [10.1051/0004-6361:200400113](https://doi.org/10.1051/0004-6361:200400113). arXiv: [astro-ph/0411720 \[astro-ph\]](https://arxiv.org/abs/astro-ph/0411720).
- Gunn, James E. and III Gott J. Richard (Aug. 1972). “On the Infall of Matter Into Clusters of Galaxies and Some Effects on Their Evolution”. In: *Astrophys. J.* 176, p. 1. DOI: [10.1086/151605](https://doi.org/10.1086/151605).
- Guo, Qi et al. (May 2011). “From dwarf spheroidals to cD galaxies: simulating the galaxy population in a  $\Lambda$ CDM cosmology”. In: *Mon. Not. R. Astron. Soc.* 413.1, pp. 101–131. DOI: [10.1111/j.1365-2966.2010.18114.x](https://doi.org/10.1111/j.1365-2966.2010.18114.x). arXiv: [1006.0106 \[astro-ph.CO\]](https://arxiv.org/abs/1006.0106).
- Hahn, ChangHoon et al. (June 2015). “PRIMUS: Effects of Galaxy Environment on the Quiescent Fraction Evolution at  $z \geq 0.8$ ”. In: *Astrophys. J.* 806.2, 162, p. 162. DOI: [10.1088/0004-637X/806/2/162](https://doi.org/10.1088/0004-637X/806/2/162). arXiv: [1412.7162 \[astro-ph.GA\]](https://arxiv.org/abs/1412.7162).
- Haines, C. P. et al. (Sept. 2007). “The different physical mechanisms that drive the star formation histories of giant and dwarf galaxies”. In: *Monthly Notices of the Royal Astronomical Society* 381.1, 7–32. ISSN: 1365-2966. DOI: [10.1111/j.1365-2966.2007.12189.x](https://doi.org/10.1111/j.1365-2966.2007.12189.x). URL: <http://dx.doi.org/10.1111/j.1365-2966.2007.12189.x>.
- Haines, C. P. et al. (Sept. 2013). “LoCuSS: THE STEADY DECLINE AND SLOW QUENCHING OF STAR FORMATION IN CLUSTER GALAXIES OVER THE

- LAST FOUR BILLION YEARS". In: *The Astrophysical Journal* 775.2, p. 126. ISSN: 1538-4357. DOI: [10.1088/0004-637x/775/2/126](https://doi.org/10.1088/0004-637x/775/2/126). URL: <http://dx.doi.org/10.1088/0004-637X/775/2/126>.
- Haines, C. P. et al. (June 2015). "LoCuSS: THE SLOW QUENCHING OF STAR FORMATION IN CLUSTER GALAXIES AND THE NEED FOR PRE-PROCESSING". In: *The Astrophysical Journal* 806.1, p. 101. ISSN: 1538-4357. DOI: [10.1088/0004-637x/806/1/101](https://doi.org/10.1088/0004-637x/806/1/101). URL: <http://dx.doi.org/10.1088/0004-637X/806/1/101>.
- Hao, Jiangang et al. (Dec. 2010). "A GMBCG Galaxy Cluster Catalog of 55,424 Rich Clusters from SDSS DR7". In: *Astrophys. J. Supp.* 191.2, pp. 254–274. DOI: [10.1088/0067-0049/191/2/254](https://doi.org/10.1088/0067-0049/191/2/254). arXiv: [1010.5503 \[astro-ph.CO\]](https://arxiv.org/abs/1010.5503).
- Harwood, Jeremy J. (Apr. 2017). "Spectral ageing in the era of big data: integrated versus resolved models". In: *Mon. Not. R. Astron. Soc.* 466.3, pp. 2888–2894. DOI: [10.1093/mnras/stw3318](https://doi.org/10.1093/mnras/stw3318). arXiv: [1612.04390 \[astro-ph.GA\]](https://arxiv.org/abs/1612.04390).
- Harwood, Jeremy J. et al. (Nov. 2013). "Spectral ageing in the lobes of FR-II radio galaxies: new methods of analysis for broad-band radio data". In: *Mon. Not. R. Astron. Soc.* 435.4, pp. 3353–3375. DOI: [10.1093/mnras/stt1526](https://doi.org/10.1093/mnras/stt1526). arXiv: [1308.4137 \[astro-ph.CO\]](https://arxiv.org/abs/1308.4137).
- Harwood, Jeremy J. et al. (Dec. 2015). "Spectral ageing in the lobes of cluster-centre FR II radio galaxies". In: *Mon. Not. R. Astron. Soc.* 454.4, pp. 3403–3422. DOI: [10.1093/mnras/stv2194](https://doi.org/10.1093/mnras/stv2194). arXiv: [1509.06757 \[astro-ph.GA\]](https://arxiv.org/abs/1509.06757).
- Helou, G. et al. (Nov. 1985). "Thermal infrared and nonthermal radio : remarkable correlation in disks of galaxies." In: *Astrophys. J. Lett.* 298, pp. L7–L11. DOI: [10.1086/184556](https://doi.org/10.1086/184556).
- Hilton, M. et al. (Feb. 2021). "The Atacama Cosmology Telescope: A Catalog of  $\sim$ 4000 Sunyaev–Zel'dovich Galaxy Clusters". In: *The Astrophysical Journal Supplement Series* 253.1, p. 3. ISSN: 1538-4365. DOI: [10.3847/1538-4365/abd023](https://doi.org/10.3847/1538-4365/abd023). URL: <http://dx.doi.org/10.3847/1538-4365/abd023>.
- Hilton, Matt et al. (Mar. 2018). "The Atacama Cosmology Telescope: The Two-season ACTPol Sunyaev-Zel'dovich Effect Selected Cluster Catalog". In: *Astrophys. J. Supp.* 235.1, 20, p. 20. DOI: [10.3847/1538-4365/aaa6cb](https://doi.org/10.3847/1538-4365/aaa6cb). arXiv: [1709.05600 \[astro-ph.CO\]](https://arxiv.org/abs/1709.05600).
- Hitomi Collaboration et al. (July 2016). "The quiescent intracluster medium in the core of the Perseus cluster". In: *Nature*. 535.7610, pp. 117–121. DOI: [10.1038/nature18627](https://doi.org/10.1038/nature18627). arXiv: [1607.04487 \[astro-ph.GA\]](https://arxiv.org/abs/1607.04487).
- Hoang, D. N. et al. (Aug. 2018). "Radio observations of the double-relic galaxy cluster Abell 1240". In: *Mon. Not. R. Astron. Soc.* 478.2, pp. 2218–2233. DOI: [10.1093/mnras/sty1123](https://doi.org/10.1093/mnras/sty1123). arXiv: [1804.11352 \[astro-ph.HE\]](https://arxiv.org/abs/1804.11352).
- Hopkins, A. M. et al. (July 2001). "Toward a Resolution of the Discrepancy between Different Estimators of Star Formation Rate". In: *Astron. J.* 122.1, pp. 288–296. DOI: [10.1086/321113](https://doi.org/10.1086/321113). arXiv: [astro-ph/0103253 \[astro-ph\]](https://arxiv.org/abs/astro-ph/0103253).
- Hopkins, A. M. et al. (Dec. 2003). "Star Formation Rate Indicators in the Sloan Digital Sky Survey". In: *Astrophys. J.* 599.2, pp. 971–991. DOI: [10.1086/379608](https://doi.org/10.1086/379608). arXiv: [astro-ph/0306621 \[astro-ph\]](https://arxiv.org/abs/astro-ph/0306621).
- Hubble, E. P. (1936). *Realm of the Nebulae*.

- Hubble, Edwin (Mar. 1929). “A Relation between Distance and Radial Velocity among Extra-Galactic Nebulae”. In: *Proceedings of the National Academy of Science* 15.3, pp. 168–173. DOI: [10.1073/pnas.15.3.168](https://doi.org/10.1073/pnas.15.3.168).
- Hubble, Edwin and Milton L. Humason (July 1931). “The Velocity-Distance Relation among Extra-Galactic Nebulae”. In: *Astrophys. J.* 74, p. 43. DOI: [10.1086/143323](https://doi.org/10.1086/143323).
- Hudson, D. S. et al. (Apr. 2010). “What is a cool-core cluster? a detailed analysis of the cores of the X-ray flux-limited HiFLUGCS cluster sample”. In: *Astron. Astrophys.* 513, A37, A37. DOI: [10.1051/0004-6361/200912377](https://doi.org/10.1051/0004-6361/200912377). arXiv: [0911.0409 \[astro-ph.CO\]](https://arxiv.org/abs/0911.0409).
- Huterer, Dragan and Daniel L. Shafer (Jan. 2018). “Dark energy two decades after: observables, probes, consistency tests”. In: *Reports on Progress in Physics* 81.1, 016901, p. 016901. DOI: [10.1088/1361-6633/aa997e](https://doi.org/10.1088/1361-6633/aa997e). arXiv: [1709.01091 \[astro-ph.CO\]](https://arxiv.org/abs/1709.01091).
- HyeongHan, Kim et al. (Sept. 2020). “Discovery of a Radio Relic in the Massive Merging Cluster SPT-CL J2023-5535 from the ASKAP-EMU Pilot Survey”. In: *Astrophys. J.* 900.2, 127, p. 127. DOI: [10.3847/1538-4357/aba742](https://doi.org/10.3847/1538-4357/aba742). arXiv: [2007.08244 \[astro-ph.HE\]](https://arxiv.org/abs/2007.08244).
- Ignesti, A. et al. (Aug. 2020). “Radio and X-ray connection in radio mini-halos: Implications for hadronic models”. In: *Astron. Astrophys.* 640, A37, A37. DOI: [10.1051/0004-6361/201937207](https://doi.org/10.1051/0004-6361/201937207). arXiv: [2006.09254 \[astro-ph.HE\]](https://arxiv.org/abs/2006.09254).
- Ilbert, O. et al. (Oct. 2006). “Accurate photometric redshifts for the CFHT legacy survey calibrated using the VIMOS VLT deep survey”. In: *Astron. Astrophys.* 457.3, pp. 841–856. DOI: [10.1051/0004-6361:20065138](https://doi.org/10.1051/0004-6361:20065138). arXiv: [astro-ph/0603217 \[astro-ph\]](https://arxiv.org/abs/astro-ph/0603217).
- Ilbert, O. et al. (Jan. 2009). “Cosmos Photometric Redshifts with 30-Bands for 2-deg<sup>2</sup>”. In: *Astrophys. J.* 690.2, pp. 1236–1249. DOI: [10.1088/0004-637X/690/2/1236](https://doi.org/10.1088/0004-637X/690/2/1236). arXiv: [0809.2101 \[astro-ph\]](https://arxiv.org/abs/0809.2101).
- Jaffe, W. J. (Feb. 1977). “Origin and transport of electrons in the halo radio source in the Coma cluster.” In: *Astrophys. J.* 212, pp. 1–7. DOI: [10.1086/155011](https://doi.org/10.1086/155011).
- Jansen, F. et al. (Jan. 2001). “XMM-Newton observatory. I. The spacecraft and operations”. In: *Astron. Astrophys.* 365, pp. L1–L6. DOI: [10.1051/0004-6361:20000036](https://doi.org/10.1051/0004-6361:20000036).
- Jansky, K.G. (1933). “Electrical Disturbances Apparently of Extraterrestrial Origin”. In: *Proceedings of the Institute of Radio Engineers* 21.10, pp. 1387–1398. DOI: [10.1109/JRPROC.1933.227458](https://doi.org/10.1109/JRPROC.1933.227458).
- Jonas, J. and MeerKAT Team (Jan. 2016). “The MeerKAT Radio Telescope”. In: *MeerKAT Science: On the Pathway to the SKA*, 1, p. 1.
- Kale, R. et al. (Sept. 2015). “Brightest cluster galaxies in the extended GMRT radio halo cluster sample. Radio properties and cluster dynamics”. In: *Astron. Astrophys.* 581, A23, A23. DOI: [10.1051/0004-6361/201526341](https://doi.org/10.1051/0004-6361/201526341). arXiv: [1506.05612 \[astro-ph.GA\]](https://arxiv.org/abs/1506.05612).
- Kale, Ruta et al. (Oct. 2012). “Spectral and polarization study of the double relics in Abell 3376 using the Giant Metrewave Radio Telescope and the Very Large Array”. In: *Mon. Not. R. Astron. Soc.* 426.2, pp. 1204–1211. DOI: [10.1111/j.1365-2966.2012.21519.x](https://doi.org/10.1111/j.1365-2966.2012.21519.x). arXiv: [1206.3389 \[astro-ph.CO\]](https://arxiv.org/abs/1206.3389).

- Kale, Ruta et al. (June 2019). “A radio halo surrounding the Brightest Cluster Galaxy in RXCJ0232.2-4420: a mini-halo in transition?” In: *Mon. Not. R. Astron. Soc.* 486.1, pp. L80–L84. DOI: [10.1093/mnrasl/slz061](https://doi.org/10.1093/mnrasl/slz061). arXiv: [1904.11670](https://arxiv.org/abs/1904.11670) [[astro-ph.CO](#)].
- Kang, Hyesung et al. (Sept. 2012). “Diffusive Shock Acceleration Simulations of Radio Relics”. In: *Astrophys. J.* 756.1, 97, p. 97. DOI: [10.1088/0004-637X/756/1/97](https://doi.org/10.1088/0004-637X/756/1/97). arXiv: [1205.1895](https://arxiv.org/abs/1205.1895) [[astro-ph.HE](#)].
- Karim, A. et al. (Mar. 2011). “The Star Formation History of Mass-Selected Galaxies in the COSMOS Field”. In: *The Astrophysical Journal* 730.2, p. 61. DOI: [10.1088/0004-637x/730/2/61](https://doi.org/10.1088/0004-637x/730/2/61). URL: <https://doi.org/10.1088/0004-637x/730/2/61>.
- Kennicutt Robert C., Jr. (May 1998). “The Global Schmidt Law in Star-forming Galaxies”. In: *Astrophys. J.* 498.2, pp. 541–552. DOI: [10.1086/305588](https://doi.org/10.1086/305588). arXiv: [astro-ph/9712213](https://arxiv.org/abs/astro-ph/9712213) [[astro-ph](#)].
- Kennicutt Robert C., Jr. et al. (Oct. 2009). “Dust-corrected Star Formation Rates of Galaxies. I. Combinations of H $\alpha$  and Infrared Tracers”. In: *Astrophys. J.* 703.2, pp. 1672–1695. DOI: [10.1088/0004-637X/703/2/1672](https://doi.org/10.1088/0004-637X/703/2/1672). arXiv: [0908.0203](https://arxiv.org/abs/0908.0203) [[astro-ph.CO](#)].
- Kennicutt, Robert C. and Neal J. Evans (Sept. 2012). “Star Formation in the Milky Way and Nearby Galaxies”. In: *Annual Review of Astronomy and Astrophysics* 50.1, 531–608. ISSN: 1545-4282. DOI: [10.1146/annurev-astro-081811-125610](https://doi.org/10.1146/annurev-astro-081811-125610). URL: <http://dx.doi.org/10.1146/annurev-astro-081811-125610>.
- Kesebonye, K. C. et al. (Jan. 2023). “The MeerKAT Galaxy Clusters Legacy Survey: star formation in massive clusters at  $0.15 \leq z \leq 0.35$ ”. In: *Mon. Not. R. Astron. Soc.* 518.2, pp. 3004–3016. DOI: [10.1093/mnras/stac3293](https://doi.org/10.1093/mnras/stac3293). arXiv: [2211.03492](https://arxiv.org/abs/2211.03492) [[astro-ph.GA](#)].
- Kewley, Lisa J. et al. (Apr. 2004). “[O II] as a Star Formation Rate Indicator”. In: *Astron. J.* 127.4, pp. 2002–2030. DOI: [10.1086/382723](https://doi.org/10.1086/382723). arXiv: [astro-ph/0401172](https://arxiv.org/abs/astro-ph/0401172) [[astro-ph](#)].
- Knowles, K. et al. (Jan. 2022). “The MeerKAT Galaxy Cluster Legacy Survey. I. Survey Overview and Highlights”. In: *Astron. Astrophys.* 657, A56, A56. DOI: [10.1051/0004-6361/202141488](https://doi.org/10.1051/0004-6361/202141488). arXiv: [2111.05673](https://arxiv.org/abs/2111.05673) [[astro-ph.GA](#)].
- Koester, B. P. et al. (May 2007a). “A MaxBCG Catalog of 13,823 Galaxy Clusters from the Sloan Digital Sky Survey”. In: *Astrophys. J.* 660.1, pp. 239–255. DOI: [10.1086/509599](https://doi.org/10.1086/509599). arXiv: [astro-ph/0701265](https://arxiv.org/abs/astro-ph/0701265) [[astro-ph](#)].
- Koester, Benjamin P. et al. (May 2007b). “MaxBCG: A Red-Sequence Galaxy Cluster Finder”. In: *Astrophys. J.* 660.1, pp. 221–238. DOI: [10.1086/512092](https://doi.org/10.1086/512092). arXiv: [astro-ph/0701268](https://arxiv.org/abs/astro-ph/0701268) [[astro-ph](#)].
- Koyama, Yusei et al. (July 2013). “On the evolution and environmental dependence of the star formation rate versus stellar mass relation since  $z \approx 2$ ”. In: *Monthly Notices of the Royal Astronomical Society* 434.1, pp. 423–436.
- Kroupa, Pavel (Apr. 2001). “On the variation of the initial mass function”. In: *Mon. Not. R. Astron. Soc.* 322.2, pp. 231–246. DOI: [10.1046/j.1365-8711.2001.04022.x](https://doi.org/10.1046/j.1365-8711.2001.04022.x). arXiv: [astro-ph/0009005](https://arxiv.org/abs/astro-ph/0009005) [[astro-ph](#)].

- Kroupa, Pavel (Jan. 2002). “The Initial Mass Function of Stars: Evidence for Uniformity in Variable Systems”. In: *Science* 295.5552, pp. 82–91. DOI: [10.1126/science.1067524](https://doi.org/10.1126/science.1067524). arXiv: [astro-ph/0201098 \[astro-ph\]](https://arxiv.org/abs/astro-ph/0201098).
- Laird, E. S. et al. (Jan. 2009). “AEGIS-X: the Chandra Deep Survey of the Extended Groth Strip”. In: *Astrophys. J. Supp.* 180.1, pp. 102–116. DOI: [10.1088/0067-0049/180/1/102](https://doi.org/10.1088/0067-0049/180/1/102). arXiv: [0809.1349 \[astro-ph\]](https://arxiv.org/abs/0809.1349).
- Large, M. I. et al. (June 1959). “A High-Resolution Survey of the Coma Cluster of Galaxies at 408 Mc./s.” In: *Nature*. 183.4676, pp. 1663–1664. DOI: [10.1038/1831663a0](https://doi.org/10.1038/1831663a0).
- Larson, R. B. et al. (May 1980). “The evolution of disk galaxies and the origin of S0 galaxies”. In: *Astrophys. J.* 237, pp. 692–707. DOI: [10.1086/157917](https://doi.org/10.1086/157917).
- Lee, Janice C. et al. (Nov. 2009). “Comparison of H $\alpha$  and UV Star Formation Rates in the Local Volume: Systematic Discrepancies for Dwarf Galaxies”. In: *Astrophys. J.* 706.1, pp. 599–613. DOI: [10.1088/0004-637X/706/1/599](https://doi.org/10.1088/0004-637X/706/1/599). arXiv: [0909.5205 \[astro-ph.CO\]](https://arxiv.org/abs/0909.5205).
- Leja, Joel et al. (Mar. 2017). “Deriving Physical Properties from Broadband Photometry with Prospector: Description of the Model and a Demonstration of its Accuracy Using 129 Galaxies in the Local Universe”. In: *Astrophys. J.* 837.2, 170, p. 170. DOI: [10.3847/1538-4357/aa5ffe](https://doi.org/10.3847/1538-4357/aa5ffe). arXiv: [1609.09073 \[astro-ph.GA\]](https://arxiv.org/abs/1609.09073).
- Lemaître, G. (Jan. 1927). “Un Univers homogène de masse constante et de rayon croissant rendant compte de la vitesse radiale des nébuleuses extra-galactiques”. In: *Annales de la Société Scientifique de Bruxelles* 47, pp. 49–59.
- Lewis, I. et al. (Aug. 2002). “The 2dF Galaxy Redshift Survey: the environmental dependence of galaxy star formation rates near clusters”. In: *Monthly Notices of the Royal Astronomical Society* 334.3, 673–683. ISSN: 1365-2966. DOI: [10.1046/j.1365-8711.2002.05558.x](https://doi.org/10.1046/j.1365-8711.2002.05558.x). URL: <http://dx.doi.org/10.1046/j.1365-8711.2002.05558.x>.
- Lilly, S. J. et al. (Mar. 1996). “The Canada-France Redshift Survey: The Luminosity Density and Star Formation History of the Universe to [ITAL]z[/ITAL]  $\sim 1$ ”. In: *The Astrophysical Journal* 460.1. DOI: [10.1086/309975](https://doi.org/10.1086/309975). URL: <https://doi.org/10.1086/309975>.
- Lindner, Robert R. et al. (Apr. 2014). “The Radio Relics and Halo of El Gordo, a Massive z = 0.870 Cluster Merger”. In: *The Astrophysical Journal* 786.1, p. 49. DOI: [10.1088/0004-637x/786/1/49](https://doi.org/10.1088/0004-637x/786/1/49). URL: <https://doi.org/10.1088/0004-637x/786/1/49>.
- Liu, A. et al. (May 2022). “The eROSITA Final Equatorial-Depth Survey (eFEDS). Catalog of galaxy clusters and groups”. In: *Astron. Astrophys.* 661, A2, A2. DOI: [10.1051/0004-6361/202141120](https://doi.org/10.1051/0004-6361/202141120). arXiv: [2106.14518 \[astro-ph.CO\]](https://arxiv.org/abs/2106.14518).
- Loeb, Abraham and Rennan Barkana (Jan. 2001). “The Reionization of the Universe by the First Stars and Quasars”. In: *Annu. Rev. Astron. Astrophys.* 39, pp. 19–66. DOI: [10.1146/annurev.astro.39.1.19](https://doi.org/10.1146/annurev.astro.39.1.19). arXiv: [astro-ph/0010467 \[astro-ph\]](https://arxiv.org/abs/astro-ph/0010467).
- Lovisari, Lorenzo and Ben J. Maughan (Feb. 2022). “Scaling relations of clusters and groups, and their evolution”. In: *arXiv e-prints*, arXiv:2202.07673, arXiv:2202.07673. arXiv: [2202.07673 \[astro-ph.CO\]](https://arxiv.org/abs/2202.07673).

- Lovisari, Lorenzo et al. (Sept. 2017). “X-Ray Morphological Analysis of the Planck ESZ Clusters”. In: *Astrophys. J.* 846.1, 51, p. 51. DOI: [10.3847/1538-4357/aa855f](https://doi.org/10.3847/1538-4357/aa855f). arXiv: [1708.02590 \[astro-ph.CO\]](https://arxiv.org/abs/1708.02590).
- Macario, G. et al. (Mar. 2013). “153 MHz GMRT follow-up of steep-spectrum diffuse emission in galaxy clusters”. In: *Astron. Astrophys.* 551, A141, A141. DOI: [10.1051/0004-6361/201220667](https://doi.org/10.1051/0004-6361/201220667). arXiv: [1302.0648 \[astro-ph.CO\]](https://arxiv.org/abs/1302.0648).
- Madau, Piero and Mark Dickinson (Aug. 2014). “Cosmic Star-Formation History”. In: *Annu. Rev. Astron. Astrophys.* 52, pp. 415–486. DOI: [10.1146/annurev-astro-081811-125615](https://doi.org/10.1146/annurev-astro-081811-125615). arXiv: [1403.0007 \[astro-ph.CO\]](https://arxiv.org/abs/1403.0007).
- Mahler, G. et al. (Jan. 2018). “Strong-lensing analysis of A2744 with MUSE and Hubble Frontier Fields images”. In: *Mon. Not. R. Astron. Soc.* 473.1, pp. 663–692. DOI: [10.1093/mnras/stx1971](https://doi.org/10.1093/mnras/stx1971). arXiv: [1702.06962 \[astro-ph.GA\]](https://arxiv.org/abs/1702.06962).
- Maier, C. et al. (Feb. 2022). “Star-formation quenching of cluster galaxies as traced by metallicity and presence of active galactic nuclei, and galactic conformity”. In: *Astron. Astrophys.* 658, A190, A190. DOI: [10.1051/0004-6361/202141498](https://doi.org/10.1051/0004-6361/202141498). arXiv: [2110.02231 \[astro-ph.GA\]](https://arxiv.org/abs/2110.02231).
- Mancone, Conor L. et al. (Sept. 2010). “The Formation of Massive Cluster Galaxies”. In: *Astrophys. J.* 720.1, pp. 284–298. DOI: [10.1088/0004-637X/720/1/284](https://doi.org/10.1088/0004-637X/720/1/284). arXiv: [1007.1454 \[astro-ph.CO\]](https://arxiv.org/abs/1007.1454).
- Mann, Andrew W. and Harald Ebeling (Mar. 2012). “X-ray-optical classification of cluster mergers and the evolution of the cluster merger fraction”. In: *Mon. Not. R. Astron. Soc.* 420.3, pp. 2120–2138. DOI: [10.1111/j.1365-2966.2011.20170.x](https://doi.org/10.1111/j.1365-2966.2011.20170.x). arXiv: [1111.2396 \[astro-ph.CO\]](https://arxiv.org/abs/1111.2396).
- Mansheim, A. S. et al. (July 2017). “Suppressed star formation by a merging cluster system”. In: *Mon. Not. R. Astron. Soc.* 469.1, pp. L20–L25. DOI: [10.1093/mnrasl/slx041](https://doi.org/10.1093/mnrasl/slx041). arXiv: [1705.03468 \[astro-ph.GA\]](https://arxiv.org/abs/1705.03468).
- Mantz, A. et al. (Aug. 2010). “The observed growth of massive galaxy clusters - II. X-ray scaling relations”. In: *Mon. Not. R. Astron. Soc.* 406.3, pp. 1773–1795. DOI: [10.1111/j.1365-2966.2010.16993.x](https://doi.org/10.1111/j.1365-2966.2010.16993.x). arXiv: [0909.3099 \[astro-ph.CO\]](https://arxiv.org/abs/0909.3099).
- Mauch, T. et al. (Jan. 2020). “The 1.28 GHz MeerKAT DEEP2 Image”. In: *Astrophys. J.* 888.2, 61, p. 61. DOI: [10.3847/1538-4357/ab5d2d](https://doi.org/10.3847/1538-4357/ab5d2d). arXiv: [1912.06212 \[astro-ph.GA\]](https://arxiv.org/abs/1912.06212).
- Mauch, Tom and Elaine M. Sadler (Mar. 2007). “Radio sources in the 6dFGS: local luminosity functions at 1.4 GHz for star-forming galaxies and radio-loud AGN”. In: *Mon. Not. R. Astron. Soc.* 375.3, pp. 931–950. DOI: [10.1111/j.1365-2966.2006.11353.x](https://doi.org/10.1111/j.1365-2966.2006.11353.x). arXiv: [astro-ph/0612018 \[astro-ph\]](https://arxiv.org/abs/astro-ph/0612018).
- McDonald, M. et al. (Nov. 2019). “Anatomy of a Cooling Flow: The Feedback Response to Pure Cooling in the Core of the Phoenix Cluster”. In: *Astrophys. J.* 885.1, 63, p. 63. DOI: [10.3847/1538-4357/ab464c](https://doi.org/10.3847/1538-4357/ab464c). arXiv: [1904.08942 \[astro-ph.GA\]](https://arxiv.org/abs/1904.08942).
- McKee, Christopher F. and Eve C. Ostriker (Sept. 2007). “Theory of Star Formation”. In: *Annu. Rev. Astron. Astrophys.* 45.1, pp. 565–687. DOI: [10.1146/annurev.astro.45.051806.110602](https://doi.org/10.1146/annurev.astro.45.051806.110602). arXiv: [0707.3514 \[astro-ph\]](https://arxiv.org/abs/0707.3514).
- Melin, J. B. et al. (Jan. 2005). “The selection function of SZ cluster surveys”. In: *Astron. Astrophys.* 429, pp. 417–426. DOI: [10.1051/0004-6361:20048093](https://doi.org/10.1051/0004-6361:20048093). arXiv: [astro-ph/0409564 \[astro-ph\]](https://arxiv.org/abs/astro-ph/0409564).

- Mercurio, A. et al. (Dec. 2021). “CLASH-VLT: Abell S1063. Cluster assembly history and spectroscopic catalogue”. In: *Astron. Astrophys.* 656, A147, A147. DOI: [10.1051/0004-6361/202142168](https://doi.org/10.1051/0004-6361/202142168). arXiv: [2109.03305 \[astro-ph.GA\]](https://arxiv.org/abs/2109.03305).
- Merten, J. et al. (Oct. 2011). “Creation of cosmic structure in the complex galaxy cluster merger Abell 2744”. In: *Mon. Not. R. Astron. Soc.* 417.1, pp. 333–347. DOI: [10.1111/j.1365-2966.2011.19266.x](https://doi.org/10.1111/j.1365-2966.2011.19266.x). arXiv: [1103.2772 \[astro-ph.CO\]](https://arxiv.org/abs/1103.2772).
- Mertens, F. G. et al. (Apr. 2020). “Improved upper limits on the 21 cm signal power spectrum of neutral hydrogen at  $z \approx 9.1$  from LOFAR”. In: *Mon. Not. R. Astron. Soc.* 493.2, pp. 1662–1685. DOI: [10.1093/mnras/staa327](https://doi.org/10.1093/mnras/staa327). arXiv: [2002.07196 \[astro-ph.CO\]](https://arxiv.org/abs/2002.07196).
- Meurer, Gerhardt R. et al. (Aug. 1999). “Dust Absorption and the Ultraviolet Luminosity Density at  $z \sim 3$  as Calibrated by Local Starburst Galaxies”. In: *Astrophys. J.* 521.1, pp. 64–80. DOI: [10.1086/307523](https://doi.org/10.1086/307523). arXiv: [astro-ph/9903054 \[astro-ph\]](https://arxiv.org/abs/astro-ph/9903054).
- Miyaji, T. et al. (May 2015). “Detailed Shape and Evolutionary Behavior of the X-Ray Luminosity Function of Active Galactic Nuclei”. In: *Astrophys. J.* 804.2, 104, p. 104. DOI: [10.1088/0004-637X/804/2/104](https://doi.org/10.1088/0004-637X/804/2/104). arXiv: [1503.00056 \[astro-ph.GA\]](https://arxiv.org/abs/1503.00056).
- Mohan, Niruj and David Rafferty (Feb. 2015). *PyBDSF: Python Blob Detection and Source Finder*. ascl: [1502.007](https://ascl.net/1502.007).
- Momcheva, Ivelina G. et al. (Feb. 2013). “Nebular Attenuation in H $\alpha$ -selected Star-forming Galaxies at  $z = 0.8$  from the NewH $\alpha$  Survey”. In: *Astron. J.* 145.2, 47, p. 47. DOI: [10.1088/0004-6256/145/2/47](https://doi.org/10.1088/0004-6256/145/2/47). arXiv: [1207.5479 \[astro-ph.CO\]](https://arxiv.org/abs/1207.5479).
- Moore, Ben et al. (Feb. 1996). “Galaxy harassment and the evolution of clusters of galaxies”. In: *Nature*. 379.6566, pp. 613–616. DOI: [10.1038/379613a0](https://doi.org/10.1038/379613a0). arXiv: [astro-ph/9510034 \[astro-ph\]](https://arxiv.org/abs/astro-ph/9510034).
- Mroczkowski, Tony et al. (Feb. 2019). “Astrophysics with the Spatially and Spectrally Resolved Sunyaev-Zeldovich Effects. A Millimetre/Submillimetre Probe of the Warm and Hot Universe”. In: *Space Sci. Rev.* 215.1, 17, p. 17. DOI: [10.1007/s11214-019-0581-2](https://doi.org/10.1007/s11214-019-0581-2). arXiv: [1811.02310 \[astro-ph.CO\]](https://arxiv.org/abs/1811.02310).
- Murphy, D. N. A. et al. (Mar. 2012). “ORCA: The Overdense Red-sequence Cluster Algorithm”. In: *Mon. Not. R. Astron. Soc.* 420.3, pp. 1861–1881. DOI: [10.1111/j.1365-2966.2011.19782.x](https://doi.org/10.1111/j.1365-2966.2011.19782.x). arXiv: [1109.3182 \[astro-ph.CO\]](https://arxiv.org/abs/1109.3182).
- Naidu, Rohan P. et al. (Nov. 2022). “Two Remarkably Luminous Galaxy Candidates at  $z \approx 10\text{--}12$  Revealed by JWST”. In: *Astrophys. J. Lett.* 940.1, L14, p. L14. DOI: [10.3847/2041-8213/ac9b22](https://doi.org/10.3847/2041-8213/ac9b22). arXiv: [2207.09434 \[astro-ph.GA\]](https://arxiv.org/abs/2207.09434).
- Norris, Ray P. et al. (Aug. 2011). “EMU: Evolutionary Map of the Universe”. In: *Pub. Astron. Soc. Australia* 28.3, pp. 215–248. DOI: [10.1071/AS11021](https://doi.org/10.1071/AS11021). arXiv: [1106.3219 \[astro-ph.CO\]](https://arxiv.org/abs/1106.3219).
- Oemler Augustus, Jr. et al. (Jan. 1997). “The Morphology of Distant Cluster Galaxies. II. HST Observations of Four Rich Clusters at  $z \approx 0.4$ ”. In: *Astrophys. J.* 474.2, pp. 561–575. DOI: [10.1086/303472](https://doi.org/10.1086/303472).
- Ogream, G. A. et al. (July 2013). “Challenges to our understanding of radio relics: X-ray observations of the Toothbrush cluster”. In: *Mon. Not. R. Astron. Soc.* 433.1, pp. 812–824. DOI: [10.1093/mnras/stt776](https://doi.org/10.1093/mnras/stt776). arXiv: [1303.1533 \[astro-ph.CO\]](https://arxiv.org/abs/1303.1533).
- Ono, Yoshiaki et al. (Aug. 2022). “Morphologies of Galaxies at  $z \simeq 9\text{--}17$  Uncovered by JWST/NIRCam Imaging: Cosmic Size Evolution and an Identifica-

- tion of an Extremely Compact Bright Galaxy at  $z \sim 12$ ”. In: *arXiv e-prints*, arXiv:2208.13582, arXiv:2208.13582. DOI: [10.48550/arXiv.2208.13582](https://doi.org/10.48550/arXiv.2208.13582). arXiv: [2208.13582 \[astro-ph.GA\]](https://arxiv.org/abs/2208.13582).
- Owers, Matt S. et al. (Feb. 2011). “The Dissection of Abell 2744: A Rich Cluster Growing Through Major and Minor Mergers”. In: *Astrophys. J.* 728.1, 27, p. 27. DOI: [10.1088/0004-637X/728/1/27](https://doi.org/10.1088/0004-637X/728/1/27). arXiv: [1012.1315 \[astro-ph.CO\]](https://arxiv.org/abs/1012.1315).
- Parekh, V. et al. (Sept. 2017). “A hot X-ray filament associated with A3017 galaxy cluster”. In: *Mon. Not. R. Astron. Soc.* 470.3, pp. 3742–3749. DOI: [10.1093/mnras/stx1457](https://doi.org/10.1093/mnras/stx1457). arXiv: [1705.07344 \[astro-ph.GA\]](https://arxiv.org/abs/1705.07344).
- Parsons, Aaron R. et al. (June 2014). “New Limits on 21 cm Epoch of Reionization from PAPER-32 Consistent with an X-Ray Heated Intergalactic Medium at  $z = 7.7$ ”. In: *Astrophys. J.* 788.2, 106, p. 106. DOI: [10.1088/0004-637X/788/2/106](https://doi.org/10.1088/0004-637X/788/2/106). arXiv: [1304.4991 \[astro-ph.CO\]](https://arxiv.org/abs/1304.4991).
- Paul, Surajit et al. (Oct. 2019). “Low-frequency radio study of MACS clusters at 610 and 235 MHz using the GMRT”. In: *Mon. Not. R. Astron. Soc.* 489.1, pp. 446–458. DOI: [10.1093/mnras/stz1965](https://doi.org/10.1093/mnras/stz1965). arXiv: [1903.06799 \[astro-ph.HE\]](https://arxiv.org/abs/1903.06799).
- Pearce, C. J. J. et al. (Aug. 2017). “VLA Radio Observations of the HST Frontier Fields Cluster Abell 2744: The Discovery of New Radio Relics”. In: *Astrophys. J.* 845.1, 81, p. 81. DOI: [10.3847/1538-4357/aa7e2f](https://doi.org/10.3847/1538-4357/aa7e2f). arXiv: [1708.03367 \[astro-ph.CO\]](https://arxiv.org/abs/1708.03367).
- Peebles, P. J. and Bharat Ratra (Apr. 2003). “The cosmological constant and dark energy”. In: *Reviews of Modern Physics* 75.2, pp. 559–606. DOI: [10.1103/RevModPhys.75.559](https://doi.org/10.1103/RevModPhys.75.559). arXiv: [astro-ph/0207347 \[astro-ph\]](https://arxiv.org/abs/astro-ph/0207347).
- Peebles, P. J. E. (1980). *The large-scale structure of the universe*.
- Pelló, R. et al. (Dec. 2009). “Photometric redshifts and cluster tomography in the ESO Distant Cluster Survey”. In: *Astron. Astrophys.* 508.3, pp. 1173–1191. DOI: [10.1051/0004-6361/200810644](https://doi.org/10.1051/0004-6361/200810644). arXiv: [0910.5418 \[astro-ph.CO\]](https://arxiv.org/abs/0910.5418).
- Peng, Ying-jie et al. (Sept. 2010). “Mass and Environment as Drivers of Galaxy Evolution in SDSS and zCOSMOS and the Origin of the Schechter Function”. In: *Astrophys. J.* 721.1, pp. 193–221. DOI: [10.1088/0004-637X/721/1/193](https://doi.org/10.1088/0004-637X/721/1/193). arXiv: [1003.4747 \[astro-ph.CO\]](https://arxiv.org/abs/1003.4747).
- Penzias, A. A. and R. W. Wilson (July 1965). “A Measurement of Excess Antenna Temperature at 4080 Mc/s.” In: *Astrophys. J.* 142, pp. 419–421. DOI: [10.1086/148307](https://doi.org/10.1086/148307).
- Perlmutter, S. et al. (June 1999). “Measurements of  $\Omega$  and  $\Lambda$  from 42 High-Redshift Supernovae”. In: *Astrophys. J.* 517.2, pp. 565–586. DOI: [10.1086/307221](https://doi.org/10.1086/307221). arXiv: [astro-ph/9812133 \[astro-ph\]](https://arxiv.org/abs/astro-ph/9812133).
- Petrosian, Vahé (Aug. 2001). “On the Nonthermal Emission and Acceleration of Electrons in Coma and Other Clusters of Galaxies”. In: *Astrophys. J.* 557.2, pp. 560–572. DOI: [10.1086/321557](https://doi.org/10.1086/321557). arXiv: [astro-ph/0101145 \[astro-ph\]](https://arxiv.org/abs/astro-ph/0101145).
- Philip, L. et al. (Jan. 2019). “Probing Radio Intensity at High-Z from Marion: 2017 Instrument”. In: *Journal of Astronomical Instrumentation* 8.2, 1950004, p. 1950004. DOI: [10.1142/S2251171719500041](https://doi.org/10.1142/S2251171719500041). arXiv: [1806.09531 \[astro-ph.IM\]](https://arxiv.org/abs/1806.09531).

- Piffaretti, R. et al. (Oct. 2011). “The MCXC: a meta-catalogue of x-ray detected clusters of galaxies”. In: *Astron. Astrophys.* 534, A109, A109. DOI: [10.1051/0004-6361/201015377](https://doi.org/10.1051/0004-6361/201015377). arXiv: [1007.1916 \[astro-ph.CO\]](https://arxiv.org/abs/1007.1916).
- Pillay, Denisha S. et al. (Nov. 2021). “A Multiwavelength Dynamical State Analysis of ACT-CL J0019.6+0336”. In: *Galaxies* 9.4, p. 97. DOI: [10.3390/galaxies9040097](https://doi.org/10.3390/galaxies9040097). arXiv: [2111.04340 \[astro-ph.HE\]](https://arxiv.org/abs/2111.04340).
- Planck Collaboration et al. (Sept. 2016). “Planck 2015 results. XXVII. The second Planck catalogue of Sunyaev-Zeldovich sources”. In: *Astron. Astrophys.* 594, A27, A27. DOI: [10.1051/0004-6361/201525823](https://doi.org/10.1051/0004-6361/201525823). arXiv: [1502.01598 \[astro-ph.CO\]](https://arxiv.org/abs/1502.01598).
- Planck Collaboration et al. (Sept. 2020). “Planck 2018 results. VI. Cosmological parameters”. In: *Astron. Astrophys.* 641, A6, A6. DOI: [10.1051/0004-6361/201833910](https://doi.org/10.1051/0004-6361/201833910). arXiv: [1807.06209 \[astro-ph.CO\]](https://arxiv.org/abs/1807.06209).
- Poggianti, B. M. et al. (Mar. 2016). “Jellyfish Galaxy Candidates at Low Redshift”. In: *Astron. J.* 151.3, 78, p. 78. DOI: [10.3847/0004-6256/151/3/78](https://doi.org/10.3847/0004-6256/151/3/78). arXiv: [1504.07105 \[astro-ph.GA\]](https://arxiv.org/abs/1504.07105).
- Pontoppidan, Klaus M. et al. (Sept. 2022). “The JWST Early Release Observations”. In: *Astrophys. J. Lett.* 936.1, L14, p. L14. DOI: [10.3847/2041-8213/ac8a4e](https://doi.org/10.3847/2041-8213/ac8a4e). arXiv: [2207.13067 \[astro-ph.IM\]](https://arxiv.org/abs/2207.13067).
- Popesso, P. et al. (Sept. 2006). “RASS-SDSS galaxy cluster survey”. In: *Astronomy & Astrophysics* 461.2, pp. 411–421. DOI: [10.1051/0004-6361:20065357](https://doi.org/10.1051/0004-6361:20065357). URL: <https://doi.org/10.1051%2F0004-6361%3A20065357>.
- Popesso, P. et al. (Jan. 2012). “The evolution of the star formation activity per halo mass up to redshift  $\sim$ 1.6 as seen by Herschel”. In: *Astron. Astrophys.* 537, A58, A58. DOI: [10.1051/0004-6361/201117973](https://doi.org/10.1051/0004-6361/201117973). arXiv: [1110.2946 \[astro-ph.CO\]](https://arxiv.org/abs/1110.2946).
- Pranger, Florian et al. (Sept. 2013). “The galaxy population of the complex cluster system Abell 3921”. In: *Astron. Astrophys.* 557, A62, A62. DOI: [10.1051/0004-6361/201321929](https://doi.org/10.1051/0004-6361/201321929). arXiv: [1305.4804 \[astro-ph.CO\]](https://arxiv.org/abs/1305.4804).
- Puschell, J. J. et al. (June 1982). “Near-infrared photometry of distant radio galaxies - Spectral flux distributions and redshift estimates”. In: *Astrophys. J. Lett.* 257, pp. L57–L61. DOI: [10.1086/183808](https://doi.org/10.1086/183808).
- Quilis, Vicent et al. (June 2000). “Gone with the Wind: The Origin of S0 Galaxies in Clusters”. In: *Science* 288.5471, pp. 1617–1620. DOI: [10.1126/science.288.5471.1617](https://doi.org/10.1126/science.288.5471.1617). arXiv: [astro-ph/0006031 \[astro-ph\]](https://arxiv.org/abs/astro-ph/0006031).
- Rajpurohit, K. et al. (Oct. 2021). “Dissecting nonthermal emission in the complex multiple-merger galaxy cluster Abell 2744: Radio and X-ray analysis”. In: *Astron. Astrophys.* 654, A41, A41. DOI: [10.1051/0004-6361/202141060](https://doi.org/10.1051/0004-6361/202141060). arXiv: [2104.05690 \[astro-ph.CO\]](https://arxiv.org/abs/2104.05690).
- Ramos-Caja, M. E. et al. (June 2019). “Projection effects in galaxy cluster samples: insights from X-ray redshifts”. In: *Astron. Astrophys.* 626, A48, A48. DOI: [10.1051/0004-6361/201935111](https://doi.org/10.1051/0004-6361/201935111). arXiv: [1904.10275 \[astro-ph.GA\]](https://arxiv.org/abs/1904.10275).
- Ranalli, P. et al. (Feb. 2003). “The 2-10 keV luminosity as a Star Formation Rate indicator”. In: *Astron. Astrophys.* 399, pp. 39–50. DOI: [10.1051/0004-6361:20021600](https://doi.org/10.1051/0004-6361:20021600). arXiv: [astro-ph/0211304 \[astro-ph\]](https://arxiv.org/abs/astro-ph/0211304).

- Richard-Laferrière, A. et al. (Dec. 2020). “On the relation between mini-halos and AGN feedback in clusters of galaxies”. In: *Mon. Not. R. Astron. Soc.* 499.2, pp. 2934–2958. DOI: [10.1093/mnras/staa2877](https://doi.org/10.1093/mnras/staa2877). arXiv: [2007.01306 \[astro-ph.GA\]](https://arxiv.org/abs/2007.01306).
- Riess, Adam G. et al. (Sept. 1998). “Observational Evidence from Supernovae for an Accelerating Universe and a Cosmological Constant”. In: *Astron. J.* 116.3, pp. 1009–1038. DOI: [10.1086/300499](https://doi.org/10.1086/300499). arXiv: [astro-ph/9805201 \[astro-ph\]](https://arxiv.org/abs/astro-ph/9805201).
- Rodríguez-Muñoz, L. et al. (May 2019). “Quantifying the suppression of the (un)-obscured star formation in galaxy cluster cores at  $0.2 \lesssim z \lesssim 0.9$ ”. In: *Mon. Not. R. Astron. Soc.* 485.1, pp. 586–619. DOI: [10.1093/mnras/sty3335](https://doi.org/10.1093/mnras/sty3335). arXiv: [1812.08804 \[astro-ph.GA\]](https://arxiv.org/abs/1812.08804).
- Rosati, Piero et al. (Jan. 2002). “The Evolution of X-ray Clusters of Galaxies”. In: *Annu. Rev. Astron. Astrophys.* 40, pp. 539–577. DOI: [10.1146/annurev.astro.40.120401.150547](https://doi.org/10.1146/annurev.astro.40.120401.150547). arXiv: [astro-ph/0209035 \[astro-ph\]](https://arxiv.org/abs/astro-ph/0209035).
- Rossetti, M. et al. (Apr. 2016). “Measuring the dynamical state of Planck SZ-selected clusters: X-ray peak - BCG offset”. In: *Mon. Not. R. Astron. Soc.* 457.4, pp. 4515–4524. DOI: [10.1093/mnras/stw265](https://doi.org/10.1093/mnras/stw265). arXiv: [1512.00410 \[astro-ph.CO\]](https://arxiv.org/abs/1512.00410).
- Rowan-Robinson, M. (2013). *Night Vision: Exploring the Infrared Universe*. Cambridge University Press. ISBN: 9781107024762. URL: <https://books.google.co.za/books?id=8-24tSFftBUC>.
- Ruhl, John et al. (Oct. 2004). “The South Pole Telescope”. In: *Z-Spec: a broadband millimeter-wave grating spectrometer: design, construction, and first cryogenic measurements*. Ed. by C. Matt Bradford et al. Vol. 5498. Society of Photo-Optical Instrumentation Engineers (SPIE) Conference Series, pp. 11–29. DOI: [10.1117/12.552473](https://doi.org/10.1117/12.552473). arXiv: [astro-ph/0411122 \[astro-ph\]](https://arxiv.org/abs/astro-ph/0411122).
- Rykoff, E. S. et al. (Apr. 2014). “redMaPPer. I. Algorithm and SDSS DR8 Catalog”. In: *Astrophys. J.* 785.2, 104, p. 104. DOI: [10.1088/0004-637X/785/2/104](https://doi.org/10.1088/0004-637X/785/2/104). arXiv: [1303.3562 \[astro-ph.CO\]](https://arxiv.org/abs/1303.3562).
- Rykoff, E. S. et al. (May 2016). “The RedMaPPer Galaxy Cluster Catalog From DES Science Verification Data”. In: *Astrophys. J. Supp.* 224.1, 1, p. 1. DOI: [10.3847/0067-0049/224/1/1](https://doi.org/10.3847/0067-0049/224/1/1). arXiv: [1601.00621 \[astro-ph.CO\]](https://arxiv.org/abs/1601.00621).
- Sadler, Elaine M. et al. (Jan. 2002). “Radio sources in the 2dF Galaxy Redshift Survey - II. Local radio luminosity functions for AGN and star-forming galaxies at 1.4 GHz”. In: *Mon. Not. R. Astron. Soc.* 329.1, pp. 227–245. DOI: [10.1046/j.1365-8711.2002.04998.x](https://doi.org/10.1046/j.1365-8711.2002.04998.x). arXiv: [astro-ph/0106173 \[astro-ph\]](https://arxiv.org/abs/astro-ph/0106173).
- Salim, Samir et al. (Dec. 2007). “UV Star Formation Rates in the Local Universe”. In: *Astrophys. J. Supp.* 173.2, pp. 267–292. DOI: [10.1086/519218](https://doi.org/10.1086/519218). arXiv: [0704.3611 \[astro-ph\]](https://arxiv.org/abs/0704.3611).
- Salpeter, Edwin E. (Jan. 1955). “The Luminosity Function and Stellar Evolution.” In: *Astrophys. J.* 121, p. 161. DOI: [10.1086/145971](https://doi.org/10.1086/145971).
- Salvato, M. et al. (Dec. 2011). “Dissecting Photometric Redshift for Active Galactic Nucleus Using XMM- and Chandra-COSMOS Samples”. In: *Astrophys. J.* 742.2, 61, p. 61. DOI: [10.1088/0004-637X/742/2/61](https://doi.org/10.1088/0004-637X/742/2/61). arXiv: [1108.6061 \[astro-ph.CO\]](https://arxiv.org/abs/1108.6061).
- Salvato, Mara et al. (June 2019). “The many flavours of photometric redshifts”. In: *Nature Astronomy* 3, pp. 212–222. DOI: [10.1038/s41550-018-0478-0](https://doi.org/10.1038/s41550-018-0478-0). arXiv: [1805.12574 \[astro-ph.GA\]](https://arxiv.org/abs/1805.12574).

- Sandstrom, Karin M. et al. (May 2009). “Measuring Dust Production in the Small Magellanic Cloud Core-Collapse Supernova Remnant 1E 0102.2-7219”. In: *Astrophys. J.* 696.2, pp. 2138–2154. DOI: [10.1088/0004-637X/696/2/2138](https://doi.org/10.1088/0004-637X/696/2/2138). arXiv: [0810.2803 \[astro-ph\]](https://arxiv.org/abs/0810.2803).
- Sarazin, Craig L. (1988). *X-ray emission from clusters of galaxies*.
- (June 2002). “The Physics of Cluster Mergers”. In: *Merging Processes in Galaxy Clusters*. Ed. by L. Feretti et al. Vol. 272. Astrophysics and Space Science Library, pp. 1–38. DOI: [10.1007/0-306-48096-4\\_1](https://doi.org/10.1007/0-306-48096-4_1). arXiv: [astro-ph/0105418 \[astro-ph\]](https://arxiv.org/abs/astro-ph/0105418).
- Schaye, Joop et al. (Jan. 2015). “The EAGLE project: simulating the evolution and assembly of galaxies and their environments”. In: *Mon. Not. R. Astron. Soc.* 446.1, pp. 521–554. DOI: [10.1093/mnras/stu2058](https://doi.org/10.1093/mnras/stu2058). arXiv: [1407.7040 \[astro-ph.GA\]](https://arxiv.org/abs/1407.7040).
- Schlafly, Edward F. et al. (Feb. 2019). “The unWISE Catalog: Two Billion Infrared Sources from Five Years of WISE Imaging”. In: *Astrophys. J. Supp.* 240.2, 30, p. 30. DOI: [10.3847/1538-4365/aafbea](https://doi.org/10.3847/1538-4365/aafbea). arXiv: [1901.03337 \[astro-ph.IM\]](https://arxiv.org/abs/1901.03337).
- Schlegel, D. et al. (Jan. 2021). “DESI Legacy Imaging Surveys Data Release 9”. In: *American Astronomical Society Meeting Abstracts*. Vol. 53. American Astronomical Society Meeting Abstracts, 235.03, p. 235.03.
- Shapley, Harlow and Heber D. Curtis (May 1921). “The Scale of the Universe”. In: *Bulletin of the National Research Council* 2.11, pp. 171–217.
- Shim, Hyunjin et al. (Jan. 2011). “Merging Galaxy Cluster A2255 in Mid-infrared”. In: *Astrophys. J.* 727.1, 14, p. 14. DOI: [10.1088/0004-637X/727/1/14](https://doi.org/10.1088/0004-637X/727/1/14). arXiv: [1011.6408 \[astro-ph.CO\]](https://arxiv.org/abs/1011.6408).
- Shimwell, Timothy W. et al. (June 2014). “Deep radio observations of the radio halo of the bullet cluster 1E 0657-55.8”. In: *Mon. Not. R. Astron. Soc.* 440.4, pp. 2901–2915. DOI: [10.1093/mnras/stu467](https://doi.org/10.1093/mnras/stu467). arXiv: [1403.2393 \[astro-ph.CO\]](https://arxiv.org/abs/1403.2393).
- Silva, David R. et al. (June 2016). “The Mayall z-band Legacy Survey”. In: *American Astronomical Society Meeting Abstracts #228*. Vol. 228. American Astronomical Society Meeting Abstracts, 317.02, p. 317.02.
- Singh, Saurabh et al. (Apr. 2018). “SARAS 2: a spectral radiometer for probing cosmic dawn and the epoch of reionization through detection of the global 21-cm signal”. In: *Experimental Astronomy* 45.2, pp. 269–314. DOI: [10.1007/s10686-018-9584-3](https://doi.org/10.1007/s10686-018-9584-3). arXiv: [1710.01101 \[astro-ph.IM\]](https://arxiv.org/abs/1710.01101).
- Skibba, Ramin A. et al. (Oct. 2009). “Galaxy Zoo: disentangling the environmental dependence of morphology and colour”. In: *Mon. Not. R. Astron. Soc.* 399.2, pp. 966–982. DOI: [10.1111/j.1365-2966.2009.15334.x](https://doi.org/10.1111/j.1365-2966.2009.15334.x). arXiv: [0811.3970 \[astro-ph\]](https://arxiv.org/abs/0811.3970).
- Skillman, Samuel W. et al. (Mar. 2013). “Cosmological Magnetohydrodynamic Simulations of Galaxy Cluster Radio Relics: Insights and Warnings for Observations”. In: *Astrophys. J.* 765.1, 21, p. 21. DOI: [10.1088/0004-637X/765/1/21](https://doi.org/10.1088/0004-637X/765/1/21). arXiv: [1211.3122 \[astro-ph.CO\]](https://arxiv.org/abs/1211.3122).
- Smith, D. J. B. et al. (Sept. 2011). “Herschel-ATLAS: counterparts from the ultraviolet-near-infrared in the science demonstration phase catalogue”. In: *Mon. Not. R. Astron. Soc.* 416.2, pp. 857–872. DOI: [10.1111/j.1365-2966.2011.18827.x](https://doi.org/10.1111/j.1365-2966.2011.18827.x). arXiv: [1007.5260 \[astro-ph.CO\]](https://arxiv.org/abs/1007.5260).

- Sobral, David et al. (Feb. 2014). “The stellar mass function of star-forming galaxies and the mass-dependent SFR function since  $z = 2.23$  from HiZELS”. In: *Mon. Not. R. Astron. Soc.* 437.4, pp. 3516–3528. DOI: [10.1093/mnras/stt2159](https://doi.org/10.1093/mnras/stt2159). arXiv: [1311.1503 \[astro-ph.CO\]](https://arxiv.org/abs/1311.1503).
- Springel, Volker et al. (Mar. 2018). “First results from the IllustrisTNG simulations: matter and galaxy clustering”. In: *Mon. Not. R. Astron. Soc.* 475.1, pp. 676–698. DOI: [10.1093/mnras/stx3304](https://doi.org/10.1093/mnras/stx3304). arXiv: [1707.03397 \[astro-ph.GA\]](https://arxiv.org/abs/1707.03397).
- Stern, Daniel et al. (June 2012). “MID-INFRARED SELECTION OF ACTIVE GALACTIC NUCLEI WITH THEWIDE-FIELD INFRARED SURVEY EXPLORER. I. CHARACTERIZINGWISE-SELECTED ACTIVE GALACTIC NUCLEI IN COSMOS”. In: *The Astrophysical Journal* 753.1, p. 30. ISSN: 1538-4357. DOI: [10.1088/0004-637x/753/1/30](https://doi.org/10.1088/0004-637x/753/1/30). URL: <http://dx.doi.org/10.1088/0004-637x/753/1/30>.
- Stroe, Andra and David Sobral (May 2021). “ENISALA. II. Distinct Star Formation and Active Galactic Nucleus Activity in Merging and Relaxed Galaxy Clusters”. In: *Astrophys. J.* 912.1, 55, p. 55. DOI: [10.3847/1538-4357/abe7f8](https://doi.org/10.3847/1538-4357/abe7f8). arXiv: [2102.10116 \[astro-ph.GA\]](https://arxiv.org/abs/2102.10116).
- Stroe, Andra et al. (Feb. 2014). “The role of cluster mergers and travelling shocks in shaping the  $\mathrm{H}\alpha$  luminosity function at  $z \sim 0.2$ : ‘sausage’ and ‘toothbrush’ clusters”. In: *Mon. Not. R. Astron. Soc.* 438.2, pp. 1377–1390. DOI: [10.1093/mnras/stt2286](https://doi.org/10.1093/mnras/stt2286). arXiv: [1311.6812 \[astro-ph.CO\]](https://arxiv.org/abs/1311.6812).
- Stroe, Andra et al. (Mar. 2017). “A large  $\mathrm{H}\alpha$  survey of star formation in relaxed and merging galaxy cluster environments at  $z \sim 0.15\text{--}0.3$ ”. In: *Mon. Not. R. Astron. Soc.* 465.3, pp. 2916–2935. DOI: [10.1093/mnras/stw2939](https://doi.org/10.1093/mnras/stw2939). arXiv: [1611.03512 \[astro-ph.GA\]](https://arxiv.org/abs/1611.03512).
- Stuardi, C. et al. (Oct. 2022). “Using the polarization properties of double radio relics to probe the turbulent compression scenario”. In: *Astron. Astrophys.* 666, A8, A8. DOI: [10.1051/0004-6361/202244179](https://doi.org/10.1051/0004-6361/202244179). arXiv: [2207.00503 \[astro-ph.CO\]](https://arxiv.org/abs/2207.00503).
- Sunyaev, R. A. and Ia. B. Zeldovich (Jan. 1980). “Microwave background radiation as a probe of the contemporary structure and history of the universe”. In: *Annu. Rev. Astron. Astrophys.* 18, pp. 537–560. DOI: [10.1146/annurev.aa.18.090180.002541](https://doi.org/10.1146/annurev.aa.18.090180.002541).
- Sutherland, Will and Will Saunders (Dec. 1992). “On the likelihood ratio for source identification.” In: *Mon. Not. R. Astron. Soc.* 259, pp. 413–420. DOI: [10.1093/mnras/259.3.413](https://doi.org/10.1093/mnras/259.3.413).
- Tauber, J. A. (Jan. 2001). “The Planck Mission”. In: *The Extragalactic Infrared Background and its Cosmological Implications*. Ed. by Martin Harwit and Michael G. Hauser. Vol. 204, p. 493.
- Taylor, Edward N. et al. (Jan. 2015). “Galaxy And Mass Assembly (GAMA): deconstructing bimodality - I. Red ones and blue ones”. In: *Mon. Not. R. Astron. Soc.* 446.2, pp. 2144–2185. DOI: [10.1093/mnras/stu1900](https://doi.org/10.1093/mnras/stu1900). arXiv: [1408.5984 \[astro-ph.GA\]](https://arxiv.org/abs/1408.5984).
- Tingay, S. J. et al. (Jan. 2013). “The Murchison Widefield Array: The Square Kilometre Array Precursor at Low Radio Frequencies”. In: *Pub. Astron. Soc. Australia* 30, e007, e007. DOI: [10.1017/pasa.2012.007](https://doi.org/10.1017/pasa.2012.007). arXiv: [1206.6945 \[astro-ph.IM\]](https://arxiv.org/abs/1206.6945).

- Toomre, Alar and Juri Toomre (Dec. 1972). “Galactic Bridges and Tails”. In: *Astrophys. J.* 178, pp. 623–666. DOI: [10.1086/151823](https://doi.org/10.1086/151823).
- Trayford, James W. et al. (Jan. 2020). “Fade to grey: systematic variation of galaxy attenuation curves with galaxy properties in the EAGLE simulations”. In: *Mon. Not. R. Astron. Soc.* 491.3, pp. 3937–3951. DOI: [10.1093/mnras/stz3234](https://doi.org/10.1093/mnras/stz3234). arXiv: [1908.08956 \[astro-ph.GA\]](https://arxiv.org/abs/1908.08956).
- Treu, Tommaso et al. (July 2003). “A Wide-Field Hubble Space Telescope Study of the Cluster Cl 0024+16 at  $z = 0.4$ . I. Morphological Distributions to 5 Mpc Radius”. In: *Astrophys. J.* 591.1, pp. 53–78. DOI: [10.1086/375314](https://doi.org/10.1086/375314). arXiv: [astro-ph/0303267 \[astro-ph\]](https://arxiv.org/abs/astro-ph/0303267).
- Twite, Jonathan W. et al. (Jan. 2012). “H-alpha star formation rates in massive galaxies at  $z \approx 1$ ”. In: *Monthly Notices of the Royal Astronomical Society* 420.2, 1061–1078. ISSN: 0035-8711. DOI: [10.1111/j.1365-2966.2011.20057.x](https://doi.org/10.1111/j.1365-2966.2011.20057.x). URL: <http://dx.doi.org/10.1111/j.1365-2966.2011.20057.x>.
- Tyler, K. D. et al. (Oct. 2014). “Star Formation Trends in the Unrelaxed, Post-merger Cluster A2255”. In: *Astrophys. J.* 794.1, 31, p. 31. DOI: [10.1088/0004-637X/794/1/31](https://doi.org/10.1088/0004-637X/794/1/31).
- van den Bosch, Frank C. et al. (June 2008). “The importance of satellite quenching for the build-up of the red sequence of present-day galaxies”. In: *Mon. Not. R. Astron. Soc.* 387.1, pp. 79–91. DOI: [10.1111/j.1365-2966.2008.13230.x](https://doi.org/10.1111/j.1365-2966.2008.13230.x). arXiv: [0710.3164 \[astro-ph\]](https://arxiv.org/abs/0710.3164).
- van Haarlem, M. P. et al. (Aug. 2013). “LOFAR: The LOw-Frequency ARray”. In: *Astron. Astrophys.* 556, A2, A2. DOI: [10.1051/0004-6361/201220873](https://doi.org/10.1051/0004-6361/201220873). arXiv: [1305.3550 \[astro-ph.IM\]](https://arxiv.org/abs/1305.3550).
- van Weeren, R. J. et al. (Apr. 2011a). “A double radio relic in the merging galaxy cluster ZwCl 0008.8+5215”. In: *Astron. Astrophys.* 528, A38, A38. DOI: [10.1051/0004-6361/201016185](https://doi.org/10.1051/0004-6361/201016185). arXiv: [1102.2235 \[astro-ph.CO\]](https://arxiv.org/abs/1102.2235).
- van Weeren, R. J. et al. (Mar. 2011b). “Diffuse steep-spectrum sources from the 74 MHz VLSS survey”. In: *Astron. Astrophys.* 527, A114, A114. DOI: [10.1051/0004-6361/201015991](https://doi.org/10.1051/0004-6361/201015991). arXiv: [1101.3865 \[astro-ph.CO\]](https://arxiv.org/abs/1101.3865).
- van Weeren, R. J. et al. (Nov. 2011c). “Using double radio relics to constrain galaxy cluster mergers: a model of double radio relics in CIZA J2242.8+5301”. In: *Mon. Not. R. Astron. Soc.* 418.1, pp. 230–243. DOI: [10.1111/j.1365-2966.2011.19478.x](https://doi.org/10.1111/j.1365-2966.2011.19478.x). arXiv: [1108.1398 \[astro-ph.CO\]](https://arxiv.org/abs/1108.1398).
- van Weeren, R. J. et al. (Feb. 2019). “Diffuse Radio Emission from Galaxy Clusters”. In: *Space Sci. Rev.* 215.1, 16, p. 16. DOI: [10.1007/s11214-019-0584-z](https://doi.org/10.1007/s11214-019-0584-z). arXiv: [1901.04496 \[astro-ph.HE\]](https://arxiv.org/abs/1901.04496).
- Vazza, F. and M. Brüggen (Jan. 2014). “Do radio relics challenge diffusive shock acceleration?” In: *Mon. Not. R. Astron. Soc.* 437.3, pp. 2291–2296. DOI: [10.1093/mnras/stt2042](https://doi.org/10.1093/mnras/stt2042). arXiv: [1310.5707 \[astro-ph.CO\]](https://arxiv.org/abs/1310.5707).
- Vazza, F. et al. (Apr. 2012). “Why are central radio relics so rare?” In: *Mon. Not. R. Astron. Soc.* 421.3, pp. 1868–1873. DOI: [10.1111/j.1365-2966.2011.20160.x](https://doi.org/10.1111/j.1365-2966.2011.20160.x). arXiv: [1111.1720 \[astro-ph.CO\]](https://arxiv.org/abs/1111.1720).

- Vazza, F. et al. (June 2016). “Constraining the efficiency of cosmic ray acceleration by cluster shocks”. In: *Mon. Not. R. Astron. Soc.* 459.1, pp. 70–83. DOI: [10.1093/mnras/stw584](https://doi.org/10.1093/mnras/stw584). arXiv: [1603.02688 \[astro-ph.GA\]](https://arxiv.org/abs/1603.02688).
- Venturi, T. et al. (May 1990). “High-Sensitivity Radio Observations of the Coma Cluster of Galaxies”. In: *Astron. J.* 99, p. 1381. DOI: [10.1086/115422](https://doi.org/10.1086/115422).
- Vikhlinin, A. et al. (Aug. 1998). “A Catalog of 200 Galaxy Clusters Serendipitously Detected in the ROSAT PSPC Pointed Observations”. In: *Astrophys. J.* 502.2, pp. 558–581. DOI: [10.1086/305951](https://doi.org/10.1086/305951). arXiv: [astro-ph/9803099 \[astro-ph\]](https://arxiv.org/abs/astro-ph/9803099).
- Vogelsberger, Mark et al. (Oct. 2014). “Introducing the Illustris Project: simulating the coevolution of dark and visible matter in the Universe”. In: *Mon. Not. R. Astron. Soc.* 444.2, pp. 1518–1547. DOI: [10.1093/mnras/stu1536](https://doi.org/10.1093/mnras/stu1536). arXiv: [1405.2921 \[astro-ph.CO\]](https://arxiv.org/abs/1405.2921).
- Vulcani, Benedetta et al. (Mar. 2011). “Galaxy stellar mass functions of different morphological types in clusters, and their evolution between  $z=0.8$  and 0”. In: *Mon. Not. R. Astron. Soc.* 412.1, pp. 246–268. DOI: [10.1111/j.1365-2966.2010.17904.x](https://doi.org/10.1111/j.1365-2966.2010.17904.x). arXiv: [1010.4442 \[astro-ph.CO\]](https://arxiv.org/abs/1010.4442).
- Walcher, Jakob et al. (Jan. 2011). “Fitting the integrated spectral energy distributions of galaxies”. In: *Astrophys. Space Sci.* 331, pp. 1–52. DOI: [10.1007/s10509-010-0458-z](https://doi.org/10.1007/s10509-010-0458-z). arXiv: [1008.0395 \[astro-ph.CO\]](https://arxiv.org/abs/1008.0395).
- Webb, N. A. et al. (Sept. 2020). “The XMM-Newton serendipitous survey. IX. The fourth XMM-Newton serendipitous source catalogue”. In: *Astron. Astrophys.* 641, A136, A136. DOI: [10.1051/0004-6361/201937353](https://doi.org/10.1051/0004-6361/201937353). arXiv: [2007.02899 \[astro-ph.HE\]](https://arxiv.org/abs/2007.02899).
- Webb, T. M. A. et al. (Oct. 2013). “The Evolution of Dusty Star formation in Galaxy Clusters to  $z = 1$ : Spitzer Infrared Observations of the First Red-Sequence Cluster Survey”. In: *Astron. J.* 146.4, 84, p. 84. DOI: [10.1088/0004-6256/146/4/84](https://doi.org/10.1088/0004-6256/146/4/84). arXiv: [1304.3335 \[astro-ph.CO\]](https://arxiv.org/abs/1304.3335).
- Weeren, R. J. van et al. (Feb. 2016). “LOFAR, VLA, and Chandra Observations of the Toothbrush Galaxy Cluster”. In: *The Astrophysical Journal* 818.2, p. 204. DOI: [10.3847/0004-637x/818/2/204](https://doi.org/10.3847/0004-637x/818/2/204). URL: <https://doi.org/10.3847/0004-637x/818/2/204>.
- Weisskopf, Martin C. et al. (July 2000). “Chandra X-ray Observatory (CXO): overview”. In: *X-Ray Optics, Instruments, and Missions III*. Ed. by Joachim E. Truemper and Bernd Aschenbach. Vol. 4012. Society of Photo-Optical Instrumentation Engineers (SPIE) Conference Series, pp. 2–16. DOI: [10.1117/12.391545](https://doi.org/10.1117/12.391545). arXiv: [astro-ph/0004127 \[astro-ph\]](https://arxiv.org/abs/astro-ph/0004127).
- Weiβmann, A. et al. (Jan. 2013). “Studying the properties of galaxy cluster morphology estimators”. In: *Astron. Astrophys.* 549, A19, A19. DOI: [10.1051/0004-6361/201219333](https://doi.org/10.1051/0004-6361/201219333). arXiv: [1210.6445 \[astro-ph.CO\]](https://arxiv.org/abs/1210.6445).
- Wen, Z. L. and J. L. Han (Nov. 2013). “Substructure and dynamical state of 2092 rich clusters of galaxies derived from photometric data”. In: *Mon. Not. R. Astron. Soc.* 436.1, pp. 275–293. DOI: [10.1093/mnras/stt1581](https://doi.org/10.1093/mnras/stt1581). arXiv: [1307.0568 \[astro-ph.CO\]](https://arxiv.org/abs/1307.0568).
- Whitehouse, D. (2009). *Renaissance Genius : Galileo Galilei & H*: Sterling. ISBN: 9781402769771. URL: <https://books.google.co.za/books?id=bGKrPVoQY8QC>.

- Williams, J. P. et al. (May 2000). “The Structure and Evolution of Molecular Clouds: from Clumps to Cores to the IMF”. In: *Protostars and Planets IV*. Ed. by V. Mannings et al., p. 97. arXiv: [astro-ph/9902246 \[astro-ph\]](#).
- Willson, M. A. G. (Jan. 1970). “Radio observations of the cluster of galaxies in Coma Berenices - the 5C4 survey.” In: *Mon. Not. R. Astron. Soc.* 151, p. 1. DOI: [10.1093/mnras/151.1.1](#).
- Wittman, David (Aug. 2019). “Dynamical Properties of Merging Galaxy Clusters from Simulated Analogs”. In: *Astrophys. J.* 881.2, 121, p. 121. DOI: [10.3847/1538-4357/ab3052](#). arXiv: [1905.00375 \[astro-ph.CO\]](#).
- Wright, Edward L. et al. (Dec. 2010). “The Wide-field Infrared Survey Explorer (WISE): Mission Description and Initial On-orbit Performance”. In: *Astron. J.* 140.6, pp. 1868–1881. DOI: [10.1088/0004-6256/140/6/1868](#). arXiv: [1008.0031 \[astro-ph.IM\]](#).
- Yokoyama, Shota L. and Yutaka Ohira (July 2020). “Particle Acceleration in a Shock Wave Propagating to an Inhomogeneous Medium”. In: *Astrophys. J.* 897.1, 50, p. 50. DOI: [10.3847/1538-4357/ab93c3](#). arXiv: [2004.05765 \[astro-ph.HE\]](#).
- Yoon, Mijin et al. (Nov. 2020). “Toward Solving the Puzzle: Dissecting the Complex Merger A521 with Multiwavelength Data”. In: *Astrophys. J.* 903.2, 151, p. 151. DOI: [10.3847/1538-4357/abb76d](#). arXiv: [2006.13535 \[astro-ph.GA\]](#).
- Yoon, Yongmin and Myungshin Im (Apr. 2020). “Star Formation Enhancement in Barred Disk Galaxies in Interacting Galaxy Clusters”. In: *Astrophys. J.* 893.2, 117, p. 117. DOI: [10.3847/1538-4357/ab8008](#). arXiv: [2004.02204 \[astro-ph.GA\]](#).
- Yuan, Z. S. and J. L. Han (Oct. 2020). “Dynamical state for 964 galaxy clusters from Chandra X-ray images”. In: *Mon. Not. R. Astron. Soc.* 497.4, pp. 5485–5497. DOI: [10.1093/mnras/staa2363](#). arXiv: [2008.01299 \[astro-ph.GA\]](#).
- Yun, Min S. et al. (June 2001). “Radio Properties of Infrared-selected Galaxies in the IRAS 2 Jy Sample”. In: *Astrophys. J.* 554.2, pp. 803–822. DOI: [10.1086/323145](#). arXiv: [astro-ph/0102154 \[astro-ph\]](#).
- Zandanel, Fabio and Shin’ichiro Ando (May 2014). “Constraints on diffuse gamma-ray emission from structure formation processes in the Coma cluster”. In: *Mon. Not. R. Astron. Soc.* 440.1, pp. 663–671. DOI: [10.1093/mnras/stu324](#). arXiv: [1312.1493 \[astro-ph.HE\]](#).
- Zhang, Y. et al. (Aug. 2019). “Dark Energy Surveyed Year 1 results: calibration of cluster mis-centring in the redMaPPer catalogues”. In: *Mon. Not. R. Astron. Soc.* 487.2, pp. 2578–2593. DOI: [10.1093/mnras/stz1361](#). arXiv: [1901.07119 \[astro-ph.CO\]](#).
- Zhang, Y. Y. et al. (Sept. 2006). “X-ray properties in massive galaxy clusters: XMM-Newton observations of the REFLEX-DXL sample”. In: *Astron. Astrophys.* 456.1, pp. 55–74. DOI: [10.1051/0004-6361:20053650](#). arXiv: [astro-ph/0603275 \[astro-ph\]](#).
- Zou, Hu et al. (Apr. 2017). “Project Overview of the Beijing–Arizona Sky Survey”. In: *Publications of the Astronomical Society of the Pacific* 129.976, p. 064101. DOI: [10.1088/1538-3873/aa65ba](#). URL: <https://doi.org/10.1088/1538-3873/aa65ba>.

Zwicky, F. (Aug. 1938). “On the Clustering of Nebulae”. In: *Pub. Astron. Soc. Pacific* 50.296, pp. 218–220. DOI: [10.1086/124935](https://doi.org/10.1086/124935).